

Centrifuge Modeling of Cyclic Lateral Response of Pile-Cap Systems and Seat-Type Abutments in Dry Sand

by

Aniruddha D. Gadre and Ricardo Dobry
Rensselaer Polytechnic Institute
Department of Civil and Environmental Engineering
Troy, New York 12180-3590

Technical Report MCEER-98-0010

October 2, 1998

This research was conducted at Rensselaer Polytechnic Institute and was supported by the Federal Highway Administration under contract number DTFH61-92-C-00112.

NOTICE

This report was prepared by Rensselaer Polytechnic Institute as a result of research sponsored by the Multidisciplinary Center for Earthquake Engineering Research (MCEER) through a contract from the Federal Highway Administration. Neither MCEER, associates of MCEER, its sponsors, Rensselaer Polytechnic Institute, nor any person acting on their behalf:

- a. makes any warranty, express or implied, with respect to the use of any information, apparatus, method, or process disclosed in this report or that such use may not infringe upon privately owned rights; or
- b. assumes any liabilities of whatsoever kind with respect to the use of, or the damage resulting from the use of, any information, apparatus, method, or process disclosed in this report.

Any opinions, findings, and conclusions or recommendations expressed in this publication are those of the author(s) and do not necessarily reflect the views of MCEER or the Federal Highway Administration.



Centrifuge Modeling of Cyclic Lateral Response of Pile-Cap Systems and Seat-Type Abutments in Dry Sands

by

Aniruddha D. Gadre¹ and Ricardo Dobry²

Publication Date: October 2, 1998

Submittal Date: September 8, 1997

Technical Report MCEER-98-0010

Task Number 112-D-3.2

FHWA Contract Number DTFH61-92-C-00112

1 Graduate Research Assistant, Department of Civil Engineering, Rensselaer Polytechnic Institute

2 Professor, Department of Civil Engineering, Rensselaer Polytechnic Institute

MULTIDISCIPLINARY CENTER FOR EARTHQUAKE ENGINEERING RESEARCH

University at Buffalo, State University of New York

Red Jacket Quadrangle, Buffalo, NY 14261

Preface

The Multidisciplinary Center for Earthquake Engineering Research (MCEER) is a national center of excellence in advanced technology applications that is dedicated to the reduction of earthquake losses nationwide. Headquartered at the University at Buffalo, State University of New York, the Center was originally established by the National Science Foundation in 1986, as the National Center for Earthquake Engineering Research (NCEER).

Comprising a consortium of researchers from numerous disciplines and institutions throughout the United States, the Center's mission is to reduce earthquake losses through research and the application of advanced technologies that improve engineering, pre-earthquake planning and post-earthquake recovery strategies. Toward this end, the Center coordinates a nationwide program of multidisciplinary team research, education and outreach activities.

MCEER's research is conducted under the sponsorship of two major federal agencies, the National Science Foundation (NSF) and the Federal Highway Administration (FHWA), and the State of New York. Significant support is also derived from the Federal Emergency Management Agency (FEMA), other state governments, academic institutions, foreign governments and private industry.

The Center's FHWA-sponsored Highway Project develops retrofit and evaluation methodologies for existing bridges and other highway structures (including tunnels, retaining structures, slopes, culverts, and pavements), and improved seismic design criteria and procedures for bridges and other highway structures. Specifically, tasks are being conducted to:

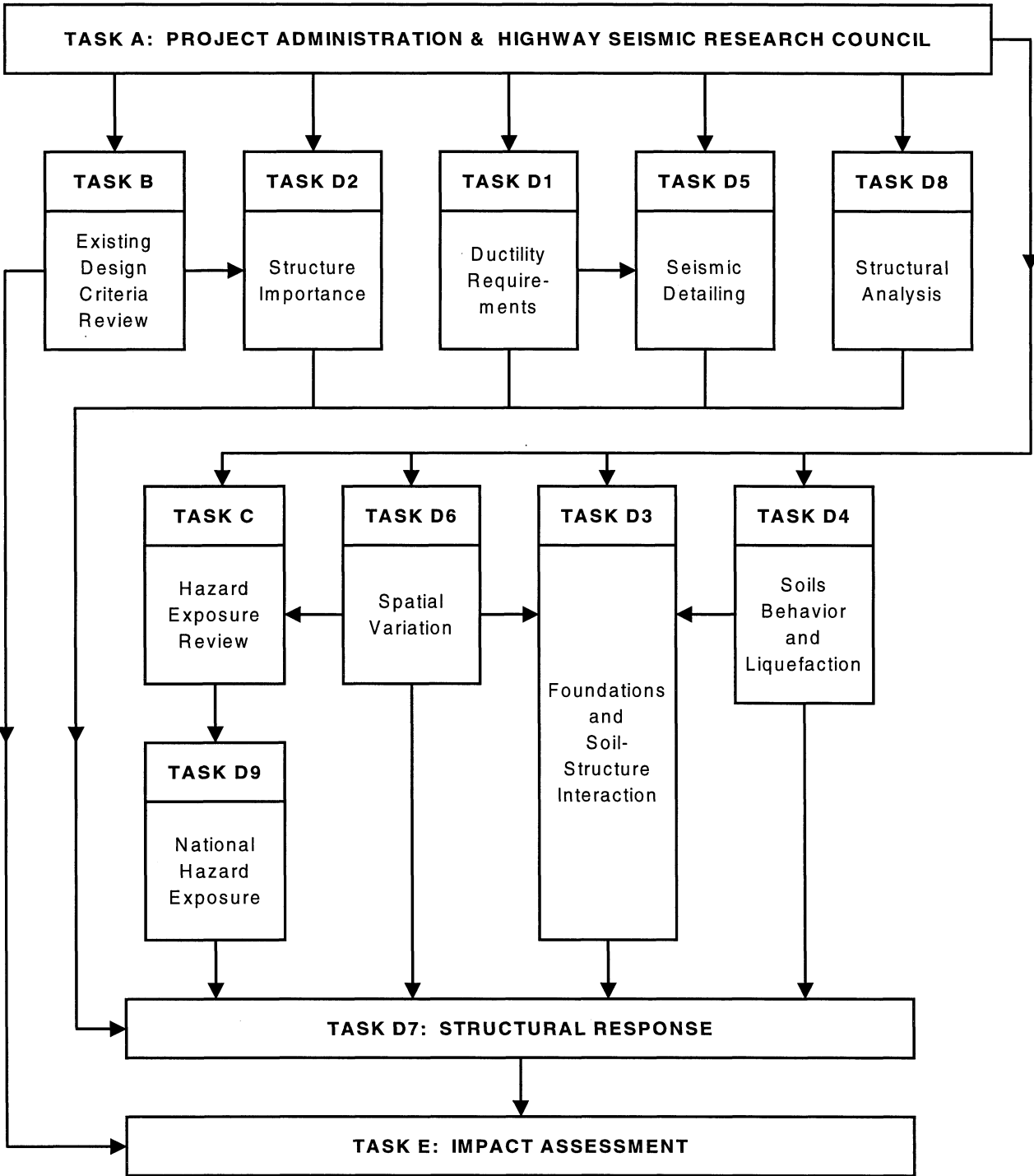
- assess the vulnerability of highway systems, structures and components;
- develop concepts for retrofitting vulnerable highway structures and components;
- develop improved design and analysis methodologies for bridges, tunnels, and retaining structures, which include consideration of soil-structure interaction mechanisms and their influence on structural response;
- review and recommend improved seismic design and performance criteria for new highway structures.

Highway Project research focuses on two distinct areas: the development of improved design criteria and philosophies for new or future highway construction, and the development of improved analysis and retrofitting methodologies for existing highway systems and structures. The research discussed in this report is a result of work conducted under the new highway structures project, and was performed within Task 112-D-3.2, "Abutment and Pile Footing Studies by Centrifuge Testing" of that project as shown in the flowchart on the following page.

The overall objective of this task was to develop guidelines for the seismic design of abutments and pile footings based on an analytical and experimental program using centrifuge testing. This report presents the results from a series of centrifuge tests, which were performed on pile-cap foundation systems (cap, single-pile and pile-cap systems) and seat-type bridge abutments, all in dense dry sand. The pile-cap foundation test results were compared to analytical models and nonlinear finite element

analyses, with good agreement. The seat-type bridge abutments were compared to established design procedures (Caltrans, ATC and AASHTO) and other evidence such as measurements obtained during past earthquakes. The test results indicate that current design procedures overestimate the measured lateral capacity and stiffness. Additional research to investigate these differences is therefore recommended.

SEISMIC VULNERABILITY OF NEW HIGHWAY CONSTRUCTION
FHWA Contract DTFH61-92-C-00112



ABSTRACT

This report presents the results of slow, cyclic, lateral-loading centrifuge tests performed on models of pile-cap foundation systems and seat-type bridge abutments in dry Nevada sand of 75 % relative density to study the lateral response of these systems. These results are compared with interpretations using simple models, results of nonlinear finite element analyses, established design procedures, as well as other evidence including measurements during earthquakes.

A total of ten centrifuge tests were performed at a centrifugal acceleration of 30-g, on models of the cap, single pile, and pile-cap system in this dense dry sand. Lateral response parameters studied included secant stiffness and material damping ratio at various displacement amplitudes, and ultimate lateral capacity of the foundation. Seven centrifuge experiments on the cap-alone simulated a reinforced concrete square, 1.14 m x 1.14 m by 0.84 m high foundation embedded in the dense dry sand. The results are relevant to both shallow foundations and embedded pile caps. The tests' objectives were to evaluate the relative contributions to stiffness, damping and capacity of the base, shearing sides, and active/passive sides of the cap to the total lateral response, as well as any possible interaction between these partial contributions. In all cases, the active/passive contribution was more than 50 % of the total stiffness, damping, and capacity. An "addition rule" is approximately valid for these contributions to secant stiffness, dissipated damping energy, and ultimate capacity. The measured lateral stiffnesses and capacities are compared with available theoretical solutions. A single test on an instrumented model of the single free-head pile - without the cap - approximately simulated a typical 40-cm diameter Cast-In-Drilled-Hole (CIDH) pile in dry sand. This test was performed primarily to backfigure p-y curves for the soil, which are in reasonable agreement with p-y curves in the literature. The results of this test are compared with established design procedures and available analytical solutions. Two centrifuge experiments on pile-cap system models were conducted with the pile rigidly clamped to the embedded cap. The measured lateral response of the pile-cap system

including load-displacement at the top, and bending moments along the pile, is compared with the measured response of the cap-alone and pile-alone.

Three-dimensional static nonlinear finite element (FE) analyses were used to predict the measured lateral load-displacement curves of centrifuge tests on cap-alone (embedded footing), with good agreement. Detailed study of these FE runs confirmed analytically the relative contributions of base, shearing sides, and active/passive sides to secant stiffness, as well as the validity of the addition rule. Parametric studies were then performed using this calibrated FE model to study the influence of the value and distribution of the soil shear modulus and of the cap/footing geometry on the nonlinear lateral response of the footing.

Three centrifuge tests at centrifugal accelerations ranging between 50 and 100 g were performed on a model of seat-type abutments in dense dry sand, simulating prototype bridge abutments of various dimensions including a typical California abutment geometry. The measured secant stiffnesses at various levels of lateral displacement and the measured ultimate lateral capacities are compared with standard design procedures, as well as with other evidence including measurements during actual earthquakes. It was found that the measured stiffness and capacities are comparable or smaller than values obtained by usual design procedures.

ACKNOWLEDGEMENT

The research presented in this report is a part of the FHWA project entitled “Seismic Vulnerability of New Highway Structures.” This project was supported by the Federal Highway Administration (FHWA) and the National Center for Earthquake Engineering Research (NCEER). Their support is gratefully acknowledged.

The authors would like to thank Prof. Geoffrey R. Martin of the University of Southern California in Los Angeles, CA, Mr. Ignatius Po Lam of Earth Mechanics Inc. in Fountain Valley, CA, Dr. Ian G. Buckle (now at Auckland University in Auckland, New Zealand) and Mr. Ian M. Friedland of NCEER in Buffalo, NY for their suggestions and feedback during this research.

The opinions, findings and conclusions or recommendations expressed in this report are those of the authors, and do not necessarily reflect the views of FHWA or NCEER.

TABLE OF CONTENTS

SECTION	TITLE	PAGE
1	INTRODUCTION	1
2	BACKGROUND	5
2.1	INTRODUCTION	5
2.2	LATERAL RESPONSE OF CAP OR EMBEDDED FOOTING	7
2.2.1	State of the Art	7
2.2.2	State of Practice	8
2.3	LATERAL RESPONSE OF SINGLE PILES	9
2.3.1	State of the Art	9
2.3.2	State of Practice – Bridge Structures	10
2.3.3	Full Scale Field Tests	11
2.3.4	Centrifuge Model Tests	11
2.4	LATERAL RESPONSE OF PILE-CAP FOUNDATION SYSTEMS	12
2.4.1	State of the Art	12
2.4.2	State of Practice	13
2.5	LATERAL RESPONSE OF BRIDGE ABUTMENTS	13
2.5.1	State of the Art	13
2.5.2	State of Practice	14
2.6	GEOTECHNICAL CENTRIFUGE MODELING	14
2.6.1	General	14
2.6.2	RPI Geotechnical Centrifuge	16
2.7	NUMERICAL MODELING OF GEOTECHNICAL PROBLEMS	19
2.8	SUMMARY	19
3	TESTING PROGRAM FOR PILE-CAP FOUNDATION SYSTEM: SCOPE AND IMPLEMENTATION	21
3.1	INTRODUCTION	21

TABLE OF CONTENTS (Cont'd)

SECTION	TITLE	PAGE
3.2	SCOPE	21
3.3	SOIL USED	27
3.4	MODEL CHARACTERISTICS	27
3.5	LATERAL LOADING ASSEMBLY	29
3.6	LATERAL DISPLACEMENT CYCLES	33
3.7	MODEL PREPARATION AND TESTING TECHNIQUE	33
4	CENTRIFUGE TESTS ON EMBEDDED FOOTING (PILE-CAP)	37
4.1	INTRODUCTION	37
4.1.1	Tests Presented in this Section	38
4.1.2	Model Footing	41
4.2	SPECIAL TECHNIQUES USED FOR THE TESTS	43
4.3	MODEL CONSTRUCTION AND TESTING PROCEDURE	44
4.3.1	Model Construction	44
4.3.2	Testing Procedure	45
4.4	TEST RESULTS	46
4.4.1	Ultimate Capacity	54
4.4.2	Secant Stiffness	58
4.4.3	Material Damping	59
4.5	COMPARISON OF INITIAL SECANT STIFFNESS WITH THEORY	62
4.6	CONCLUSIONS	68
5.	CENTRIFUGE TESTS ON FREE-HEAD PILE WITHOUT CAP	71
5.1	INTRODUCTION	71
5.2	MODEL CONFIGURATION	71

TABLE OF CONTENTS (Cont'd)

SECTION	TITLE	PAGE
5.3	MODEL CONSTRUCTION AND TESTING PROCEDURE	72
5.4	TEST RESULTS	76
5.4.1	Ultimate Capacity	76
5.4.2	Secant Stiffness	78
5.4.3	Material Damping	81
5.4.4	Measured Bending Moments	81
5.5	DETERMINATION OF p-y CURVES FOR THE SOIL	81
5.6	COMPARISON OF EXPERIMENTAL RESULTS WITH THEORY	85
5.6.1	Initial Secant Stiffness	85
5.6.2	Lateral Load Deflection Characteristics	87
5.6	CONCLUSIONS	89
6	CENTRIFUGE TESTS ON PILE-CAP SYSTEM	93
6.1	INTRODUCTION	93
6.2	MODEL CONFIGURATION	93
6.3	MODEL CONSTRUCTION AND TESTING PROCEDURE	94
6.4	TEST RESULTS	96
6.4.1	Ultimate Capacity	100
6.4.2	Secant Stiffness	100
6.4.3	Material Damping	103
6.4.4	Measured Bending Moments	103
6.5	COMPARISON OF MEASURED AND CALCULATED RESPONSE	107
6.5.1	Bending Moments	110
6.5.2	Lateral Load	110
6.5.3	Rotation of Cap	111
6.5.4	Response at Large Displacements	112

TABLE OF CONTENTS (Cont'd)

SECTION	TITLE	PAGE
6.6	CONCLUSIONS	113
7.	FINITE ELEMENT ANALYSES OF CAP-ALONE (EMBEDDED FOUNDATION) WITH UNIFORM SOIL MODULUS	117
7.1	INTRODUCTION	117
7.2	MODEL DESCRIPTION	117
7.2.1	Constitutive Models	118
7.3	NUMERICAL SIMULATION OF CENTRIFUGE TESTS	124
7.3.1	Parameters Used in the FE Model	126
7.3.2	Results of FE Analyses	128
7.3.3	Comparison of Computed and Measured Material Damping	128
7.3.4	Contributions of Base and Sides of Cap to Total Lateral Response	130
7.4	COMPARISON OF LATERAL RESPONSE OF CAP IN TESTS CBSP AND PCBSPI	139
7.5	PARAMETRIC FE STUDY FOR LATERAL RESPONSE OF CAP/FOOTING	140
7.5.1	Effect of Soil Modulus on Lateral response	140
7.5.2	Effect of Foundation Geometry on Lateral Response	140
7.6	CONCLUSIONS	145
8.	FINITE ELEMENT ANALYSES OF CAP/FOOTING WITH SOIL MODULUS DEPENDENT ON MEAN NORMAL STRESS	149
8.1	INTRODUCTION	149
8.2	NUMERICAL SIMULATION OF CENTRIFUGE TESTS CBSP AND CBSPL	150
8.2.1	FE Analyses	150

TABLE OF CONTENTS (Cont'd)

SECTION	TITLE	PAGE
8.2.2	Contribution of Base and Sides of Cap to Total Lateral Response	154
8.3	EFFECT OF FOUNDATION GEOMETRY ON LATERAL RESPONSE	157
8.4	CONCLUSIONS	161
9	CENTRIFUGE TESTS ON SEAT-TYPE MODEL ABUTMENT	165
9.1	INTRODUCTION	165
9.2	TESTING PROGRAM: SCOPE AND IMPLEMENTATION	166
9.2.1	Model of Seat-Type Abutment	166
9.2.2	Centrifuge Tests Performed	169
9.2.3	Lateral Loading	169
9.3	MODEL CONSTRUCTION AND TESTING PROCEDURE	175
9.3.1	Model Construction	175
9.3.2	Testing Procedure	175
9.4	TEST RESULTS	176
9.4.1	Ultimate Capacity	178
9.4.2	Secant Stiffness	179
9.4.3	Normalized Non-dimensional Backbone Curve	181
9.5	CONCLUSIONS	182
10	CONCLUSIONS	189
11	RECOMMENDATIONS	193
11.1	ENGINEERING RECOMMENDATIONS	193
11.2	SUGGESTIONS FOR FUTURE WORK	194
12	REFERENCES	195

LIST OF ILLUSTRATIONS

FIGURE	TITLE	PAGE
2-1	Pile foundation with embedded cap.	6
2-2	Bridge abutment in dense dry sand subjected to lateral load.	6
2-3	Plan view of RPI geotechnical facilities (after Elgamal et al., 1991)	17
2-4	Schematic of RPI geotechnical centrifuge (after Van Laak, 1996).	17
2-5	Performance envelope for RPI centrifuge (after Elgamal et al., 1996).	18
3-1	Pile foundation with embedded cap.	22
3-2	Isolation of forces contributing to lateral response of pile-cap system.	24
3-3	Grain size distribution for Nevada sand (after Arulmoli et al., 1992).	28
3-4	Model container used for centrifuge tests.	30
3-5	Load transfer mechanism.	31
3-6	General setup showing the lateral loading assembly for pile-cap foundation system.	32
3-7	Applied lateral cyclic displacement time history in prototype scale.	32
4-1	Forces contributing to the lateral resistance of the embedded foundation (pile cap).	39
4-2	Dimensions of the footing/cap model used in the centrifuge tests in prototype scale.	39
4-3	General set-up for centrifuge tests on embedded footing (pile cap).	42
4-4	Schematic representation of set-ups for centrifuge tests on model footing/cap.	42
4-5	Load-displacement response for Test CB in prototype scale.	47
4-6	Load-displacement response for Test CBL in prototype scale.	48
4-7	Load-displacement response for Test CS in prototype scale.	49
4-8	Load-displacement response for Test CP in prototype scale.	50
4-9	Load-displacement response for Test CSP in prototype scale.	51

LIST OF ILLUSTRATIONS (Cont'd)

FIGURE	TITLE	PAGE
4-10	Load-displacement response for Test CBSP in prototype scale.	52
4-11	Load-displacement response for Test CBSPL in prototype scale.	53
4-12	Normal force versus ultimate lateral capacity for Tests CB and CBL.	55
4-13	Measured secant stiffness versus displacement amplitude in tests on footing /cap.	55
4-14	Measured normalized secant stiffness versus displacement amplitude.	60
4-15	Measured area of loop versus displacement amplitude for tests on footing/cap.	60
4-16	Measured equivalent damping ratio versus displacement amplitude.	63
4-17	Correlation chart for shape factor for abutment stiffness (after Wilson, 1988).	63
5-1	Model pile used in Test PI.	73
5-2	Set-up for centrifuge Test PI.	75
5-3	Load-displacement response for Test PI in prototype scale.	77
5-4	Stiffness versus displacement amplitude in prototype scale.	79
5-5	Measured bending moments versus time in Test PI in prototype scale.	79
5-6	Measured prototype bending moments along the length of the pile in Test PI.	82
5-7	p-y curves for the soil backfigured from the results of Test PI in prototype scale.	82
5-8	Measured and calculated bending moments for Test PI.	84
5-9	Comparison of p-y curves backfigured from centrifuge Test PI with the p-y curves modified after Bouafia and Garnier (1991).	86
5-10	Correlation chart for I_{pH} (after Poulos and Davis, 1980).	86

LIST OF ILLUSTRATIONS (Cont'd)

FIGURE	TITLE	PAGE
5-11	Correlation chart for F_p (after Poulos and Davis, 1980).	90
5-12	Measured and calculated load-deflection curves for Test PI.	90
6-1	Model of pile-cap system used in Test PCBSPI.	95
6-2	Set-up for centrifuge tests on pile-cap system.	97
6-3	Measured load-displacement response for Test PCBSPI in prototype scale (pile-cap system).	98
6-4	Measured load-displacement response for Test PCBSPI (pile-cap system with instrumented pile).	99
6-5	Measured secant stiffness versus displacement amplitude.	102
6-6	Measured area of loop versus displacement amplitude.	102
6-7	Measured bending moments versus time in Test PCBSPI in prototype scale.	105
6-8	Measured Bending Moments along the Length of the Pile in Test PCBSPI.	105
6-9	Measured bending moments for Test PCBSPI superimposed on moment distributions calculated using p-y curves obtained from Test PI for free-head and fixed-head conditions.	108
6-10	p-y Curves Used for Large Displacement Amplitudes.	114
6-11	Measured and Calculated Bending Moments for Test PCBSPI at Large Displacements.	115
7-1	Dimensions of the square embedded foundation/pile-cap used in basic FE analyses.	119
7-2	Finite element mesh simulating set-up for centrifuge tests on cap-alone.	119
7-3	Modified Drucker-Prager/Cap model yield surface in the p-t plane (after Hibbit, Karlsson & Sorensen Inc., 1994).	121
7-4	Modified Drucker-Prager/Cap model typical yield/flow surfaces in the deviatoric plane (after Hibbit, Karlsson & Sorensen Inc., 1994).	121

LIST OF ILLUSTRATIONS (Cont'd)

FIGURE	TITLE	PAGE
7-5	Modified Drucker-Prager/Cap model flow potential in the p-t plane (after Hibbit, Karlsson & Sorensen Inc., 1994).	125
7-6	Cap hardening rule for the sand used in the FE analysis.	125
7-7	Measured and computed load-displacement response for Tests CBSP and CBSPL.	129
7-8	Load-displacement loops generated for Test CBSP from finite element results using Masing criterion.	131
7-9	Measured and computed equivalent damping ratios for Test CBSP.	132
7-10	Shear and normal forces at the base of the cap. (FE results are for Test CBSP with parameters of table 7-1).	132
7-11	Shear and normal forces along the shearing sides of the cap (FE results are for Test CBSP with parameters of table 7-1).	135
7-12	Normal forces at active/passive sides of the cap (FE results are for Test CBSP with parameters of table 7-1).	135
7-13	Measured and computed contributions to the load-displacement response of the cap. (FE results are for Test CBSP with parameters in table 7-1).	137
7-14	Measured and computed secant stiffness contributions versus displacement amplitude. (FE results are for Test CBSP with parameters in table 7-1).	137
7-15	Measured and computed contributions to the load-displacement response of the cap. (FE results are for Test CBSPL with parameters in table 7-1).	138
7-16	Measured and computed secant stiffness contributions versus displacement amplitude. (FE results are for Test CBSPL with parameters in table 7-1).	138
7-17	Computed load-displacement responses for Test CBSP with different soil shear moduli.	141

LIST OF ILLUSTRATIONS (Cont'd)

FIGURE	TITLE	PAGE
7-18	Computed horizontal secant stiffness versus displacement amplitude for Test CBSP with different soil shear moduli.	141
7-19	Results of parametric FE analyses conducted to study the influence of footing geometry on lateral secant stiffness. (FE analyses performed with $G = 1.73$ MPa).	147
8-1	Measured and computed load-displacement response for Tests CBSP.	152
8-2	Measured and computed load-displacement response for Test CBSPL.	152
8-3	Measured and computed secant stiffness for Test CBSP.	153
8-4	Measured and computed contributions to the load displacement response in Test CBSP. (FEM analyses are with $G = 584 \sigma_0^{0.5}$).	153
8-5	Measured and computed contributions to secant stiffness in Test CBSP (FEM analyses are with $G = 584 \sigma_0^{0.5}$).	155
8-6	Measured and computed contribution to load-displacement response in Test CBSPL (FEM analyses are with $G = 584 \sigma_0^{0.5}$).	155
8-7	Measured and computed contributions to secant stiffness of Test CBSPL. (FEM analyses are with $G = 584 \sigma_0^{0.5}$)	156
8-8	Results of parametric FE analyses conducted to study the influence of footing geometry on lateral secant stiffness.	160
8-9	Normalized equivalent depth versus normalized side of the footing ($m/D_f = 0.26$).	163
9-1	Schematic view of model abutment.	167
9-2	General setup for centrifuge tests on abutments.	168
9-3	Plan view of model abutment used in centrifuge tests.	168
9-4	Measured load-displacement response for Test AB50g in prototype scale.	172

LIST OF ILLUSTRATIONS (Cont'd)

FIGURE	TITLE	PAGE
9-5	Measured load displacement response for Test AB80g in prototype scale.	173
9-6	Measured load-displacement response for Test AB100g in prototype scale.	174
9-7	Measured and computed secant stiffnesses for Test AB50g.	185
9-8	Measured and computed secant stiffnesses for Test AB80g.	185
9-9	Measured and computed secant stiffnesses for Test AB100g.	186
9-10	Measured secant stiffness per unit length for centrifuge tests on abutments.	186
9-11	Measured secant stiffness per unit area for centrifuge tests on abutments.	187
9-12	Normalized backbone curves obtained from the centrifuge tests and the half-scale load test described by Maroney et al. (1994).	187

LIST OF TABLES

TABLE	TITLE	PAGE
2-1	Partial list of scaling relations for centrifuge modeling.	15
3-1	Centrifuge tests performed on pile-cap system.	25
3-2	Parameters considered for centrifuge model experiments.	25
4-1	Centrifuge tests performed on embedded footing/pile-cap.	40
4-2	Measured secant stiffness for loops of increasing displacement amplitudes in centrifuge tests on footing/cap.	40
4-3	Measured material damping for loops of increasing displacement amplitudes in centrifuge tests on footing /cap.	61
4-4	Parameters used for analytical calculation of initial horizontal secant stiffness.	61
4-5	Comparison of measured initial secant stiffness with theory.	67
5-1	Secant stiffness for loops of increasing displacement amplitude in Test CBSP, Test CBSPL, and Test PI.	80
5-2	Material damping for loops of increasing amplitude.	80
5-3	Comparison of measured and calculated pile-head shear forces.	80
5-4	Parameters used for initial stiffness calculations.	88
5-5	Calculation of lateral load-deflection curve for Test PI according to Poulos and Davis (1980) recommendations.	88
6-1	List of Centrifuge Tests Performed.	101
6-2	Secant Stiffness for Loops of Increasing Displacement Amplitude.	101
6-3	Material Damping for Loops of Increasing Displacement Amplitude.	104
6-4	Calculated Negative Bending Moments at the Pile-head in Test PCBSPI.	104
6-5	Pile-head configurations used for bending moment predictions using LPILE.	109
6-6	Measured and calculated lateral load contribution of pile in Test PCBSPI.	109

LIST OF TABLES (Cont'd)

TABLE	TITLE	PAGE
7-1	Parameters used in the finite element analyses of centrifuge Tests CBSP.	127
7-2	Comparison of lateral resistance of the cap with no rotation and with rotation equal to the pile-head rotation in the free-head case.	127
7-3	Comparison of ultimate capacity calculated by adding contributions of different sides with the capacity obtained using FE analyses. (Note 2B = 1.14 m, D = 1.14 m, G = 1.73 MPa).	142
7-4	Comparison of initial secant stiffness computed in the FE parametric study with the stiffness calculated using Pais-Kausel and Gazetas-Tassoulas solutions. (Note 2B = 1.14 m, D = 1.14 m, G = 1.73 MPa).	142
8-1	Comparison of ultimate capacity calculated by adding contributions of different sides with the capacity obtained using FE analyses. (Note 2B = 1.14 m, D = 1.14 m, G = 584 $\sigma_0^{0.5}$)	158
8-2	Comparison of initial secant stiffness at 0.3-cm deflection computed with G = 1.73 MPa and G = 584 $\sigma_0^{0.5}$. (Note 2B = 1.14 m, D = 1.14 m.)	158
8-3	Equivalent uniform soil shear modulus for the FE analyses with G = 584 $\sigma_0^{0.5}$ (Note 2B = 1.14 m, D = 1.14 m.)	162
9-1	Centrifuge tests performed on abutments.	170
9-2	Analysis of negative forces measured in the final displacement cycle of centrifuge tests on abutments.	170
9-3	Measured and computed stiffnesses for centrifuge tests on abutments.	184
10-1	Summary of centrifuge tests and FE analyses performed.	192

SECTION 1

INTRODUCTION

Evaluation of the cyclic lateral response of pile-cap foundation systems is very important for the design of foundations subjected to lateral loading, especially those arising from dynamic phenomena. This kind of loading in buildings, bridges and other structures arises due to earthquake shaking, wind, offshore wave loadings, and man-induced vibrations. Also, a reasonable assessment of the lateral stiffness and capacity of bridge abutments is essential for the seismic design of bridges. A research program was conducted to study the lateral response of highway bridge foundations and abutments. This project is part of the ongoing effort by the Federal Highway Administration (FHWA) and the National Center for Earthquake Engineering Research (NCEER) to assess seismic vulnerability of new highway structures, as well as to develop guidelines for seismic design of bridge foundations and abutments. Although this study refers to highway bridge structures, the results can also be used for other similar geotechnical engineering problems.

The lateral response of a pile-cap foundation system with an embedded cap has contributions from both the cap and the pile. The response of a single pile has been studied fairly well, and various design charts and computer programs have been developed. The lateral response of a cap, which can be viewed as equivalent to an embedded footing, is not completely understood, especially at large displacement amplitudes. The interaction between embedded-cap and pile contributions to the lateral response of a pile-cap foundation system also needs to be investigated. Better understanding of the lateral response of seat-type abutments, especially at large displacements, is very important for the seismic design of highway bridge structures.

The cyclic lateral response of foundations and abutments has three main aspects: stiffness, damping (both radiation and material damping components), and ultimate lateral capacity. As the response is nonlinear, both stiffness and damping generally

change with the level of applied lateral displacement. Hence, the elastic analytical solutions found in the available literature for determination of lateral stiffness are strictly applicable only at very small displacements. For pile-cap systems such as used in bridge foundations, the lateral pile-head deflection may range from 1.3 cm (0.5 in) to 2.5 cm (1 in) even at normal working load levels. In the case of offshore foundations, the lateral displacements for normal working loads can be even larger. The lateral response of bridge abutments during earthquakes is also highly nonlinear. Lateral abutment movements on the order of 6 cm or more have been observed during strong earthquake-shakings without major damage to the structure. Thus, the elastic solutions available in the literature are no longer adequate to determine the lateral stiffness of foundations and abutments during strong earthquake motions.

In order to study the lateral response of pile foundations and abutments at large displacements, one may resort to nonlinear analyses and/or full-scale lateral loading tests. However, with the advent of geotechnical centrifuge technology, it has become possible to model complicated geotechnical engineering problems in a controlled laboratory environment. Centrifuge testing is much less expensive than full-scale testing, and it captures the prototype stress conditions in a small-scale model. Since soil behavior is highly stress-dependent, centrifuge testing provides a viable alternative to full scale testing.

The focus of the research program conducted was to get a better understanding of the lateral response of the pile-cap systems and seat-type bridge abutments, and to verify the current design procedures used for estimation of stiffness and capacity. This was accomplished through centrifuge tests, nonlinear finite element modeling, interpretations using simple models and comparison with other evidence including measurements during actual earthquakes. This document presents and discusses the results of cyclic slow lateral loading centrifuge tests performed on small-scale models of pile-cap foundation systems and seat-type abutments in dense dry sand, where rough interfaces, sand-foundation and sand-abutment, are modeled to simulate reinforced concrete foundation and abutment. Three-dimensional nonlinear finite element (FE) analyses were performed

to predict the measured lateral response for the cap-alone experiments. Using these results, parametric studies were performed to investigate the influence of the value and distribution of the soil shear modulus, and of the foundation geometry on the nonlinear lateral response. The results of this study are presented in this document.

The organization of the document is straightforward. Section 2 examines the available literature on evaluation of the lateral response of foundations and abutments. Both the current *state of the art* and *state of practice* are reviewed. Several aspects of centrifuge modeling and finite element analysis are also discussed in Section 2.

The scope of the centrifuge testing program on the pile-cap system is discussed in Section 3. This section also gives the soil properties and model dimensions used in these centrifuge tests. The lateral loading assembly used for the in-flight cyclic loading of the scaled models of foundations and abutments is described. Various modeling techniques used in the different centrifuge tests are also explained.

Section 4 presents results of the centrifuge testing program conducted to evaluate the contributions of the various foundation-soil interfaces to the lateral response of the cap-alone at various displacement levels. These results are also applicable to embedded footings. The results are compared with the analytical formulations available in the literature.

Results of a single centrifuge test performed on an instrumented free-head pile-alone are presented in Section 5. This test was conducted primarily to evaluate the p-y curves of the soil. The results are compared with the relevant information available in the literature.

Section 6 describes the setup and results of centrifuge tests performed on the pile-cap foundation system. The pile was rigidly clamped to the embedded cap in these experiments. The lateral response of the pile-cap system is compared with the responses of the cap-alone and free head pile-alone from the previous sections. The bending

moment distributions measured in the pile with a cap on top are compared with the distributions obtained for the free-head pile.

Section 7 describes the finite element models used to numerically predict the results of the cap-alone experiments in which all sides and the base of the cap were in contact with the soil. The results of the parametric studies performed to investigate the influence of soil shear modulus and foundation geometry on the nonlinear lateral response are also presented. A uniform soil shear modulus was used in the FE analyses presented in Section 7.

Additional nonlinear FE analyses were performed with the soil shear modulus proportional to the square root of the initial mean normal stress. These analyses are described in Section 8. This section also includes results of a parametric study performed using such nonlinear FE analyses to understand the influence of cap/footing geometry on the lateral response. These results are compared with the results of the parametric study presented in Section 7.

The centrifuge tests performed on models of seat-type bridge abutments are described in Section 9. The lateral stiffnesses and capacities measured in these tests are compared with the design values obtained from current procedures.

Finally, Section 10 summarizes the significant results of the centrifuge testing program and finite element analyses. This section also presents some major conclusions drawn from these results, as well as recommendations for future research.

SECTION 2

BACKGROUND

2.1 INTRODUCTION

Evaluating the lateral stiffness, damping and capacity of pile foundations is an important problem to geotechnical and structural engineers dealing with the dynamic response of foundations to phenomena such as earthquakes, machine vibrations, and ocean wave loadings. Determination of the lateral stiffness and capacity of abutments is an important issue for seismic design of bridges and retaining structures. The research presented in this report pertains to the earthquake responses of bridge foundations and seat-type abutments, and is also generally applicable to other structures and sources of loading.

The lateral responses of both a single pile and an embedded footing have been studied fairly well. Less is known about the response of a pile-cap system when the cap is fully embedded in soil. The lateral response of a pile foundation such as shown in figure 2-1 includes contributions from both piles and cap. This is true for the lateral stiffness, damping, and capacity of the system. The lateral response at small amplitudes of motion of abutments, such as schematically shown in figure 2-2, has been studied extensively through elastic FE analyses and small-amplitude field vibration tests. However, these results are not useful in the design of bridges for intense earthquake motion, because the stiffness of the abutment depends on the amplitude of the motion.

In this section, the available literature and the *state of the art* of evaluation of lateral response of shallow footings, piles, pile-cap systems and abutments is briefly surveyed, plus the current *state of practice* used for the seismic design of highway bridges is reviewed. In addition, various relevant aspects of centrifuge modeling and finite element analysis are examined.

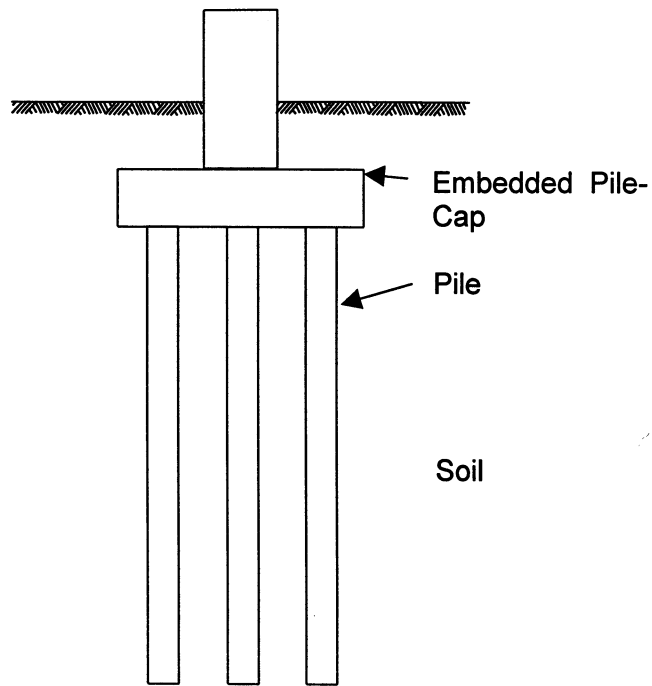


FIGURE 2-1: Pile foundation with embedded cap.

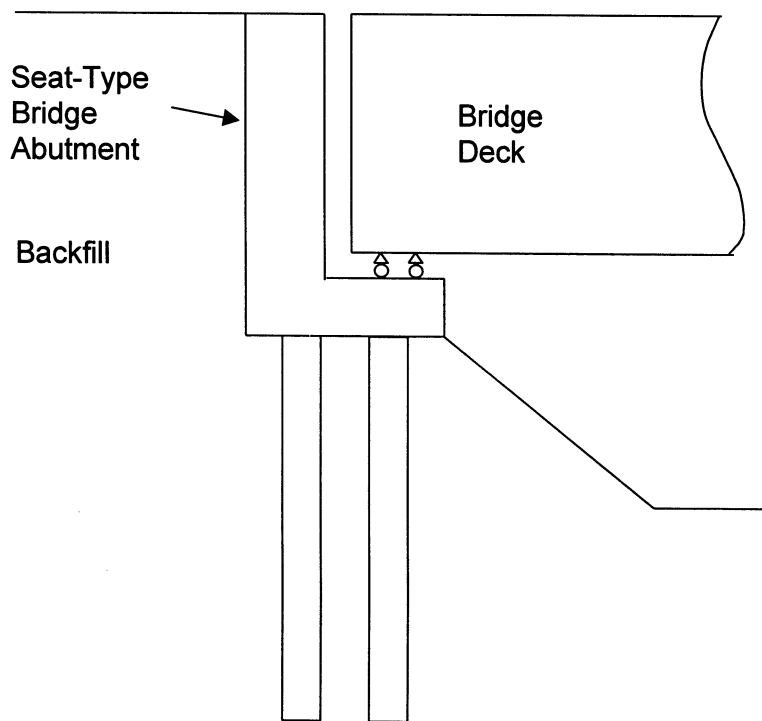


FIGURE 2-2: Bridge abutment in dense dry sand subjected to lateral load.

2.2 LATERAL RESPONSE OF CAP OR EMBEDDED FOOTING

2.2.1 State of the Art

A pile-cap without the pile can be assumed to be equivalent to a shallow footing. A number of solutions have been reported in the literature for the horizontal stiffness of a square or circular surface foundation on an elastic half space (Wong and Luco, 1978; Dominguez, 1978; Dobry and Gazetas, 1986; Pais and Kausel, 1988, Wolf, 1988). Dobry and Gazetas provide expressions for the stiffness of a surface footing having an arbitrary shape. Solutions for determination of the horizontal stiffness and radiation damping of embedded spread footings of various shapes in linear soils have been provided by several authors (Johnson et al., 1975; Kausel and Roesset, 1975; Gazetas and Tassoulas, 1987a,b; Pais and Kausel, 1988; Wolf, 1988; Gazetas, 1991b). Dynamic experimental investigations of the lateral response of an embedded foundation have also been reported (Stokoe and Richart, 1974; Crouse et al., 1985, 1990; Gazetas and Stokoe, 1991). Gazetas and Tassoulas (1987a, b) discuss the effect of embedment on the lateral impedance of a footing of arbitrary shape. The main consequences of embedding a footing are to increase its resonance frequency and decrease the amplification at resonance. This points out to increases in both the stiffness and the damping of the embedded foundation as compared with the same foundation placed on the surface of the medium. Placing the foundation at the bottom of an excavation without contact between the foundation walls and the surrounding soil typically results in a moderate increase in stiffness and little or no effect on damping. This “trench” effect results from the different boundary conditions when the footing is on the bottom of the trench instead of the surface of the medium. Contact between foundation sidewalls and soil results in a further increase in stiffness and a drastic increase in radiation damping. This “side-wall” effect on stiffness and damping is very sensitive to how good the contact is and how much wall area is in actual contact with the soil. Gazetas and Tassoulas (1987a) have suggested an expression for the lateral static stiffness of an embedded footing of the form:

$$K_h = K_{sur} I_{tre} I_{wall} \quad (2-1)$$

thus explicitly separating the trench (I_{tre}) and the side-wall (I_{wall}) contributions. In this expression, K_{sur} is the lateral static stiffness of an equivalent surface footing. Typically,

the dimensionless factor I_{wall} is much larger than I_{tre} . The dynamic stiffness is $K_{\text{hd}} = \chi_1 K_{\text{h}}$, where the dimensionless coefficient χ_1 is a function of the excitation frequency and of the geometry and embedment characteristics of the foundation. Gazetas and Tassoulas (1987a) have provided parametric charts for obtaining the value of χ_1 under different conditions. For the low frequencies typically of interest in seismic design, generally $\chi_1 \approx 1$ can be used. Pais and Kausel (1988) have also provided very simple approximate expressions for the increase in static horizontal stiffness of circular, square, and rectangular foundations due to embedment in an elastic half-space. They have expressed the embedded lateral stiffness (K_{h}) as a product of the corresponding surface foundation stiffness of the same base shape and area (K_{sur}) times a factor that increases with embedment depth.

2.2.2 State of Practice

Lam et al. (1991) reviewed the current *state of practice* for analysis and evaluation of the lateral response of a cap-alone or of an embedded footing, for highway bridge foundations. They present a method for solutions of stiffness of an embedded rectangular footing. This method determines the stiffness contribution of the base of the footing by using the radius of an equivalent circular footing in conjunction with stiffness equations for a rigid circular footing embedded in a semi-infinite elastic half space. The detailed procedure and corresponding equations are given by Lam, et al. (1991). This procedure gives the lateral stiffness contribution of the base as a horizontal spring located at the base of the cap. The additional contribution to the lateral stiffness of the embedded footing due to the passive pressure on the vertical face of the footing is determined based on Wilson's (1988) recommendations for abutment wall-backfill stiffness. Lam and Martin (1991) note that the contributions to lateral stiffness arising from soil resistance on the passive side of the cap, and from shear at the base of the cap, can be significant compared to the contribution of the piles.

2.3 LATERAL RESPONSE OF SINGLE PILES

2.3.1 State of the Art

The lateral response of a pile involves the assessment of stiffness, damping and capacity of the pile. Gazetas (1991a), Whitman and Dobry (1993) and Martin and Lam (1995) summarize the *state of the art* for evaluation of lateral-rocking stiffness and damping of single piles and pile groups with emphasis on seismic response. For piles, horizontal translation and rocking are strongly coupled, which makes it necessary to consider them together. For a single linear pile in linear soil, the dynamic harmonic force Q and moment T can be expressed as:

$$Q = (K_h u + C_h \dot{u}) + (K_{hr} q + C_{hr} \dot{q}) \quad (2-2)$$

$$T = (K_{hr} u + C_{hr} \dot{u}) + (K_r q + C_r \dot{q})$$

where u , q are horizontal displacement and rotation; K_h , C_h are the horizontal spring and dashpot; K_r , C_r are the rocking spring and dashpot; and K_{hr} , C_{hr} correspond to coupled horizontal and rocking spring and dashpot. All these springs and dashpots are functions of excitation frequency. Results for the static stiffnesses K_{ho} , K_{ro} , and K_{hro} and the dynamic impedance functions have been presented for a single floating pile by Kuhlemyer (1979), Poulos and Davis (1980), Dobry et al. (1982), Nogami (1987), Banerjee and Sen (1987), and Nogami et al. (1992). The following trends have been observed: (a) for a given pile/soil ratio of Young's moduli, E_p/E_s , and an aspect ratio, L/d , the static stiffness K_{ho} is proportional to $E_s d$, K_{ro} is proportional to $E_s d^3$, and K_{hro} is proportional to $E_s d^2$; and (b) for long piles, stiffness depends only on the ratio E_p/E_s . Plots for dynamic springs and dashpots versus frequency for the horizontal rocking case show that the results are generally insensitive to variation in the soil Poisson's ratio and of the pile/soil density ratio. Dobry et al. (1982) and Gazetas (1991a) have shown that the dynamic spring constants K_h , K_r , and K_{hr} , do not vary much with frequency, and thus the use of their static values constitutes a good approximation. The corresponding equivalent radiation dashpots C_h , C_r , and C_{hr} , can also be considered as constants in the low frequency range. For piles embedded in a soil with a material damping ratio β , the equivalent horizontal, rocking and coupled dashpots at top of the pile must be corrected

to incorporate the contribution of β . The effect of β on equivalent stiffness is small and can generally be neglected. The correspondence principle can be used to obtain the modified dashpots (Whitman and Dobry, 1993).

A convenient approximate way to analyze the lateral response of piles is to replace the soil by a bed of linear or nonlinear horizontal soil springs. In the literature, the nonlinear springs are often referred to as “p-y curves” (Reese et al., 1974; Martin and Lam, 1995).

2.3.2 State of Practice – Bridge Structures

The *state of practice* for calculating the ultimate lateral capacity of pile foundations recognizes that capacity depends on the characteristics of both pile and soil. Pile analysis typically involves the use of a set of p-y curves along the entire length of the pile, which includes formulation of an ultimate resistance, P_u , of the soil at that elevation expressed in force per unit length of pile. The Applied Technology Council (ATC) Seismic Design Guidelines for Highway Bridges (1986) indicates that the P_u for lateral loading is reached for a pile deflection, Y_u , of about $3d/80$, where d is the pile diameter in inches. Lam and Martin (1986) state that for sand, the P_u can be developed, in concept, based on either failure of an assumed soil wedge around the upper portion of the pile or a horizontal plane strain plastic flow around the pile. They provide charts and formulas to calculate P_u .

Lam and Martin (1986) describe a procedure to evaluate the load-deformation characteristics of a single pile under lateral and axial loading conditions. They also suggest a method to develop an equivalent pile-head stiffness matrix based on the load-deformation characteristics. Due to strong cross coupling between the shear and bending moment in the pile, a careful examination of the pile-head rotational constraint is needed to evaluate lateral stiffness, as well as bending moment and stress distributions along the pile. Lam and Martin (1991) provide design charts, which give the pile-head stiffness coefficients for a combination of the pile bending stiffness, $E_p I_p$ and the rate of increase of the soil reaction modulus with depth, f . The lateral pile-head stiffness obtained by this method compares favorably with California Department of Transportation (CALTRANS,

1989) practice. They also give a method to calculate axial stiffness. For pile groups, the translational and cross-coupling stiffnesses are obtained merely by multiplying the corresponding stiffness components of an individual pile by the number of piles. However, the rotational stiffness terms require consideration of an additional stiffness component due to pile-group interaction.

2.3.3 Full Scale Field Tests

Full-scale lateral loading tests on pile foundations in sandy soils have been reported extensively (McNulty, 1956; Cox et al., 1974; Reese et al., 1974; Abcarius, 1991). McNulty (1956) suggested values for safe allowable lateral capacities of typical piles in typical soils based on field experiments. Cox et al. (1974) and Reese et al. (1974) presented pioneering research work in understanding the lateral response of piles in sand, based on full-scale tests in Mustang Island, near Corpus Christi in Texas. They developed several guidelines for determination of the lateral response of piles in sand. Based on these recommendations, Reese and Wang (1993) developed the computer program LPILE, currently commercially available, for determining the lateral response of pile foundations.

Abcarius (1991) performed a full-scale lateral load test on a group of driven piles in a typical highway bridge footing at the Cypress Street viaduct in Oakland, California. He found that the lateral capacity at $\frac{1}{4}$ in (0.635-cm) deflection greatly exceeds the CALTRANS Bridge Design Aids (1989) criteria, and he suggested modifications in the code.

2.3.4 Centrifuge Model Tests

Several authors have reported lateral loading tests on model piles in the centrifuge. Scott (1979) performed lateral loading centrifuge experiments on an instrumented pile model placed in medium-dense saturated sand, to approximately simulate the full scale Mustang Island tests reported by Cox et al. (1974) and Reese et al. (1974). Scott recommended that the results of centrifuge tests on laterally loaded piles could be used to check analytical and empirical procedures for determining pile-soil stiffness and load capacities. Barton and Pande (1982) also modeled the Mustang Island tests and developed finite element

methods for modeling pile behavior. Oldham (1985) reported centrifuge lateral loading tests on single piles in sand, in which the model pile was driven “in flight.” Barton (1984) conducted lateral loading experiments on pile groups in sand and found that soil non-linearity strongly affects the strain field around a laterally loaded pile. Terashi et al. (1991) studied the influence of slope on the lateral resistance of long piles in sand using a series of geotechnical centrifuge model tests. Dickin and Wei (1991) investigated the moment carrying capacity of short piles in sand using centrifuge-modeling techniques. Bouafia and Garnier (1991) performed an experimental study to determine p-y curves for piles in sand. They found that the soil stiffness values backfigured from the tests, were several times smaller than those recommended in usual methods based on density index and angle of shearing resistance. McVay et al. (1995) presented results of centrifuge tests to evaluate the lateral response of three-row pile-groups in loose to dense sands. Dobry et al. (1995) presented results of centrifuge tests to study the response of pile foundations in liquefying sand.

2.4 LATERAL RESPONSE OF PILE-CAP FOUNDATION SYSTEMS

2.4.1 State of the Art

Static and dynamic pile-pile cap interactions have been studied by looking first at single pile-cap systems similar to that shown in figure 2-1, but with a surface rather than an embedded cap. Poulos and Davis (1980) proposed the use of interaction factors derived from studies of such single pile-cap configurations, for approximate evaluation of vertical and horizontal static springs of larger pile group-cap systems. Using the finite element method, Nasim and O'Rourke (1987) investigated the static and dynamic lateral impedance of such pile-cap foundations. For the cases studied, the static lateral stiffness was found to be dominated by cap-soil rather than pile-soil interaction. The radiation damping for a contact pile foundation was found to be somewhat higher than the sum of the damping for the cap and the pile acting alone. In general, the pile's contribution to the overall radiation damping was found to be significant.

2.4.2 State of Practice

Pile foundations are typically installed in a group of piles under a cap. The current *state of practice* for determining the lateral stiffness of such foundations in highway bridge design involves the use of the following simplified procedure (Lam et. al., 1991):

1. Solve for the stiffness matrix at the top of a single pile under lateral loading.
2. Obtain the stiffness matrix at the top of the single pile under axial loading.
3. Superimpose the stiffness of the individual piles to obtain the pile-group stiffness.
4. Determine the stiffness contribution of the cap.
5. Superimpose the stiffness of the cap to that of the pile group.

Interaction between the piles and the cap, and the pile-group effect, are neglected in this method.

2.5 LATERAL RESPONSE OF BRIDGE ABUTMENTS

2.5.1 State of the Art

The lateral response of abutments has been studied through theoretical models, small-amplitude field vibration tests, centrifuge tests, and analyses of recorded motions of actual bridges during earthquakes. Schematic of a typical seat-type bridge abutment is shown in figure 2-2. Wilson (1988), Levine and Scott (1989), and Wilson and Tan (1990) proposed theoretical models for determining abutment stiffness based on the soil properties and abutment dimensions. However, these models do not include the significant effects of nonlinear soil behavior (Siddharthan et al., 1995). Several researchers have attempted to determine abutment stiffness and/or vibration properties from field vibration tests on highway bridges (Crouse et al., 1987; Gates and Smith, 1982; Douglas et al., 1990; Ventura et al., 1995). However, such small amplitude tests lead to results that are not useful in design for intense earthquake motions, because the stiffness of abutment depends on level of shaking. Recognizing this limitation of small-amplitude tests, several investigations to estimate abutment stiffness from motions of bridges recorded during earthquakes have been reported (Maroney et al., 1990, McCallen and Romstad, 1994; Werner et al., 1994; Goel and Chopra, 1997). Hushmand et al. (1986) presented results of centrifuge testing of a bridge-soil model in sand. They also predicted their results with numerical analysis. Maroney et al. (1994) describe the results

of a half scale load test on a monolithic abutment tested to failure. Sweet and Morill (1993) presented the nonlinear finite element analyses of abutment-soil systems.

2.5.2 State of Practice

Most specifications and guidelines for earthquake design of highway bridges require that the abutment-soil system be included in the analytical model as discrete equivalent linear springs (CALTRANS, 1988 and 1989; ATC-6, 1981; AASHTO-83, 1988). In design applications, stiffness values of these springs are usually determined based either on simplified rules and an iterative process, or from abutment capacity and expected deformation during the earthquake. It is not entirely clear how well the stiffness value thus determined represents the complex behavior of the abutment-soil system, which is influenced by soil-structure interaction and nonlinear behavior of the soil. Martin et al. (1996) developed improved modeling procedures to simulate abutment stiffness, passive capacity and damping characteristics for use in seismic response analysis of bridge structures.

2.6 GEOTECHNICAL CENTRIFUGE MODELING

2.6.1 General

Centrifuge geotechnical testing of small-scale models of soil and soil-structure systems is a useful means of studying a wide range of problems in geotechnical engineering. The centrifuge permits cost effective experimental investigations of phenomena of concern in large-scale civil engineering projects. Dynamic centrifuge testing of soil models can be an effective way for studying basic soil behavior in response to static and dynamic loading. Through proper application of scaling laws, measurements of model soil stresses, strains, and pore pressures can be related to the response of full-scale soil structures. Table 2-1 shows a partial list of the scaling relations that are often used for centrifuge modeling. Highly controlled nature of centrifuge experiments permits calibration of numerical analysis codes.

TABLE 2-1: Partial list of scaling relations for centrifuge modeling.

Parameter	Model Units	Prototype Units
Length	$1/n$	1
Area	$1/n^2$	1
Moment of Inertia	$1/n^4$	1
Stress	1	1
Strain	1	1
Time (dynamic)	$1/n$	1
Frequency	n	1
Elastic Modulus, E	1	1
Flexural Rigidity, EI	$1/n^4$	1

In recent years, the field of geotechnical centrifuge modeling has experienced tremendous growth and has attained wide acceptance as a viable method of testing scaled models of geotechnical structures for which gravity effects are important. Several new centrifuge facilities are being built. For the research presented in this thesis, the medium size geotechnical centrifuge facility at Rensselaer Polytechnic Institute (RPI) in Troy, NY was used. The following subsection gives a brief description of this facility.

2.6.2 RPI Geotechnical Centrifuge

The 100 g-ton RPI centrifuge was manufactured by Acutronic, France, according to RPI specifications, and it became the first Acutronic Model 665-1. The centrifuge is located on the first floor of the Jonsson Engineering Center on the RPI campus, and is integrated with the Class of 1933 Earthquake Engineering and Cyclic Loading Soils Laboratory (figure 2-3). The enclosure containing the machine is connected to the model preparation room and the control room through a tunnel, which makes the access to the machine very convenient. This arrangement also facilitates the interaction between the centrifuge and the rest of the experimental facilities. Three closed-circuit television cameras and attached monitors provide view of the centrifuge, plan view of the model, and side view of the soil model, during operation.

A sketch of the centrifuge is shown in figure 2-4. It has a radius (to the platform) of 3.0 m, and usable payload dimensions of 100 cm in depth by 80 cm in both width and height. The performance of a centrifuge is generally limited by three factors: the maximum motor rotation speed, the maximum effective payload mass, and the tolerable structure stresses. The performance envelope of Model 665-1, which is depicted in figure 2-5, is defined on the basis of these three factors. The machine can be operated safely within the three boundaries of this envelope. The centrifuge is equipped with 64 sliprings, of which 50 are for analog signals, 12 for power supplies and 2 for video signals. A hydraulic rotary joint with 6 passages is installed, with two of them rated for a pressure of 3000-psi (20.7 MPa).

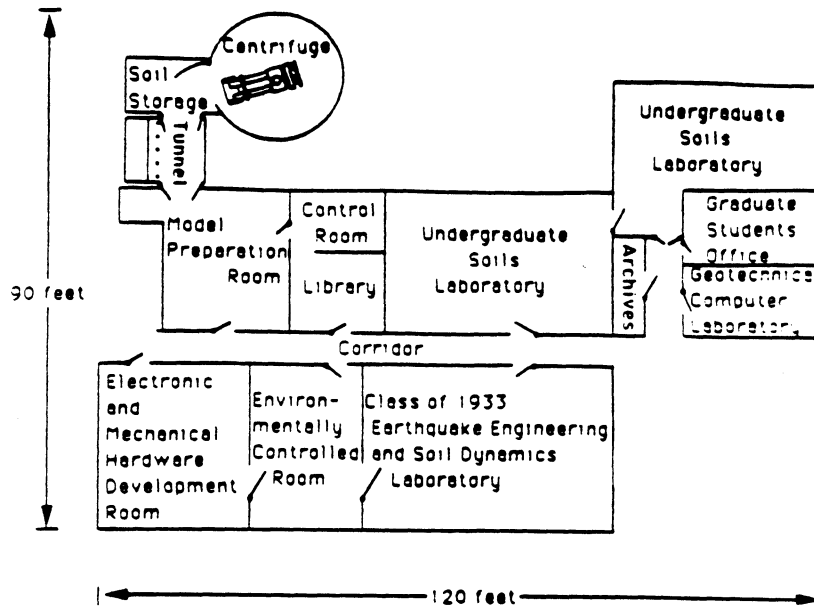


FIGURE 2-3: Plan view of RPI geotechnical facilities (after Elgamal et al., 1991)

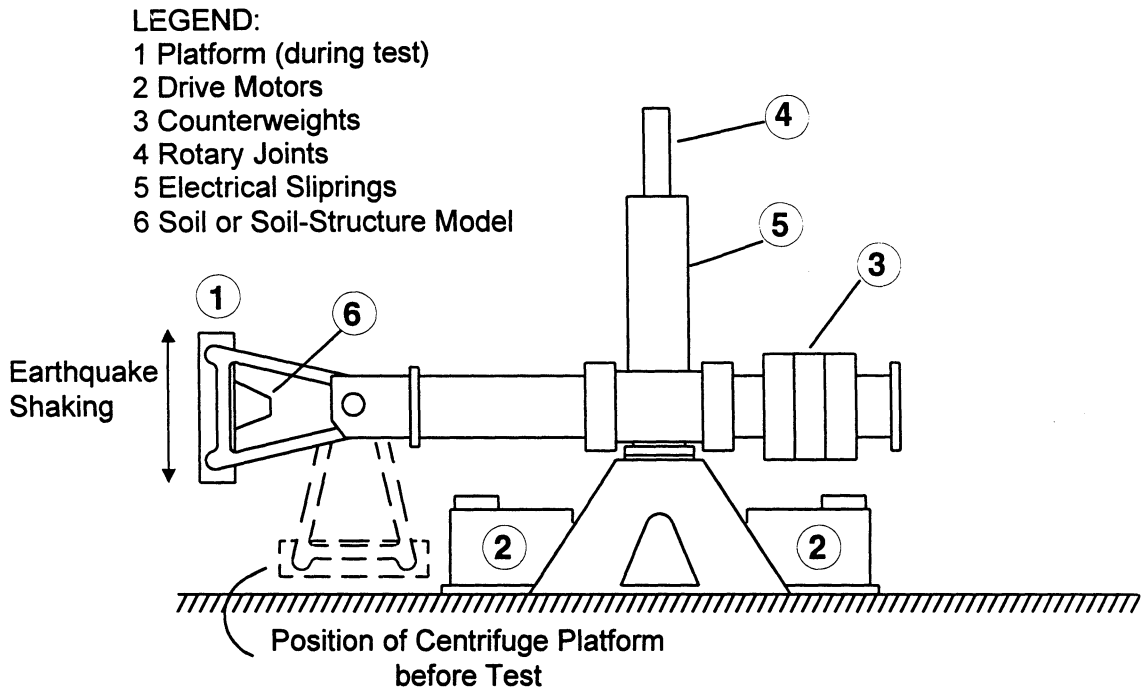


FIGURE 2-4: Schematic of RPI geotechnical centrifuge (after Van Laak, 1996).

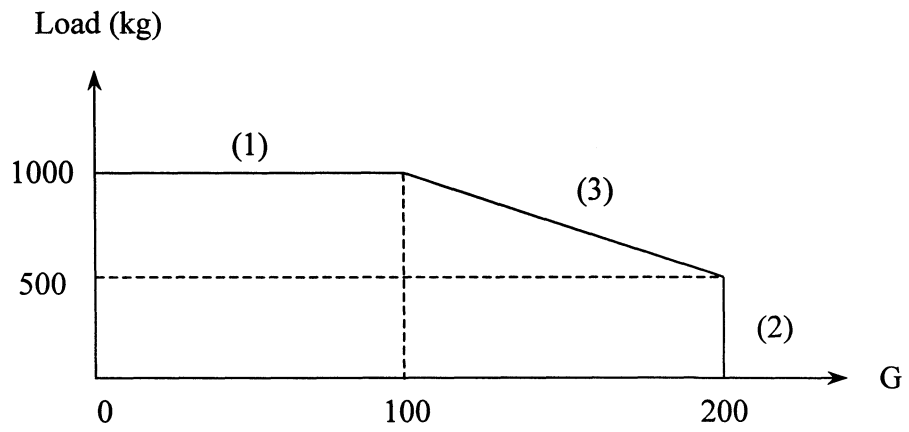


FIGURE 2-5: Performance envelope for RPI centrifuge (after Elgamal et al., 1996).

Other specifications of the centrifuge include a 50 KN maximum acceptable imbalance, a 3-minute run up and down time for 0-100 g and an in-flight automatic balancing system. More details of the features of the Model 665-1 centrifuge may be found in Elgamal et al. (1991) and Van Laak (1996).

2.7 NUMERICAL MODELING OF GEOTECHNICAL PROBLEMS

Due to the advent of computer technology, numerical modeling of complex geotechnical problems has become a common occurrence in recent years. Both linear elastic and nonlinear constitutive models for soils are prevalent. For very small strains, linear elastic models are adequate for modeling the behavior of the soil. These models are simple to implement numerically, and require limited computational effort. For problems involving large strains, simple linear models may not be able to predict the behavior of foundations and structural systems involving soils accurately, due to the highly nonlinear nature of the stress-strain relations for soils. More complex constitutive equations are needed to model the behavior of soils at large strains. Saada (1988) presented a compilation of different constitutive models developed for granular non-cohesive soils.

Several authors have reported elastic finite element analyses of laterally loaded foundations (Kuhlemeyer, 1979; Gazetas and Tassoulas, 1987a, b; Nasim and O'Rourke, 1987). Although simple in implementation, elastic analyses do not capture the nonlinearity inherent in the problem. Kooijman (1989) used an elastoplastic quasi three-dimensional model for laterally loaded piles, and compared the results with field tests. Brown and Shie (1990) presented three-dimensional finite element analyses of laterally loaded piles using two different types of plasticity models for the soil.

Computer programs such as LPILE (Reese and Wang, 1993) use finite difference techniques and p-y soil springs to include pile-soil interaction into the analysis.

Martin and Lam (1995) present a comprehensive review of the *state of the art* of both sophisticated and simple analyses of seismic response of pile foundations with emphasis on seismic response of bridges.

2.8 SUMMARY

The lateral response of a pile-cap foundation system with an embedded cap includes contributions from both the pile and cap. Comprehensive research has been done to evaluate the initial stiffness and damping of laterally loaded footings and piles, using elastic theory. The lateral response of piles has also been studied, at both small and large displacements, through large-scale field tests and centrifuge tests. Much less is known about the combined response of a pile and an embedded cap in a pile-cap foundation system.

Current *state of practice* for highway bridge design advocates the use of the available information coupled with some simplified assumptions, to evaluate the lateral response of pile-cap systems. Simplified design approaches to the soil-pile-structure interaction problem, considering primarily a Winkler spring approach to inertial interaction are also available. The lateral response of abutments has been studied through theoretical models, small-amplitude field vibration tests, centrifuge tests, and analyses of recorded motions of actual bridges during earthquakes. In the current *state of practice*, the lateral stiffness is determined based either on simplified rules and an iterative process, or from abutment capacity and expected deformation during the earthquake.

Centrifuge testing coupled with numerical analysis is a very efficient tool to study the lateral response of foundations and abutments.

SECTION 3

TESTING PROGRAM FOR PILE-CAP FOUNDATION SYSTEM: SCOPE AND IMPLEMENTATION

3.1 INTRODUCTION

A centrifuge model testing program was conducted to study the cyclic lateral response of pile-cap foundation systems and seat-type bridge abutments in new highway bridge constructions. The scope and specific objectives, as well as general techniques used for the centrifuge tests on pile-cap system models are discussed in this section. Sections 4, 5 and 6 give thorough descriptions of the centrifuge tests on cap-alone, single pile and pile-cap system, respectively, and discuss the corresponding test results. The scope and implementation techniques for the centrifuge tests on seat-type abutments, as well as results of these tests, are discussed separately in Section 9. Dry Nevada sand of 75 % relative density was used in all centrifuge experiments. The properties of this sand are given in this section. Descriptions of the miniature models of the cap, pile and pile-cap system, and of the model container used in the centrifuge tests are provided. The lateral loading assembly utilized in the centrifuge tests is also described. The same assembly was used in all centrifuge tests on pile-cap system and abutment models. The lateral displacement cycles applied to the models of pile-cap system are described, and general description of model preparation and testing techniques is also given.

3.2 SCOPE

The centrifuge testing program on pile-cap foundation system addressed the stiffness and material damping of the foundation at various displacement levels, as well as its ultimate capacity. As the lateral load was applied slowly, no inertia forces were generated, and thus the radiation-damping component of the lateral response was not studied in this research. A schematic of the typical pile-cap system studied in this research, including a single pile with a pile-cap fully embedded in soil, is shown in figure 3-1. The goal of the centrifuge-model testing program was to understand the role of the embedded cap and the pile in the total lateral stiffness, material damping and capacity of the pile-cap foundation

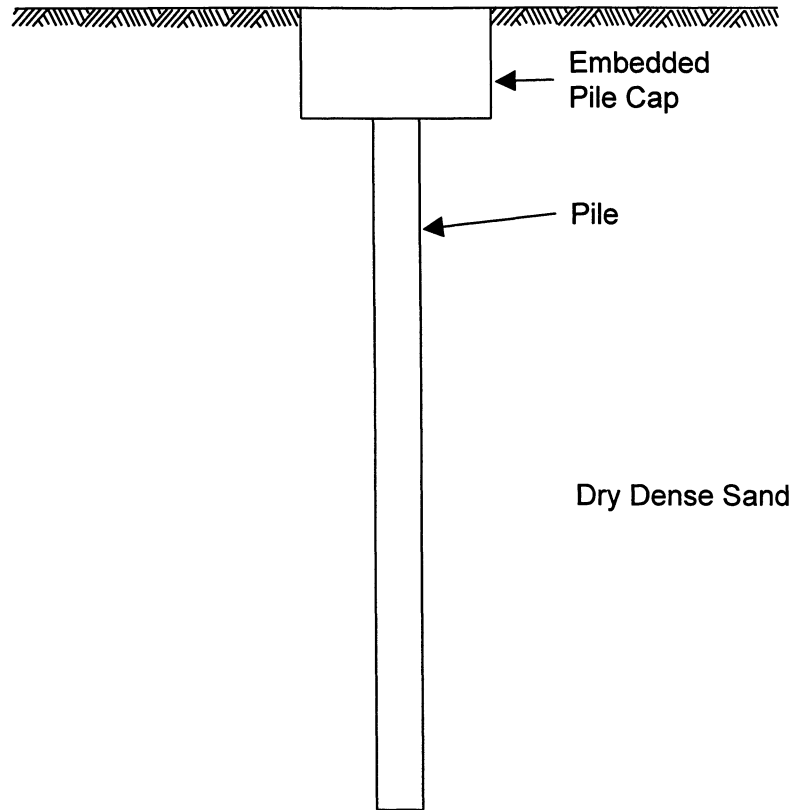


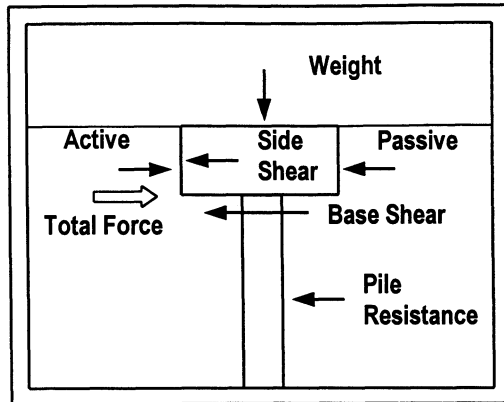
FIGURE 3-1: Pile foundation with embedded cap

system in typical highway structures. Specifically, can addition rules, where the stiffness, material damping, and capacity of the piles and cap are separately evaluated and then added, be used to represent the response of the pile-cap foundation system?

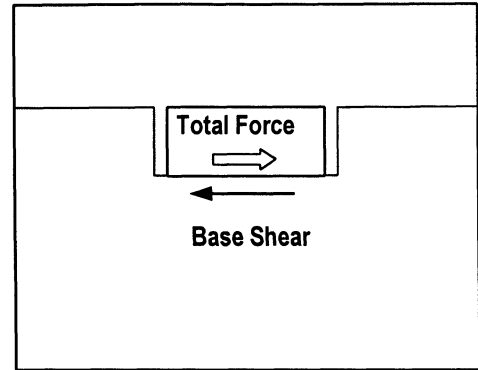
The different factors contributing towards the lateral response of the idealized pile-cap system of figure 3-1 are shown in figure 3-2. While the total lateral response has contributions from both the pile and cap, the contribution of the cap can be further subdivided into contributions due to the base shear, soil active/passive resistances from two sides, and side-shear from the other two sides. The weight of the foundation also has an effect on the lateral response of the system. Centrifuge tests were performed on the model of the embedded footing/pile-cap to evaluate the relative contributions of the base, shearing sides, and active/passive sides of the cap to the total lateral response, as well as to study any possible interaction between these partial contributions.

The cyclic lateral loading tests conducted in the centrifuge on small-scale models of various components of the pile-cap foundation system are listed in table 3-1. All tests were performed at 30-g centrifugal acceleration. Therefore, all model dimensions, measured displacements, and times were multiplied by 30 to obtain the corresponding prototype values; while the forces in the model were multiplied by $(30)^2 = 900$. Also, these tests were conducted relatively slowly, with an actual duration of each load cycle of about 2 seconds or about 60 seconds in prototype time. That is, the strain rate was slow, and no significant inertia forces were generated in the system.

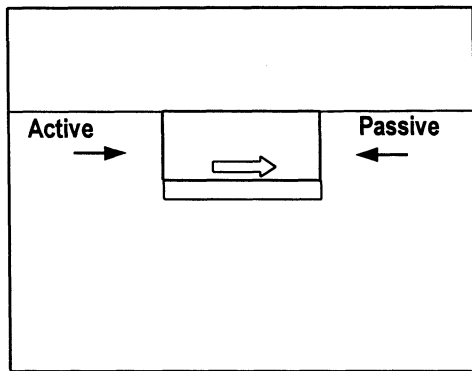
The objective of this research was to isolate the contribution of different factors towards the total lateral response of the pile-cap foundation system, and to study any interaction between these contributions. In order to accomplish this goal, cyclic lateral loading tests were performed on scaled models of the cap-alone, pile-alone, and pile-cap system in centrifuge. The tests on the embedded footing/cap-alone were extended to study the interaction between the base, shearing sides, and active/passive sides. Centrifuge tests were also performed on models of the free-head pile-alone and of the entire pile-cap system. The test on the free-head pile was utilized to evaluate the p-y characteristics of



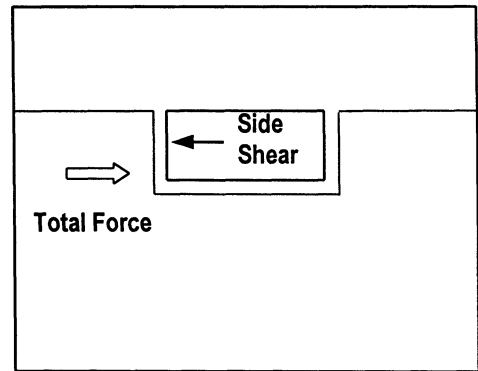
(a)



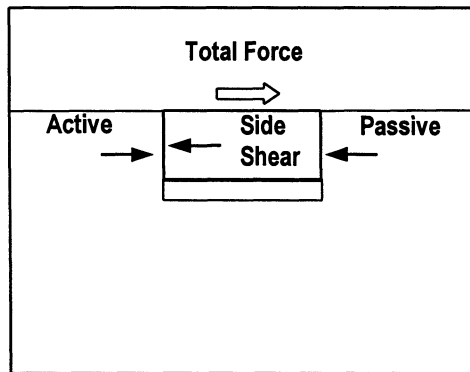
(b)



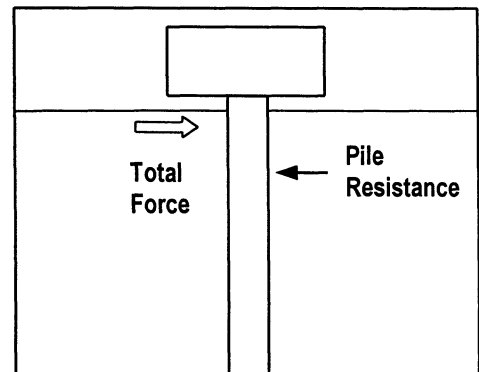
(c)



(d)



(e)



(f)

FIGURE 3-2: Isolation of forces contributing to lateral response of pile-cap system.

TABLE 3-1: Centrifuge tests performed on pile-cap system.

Test Code	Pile Contribution	Cap Contribution			Vertical Load at the base* (KN)	Remarks
		Base Friction	Side wall Shear	Passive/active Force		
CB	NO	YES	NO	NO	53	
CBL	NO	YES	NO	NO	108	
CS	NO	NO	YES	NO	53	
CP	NO	NO	NO	YES	53	
CSP	NO	NO	YES	YES	53	
CBSP	NO	YES	YES	YES	53	
CBSPL	NO	YES	YES	YES	108	
PI	YES	NO	NO	NO	-	Free-head, Instrumented pile
PCBSP	YES	YES	YES	YES	53	
PCBSPI	YES	YES	YES	YES	53	Instrumented pile

*This includes the cap's self weight and any additional static vertical load applied to the cap.

TABLE 3-2: Parameters considered for centrifuge model experiments.

Parameter	Model at 30g	Prototype
Material for cap	Aluminum with sand glued to sides	Rigid Reinforced Concrete cap
Dimensions of the cap	38 mm x 38 mm x 28 mm	1.14 m x 1.14 m x 0.84 m
Material for pile	Aluminum Pipe	Typical Highway Cast-In-Drilled-Hole (CIDH) pile
External Diameter of pile	12.7 mm	38.1 cm
Flexural Rigidity (EI)	$3.73 \times 10^5 \text{ N-cm}^2$	$3.23 \times 10^{11} \text{ N-cm}^2$
Effective Length	19 cm	571.5 cm
Length/Diameter	15	15
Ultimate Lateral Resistance of single pile	200 N/pile (Estimated)	180 KN/pile (Recommended)

the soil. Results from all experiments were used to study the interaction between the different contributing factors to the lateral response of the entire pile-cap system.

The nomenclature of the centrifuge tests listed in table 3-1 is characteristic of the components contributing towards the lateral response in that test. The letters “C” and “P” at the beginning of the test code indicate the presence of the cap/footing and the pile in that test, respectively. The letters “B,” “S,” and “P” are appended to the codes of the centrifuge tests with cap model to indicate that the contributions of the base, shearing sides, and active/passive sides of the cap, respectively, were measured in that test. The letter “L” is added to connote the presence of an additional vertical static load applied to the foundation. The letter “I” is added to the test code when the pile is instrumented. For example, Test CBSPL was performed on a model of the cap-alone (embedded footing), with its base and all sides in contact with the soil, and with a vertical static load in addition to the self weight of the cap being applied; while Test PCBSPI was performed on the entire pile-cap system including an instrumented pile.

The various experiments listed in table 3-1 are shown schematically in figure 3-2. In the setup of figure 3-2a, the entire pile-cap foundation system is in contact with the soil (Test PCBSP). Figure 3-2b shows a case, where there is no pile and only the base of the cap is in contact with the soil (Test CB). In the setup shown in figure 3-2c, only the active/passive sides of the cap are in contact with the soil (Test CP). In figure 3-2d, the test setup has only the shearing sides in contact with the soil (Test CS). Figure 3-2e shows a configuration, where both the shearing and the active/passive sides of the cap are in contact with the soil (Test CSP). In figure 3-2f, only the pile resistance is measured (Test PI). In order to isolate the contribution of any component towards the lateral response of the system, contributions from the remaining factors are eliminated, keeping only the component of interest activated. It should be noted that in Tests PCBSP and PCBSPI on the pile-cap system the pile was rigidly clamped to the cap, and hence could rotate only together with the cap, while Test PI was performed on a free-head pile model.

3.3 SOIL USED

The focus of the testing program was to study the lateral response of pile-cap foundation systems for new highway structures constructed in dry sand. In new constructions, foundation soil (sand) is usually compacted. Hence, it was decided to use sand with high relative density in the centrifuge experiments. In all centrifuge tests, dry Nevada No. 120 sand with relative density of about 75% was used. The specific gravity and maximum and minimum void ratios for this sand, which were supplied by Arulmoli et al. (1992), are $G_s = 2.68$, $e_{max} = 0.894$, and $e_{min} = 0.516$, respectively. At 75% relative density, the void ratio $e = 0.605$ and the unit weight of the sand is about 16.2 KN/m^3 . The grain size distribution curve for the sand, also supplied by Arulmoli et al (1992) is shown in figure 3-3. This same sand at 75 % relative density was also used for the centrifuge tests on seat-type bridge abutments described in Section 9.

3.4 MODEL CHARACTERISTICS

Miniature models of a single pile and cap were used in these experiments, so as to simulate realistic prototype pile and cap at 30-g centrifugal acceleration. The parameters considered for the model experiments are listed in table 3-2, in model and corresponding prototype environments. The prototype parameters were obtained by multiplying the values of the parameters in model scale by an appropriate scaling factor from table 2-1. The cap was modeled with an aluminum block of dimensions 38-mm in length (L) by 38-mm in width (W) by 28-mm in height (H), which at 30-g simulates a prototype cap (rigid embedded foundation) of dimension 1.14-m (L) x 1.14-m (W) x 0.84-m (H). Sand was glued to the sides and the base of the model cap to represent a rough concrete surface. The model cap had a vertical hole at the center, of diameter of about 12.7 mm, to receive the rounded end of the loading rod of the lateral loading assembly described later in this section.

In order to model lateral loading of piles in the centrifuge, appropriate scaling of the pile length, diameter and flexural stiffness is required. These parameters are listed in both the model and prototype scales in table 3-2. The model pile was fabricated with an aluminum pipe of outer diameter of 12.7 mm and a wall thickness of 0.9 mm. This corresponds to a

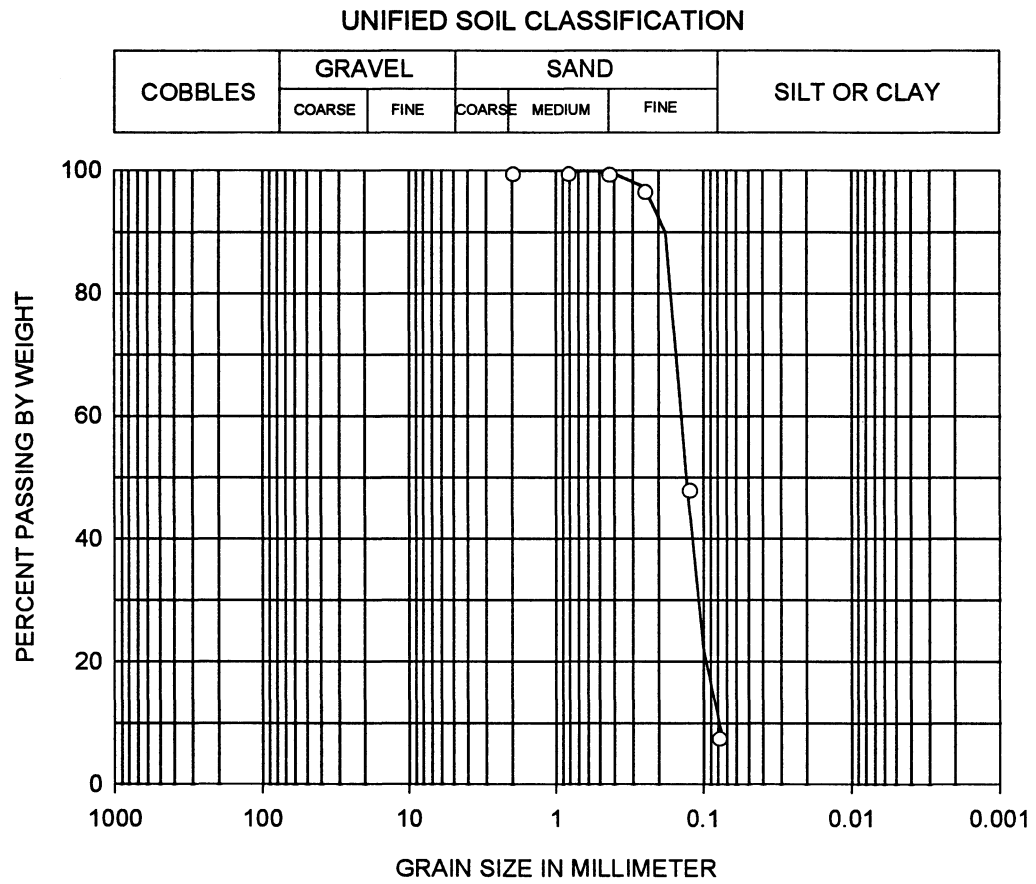


FIGURE 3-3: Grain size distribution for Nevada sand (after Arulmoli et al., 1992).

prototype pile of outer diameter 0.381 m and flexural stiffness 3.23×10^{11} N-cm² at 30-g centrifugal acceleration. For lateral loading, this represents a typical Cast-In-Drilled-Hole (CIDH) highway bridge foundation pile (Abcarius, 1991; Lam et al., 1991). The length of the model pile was about 19 cm, which at 30-g centrifugal acceleration simulates a pile of length 5.715-m. The length - diameter ratio of the pile is about 15. Hence, the pile was a “long pile” for lateral loading, according to criteria given by Poulos and Davis (1980).

A rigid aluminum box of dimensions 914-mm (L) x 610-mm (W) x 356-mm (H) (figure 3-4) was used as the model container in all centrifuge tests. The dimensions of this container are much larger than the model dimensions, which should eliminate any boundary effects in these centrifuge tests. Holes were tapped in the skirt of the model container to receive screws from the housing plate of the lateral loading assembly, described in the following subsection. Holes in the four-corners of the box were used to attach steel cables to the box, to facilitate its transportation with a forklift.

3.5 LATERAL LOADING ASSEMBLY

A displacement-controlled lateral loading assembly was used in the centrifuge experiments on models of pile-cap system (Sections 4, 5 and 6) as well as seat-type bridge abutments (Section 9). This assembly consists of a servo valve (Model 760-100A from Moog Inc.), a hydraulic actuator (Model H-17-DUZ from Bimba Manufacturing Company) and a feedback displacement transducer (LVDT Model MHR 100 from Schaevitz Engineering). The lateral load is measured through a load cell (Model ELF TC 1000-250 from Eltran Devices Inc.). The load from the hydraulic actuator is transmitted to the foundation through a load transfer mechanism consisting of a bearing plate and a loading rod (see figure 3-5). The lateral load applied to the bearing plate is conveyed to the foundation through the rounded end of the loading rod, which acts like a hinge-type connection. Hence, no moment is applied to the foundation. The moment balance is achieved through the vertical forces in the roller bearings. All components of the lateral loading assembly are mounted on a thick housing plate. The housing plate is placed and secured on top of the model container with screws. The entire assembly, mounted on the model container, is shown in figure 3-6.

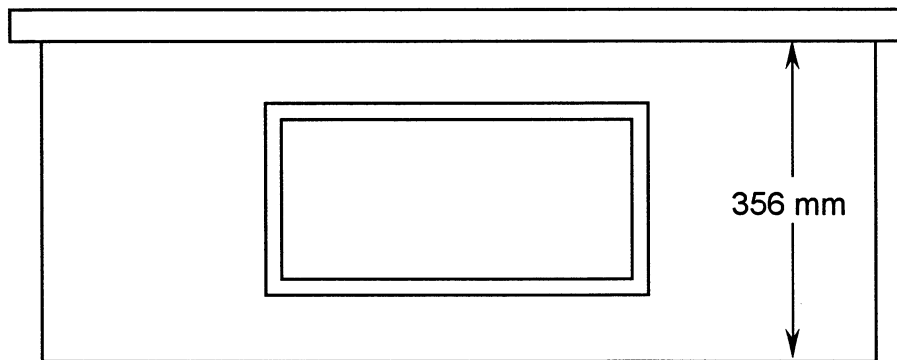
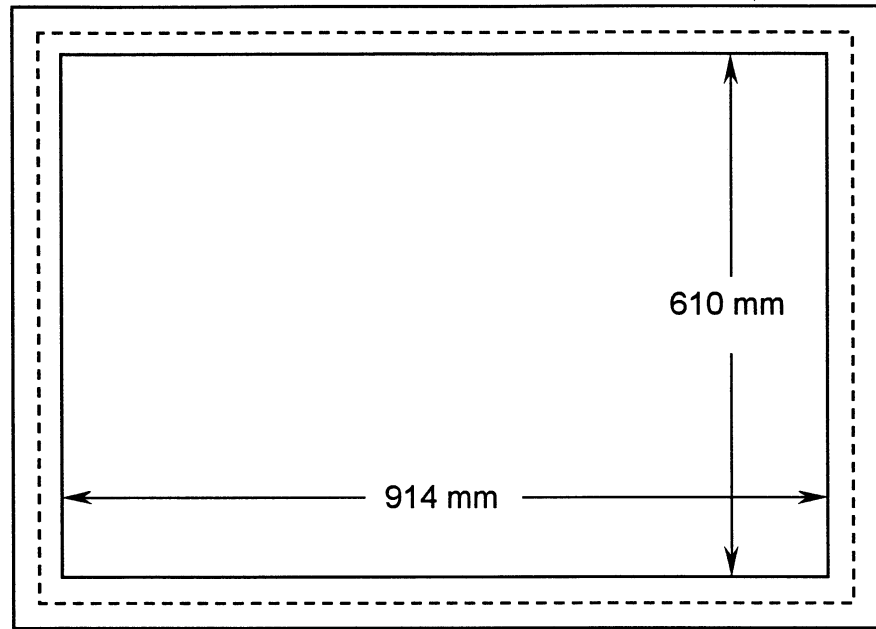


FIGURE 3-4: Model container used for centrifuge tests.

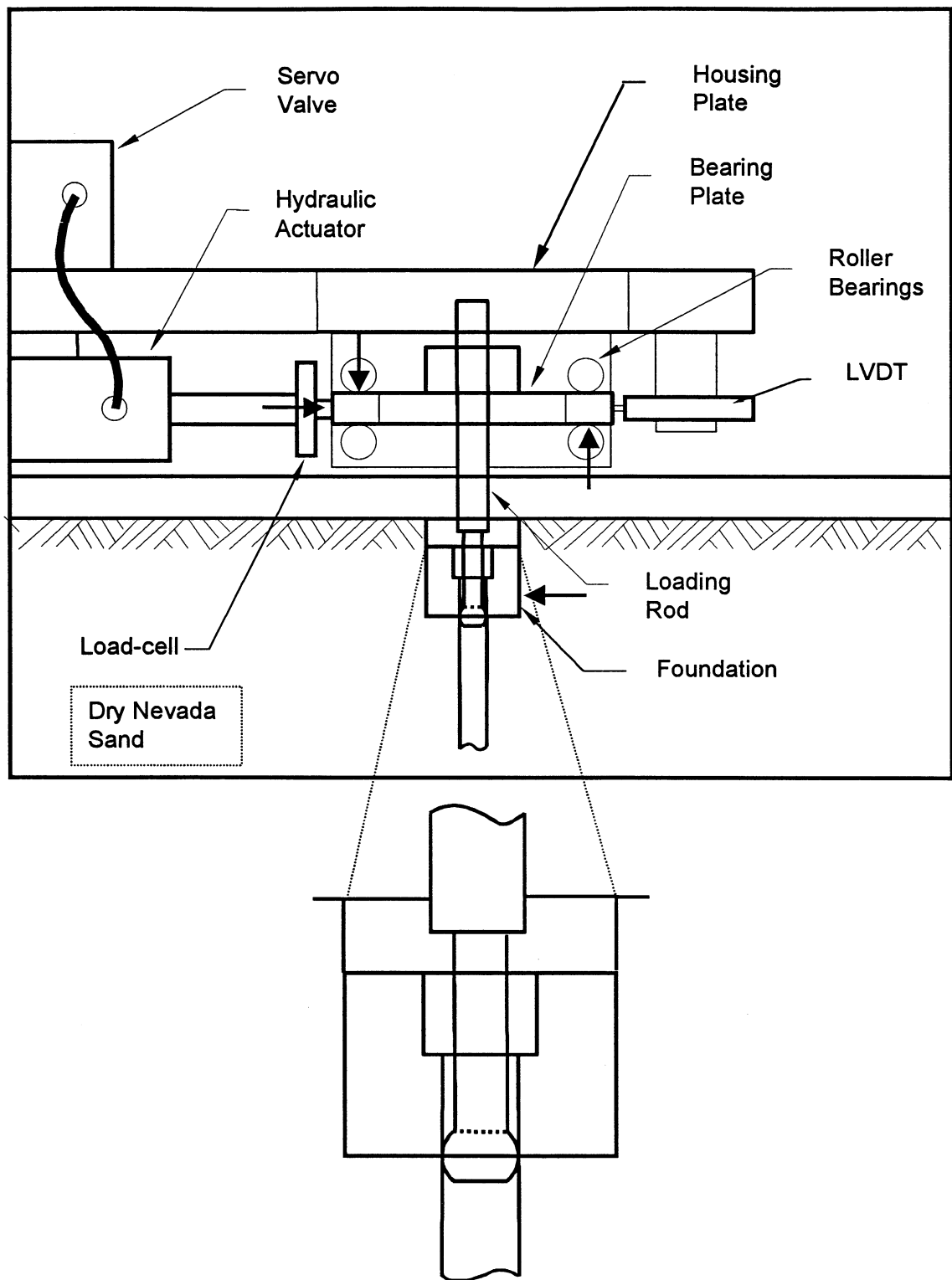


FIGURE 3-5: Load transfer mechanism.

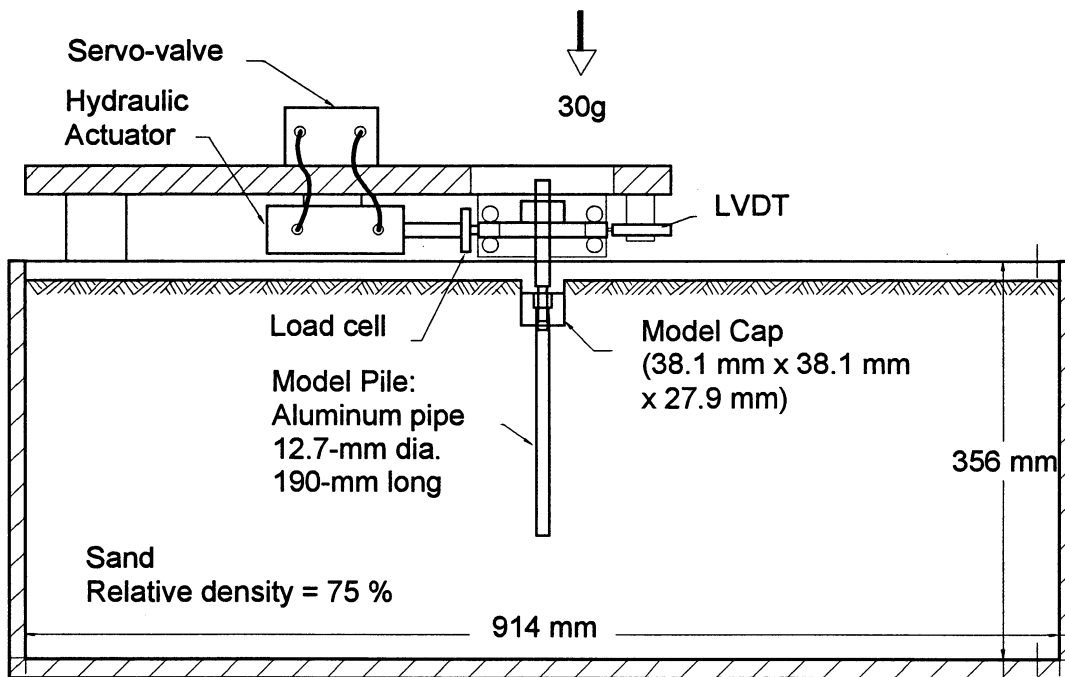


FIGURE 3-6: General setup showing the lateral loading assembly for pile-cap foundation system.

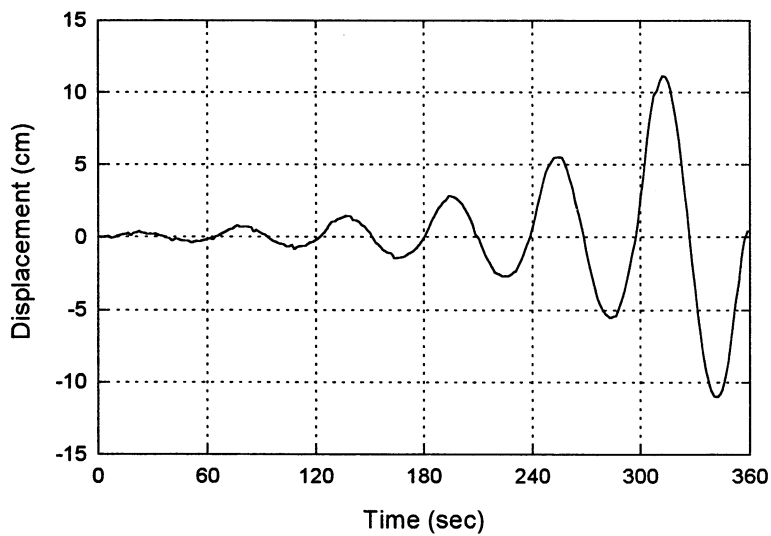


FIGURE 3-7: Applied lateral cyclic displacement time history in prototype scale.

The digital input signal, representing input displacement cycles, is generated on a PC386 computer. It is then converted into an analog signal through the digital I/O board plugged into the computer, and finally sent to the servo-controller on the arm of the centrifuge through electrical sliprings. The servo controller monitors the oil pressure in the hydraulic actuator through the servo valve, depending on the input signal; and the feedback signal is recorded by the displacement transducer. This causes backward or forward lateral movement of the foundation, consistent with the input displacement cycles. The corresponding load is measured through the load cell.

3.6 LATERAL DISPLACEMENT CYCLES

Lateral displacement cycles of increasing amplitude were applied to the model foundation through the servo-controlled lateral loading assembly. The typical applied displacement versus time response is shown in figure 3-7 in the prototype scale. The frequency of the displacement cycles was 0.5 Hz in the model scale, that is 0.0167 Hz (0.1 cycles per second) in the prototype scale at 30-g centrifugal acceleration. The stress-strain behavior of dry cohesionless soils is frequency independent at least for frequencies from zero to a few hundred cycles per second (Dobry et al. 1971). Hence, any dynamic frequency dependent effects during the loading may be neglected, and the loading can be considered as both static and cyclic. Six sinusoidal displacement cycles of increasing amplitude were applied to the foundation, with amplitudes ranging from about 0.28 cm for the first cycle, to about 11 cm for the last cycle, in the prototype scale. This arrangement captured the initial close to linear response, as well as the failure response when the foundation-soil system reached its ultimate lateral capacity. According to Lam et al. (1991), for normal working load levels in highway bridge foundations, the lateral pile-head deflection ranges from 1.3 cm (0.5 in) to 2.5 cm (1 in). The prescribed displacement cycles of figure 3-7 captured the response of the foundation for this displacement range.

3.7 MODEL PREPARATION AND TESTING TECHNIQUE

A similar general procedure was used in all centrifuge experiments for model preparation, with some differences depending on the type of the test. Dry Nevada sand was deposited in layers having a thickness of about 6 cm or less. The amount of sand

needed for each layer to achieve the required relative density of 75 % was weighed, and the sand was placed in the container by dry raining. Once the top surface of the sand deposit was reached at the estimated elevation of the bottom of the model foundation, the model foundation (cap, pile, or pile-cap system) with the loading rod was placed in the box. Sand was then deposited around the model foundation.

Specially designed confining boxes and roller bearings were used to eliminate the contribution of different sides and the base of the cap to the lateral response, and to retain sand above the top rim of the model foundation. This was done to maintain approximately the same state of stresses in the soil around the model in all experiments. A more detailed description of these assemblies can be found in Section 4. Special holding devices (clamps) were designed to keep the pile foundation in an upright position, while sand was being deposited around it, in tests on the free-head pile and the entire pile-cap system. These clamps were removed as soon as the confining pressure of the sand around the pile was enough to retain the pile in the vertical position.

The thick housing plate, bearing the lateral loading assembly, was placed on top of the model container, ensuring that the loading rod was inserted in the central hole of the bearing plate. Specially designed clamps were used to eliminate any model disturbance, and to keep the loading rod vertical during this operation. These clamps were removed as soon as the housing plate was secured to the model container. The loading rod was then clamped to the bearing plate and the model was ready for spinning in the centrifuge.

Due to the massive size and weight of the model including the model container, an electric forklift had to be used to transport it from the model preparation area to the centrifuge basket. Once the model was placed on the centrifuge basket, pneumatic hoses from the servo valve of the lateral loading assembly were connected to the hydraulic input/output valves located on the arm of the centrifuge. All instruments were then connected to appropriate sockets on the data acquisition panel of the centrifuge. The data acquisition computers were turned on. Signal conditioners, amplifiers, and servo-control system on the arm of the centrifuge were powered to warm up the system, and the feed-

back-displacement transducer (LVDT) was adjusted to the mean position. The counterweight of the centrifuge was adjusted to the appropriate position so as to balance the weight of the model container during flight.

The centrifuge was spun to achieve 30-g centrifugal acceleration at the location of the model foundation. The hydraulic pump was started, and the input signal was sent to the servo-control assembly. The lateral displacement cycles were applied to the foundations through the servo-controlled-feed-back system. The load-displacement response was measured through the load-cell and displacement transducer (LVDT). For tests involving piles, the strain-gage response was also recorded during loading.

SECTION 4

CENTRIFUGE TESTS ON EMBEDDED FOOTING (PILE CAP)

4.1 INTRODUCTION

Evaluation of the cyclic lateral response (stiffness, damping and capacity) of an embedded footing is an important problem in geotechnical engineering. In the case of a pile foundation with an embedded cap, the lateral response of the cap, which may be considered as equivalent to an embedded footing, plays an important role in the total response of the entire pile-cap system. A number of solutions have been reported in the literature for the static horizontal stiffness of circular and square surface footings on linear soil (Wong and Luco, 1978; Dominguez, 1978; Dobry and Gazetas, 1986; Pais and Kausel, 1988). Dobry and Gazetas also provide an expression for the stiffness of a surface footing having an arbitrary shape. Solutions for determination of the horizontal stiffness and radiation damping of embedded shallow footings of various shapes in linear soils have also been reported in the literature (Johnson et al., 1975; Kausel and Roesset, 1975; Gazetas and Tassoulas, 1987a,b; Pais and Kausel, 1988; Wolf, 1988; Gazetas, 1991). Results of dynamic experimental investigations of lateral embedded foundation response have also been published (Stokoe and Richart, 1974; Crouse, et. al., 1985, 1990; Gazetas and Stokoe, 1991). The current *state of practice* in highway bridge design for estimation of lateral impedance functions of spread footings or pile caps involves the use of stiffness equations for rigid surface footings on a semi-infinite elastic half space (Lam et al., 1991). For embedded footings or pile caps, the additional contribution of the passive side due to embedment is determined using Wilson's (1988) equation for lateral abutment stiffness as an engineering approximation.

Most published results for the horizontal stiffness of an embedded footing consider the soil as an elastic half-space, and thus are strictly applicable only at low strain levels in the soil. Little work is available on the secant stiffness and damping of a foundation at larger displacement amplitudes. This section presents the results of a centrifuge-testing program conducted to evaluate the horizontal secant stiffness, material damping, and ultimate

capacity of an embedded foundation at various levels of lateral displacement. While these lateral load centrifuge tests were slow, it is believed that for dry sand the results are applicable to faster earthquake loadings. The results of these centrifuge tests are compared with available analytical formulations from the literature at the end of this section, as well as with results of three-dimensional nonlinear finite element analyses in Sections 7 and 8.

4.1.1 Tests Presented in this Section

The lateral response of a square or rectangular embedded foundation is influenced by contributions from the base, shearing sides, and active/passive sides. The weight and the vertical load on the foundation should also have an effect on the lateral response, by generally increasing the level of normal stress in the soil, especially under the footing. These various forces contributing to the lateral resistance of the soil-foundation system are shown in figure 4-1. A main objective of the centrifuge tests performed was to evaluate separately the relative contributions of the base, shearing sides, and active/passive sides of the foundation to the total lateral response; as well as any possible interaction between these partial contributions. The influence on the lateral response of an additional vertical load on the footing was also investigated. Lateral response parameters studied included the secant stiffness and material damping ratio at various displacement amplitudes, and the ultimate lateral capacity of the foundation. The seven cyclic lateral loading centrifuge tests performed on a model of an embedded footing are listed in table 4-1. All these tests were conducted relatively slowly, with an actual duration of each load cycle of about 2 seconds or about 60 seconds in prototype time. That is, the strain rate was slow, and no significant inertia forces were generated in the system.

In Tests CB and CBL, only the base of the footing was in contact with the soil, as the footing was separated from the surrounding soil. The active/passive and shearing sides were not in contact with the sand, and did not contribute to the lateral response in this test. The ways in which this separation of the sides or the bottom was implemented in this and other tests is discussed in the next subsection. In Test CBL, an additional load was

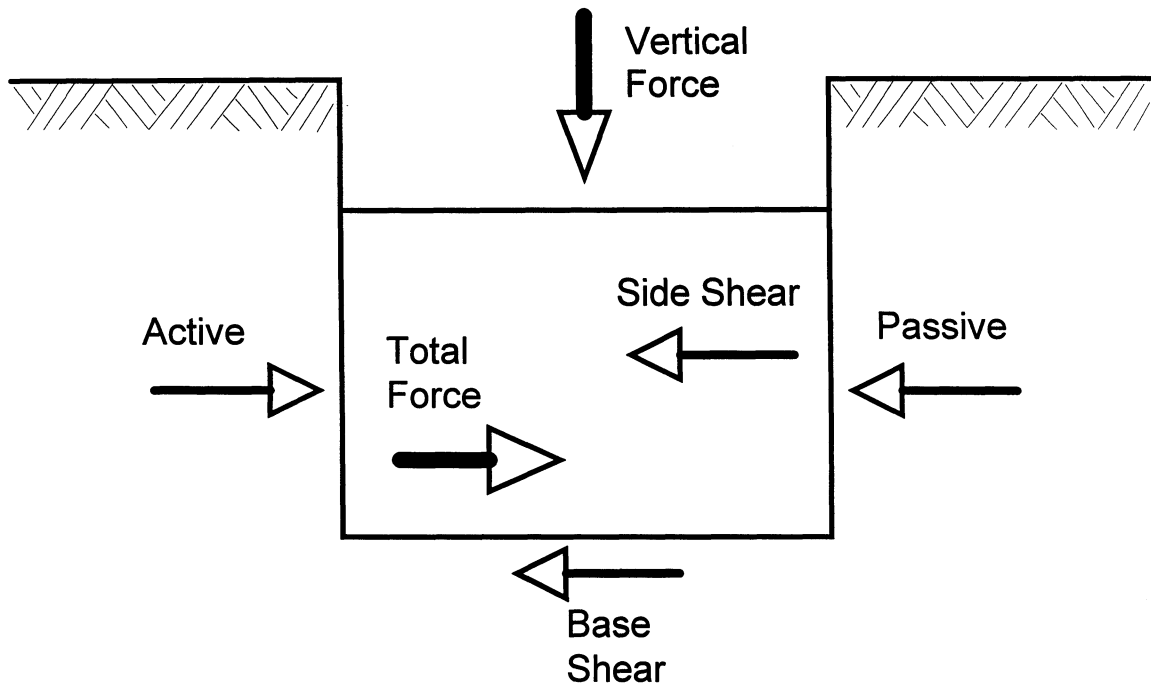


FIGURE 4-1: Forces contributing to the lateral resistance of the embedded foundation (pile cap).

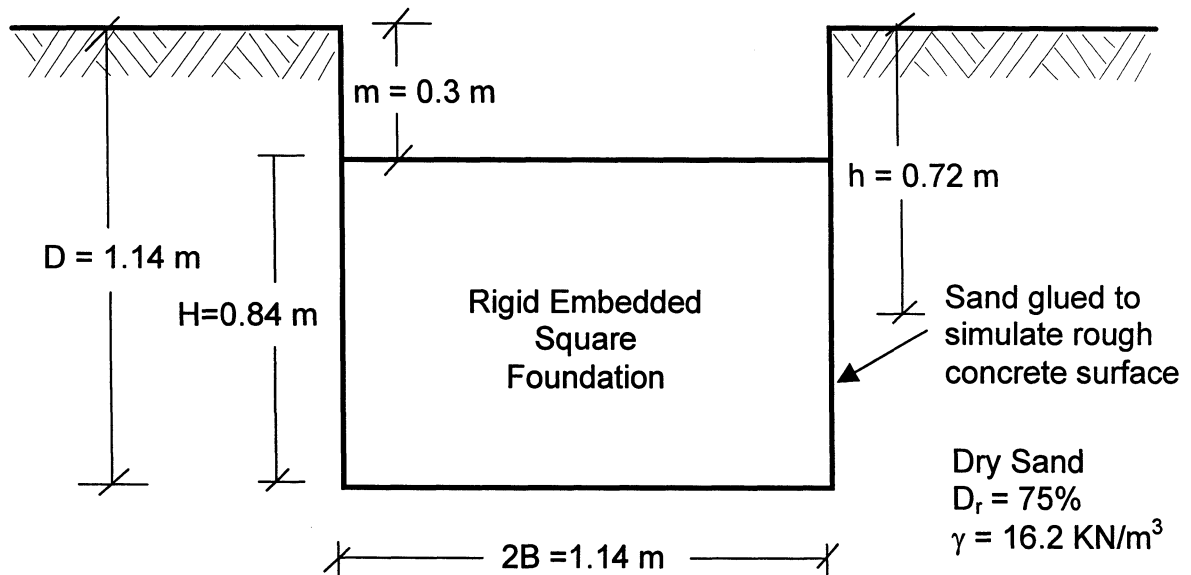


FIGURE 4-2: Dimensions of the footing/cap model used in the centrifuge tests in prototype scale.

TABLE 4-1: Centrifuge tests performed on embedded footing/pile-cap.

Test Code	Pile Contribution	Cap Contribution			Vertical Load at the base* (KN)	Ultimate Lateral Capacity (KN)	Remarks
		Base Friction	Side wall Shear	Passive /active Force			
CB	NO	YES	NO	NO	53	44	$\mu \approx 0.82$
CBL	NO	YES	NO	NO	108	88	
CS	NO	NO	YES	NO	53	38	$K_s \approx 2.1$
CP	NO	NO	NO	YES	53	124	$K_p \approx 14.3$
CSP	NO	NO	YES	YES	53	165	
CBSP	NO	YES	YES	YES	53	214	
CBSPL	NO	YES	YES	YES	108	245	

* This includes the cap's self weight and any additional static vertical load applied to the cap.

TABLE 4-2: Measured secant stiffness for loops of increasing displacement amplitudes in centrifuge tests on footing/cap.

Loop No.	1	2	3	4	5	6	
Displacement Amplitude, ρ (cm)	0.3	0.7	1.4	2.8	5.6	10.9	
Stiffness K_{test} (KN/cm)	K_{CB}	52.6	31.5	21.1	15.3	8	4.1
	K_{CBL}	68	54.4	41.3	29.8	16.1	8.2
	K_{CS}	25.5	18.3	14	8.9	5.6	3.5
	K_{CP}	97.8	47.9	38.4	31.7	19.5	11.4
	K_{CSP}	117.1	64.5	48.9	37.4	23	15.1
	K_{CBSP}	161	96.1	71.3	53.9	32.1	19.6
	K_{CBSPL}	173.1	120.1	95.8	68.1	43	22.5
$\frac{(K_{CS} + K_{CP}) - K_{CSP}}{K_{CSP}} (\%)$	5.3	2.6	7.2	8.6	9.1	-1.3	
$\frac{(K_{CB} + K_{CS} + K_{CP}) - K_{CBSP}}{K_{CBSP}} (\%)$	9.3	1.7	3.1	3.7	3.1	-3.1	
$\frac{(K_{CBL} + K_{CS} + K_{CP}) - K_{CBSPL}}{K_{CBSPL}} (\%)$	10.5	0.4	-2.2	3.4	-4.2	2.7	

placed on top of the footing, which approximately doubled the normal force acting on the base. In Test CS, only the shearing sides of the footing were in contact with the sand, while the base and active/passive sides were not, and thus did not contribute to the lateral response. Test CP isolated the contribution of the active/passive sides; the base and shearing sides were not in contact with the soil in this case. In Test CSP, both side shear and active/passive resistances were activated, while the base did not contribute. In Test CBSP, the base, shearing sides, and active/passive sides were in contact with the soil. In other words, this test corresponds to the regular situation, in which all available contact surfaces contribute to lateral response. Test CBSPL was similar to Test CBSP, except that an additional vertical load was kept on the footing similar to Test CBL.

4.1.2 Model Footing

All centrifuge tests were performed at 30-g centrifugal acceleration with dry Nevada sand of 75% relative density. Therefore, all model dimensions, measured displacements and times were multiplied by 30 to obtain the corresponding prototype values; while the forces in the model were multiplied by $(30)^2 = 900$. The footing was modeled with a rigid aluminum block of dimensions 38-mm (length) x 38-mm (width) x 28-mm (height), which at 30-g centrifugal acceleration, simulates a prototype foundation of dimensions 1.14-m (length) x 1.14-m (width) x 0.84-m (height) (see figure 4-2). Sand was glued to the base and sides of the model footing to simulate a rough concrete surface. A rigid aluminum box of dimensions 914-mm (length) x 610-mm (width) x 356-mm (height) was used as model container for all seven-centrifuge tests. The dimensions of this container are much larger than the dimensions of the foundation model, which should eliminate any boundary effects for these centrifuge experiments.

The general setup for centrifuge tests on the footing is shown in figure 4-3. Lateral displacement cycles of increasing amplitude were applied to the model using a servo controlled hydraulic actuator. The load-displacement response was recorded using a load cell and a displacement transducer (LVDT). The lateral load from the hydraulic actuator was transmitted to the foundation through the load transfer mechanism, which ensured that the horizontal load was applied within the bottom third depth of the model

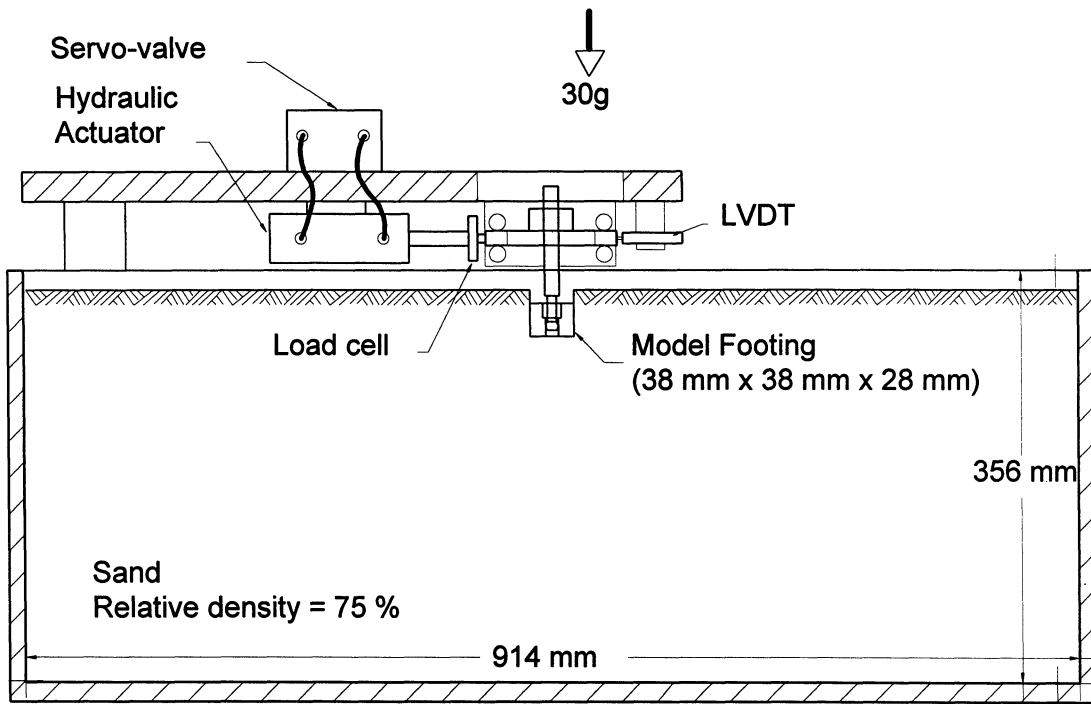


FIGURE 4-3: General set-up for centrifuge tests on embedded footing (pile cap).

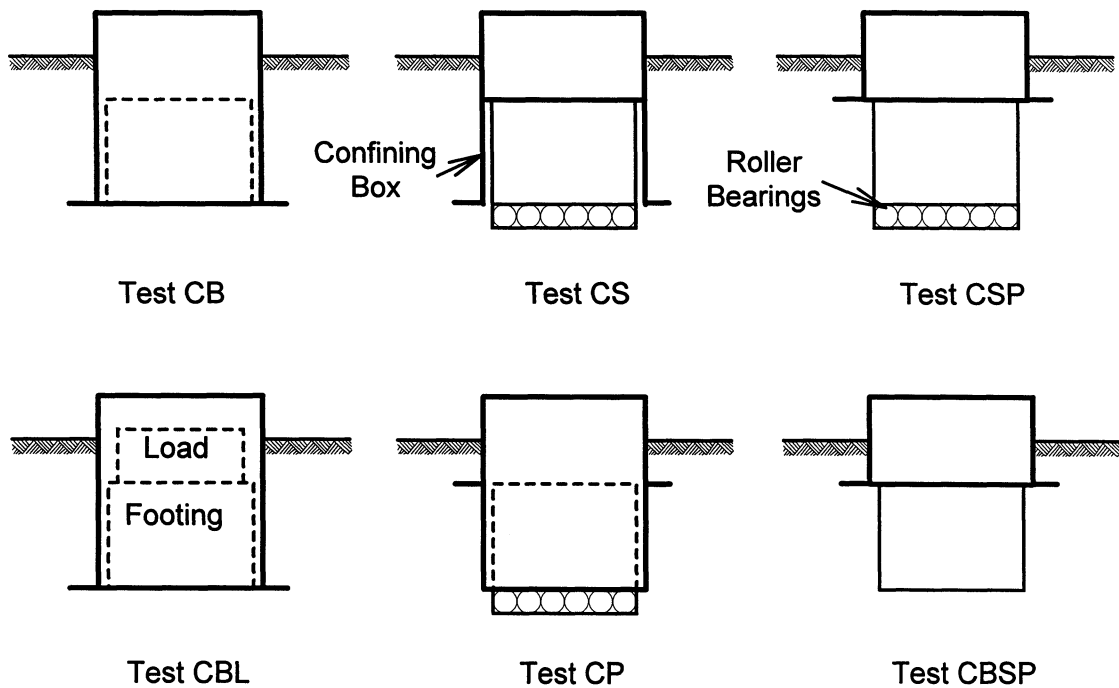


FIGURE 4-4: Schematic representation of set-ups for centrifuge tests on model footing/cap.

foundation, with no rocking moment, or with a minimum moment transmitted to the foundation. This minimized any possible rotation of the footing. The following subsections provide detailed descriptions of the tests performed, and discuss the test results.

4.2 SPECIAL TECHNIQUES USED FOR THE TESTS

The objective of the testing program was to isolate successively the contributions of the base, shearing sides, and active passive sides of the footing. It was important to keep approximately the same state-of-stresses in the soil in all experiments, in order to facilitate comparison of the results from different centrifuge tests. Also, it was decided to provide some soil confinement above the top rim of the footing, to prevent loss of contact of the footing with the soil at large displacements. The ground surface was held at about 1 cm in model scale (0.3 m in prototype scale) above the top edge of the model footing (figure 4-2). To achieve this, specially designed confining boxes were used in each centrifuge test, which retained the soil located above the top edge of the foundation, and along the sides of the foundation which were not in contact with the soil in that test. Roller bearings were used at the bottom of the model footing, when performing the “no base shear” experiments, so as to transmit the vertical load to the base.

The set-ups for the different centrifuge experiments on the footing are shown schematically in figure 4-4. The confining box for Tests CB and CBL retains sand vertically along the sides of the footing, while preventing their contact with the soil. Thus, only the base of the footing remains in contact with the soil. In the set-up shown for Test CS, the confining box retains soil vertically only along the active/passive sides of the footing. It also holds soil above the rim of the footing along all sides to provide sufficient confining soil pressure at the top rim of the footing. In this Test CS, the footing is resting on roller bearings, which eliminates the base shear. Hence only the shearing sides participate in the lateral response. In Test CP, the confining box retains the soil along the shearing sides of the footing to prevent their contact with soil, as well as above the rim of the footing along all sides to provide confinement; roller bearings at the base of the footing eliminate the base shear. Therefore, only the active/passive sides remain in

touch with the soil in Test CP. In the set-ups for Tests CSP and CBSP, the only task of the confining box is to retain soil above the top rim of the footing. Both shearing sides and active passive sides are in contact with the soil in these tests. In Test CSP, bearings at the bottom of the footing eliminate its contact with the base. In Test CBSP, all sides as well as the base take part in the lateral response.

In all set-ups, sufficient gaps were maintained between the sidewalls of the footing and the inner walls of the confining boxes to allow lateral displacement without contact. A latex membrane of very low elastic modulus was used to prevent entry of soil in the gaps. The roller bearings were also sealed off from the soil with a latex membrane. Every attempt was made to maintain a comparable state-of-stresses in the soil in all experiments.

4.3 MODEL CONSTRUCTION AND TESTING PROCEDURE

4.3.1 Model Construction

The general procedure of model construction for centrifuge tests on the cap/footing is as follows:

1. Dry sand with relative density of about 75% was deposited in layers of thickness of 6 cm or less. The amount of sand needed for each layer to achieve the required density was weighed and sand was placed in the container by a raining technique.
2. Once the height of the sand layer reached about 30 cm from the bottom of the box, the model footing with the loading rod was placed on the soil. The footing was positioned such that the loading rod would be aligned vertically with the hole in the bearing plate of the lateral loading assembly (see Section 3), when the housing plate was placed on top of the container. Roller bearings were placed below the footing in the “no base resistance” experiments.
3. The appropriate confining box was placed around the footing to eliminate contact of the soil with the sides of the footing not participating in lateral response in that test, and to retain soil above the top rim of the footing.

4. Sand was deposited around the foundation and the confining box, maintaining the required density, until the top of the soil surface was about 1 cm above the top rim of the footing model.
5. The thick housing plate, bearing lateral loading assembly (see Section 3) was placed on top of the model container, ensuring that the loading rod was inserted in the central hole of the bearing plate. Specially designed clamps were used to eliminate any model disturbance, and to keep the loading rod vertical during this process. The clamps were removed after the housing plate was secured to the model container.
6. The loading rod was clamped to the bearing plate, ensuring that the rounded end of the loading rod remained within the bottom one-third height of the footing. This ascertained that no moments were transmitted to the footing, and that the horizontal force transmitted through the loading rod caused minimal rocking. The housing plate was fitted to the model container with screws. The general final setup is schematically shown in figure 4-3.
7. Finally, the model was transported to the centrifuge basket with a forklift.

4.3.2 Testing Procedure

1. The model was placed on the centrifuge basket very gently.
2. The data acquisition computers were turned on.
3. Signal conditioners, amplifiers, and the servo-control system on the arm of the centrifuge were powered to warm up the system.
4. The load-cell and the displacement transducer (LVDT) were connected to the data acquisition panel on the centrifuge arm. The cord of the feedback LVDT was adjusted to the mean position. The servo valve was connected to the servo controller system.
5. Video cameras in the centrifuge room and the video monitors in the control room were turned on to observe the model in-flight.
6. The centrifuge was spun to 30-g centrifugal acceleration.
7. The hydraulic pump was started, and an input signal was sent to the servo-control system.

8. Lateral displacement cycles of increasing amplitudes were applied to the foundation through the hydraulic actuator. The displacements were monitored through the feedback-LVDT, and the corresponding loads were measured through the load-cell.

4.4 TEST RESULTS

Results of the seven centrifuge tests of table 4-1 performed on models of the embedded cap/footing are presented in this subsection. Data presented in this and the following subsections are in prototype scale, unless specified otherwise. Load displacement responses for the centrifuge tests are plotted in figures 4-5 to 4-11. Several general trends can be observed from these results. Some of the peaks of the load cycles lag behind the corresponding peaks of displacement cycles while others do not. On the other hand, the zero crossings of load and displacement lag with respect to each other in all cases, as anticipated due to the nonlinear hysteretic behavior of soil. As a result, hysteresis load-displacement cycles of increasing displacement amplitude and increasing nonlinearity could be plotted for all seven tests. While the load-displacement response is nonlinear even at low values of the lateral displacement, clear yielding occurs in all tests at a yield displacement of about 2.5 ± 1 cm, with failure happening typically shortly afterwards at a displacement somewhat between 3.5 and 5 cm. The corresponding displacement normalized to the height of the cap is about $4/80 \approx 5\%$, reasonably in agreement with the displacement needed to mobilize passive thrust in sand behind rigid retaining walls. If both the initial nonlinearity and the transition between yielding and ultimate failure are ignored, the footing response can be regarded in first approximation as an elastic-perfectly-plastic system, with corresponding large hysteretic loops after yielding.

It is interesting to examine the individual features of figures 4-5 to 4-11 and speculate about the source of these features. Test CS (figure 4-7) corresponds to the pure shear of two sides of the cap, and exhibits a more or less rigid-elastic-plastic behavior, with three steps in the initial backbone curve, and the same corresponding three steps during the unloading and reloading parts of the cycles. Therefore, it seems that the loops in figure 4-7 more or less follow Masing's Criterion (Masing, 1926). As a result, in figure 4-7 there is no significant displacement lag between peaks of load and displacement cycles.

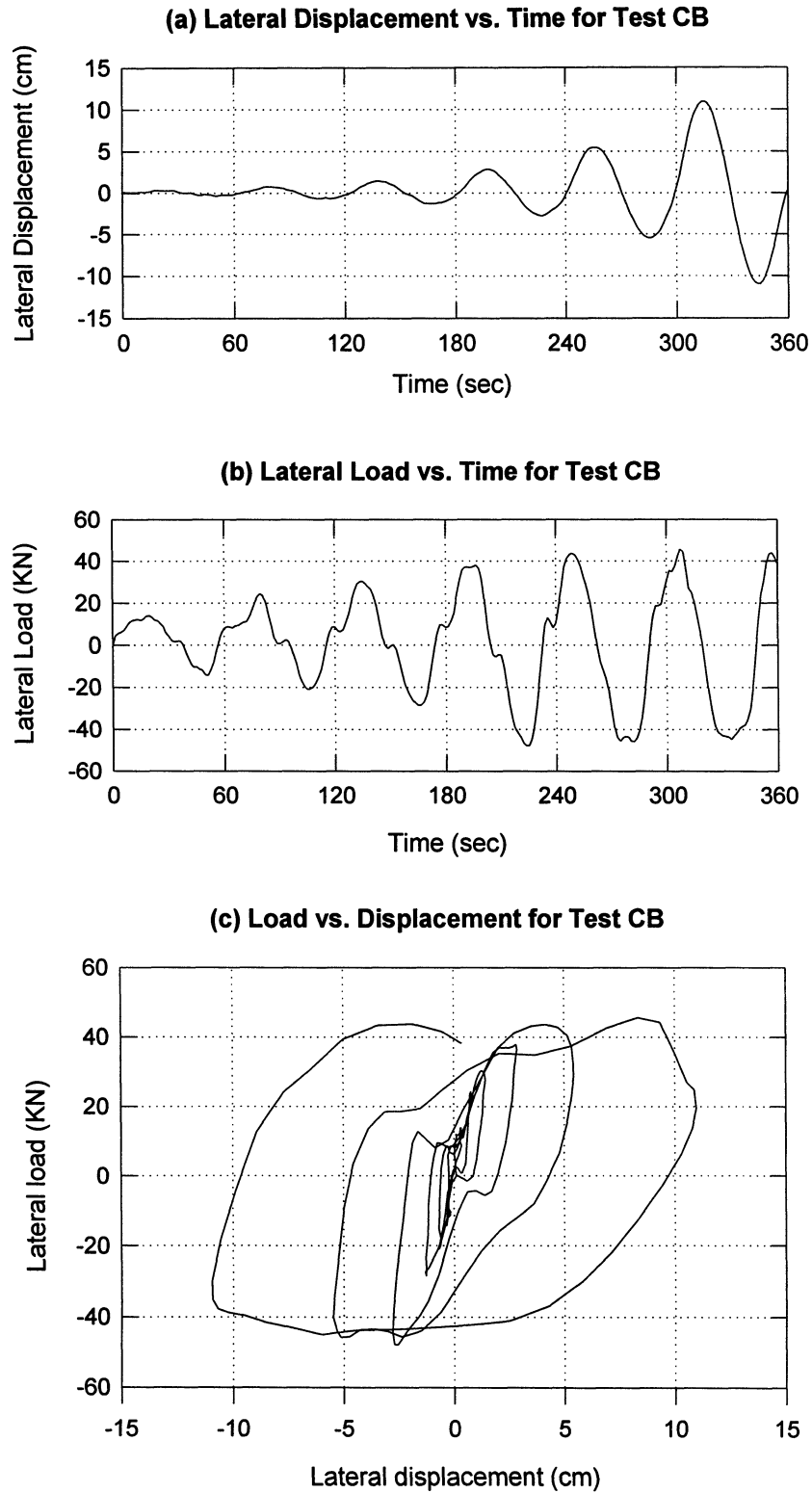


FIGURE 4-5: Load-displacement response for Test CB in prototype scale.

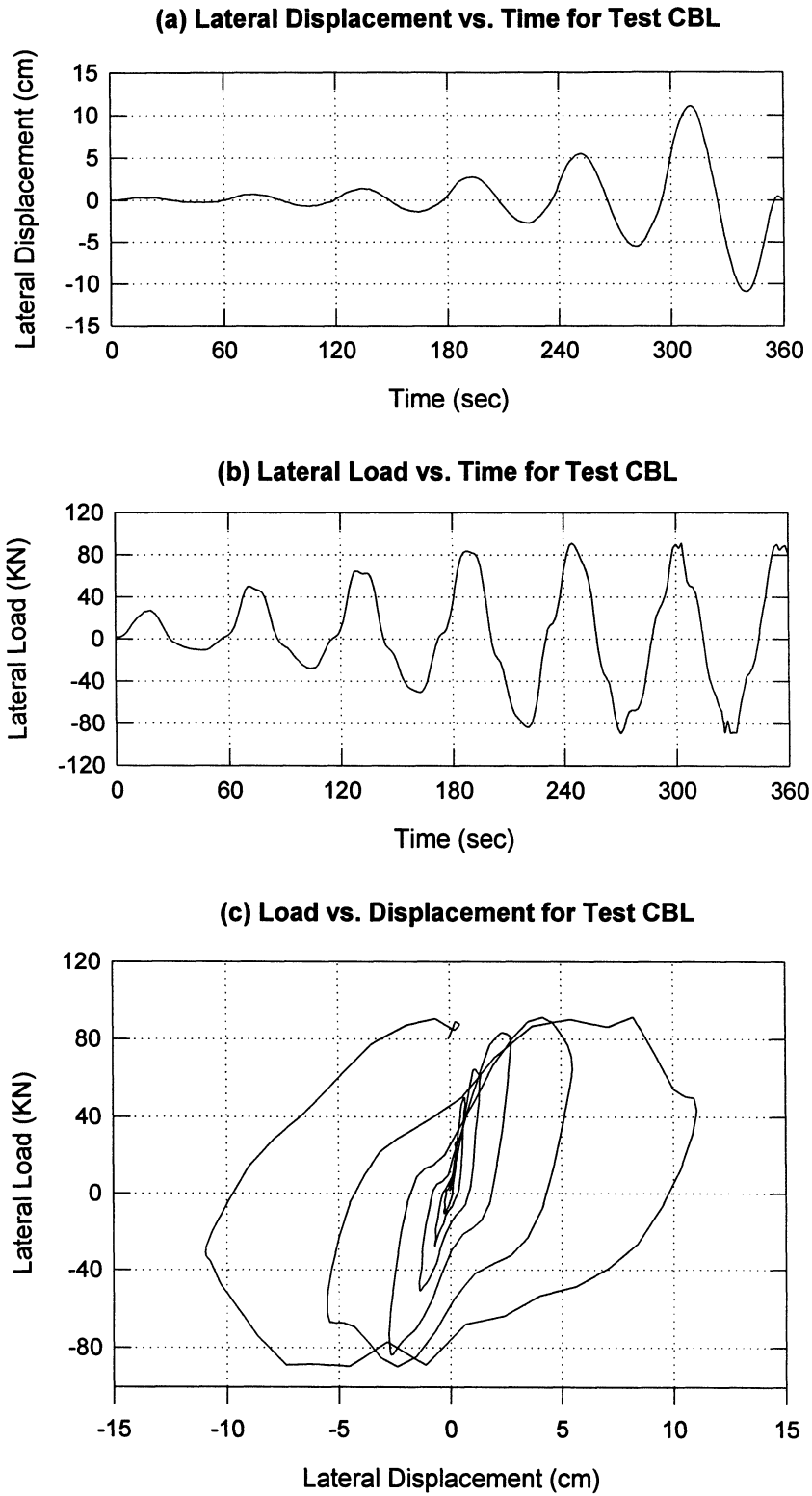


FIGURE 4-6: Load-displacement response for Test CBL in prototype scale.

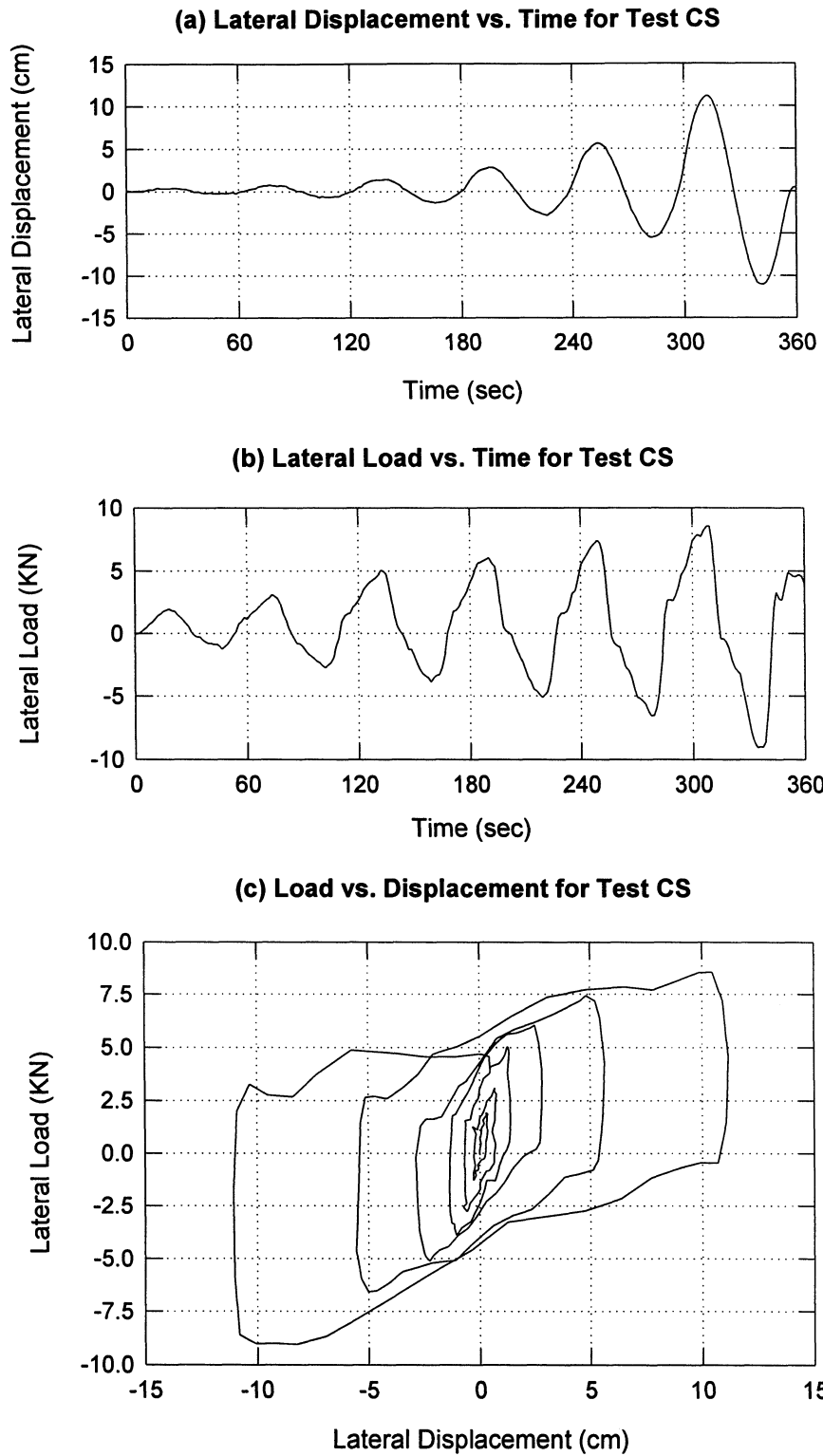


FIGURE 4-7: Load-displacement response for Test CS in prototype scale.

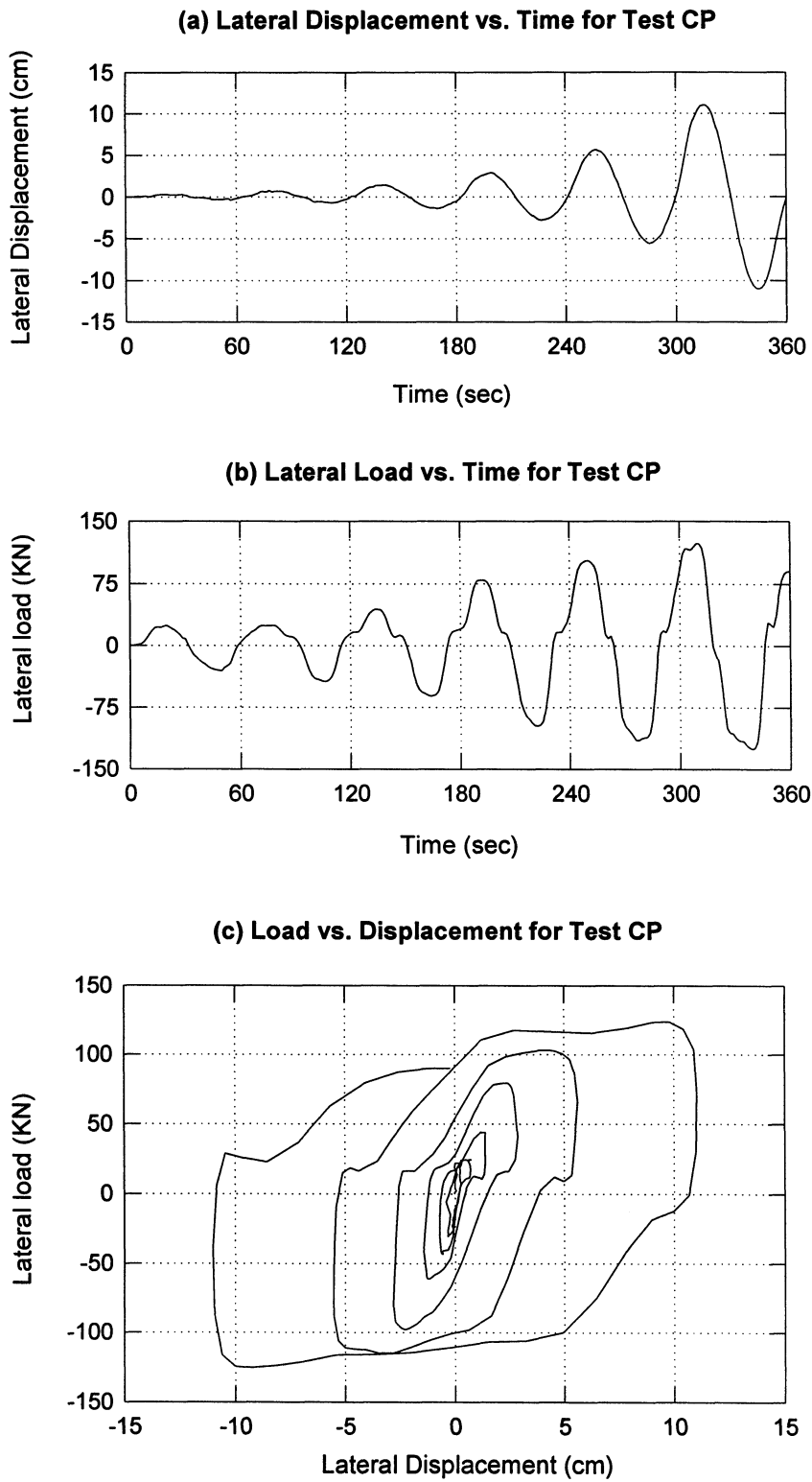


FIGURE 4-8: Load-displacement response for Test CP in prototype scale.

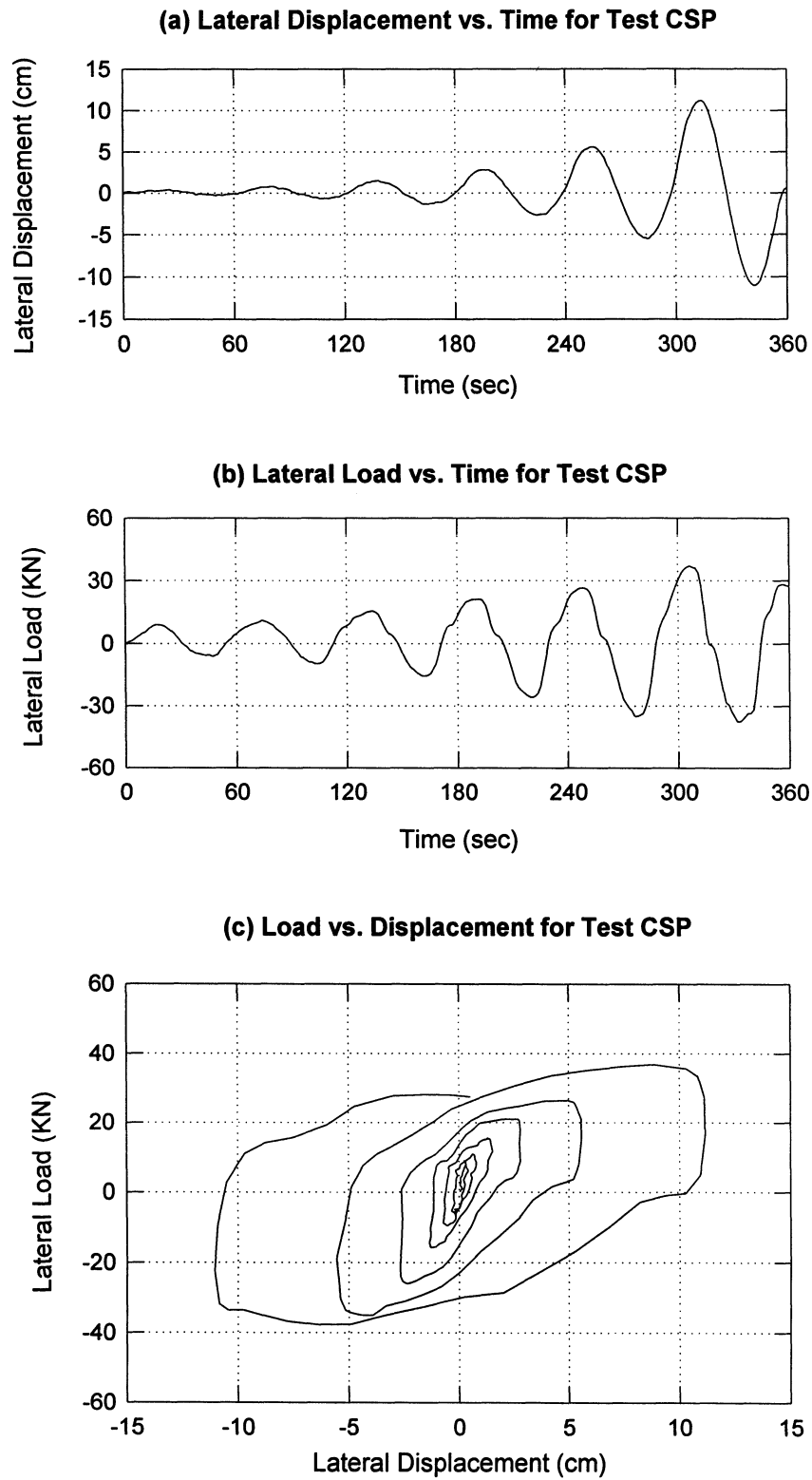
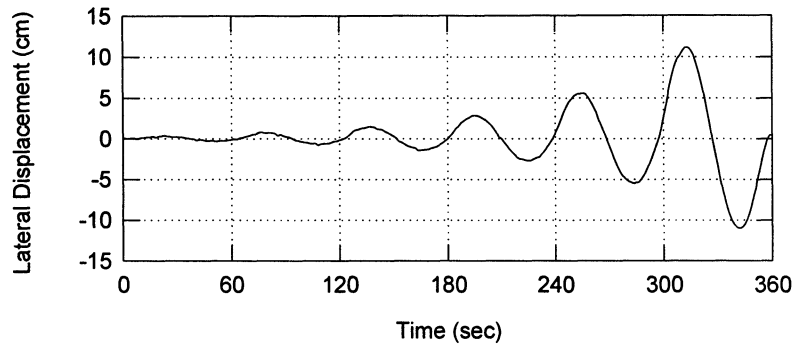
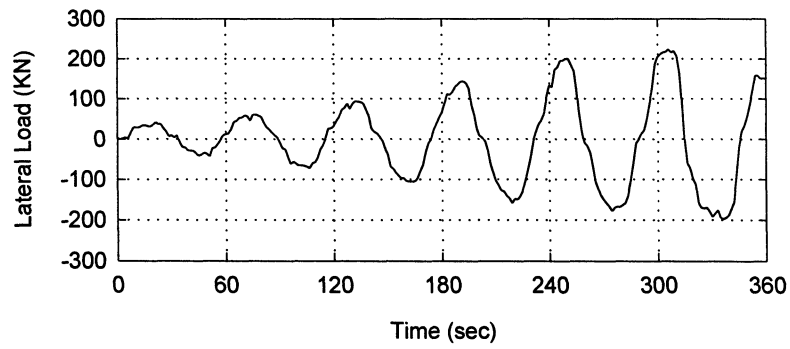


FIGURE 4-9: Load-displacement response for Test CSP in prototype scale.

(a) Lateral Displacement vs. Time for Test CBSP



(b) Lateral Load vs. Time for Test CBSP



(c) Load vs. Displacement for Test CBSP

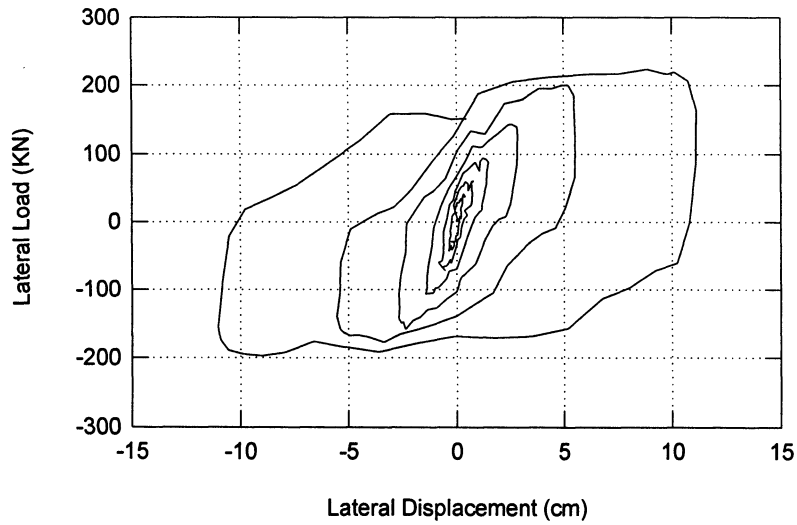


FIGURE 4-10: Load-displacement response for Test CBSP in prototype scale.

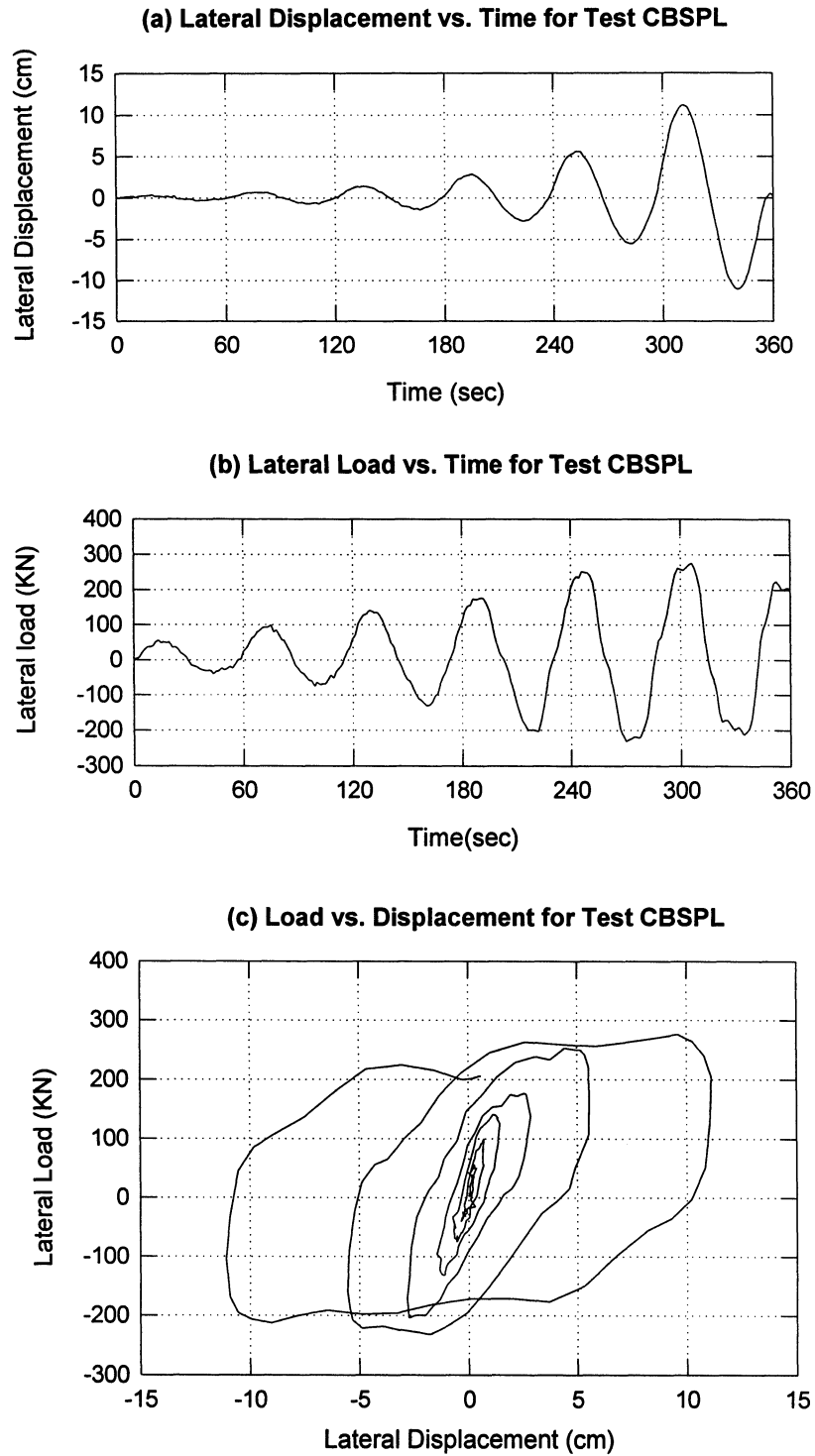


FIGURE 4-11: Load-displacement response for Test CBSPL in prototype scale.

Tests CB (figure 4-5) and CBL (figure 4-6) also correspond in principle to pure shear at the base of the cap. However, the loops in these tests are more rounded and complicated than in Test CS, with corresponding lag between load and displacement peaks. This is attributed to the complex boundary condition at the interface between cap base and soil at the bottom of the trench.

Test CP (figure 4-8) involves only the passive and active forces of the cap. The most prominent feature in all loops is the large drop-off in load immediately after unloading or reloading occurs, with consequent vertical segments of the loops. These vertical segments are similar, but not as prominent as those noticed in Test CS. Probably the best way to explain the shape of figure 4-8 is to neglect the contribution of the active side altogether, and to explain the vertical drop-off, in first approximation, by “separation” of the cap from the passive side until the other side makes contact with the soil and passive thrust starts building at this other side.

Tests CSP (figure 4-9), CBSP (figure 4-10) and CBSPL (figure 4-11) exhibit intermediate features, which are closer to those of Test CP. This is not surprising since, as discussed later, the contribution of the passive side to total response is paramount.

4.4.1 Ultimate Capacity

The ultimate lateral resistance (capacity) of the cap/footing was defined as the maximum load measured in the last displacement cycle of amplitude about 11 cm. The ultimate capacities measured in the centrifuge tests on the cap are listed in table 4-1.

Tests CB and CBL (figures 4-5 and 4-6) involved only the base shear resistance of the footing. In Test CBL, an additional load was placed on the top of the footing, which approximately doubled the normal force on the base. As a result, the ultimate capacity for Test CBL (88 KN) was twice the capacity for Test CB (44 KN). The vertical normal force versus ultimate capacity in these two tests is plotted in figure 4-12. The best fit line for this data passes through the origin. As these ultimate capacities are solely due to

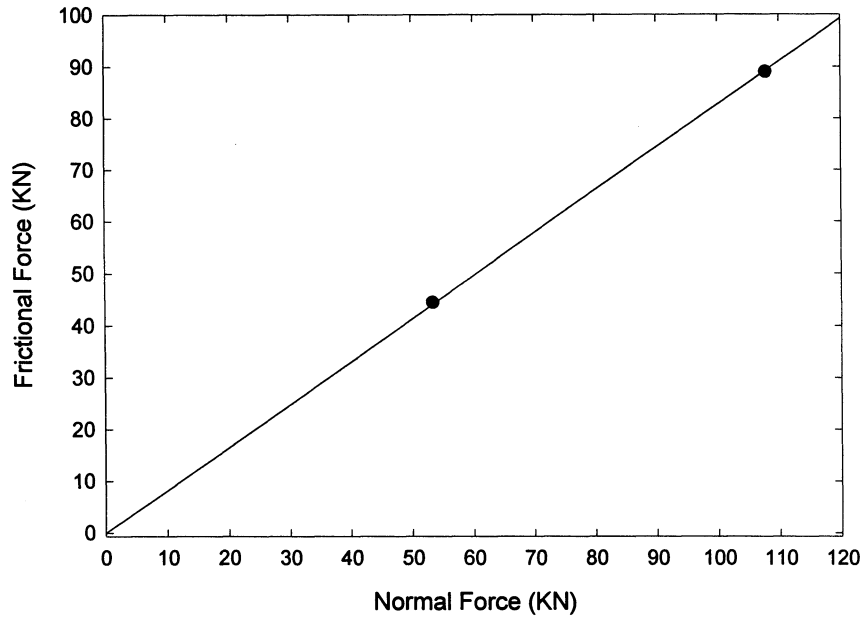


FIGURE 4-12: Normal force versus ultimate lateral capacity for Tests CB and CBL.

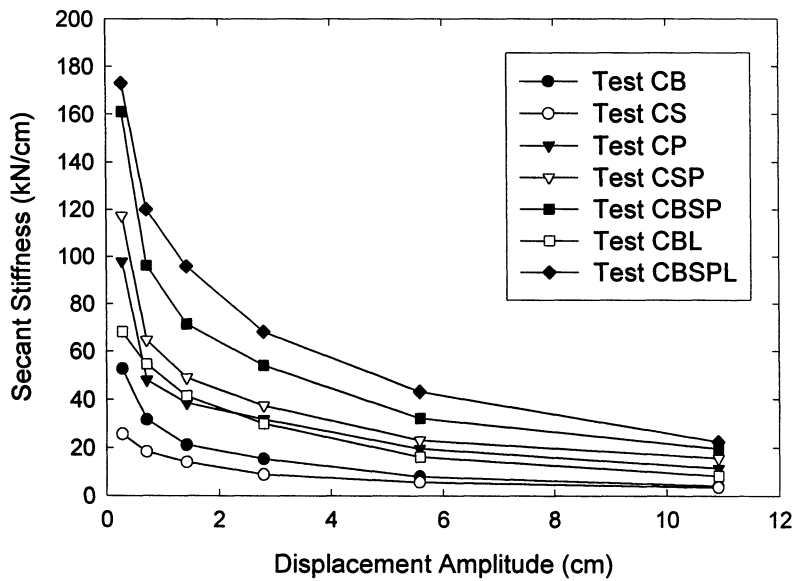


FIGURE 4-13: Measured secant stiffness versus displacement amplitude in tests on footing /cap.

friction at the base, a kinematic friction coefficient of $\mu=0.82$ is obtained from the slope of the best-fit line. This value of μ has been listed in table 4-1.

The results of Test CS are shown in figure 4-7. In this case, only the shearing sides were in contact with the sand, while neither the base nor the active/passive sides contribute. The ultimate capacity measured in Test CS was about 38 KN. Since sand was glued to the shearing sides, and assuming the frictional coefficient to be 0.82 measured in Tests CB and CBL, the estimated total normal force on the two shearing sides at the time of failure becomes $38/0.82 = 46$ KN. Based on this estimated value of the normal force, a lateral earth pressure coefficient K_s may be defined as:

$$K_s = \frac{46}{(\gamma mH + \frac{1}{2}\gamma H^2)(2)(2B)} = \frac{46}{(16.2 \times 0.3 \times 0.84 + 0.5 \times 16.2 \times 0.84^2)2 \times 1.14} \approx 2.1 \quad (4-1)$$

where $2B$ is the side and H is the height of the cap; m is the distance of the top edge of the cap from ground surface (figure 4-2); and γ is the unit weight of the sand. That is, the measured value of lateral capacity contributed by each shearing side can be calculated as $(0.82)(2.1)(\gamma mH + \frac{1}{2}\gamma H^2)(2B)$, where $K_s = 2.1$ plays the role of lateral earth pressure coefficient. This value of $K_s = 2.1$ is much larger than the estimated lateral earth pressure coefficient at rest, $K_o \approx 0.5$ or 0.6 of the sand at the time of placement. The increase is attributed to dilation of this dense sand during the shearing. As this increased K_s due to dilation increases significantly the side shear resistance of the cap, it is important for practical applications. This value of $K_s = 2.1$ has been listed in table 4-1.

In Test CP, only the active and passive sidewalls were activated, without contributions of the shearing walls or of the base shear. The measured ultimate capacity, which in this case is mainly due to passive thrust, is about 124 KN (see figure 4-8). If the contribution of the active side is neglected, this gives, for a wall friction angle of $\phi_w = 39^\circ = \tan^{-1}0.82$, and using the dimensions of figure 4-2, a backfigured passive lateral earth pressure coefficient K_p in the soil:

$$K_p = \frac{124}{\cos \phi_w (\gamma mH + \frac{1}{2}\gamma H^2)2B} \approx 14.3 \quad (4-2)$$

This value of K_p is listed in table 4-1. Using the same wall friction angle $\phi_w = 39^\circ$, as well as an internal friction angle of $\phi = 39^\circ$ for the soil, we get a theoretical $K_p \approx 14$ (Caquot and K erisel, 1949; Lambe and Whitman, 1969). This value is in excellent agreement with $K_p \approx 14.3$, backfigured from Test CP. This agreement is not a priori obvious, as the passive side of the cap has an aspect ratio of $1.14/0.84 = 1.36$, quite different from the infinite aspect ratio assumed in this passive limiting equilibrium analysis. The agreement between theoretical and measured K_p suggests that this solution can be used even in rather short caps and footings. The assumption that ϕ in the soil is equal to that measured between soil and footing is reasonable given the roughness of the footing model. In turn, this value, $\phi = 39^\circ$, associated with a sand of relative density, $D_r = 75\%$, is consistent with the values $\phi = 33^\circ$ and 36° obtained from laboratory triaxial tests on Nevada sand of relative densities 40% and 60%, respectively, as reported by Arulmoli, et al. (1992).

The load-displacement response for Test CSP is shown in figure 4-9. For this experiment, both the side shear and active/passive contributions were activated, while the base was not in contact and thus there was no base shear contribution. The measured ultimate resistance in this case was 165 KN. Note that the addition of ultimate load values for Tests CS and CP is 162 KN, which is very close to the value measured in Test CSP. The validity of such an addition rule for ultimate capacity is as expected from limiting equilibrium considerations for a system undergoing plastic rather than brittle failure.

In Test CBSP (figure 4-10), the base, shearing sides, and active/passive sides were in contact with soil. That is, all available contact surfaces contribute in this case. The measured ultimate capacity in this test is about 214 KN, which matches well with the addition of ultimate capacities for Tests CB, CS and CP (206 KN), again as expected from limiting equilibrium. Notice that most of this total lateral capacity of the footing ($\approx 60\%$) is provided by the passive contribution.

The results of Test CBSPL are shown in figure 4-11. This experiment was also performed with the base and all sides of the footing in contact with the soil. An additional vertical load was kept on top of the footing for a total vertical load of 108 KN, similar to the

vertical load used in Test CBL. The measured ultimate capacity in this test is around 245 KN, which matches well with the addition of ultimate capacities from Tests CBL, CS and CP (251 KN), again consistent with the basic limiting equilibrium conclusion that an addition rule is valid.

4.4.2 Secant Stiffness

The secant stiffness values measured in all seven-centrifuge tests at various levels of displacement are listed in table 4-2 and plotted in figure 4-13. These values were calculated by dividing the maximum load measured in each cycle by the corresponding maximum displacement amplitude. In all tests, the secant stiffness decreases as the displacement amplitude increases. This is as expected for this nonlinear system, and is analogous to the reduction in secant shear modulus in soils with increasing shear strain.

The errors in applying a simple addition rule to evaluate the effect of partial contributions to lateral stiffness are calculated in the three bottom rows of table 4-2. The first row evaluates the addition rule for Tests CS, CP and CSP, that is the contribution of the shear and active-passive sides. The maximum error of the addition rule is less than 10%. The second row evaluates the addition rule for Tests CB, CS, CP and CBSP, that is the contributions of the base and active-passive and shear sides. Again, the maximum error is less than 10%. The last row evaluates the addition rule for Tests CBL, CS, CP and CBSPL. The addition rule is verified again with a maximum error of about 10%, for the base, active-passive and shear sides, and for the case of a larger vertical load, under the assumption that the whole vertical load is taken by the base. From all this it is clear that there is not much interaction in these tests between the stiffness contributions due to base shear, side shear, and active/passive resistances of the footing, with the errors of simply adding the partial contributions being always less than 10%. The sum of partial stiffnesses in table 4-2, however, is generally slightly greater than the total measured stiffness, suggesting a small but systematic interaction. The predominant contributor to the lateral stiffness of the foundation in this test is invariably the passive side, with this passive side contribution being more than 50% of the total stiffness at all displacement amplitudes.

The same information is plotted in figure 4-14 as curves of normalized secant stiffness versus displacement amplitude. For each test, the normalized stiffness was obtained by dividing the secant stiffness for any displacement amplitude by the secant stiffness in the same test at displacement amplitude of 0.3 cm (corresponding to the first load-displacement loop). The reduction in normalized stiffness with increasing displacement amplitude falls within a relatively narrow band in figure 4-14, with the secant stiffness being 30 to 45% of its initial value at a displacement of 2.5 cm, and only about 10% of its initial value at a displacement of 11 cm.

4.4.3 Material Damping

The cyclic lateral loading centrifuge tests listed in table 4-1 were performed at a frequency of 0.0167 Hz (0.1 cycles per second) in prototype scale. At this very low frequency, radiation damping is negligible. Hence, the energy dissipation in these tests is entirely attributed to internal (material) damping developed within the soil and at the soil-foundation interfaces.

The measured areas of loops of different displacement amplitudes for all tests are listed in table 4-3 and plotted in figure 4-15. These areas represent the internal damping or energy dissipated per cycle within the sand and at the sand-foundation interfaces. It can be seen that a simple addition rule also works for the partial contributions of sides and base to energy dissipation. That is, for each displacement amplitude, the sum of the areas of loops for Tests CS and CP, is approximately equal to the area of the corresponding loop for Test CSP. Also, the sum of areas of loops for Tests CB, CS and CP, is just about equal to the area of corresponding loop for Test CBSP. A similar addition law for areas holds true in case of the loops for Tests CBL, CS and CP matched against the corresponding loop for Test CBSPL. Again, the dominant contributor to the damping of the foundation was invariably the passive side. This validity of the addition rule for the areas of the loops is as expected for a system of soil horizontal dashpots or nonlinear energy dissipaters in parallel, all subjected to the same lateral foundation displacement. The equivalent material damping ratios, β_{eq} , calculated for all tests and all cycles, are also listed in table 4-3. These damping ratios were calculated using the standard expression:

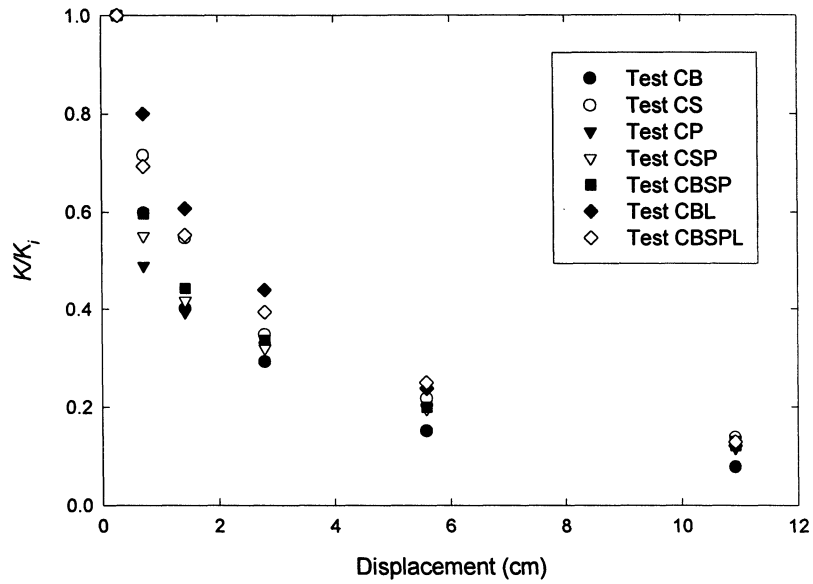


FIGURE 4-14: Measured normalized secant stiffness versus displacement amplitude.

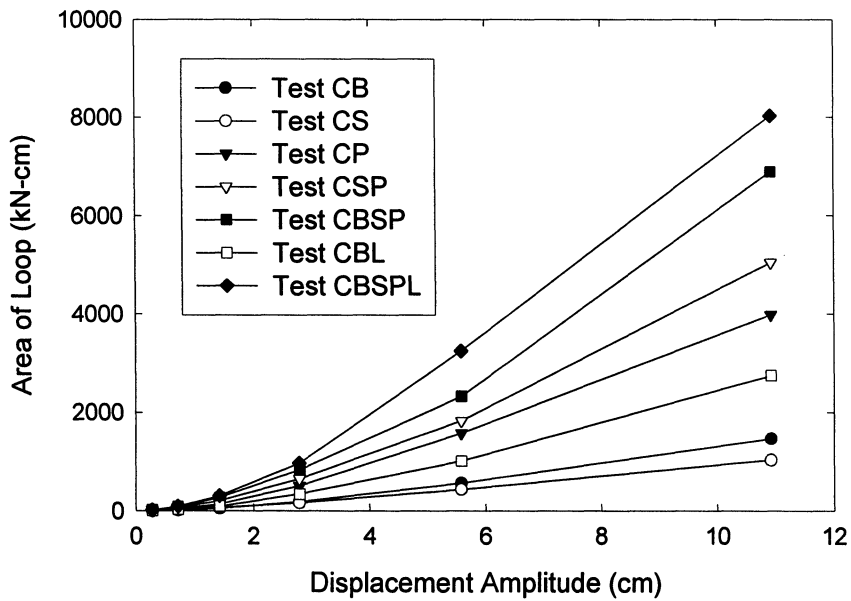


FIGURE 4-15: Measured area of loop versus displacement amplitude for tests on footing/cap.

TABLE 4-3: Measured material damping for loops of increasing displacement amplitudes in centrifuge tests on footing /cap.

Test	Loop	1	2	3	4	5	6
		ρ (cm)	0.3	0.7	1.4	2.8	5.6
CB	Area (KN-cm)	3.6	13.2	50.1	181.5	557.6	1463.6
	β_{eq}	0.12	0.14	0.18	0.24	0.36	0.47
CBL	Area (KN-cm)	3.8	23.1	91.6	334.4	1006.9	2747.8
	β_{eq}	0.11	0.13	0.17	0.23	0.32	0.45
CS	Area (KN-cm)	4.0	21.5	65.2	160.6	429.1	1032.9
	β_{eq}	0.32	0.37	0.37	0.37	0.39	0.39
CP	Area (KN-cm)	14.9	44.7	135.5	500.2	1571.6	3981.5
	β_{eq}	0.31	0.29	0.29	0.32	0.41	0.47
CSP	Area (KN-cm)	18.7	69.4	202.4	644.9	1825.6	5043.2
	β_{eq}	0.32	0.33	0.33	0.35	0.38	0.44
CBSP	Area (KN-cm)	21.1	83.8	267.5	825.8	2324.2	6880.6
	β_{eq}	0.28	0.30	0.30	0.31	0.37	0.47
CBSPL	Area (KN-cm)	21.5	91.9	300.0	962.1	3244.2	8027.5
	β_{eq}	0.24	0.24	0.25	0.29	0.38	0.48

TABLE 4-4: Parameters used for analytical calculation of initial horizontal secant stiffness.

Foundation Parameters:	Width, 2B	1.14 m
	Depth of footing base below ground surface, D	1.14 m
	Depth from the ground surface to the side-wall center of gravity, h	0.72 m
	Area of vertical side-wall surface in contact with the surrounding soil, A_w	3.83 m ²
Soil Parameters:	Shear Modulus, G	1.73 MPa
	Elastic Modulus, E	4.67 MPa
	Poisson's Ratio, ν	0.35

$$\beta_{eq} = \frac{A}{2\pi K_h u^2} \quad (4-3)$$

where A = measured area of loop; K_h = secant stiffness for that cycle; and u = displacement amplitude of the loop. The variation of this equivalent material-damping ratio with displacement amplitude is shown in figure 4-16 for all tests. While there is more or less a general trend for damping ratio to increase with displacement amplitude, this is not true in all cases. Some very interesting detailed trends can be observed in table 4-3 and figure 4-16, especially for the range of displacements up to $u = 6$ cm. These trends are: (i) for the tests in which only the base contributes (CB and CBL), $\beta_{eq} \approx 0.1$ is low at small displacements, and increases rapidly to $\beta_{eq} \approx 0.3$ or more at $u \approx 6$ cm; (ii) Tests CS, CP and CSP in which only the side walls contribute, have the highest value of $\beta_{eq} \approx 0.3$ to 0.4, with little variation of β_{eq} with amplitude; and (iii) the tests including contributions of both base and walls (CBSP and CBSPL) have intermediate values of $\beta_{eq} \approx 0.25$ to 0.30, and exhibit only a moderate tendency to increase with displacement.

4.5 COMPARISON OF INITIAL SECANT STIFFNESS WITH THEORY

The discussion of ultimate lateral capacities in the previous subsection allowed some theoretical comparisons and conclusions, summarized in the values of μ , K_S and K_P listed in table 4-1. Some theoretical predictions for the measured damping ratios are discussed in Section 7, in the context of finite element analyses of the centrifuge tests. This subsection focuses on comparison with theory of the measured initial secant stiffnesses in the centrifuge experiments.

Pais and Kausel give the following expression for evaluating the static stiffness, K_{sur} , of a square surface footing of side $2B$ on a homogeneous isotropic elastic half-space with shear modulus G , and Poisson ratio ν ,

$$K_{sur} = \frac{9.2BG}{(2 - \nu)} \quad (4-4)$$

Gazetas and Tassoulas (1987a), using an elastic soil model and a boundary element formulation along with solutions published by several researchers, performed a parametric study on the static and dynamic horizontal stiffnesses of rigid foundations of

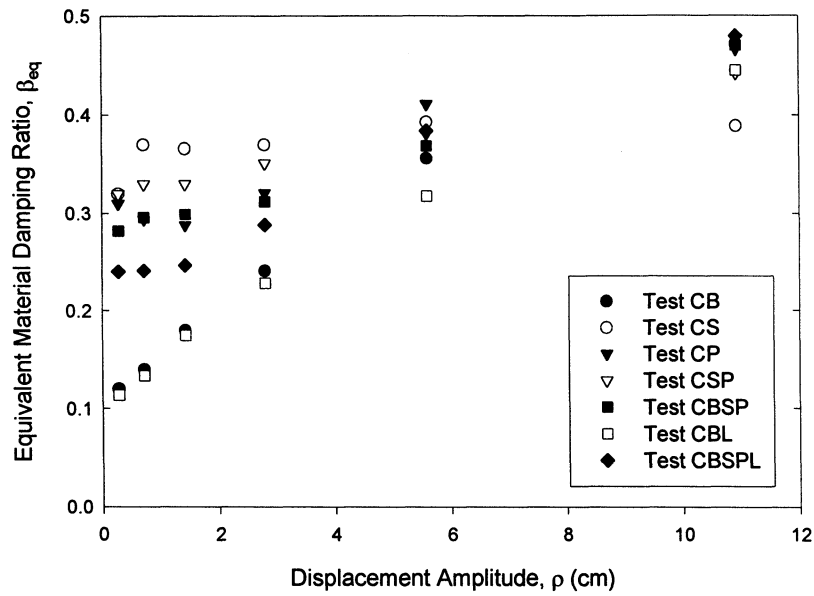


FIGURE 4-16: Measured equivalent damping ratio versus displacement amplitude.

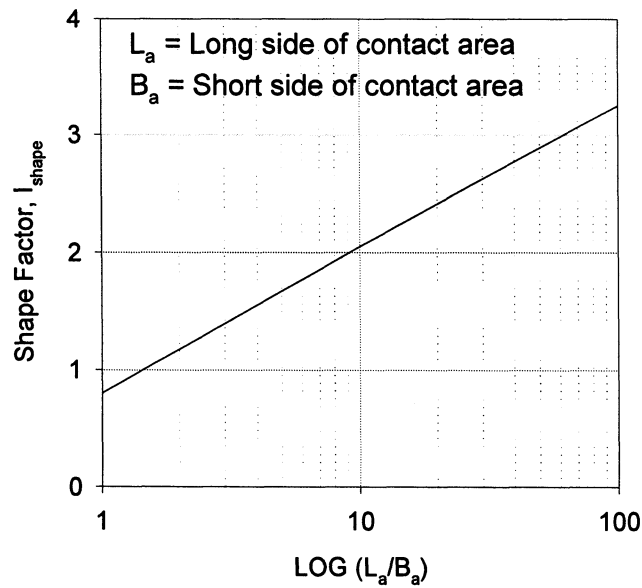


FIGURE 4-17: Correlation chart for shape factor for abutment stiffness (after Wilson, 1988).

various shapes embedded in a reasonably deep and homogeneous soil deposit. The results of this study show that the static stiffness of the embedded foundation is always greater than the stiffness of the same foundation placed on the surface of the medium. Placing the foundation at the bottom of the excavation, without contact between the foundation walls and the surrounding soil, typically results in a moderate increase in the stiffness. This “trench effect” results from the different boundary conditions when the footing is at the bottom of the trench instead of on the surface of the medium. The horizontal static stiffness of the foundation, K_{tre} , is given by:

$$K_{tre} = K_{sur} I_{tre} \quad (4-5)$$

which accounts for the “trench effect” through the dimensionless factor $I_{tre} > 1$. Contact between the foundation sidewalls and soil results in a further increase in stiffness. This “side-wall effect” on stiffness predicted by elastic theory is very sensitive to how good the contact is and how much wall area is in actual contact with the soil. The final expression for the lateral static stiffness of an embedded foundation, K_h , proposed by Gazetas and Tassoulas, is of the form:

$$K_h = K_{sur} I_{tre} I_{wall} \quad (4-6)$$

which incorporates both the trench (I_{tre}) and sidewall (I_{wall}) contributions. For a square embedded foundation of side $2B$, the “trench factor”, I_{tre} and the “side-wall factor” I_{wall} are given as:

$$I_{tre} = 1 + 0.15 \sqrt{\frac{D}{B}} \quad (4-7)$$

$$I_{wall} = 1 + 0.52 \left(\frac{hA_w}{B^3} \right)^{0.40} \quad (4-8)$$

where D = depth of the base of the foundation from ground surface; A_w = vertical area of the foundation sidewalls actually in contact with the soil; h = depth from ground surface of the centroid of the sidewall area in contact with the soil.

The secant stiffness measured in the first displacement cycle applied in the centrifuge experiments can be compared with the results of the elastic solution provided by (4-4) to (4-8). In Tests CB and CBL, only the base of the foundation was in contact with the soil. Soil was retained vertically around the foundation without contact with it. This situation

includes the “trench effect” described by Gazetas and Tassoulas. In Tests CBSP and CBSPL, all sides and the base of the foundation were in contact with the soil; thus, both “trench” and “side-wall” effects were acting in these tests. Hence, the Pais-Kausel and Gazetas-Tassoulas solutions could be used to compare the measured initial secant stiffness of these tests with the trends predicted by elastic theory.

A first comparison was made by comparing the empirical values of $I_{\text{wall}} = K_{\text{CBSP}}/K_{\text{CB}} = K_{\text{CBSPL}}/K_{\text{CBL}}$, with the value of $I_{\text{wall}} = 2.53$ obtained from Gazetas-Tassoulas equation (4-8). The empirical values from the centrifuge tests are $K_{\text{CBSP}}/K_{\text{CB}} = 161/52.6 = 3.06$ and $K_{\text{CBSPL}}/K_{\text{CBL}} = 2.55$, which are in very good agreement with the analytical $I_{\text{wall}} = 2.53$. This agreement is really excellent when considering that Gazetas and Tassoulas assume that G is the same at all points throughout the soil mass, while G must have varied in the soil mass in the centrifuge tests due to both variations in confining pressure and in shear strain level. It is interesting to note that up to displacement amplitudes of about 2.8 cm, the empirical values of I_{wall} range between 2.2 and 3.5, which are still in reasonable agreement with the analytical $I_{\text{wall}} = 2.53$.

The foundation and soil parameters used for this comparison with theory are listed in table 4-4. The foundation parameters correspond to the dimensions of the model footing in prototype scale. A soil Poisson’s ratio $\nu = 0.35$, typical of dry sand was selected. Values of $G = 1.43$ and 1.84 MPa are backfigured from applying (4-4), (4-5) and (4-7) to the measured first cycle stiffnesses in Tests CB and CBL, respectively. A constant shear modulus, G , of 1.73 MPa was chosen as an average engineering approximation for both tests, as well as for Tests CBSP and CBSPL. This approximation neglects the 29% increase in initial horizontal stiffness between Tests CB and CBL, and the corresponding 7% increase between Tests CBSP and CBSPL. The FE analyses described later in Section 7 indicated that maximum shear strains of the order of 0.5% were developed in the sand around the footing for a lateral foundation displacement of 0.3 cm. For the low mean confining pressures acting in the sand in the free field at or about the foundation base level ($\sigma_m \leq 10$ KPa), and for this high shear strain level, $G/G_{\text{max}} < 0.1$ in sands. That is, a value of $G_{\text{max}} > 17$ MPa is estimated for the soil, corresponding to a shear wave velocity,

V_s of 100 m/sec or more. In the absence of direct measurements of G_{max} or V_s in the sand tested, it is not possible to estimate exactly the value of the G_{max} or V_s that should be used, nor the depth at which it should be selected to be able to predict the lateral stiffnesses measured in the centrifuge tests. The reasons for this are the uncertainty in the value of G/G_{max} at large strains, noted above, and the fact that available empirical correlations for G_{max} in sand (e. g., Richart et al., 1970) correspond to significantly higher levels of confining stresses, $\sigma_m \geq 20$ KPa. However, reasonable extrapolations of measured G_{max} and V_s to lower σ_m suggest that the $G_{max} \geq 17$ MPa backfigured from the measured stiffnesses is a reasonable average of the shallow strain stiffness of Nevada sand at depths above the foundation base level, $D = 1.14$ m, used in the centrifuge tests.

Therefore, using $G = 1.73$ MPa, and the rest of foundation and soil parameters listed in table 4-4, together with the Pais-Kausel and Gazetas-Tassoulas equations (4-4) to (4-8), the predicted stiffnesses for Tests CB, CBL, CBSP and CBSPL are listed in table 4-5. These predicted values and corresponding predicted trends between experiments match quite well with the measured values from the centrifuge tests, also included in table 4-5.

Pais and Kausel (1988) also give formulae for evaluation of the static horizontal stiffness of embedded circular and rectangular foundations. For a square embedded foundation of side $2B$ and depth of embedment D_e ,

$$K_h = K_{sur} \left[1 + \left(\frac{D_e}{B} \right)^{0.8} \right] \quad (4-9)$$

where K_{sur} is the stiffness of equivalent surface footing given by the Pais-Kausel equation (4-4). Note that, unlike the Gazetas-Tassoulas expressions determining the effect of embedment on lateral stiffness (4-4 to 4-7), the Pais-Kausel equation (4-9) does not take into account the effective vertical area of sidewall actually in contact with the soil. Assuming the depth of embedment, D_e in (4-9) equal to the depth of the foundation base from the ground surface, D , and using (4-4) and (4-9) along with the parameters of table 4-4, the calculated value of horizontal stiffness is 150.7 KN/cm, which is in reasonable agreement with the measured initial secant stiffnesses for Tests CBSP (161 KN/cm) and CBSPL (173.1 KN/m).

TABLE 4-5: Comparison of measured initial secant stiffness with theory.

Test	Initial Horizontal Secant Stiffness, K_h , KN/cm	
	Measured in Centrifuge Test	Calculated using Gazetas and Tassoulas (1987a) Solutions and $G = 1.73$ MPa
CB	52.6	66.6
CBL	68	66.6
CBSP	161	168.7
CBSPL	173.1	168.7

Wilson (1988) developed a general equation for the abutment wall-backfill stiffness, K^* , which considers the passive resistance of the soil. The equation is given by:

$$K^* = \frac{E}{(1 - \nu^2)I_{\text{shape}}} \quad (4.10)$$

where E and ν are the Young's Modulus and the Poisson's Ratio of the soil respectively; and I_{shape} is a shape factor. Wilson (1988) provided correlation chart for I_{shape} with the aspect ratio of the contact area (L^*/B^*), which is reproduced in figure 4-17. Lam et al. (1991) recommended the use of Wilson's equation, as an engineering approximation to find the stiffness contribution of the passive side of the footing. The value of K^* obtained using the parameters in table 4-4, in conjunction with the Wilson's correlation chart (figure 4-17) and with (4-9) was about 5.3 MPa. This value compares reasonably well with the measured value of 8.4 MPa obtained from Test CP, considering the fact that Wilson's equation is only approximately applicable to the situation in Test CP.

4.6 CONCLUSIONS

The following conclusions can be drawn from this series of centrifuge tests.

1. For all tests, the measured values of ultimate lateral capacity agree reasonably well with theory, and also satisfy the addition rule expected from limiting equilibrium.
2. There is little interaction between the stiffness contributions of the base, shearing sides, and active/passive sides, with an addition rule for secant stiffness being approximately valid.
3. The measured areas of the load-displacement loops, representing material damping, also satisfy the "addition rule," as expected from the response of dashpots or other energy dissipators in parallel.
4. For all parameters measured in tests on the model foundation/cap (ultimate lateral capacity, lateral stiffness, and material damping), the contribution of the passive side accounts for more than half of the total. The contribution of the passive side to capacity is well predicted by passive thrust theory, if the soil-wall friction is considered and a corresponding high passive pressure coefficient is used ($K_p = 14$ in this case).

5. The measured initial secant stiffness values, including their increase when the foundation walls make contact with the surrounding soil, agree well with the available elastic solutions in the literature, if a maximum shear modulus at a shallow depth is selected.

SECTION 5

CENTRIFUGE TEST ON FREE-HEAD PILE WITHOUT CAP

5.1 INTRODUCTION

The lateral response of a pile-cap foundation system has contributions from both cap and pile(s). In Section 4, results of centrifuge tests on the cap-alone were given. In this section, results of a centrifuge model test of a single free head pile-alone without cap are presented. This test was done primarily to estimate the p-y curves for the soil, which will be used later in Section 6 to evaluate the response of the pile in centrifuge tests done on the entire pile-cap system. The measured lateral response parameters of the free-head pile (ultimate capacity, secant stiffness, and material damping) are compared in this section, with the corresponding values obtained from the tests on the cap, already discussed in Section 4. Bending moments measured along the length of the pile were used to backfigure the p-y curves for the soil. These measured p-y curves, initial secant stiffness, as well as the measured load-deflection characteristics of the pile are compared with available results in the literature.

5.2 MODEL CONFIGURATION

Centrifuge Test PI was performed on a model of a free-head pile at 30-g centrifugal acceleration. There was no pile-cap in this test. Dry Nevada sand of 75% relative density was used for this experiment. The pile was simulated with an aluminum pipe of external diameter 12.7-mm and wall thickness 0.9-mm. This corresponds to a prototype pile of outer diameter 0.381 m and flexural stiffness 3.23×10^{11} N-cm². For lateral loading, this approximately represents a typical Cast-In-Drilled-Hole (CIDH) highway bridge foundation pile (Abcarius, 1991, Lam et al, 1991). In this simulation the effect of the pile roughness on the lateral response is neglected. Bouafia and Garnier (1991) performed lateral loading centrifuge tests on piles to study the influence of the roughness of the pile-shaft on the lateral response. The results of their study show that for the same lateral load, the deflection of rough pile was only about 15 % lower than the deflection of the smooth pile. Hence, the assumption made above in our case, of neglecting the effect of pile

roughness is rational. The length of the model pile was about 19 cm. At 30-g centrifugal acceleration, this simulates a pile of length 5.715-m. The ratio of length to diameter of the pile was about 15. Therefore, this is a prototype “long pile” for lateral loading, according to the criteria given by Poulos and Davis (1980).

The model pile was instrumented with five pairs of strain gages in a half-bridge Wheatstone circuit, to allow measurement of bending moments along its length. These strain-gages were of type CEA-13-032UW-120, manufactured by Measurements Group, Inc. and were excited by a 2-Volt power supply. The pattern of strain gages installed on the model pile is shown in figure 5-1. The strain gage spacing was biased starting with a close spacing at the top to a more distant spacing at the bottom. The purpose of this arrangement was to capture the rapid variation of bending moments expected near the pile-head.

The bottom of the cap model in the centrifuge tests conducted on the cap-alone (discussed earlier in Section 4) was at a depth of about 3.8-cm (model scale) from the soil surface. In Test PCBSPI on the entire pile-cap system (discussed later in Section 6), the pile was clamped to the cap, and consequently, the pile-head was also located at a depth of about 3.8-cm, from the soil surface. Hence, the top of the pile in the free-head pile Test PI was positioned at this same depth of about 3.8-cm from the soil surface, in model scale (1.14 m in prototype scale). This ensured that the pile-head locations are at an identical depth in both Test PCBSPI on the pile-cap system and Test PI on the free-head pile. This facilitated direct comparison of the lateral responses of the foundations in these two tests. A cylindrical confining box was used to retain sand above the pile-head in Test PI (figure 5-1).

5.3 MODEL CONSTRUCTION AND TESTING PROCEDURE

The process of model construction for Test PI on the free-head pile is as follows:

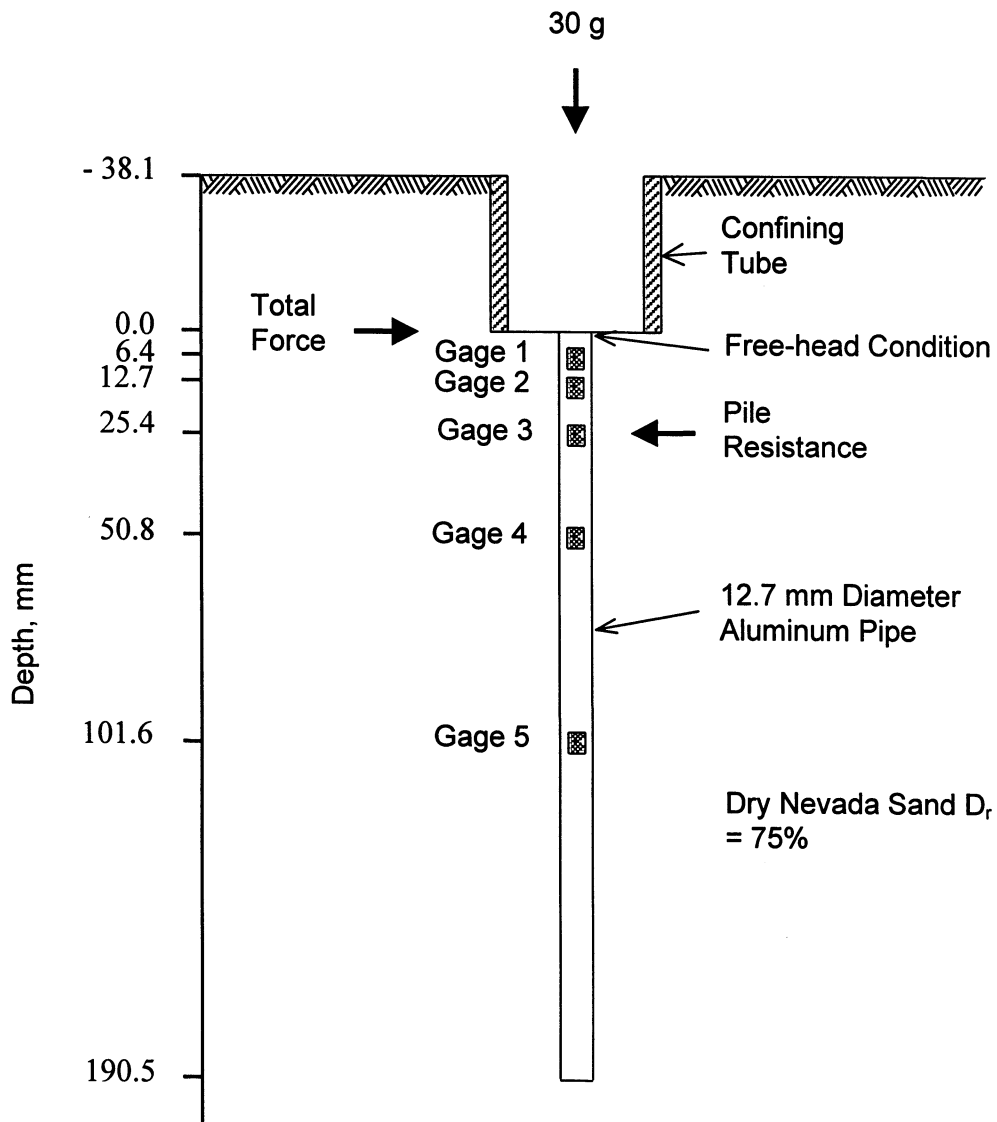


FIGURE 5-1: Model pile used in Test PI.

1. Dry sand with relative density of about 75% was deposited in layers of thickness 6 cm or less. The amount of sand needed for each layer to achieve required density was weighed, and sand was rained in the container.
2. Once the top surface of the sand reached about 11 cm from the bottom of the box, the model pile with loading rod was placed in the box. The pile was held vertical with the help of specially designed clamps. The pile and the loading rod were positioned such that the loading rod would be in a vertical alignment with the hole in the bearing plate of the lateral loading assembly (see Section 3), when the housing plate was placed on the top of the container.
3. Sand was rained around the pile, maintaining the required density. The pile-holding clamps were removed after sufficient sand had been deposited around the pile. The pile remained in an upright position due to the confining pressure of the sand.
4. When the top surface of the sand reached the level of the pile-head, the confining box was placed around it to retain the soil vertically above the pile-head. Sand was deposited around the confining box until the sand surface was 3.8 cm above the pile-head.
5. The thick housing plate, bearing lateral loading assembly (see Subsection 3.4) was placed on top of the model container, ensuring that the loading rod is inserted in the central hole of the bearing plate. Specially designed clamps were used to eliminate any model disturbance and to keep the loading rod vertical during this process. The clamps were removed after the housing plate was in place.
6. The loading rod was clamped to the bearing plate, ensuring that the rounded end of the loading rod was located at the pile-head. This arrangement ensured that no moments were transmitted to the pile-head. The housing plate was fitted to the model container with screws. The general final setup is schematically shown in figure 5-2.
7. Finally, the model was transported to the centrifuge basket with the help of a forklift. The testing procedure for Test PI was similar to the general procedure for tests on the cap-alone, described in Subsection 4.3.2. Lateral displacement cycles of increasing amplitude were applied to the model using a servo controlled feedback system. The load-displacement response was recorded using a load-cell and a displacement transducer

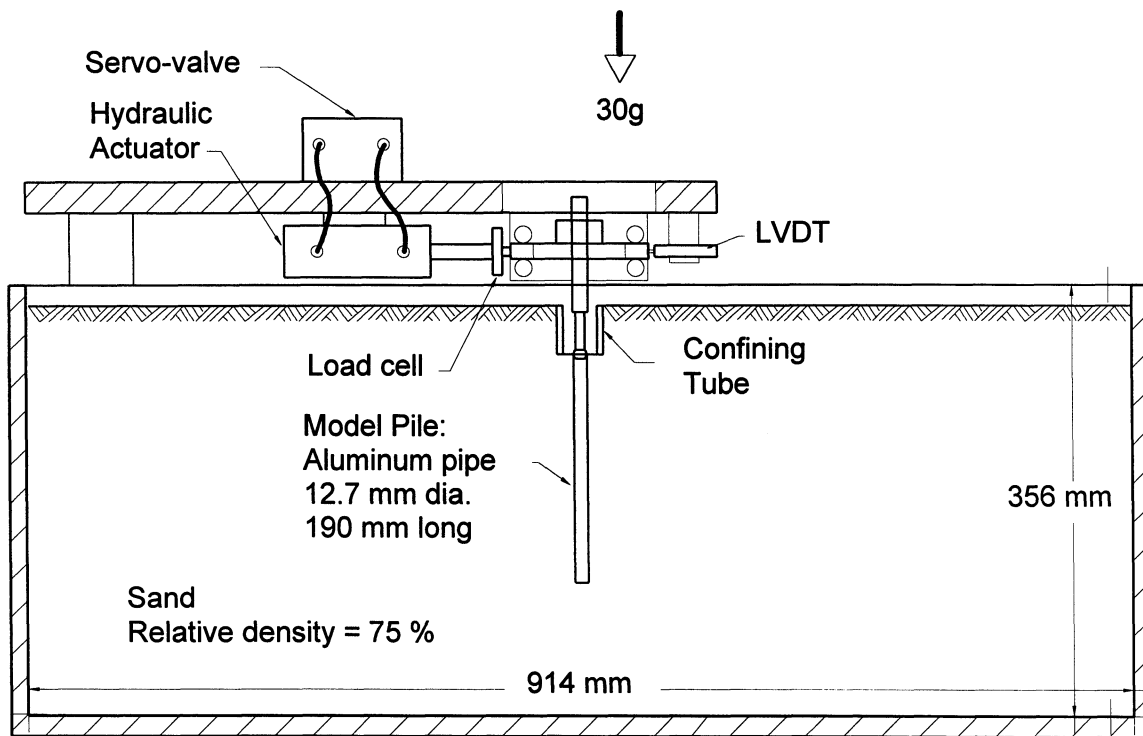


FIGURE 5-2: Set-up for centrifuge Test PI.

(LVDT). In addition, the bending moments along the length of the pile were recorded through the strain-gages glued on the pile.

5.4 TEST RESULTS

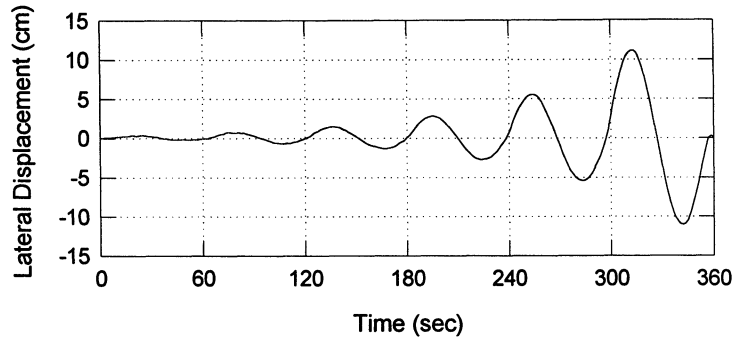
Results of centrifuge Test PI, conducted on the model of a free-head pile, are presented in this subsection. The data presented in the following subsections is in prototype scale, unless mentioned otherwise. The load-displacement response of Test PI is given in figure 5-3. The load-displacement loops look sharper than the corresponding loops for any of the tests on the cap-alone presented in Section 4. Even at the final displacement-amplitude used of about 11-cm, the response of the pile does not show any clear failure.

5.4.1 Ultimate Capacity

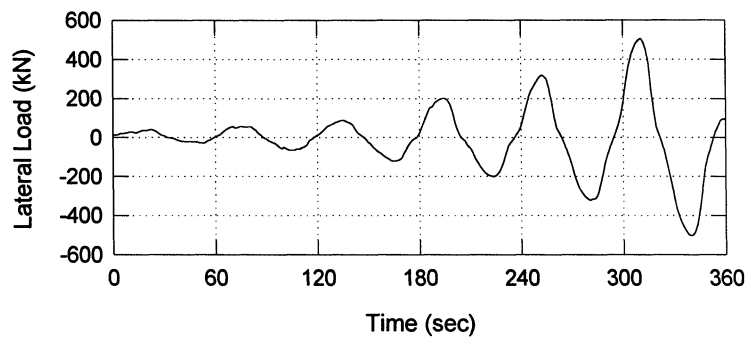
The load-displacement response of the free-head pile (figure 5-3) did not show clear failure even at large displacements. Hence, the pile may not have reached its ultimate capacity. At the final displacement amplitude used of about 11 cm, the lateral load carried by the pile was about 500 KN.

In many practical cases, the design of piles for lateral loading depends on satisfying a limiting lateral deflection requirement. This results in specification of the allowable lateral loads that are much less than the ultimate lateral capacity of the foundation. McNulty (1956) suggested a safe allowable lateral force of about 31 KN for a 40-cm diameter free-head concrete pile, based on a safety factor of 3 applied to the load required for 0.635-cm ($\frac{1}{4}$ in) deflection. The CALTRANS Bridge Design Aids (1988) specifies 22.25 KN of lateral resistance at 0.635 cm deflection of a 30.5-cm diameter concrete pile driven in soil with a standard penetration resistance value, $N = 10$. Abcarius (1991) reported results of a full-scale lateral loading test on driven pile footings. For groups of 30.5-cm diameter steel pipe piles in sandy silt, the lateral load per pile for a 0.635-cm deflection was observed to be about 111 KN. At 30-g centrifugal acceleration, the pile modeled in Test PI approximately represents a typical Cast-in-Drilled-Hole (CIDH) concrete pile of 38.1-cm diameter (see Subsection 5.2). At a lateral displacement of 0.7 cm, the lateral load taken by the pile in Test PI was about 62 KN, which is within the range of the values reported in the literature. The maximum load observed by Abcarius

(a) Lateral Displacement vs. Time for Test PI



(b) Lateral Load vs. Time for Test PI



(c) Load vs. Displacement for Test PI

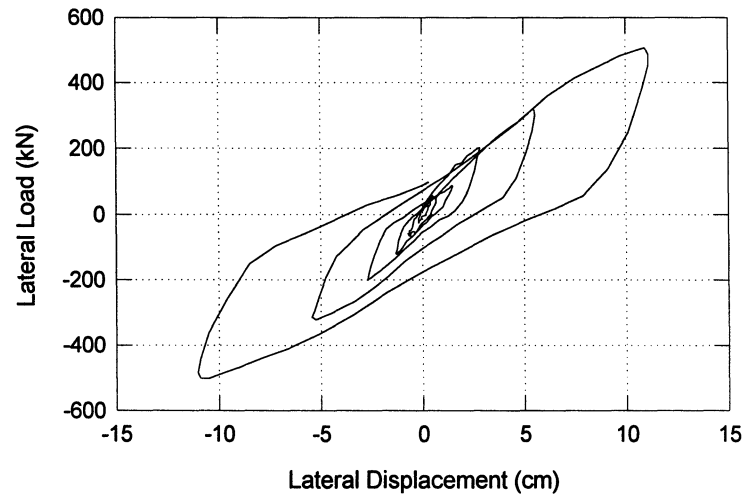


FIGURE 5-3: Load-displacement response for Test PI in prototype scale.

(1991) for the experiment on pile groups in sandy silt described above, was about 402 KN per pile for a lateral deflection of about 12-cm. The observed maximum load in Test PI of 500 KN corresponding to 11-cm lateral displacement is similar to the field value observed by Abcarius.

The pile modeled in Test PI represents approximately a standard 40-cm (16-in) CIDH (Cast-in-Drilled-Hole) pile described in the CALTRANS Bridge Design Aids (1988). The specified capacity of this pile for the allowable lateral displacement of 2.5-cm (1-in) is about 178 KN (40 Kip). This matches well with the measured lateral load of 196 KN for a lateral displacement of 2.8-cm in Test PI.

5.4.2 Secant Stiffness

The secant stiffness values measured in Test PI on the free-head pile are listed in table 5-1, along with the values for Tests CBSP and CBSPL on the cap-alone. These values are plotted against the corresponding displacement amplitudes in figure 5-4. All sides and the base were in contact with the soil in both tests on the cap. For low displacement amplitudes, the secant stiffness of the free-head pile (Test PI) is smaller than the corresponding stiffness of the cap (Tests CBSP and CBSPL). In all tests, the secant stiffness decreases with increasing displacement amplitudes. However, in the tests of cap-alone, this stiffness reduction is much faster than in the test of pile-alone. Eventually, for displacement amplitudes of more than 3 cm, the stiffness of the cap becomes smaller than that of the pile. That is, unlike the cap, the pile retains much of its initial stiffness at larger displacement amplitudes.

In the CALTRANS Bridge Design Aids (1988), a pile head stiffness of 70 KN/cm (40 Kips per inch deflection) is recommended for a standard 40-cm (16 in) diameter CIDH (Cast-in-Drilled-Hole) pile having bending stiffness 2.8×10^{11} N-cm² (9.7×10^9 in²-lb). The pile modeled in Test PI approximately represents a Cast-In-Drilled-Hole (CIDH) concrete pile of 38.1-cm diameter, and flexural stiffness 3.23×10^{11} N-cm² at 30-g centrifugal acceleration, which is approximately equivalent to the standard pile considered by CALTRANS. At normal working load levels (pile-head deflection between

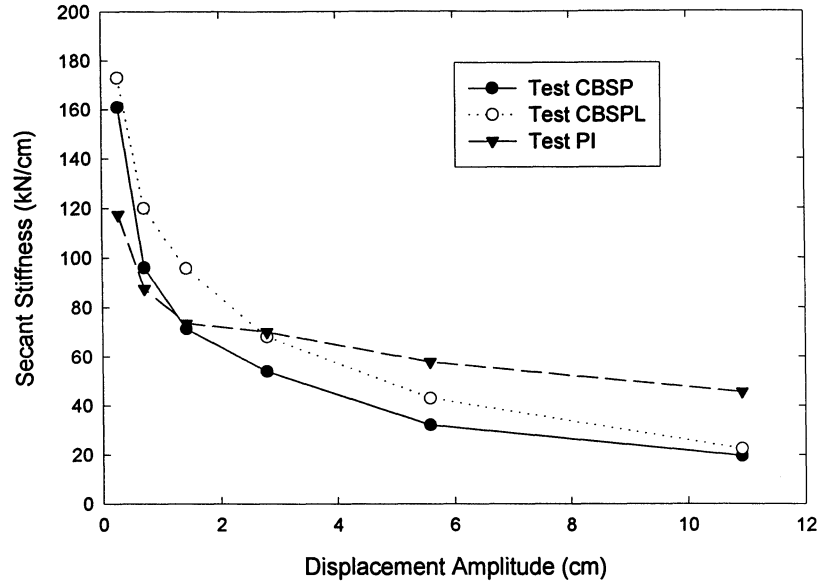


FIGURE 5-4: Stiffness versus displacement amplitude in prototype scale.

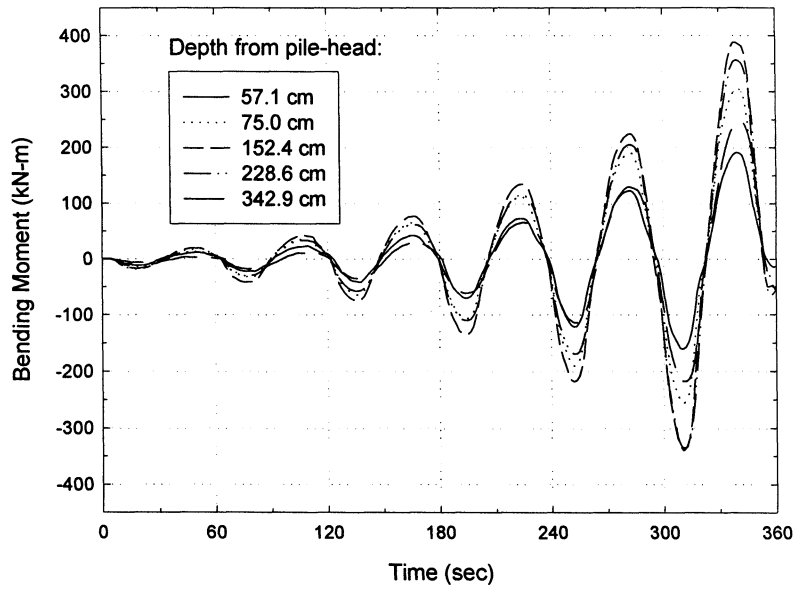


FIGURE 5-5: Measured bending moments versus time in Test PI in prototype scale.

TABLE 5-1: Secant stiffness for loops of increasing displacement amplitude in Test CBSP, Test CBSPL, and Test PI.

Loop No.		1	2	3	4	5	6
Displacement Amplitude, ρ (cm)		0.3	0.7	1.4	2.8	5.6	10.9
Stiffness K_{test} (KN/cm)	K_{CBSP}	161	96.1	71.3	53.9	32.1	19.5
	K_{CBSPL}	173.1	120.1	95.8	68.1	43	22.3
	K_{PI}	117.3	87.5	73.5	70	58	45.5

TABLE 5-2: Material damping for loops of increasing amplitude.

Test	Loop	1	2	3	4	5	6
	ρ (cm)	0.3	0.7	1.4	2.8	5.6	10.9
P	Area (KN-cm)	10.6	51.0	125.5	525.5	1768	6371
	β_{eq}	0.18	0.18	0.13	0.15	0.16	0.19
CBSP	Area (KN-cm)	21.1	83.8	267.5	825.8	2324.2	6880.6
	β_{eq}	0.28	0.30	0.30	0.31	0.37	0.47
CBSPL	Area (KN-cm)	21.5	91.9	300.0	962.1	3244.2	8027.5
	β_{eq}	0.24	0.24	0.25	0.29	0.38	0.48

TABLE 5-3: Comparison of measured and calculated pile-head shear forces.

Displacement Amplitude, ρ (cm)		0.3	0.7	1.4	2.8	5.6	10.9
Pile-head Lateral Load for Test PI (KN)	Measured in Test PI	32.9	57.9	102.8	195.8	323.1	507.3
	Calculated using LPILE	31.1	61.0	104.6	179.0	289.2	498.4

1.3 and 2.5 cm) the measured secant stiffness (74-70 KN/cm) is very consistent with the recommended value of 70 KN/cm.

5.4.3 Material Damping

The areas of loops for different displacement amplitudes are listed in table 5-2 for Tests PI, CBSP, and CBSPL. These areas represent energy dissipated per cycle within the sand and at the sand-foundation interfaces. For all displacements, the areas of loops in Test PI on the free-head pile are less than the corresponding areas of loops for Tests CBSP and CBSPL on cap-alone, indicating that more energy is dissipated through cap-soil interaction than through pile-soil interaction. This is consistent with the observation made before from inspection of the corresponding load-displacement plots that the response of the pile was much more linear than that of the cap. Table 5-2 also lists the equivalent damping ratios (β_{eq}) calculated using (4-3). Again, the damping ratios are much smaller for the free-head pile than the cap, for all displacement amplitudes.

5.4.4 Measured Bending Moments

The bending moments recorded during Test PI by the strain gages glued to the pile at different depths are shown in figure 5-6. The moments recorded by all strain gages are in phase. As the pile-head displacement amplitude increases, the recorded maximum bending moment in the pile increases. The bending moment distributions along the length of the pile are shown in figure 5-6 for different displacement amplitudes of the pile-head. The pile-head bending moments (at depth zero) are assumed to be zero, as it is a free-head pile. The measured bending moments seem to be consistent with the free-head pile condition.

5.5 DETERMINATION OF p-y CURVES FOR THE SOIL

The equilibrium equation for the lateral loading of a pile is:

$$E_p I_p \frac{d^4 y}{dz^4} - p = 0 \quad (5-1)$$

where $E_p I_p$ = Flexural Rigidity of the pile; p = soil reaction per unit length of pile; and y = lateral deflection of the pile at depth z from the pile-head. The nonlinear lateral soil spring at a given depth is typically specified as a p - y curve.

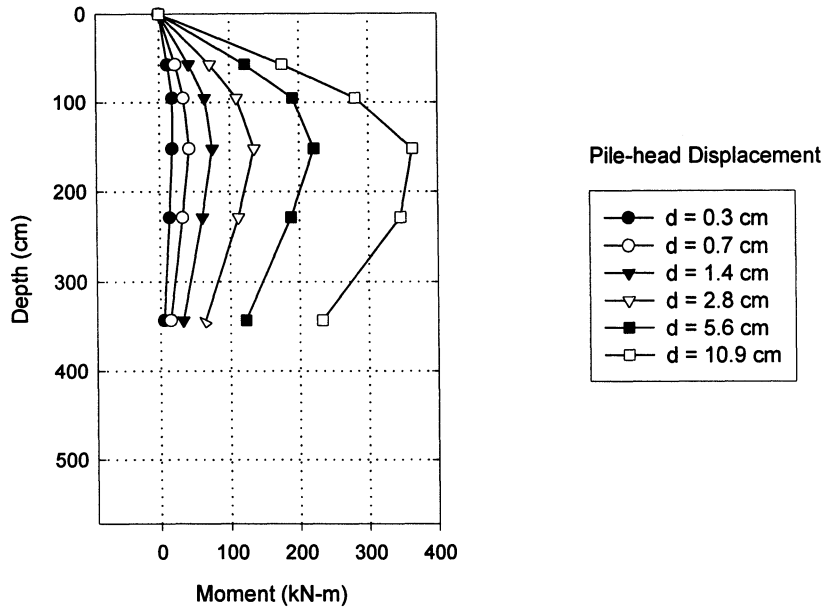


FIGURE 5-6: Measured prototype bending moments along the length of the pile in Test PI.

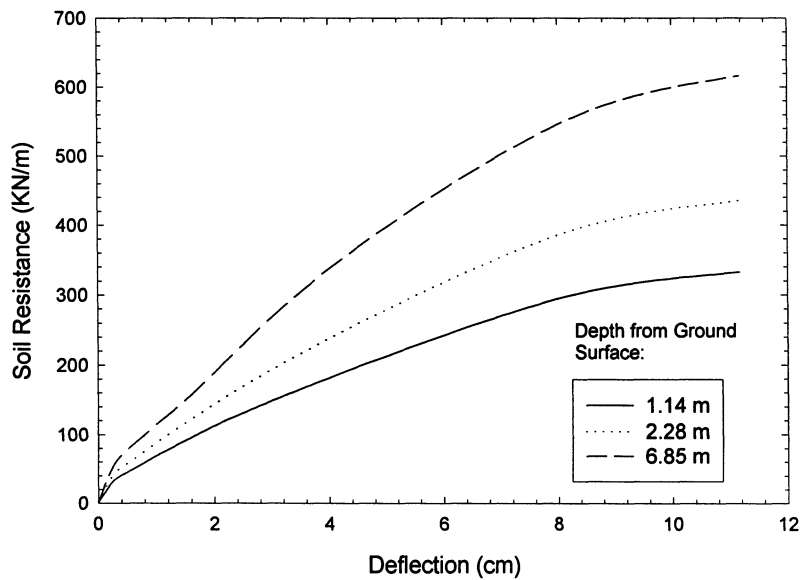


FIGURE 5-7: p-y curves for the soil backfigured from the results of Test PI in prototype scale.

$$p = -K_{hd} \cdot y \quad (5-2)$$

where K_{hd} is the equivalent nonlinear horizontal soil spring. The p-y curves for various soil types have been empirically determined from field lateral loading tests on instrumented piles (Reese and Wang, 1993). Liu and Dobry (1995) and Dobry et al. (1995) reported a technique for determination of p-y curves from centrifuge experiments. A similar approach was used to develop the p-y curves from the results of the free-head pile Test PI, using the laterally loaded pile analysis package LPILE (Reese and Wang, 1993). The p-y curves for the soil, backfigured from the results of Test PI are shown in figure 5-7. The slope of the p-y curves increases with depth, which is typical for sands. The curves of bending moment versus depth for different pile-head displacement amplitudes, calculated with LPILE using the p-y curves in figure 5-7, are plotted in figure 5-8, along with the measured bending moments in Test PI (data points). The calculated and measured values match well, confirming the validity of the p-y curves selected. Table 5-3 compares the corresponding calculated (by LPILE) and measured pile-head shear force values for Test PI, again with very good agreement.

The initial tangent and secant slopes of the p-y curves in figure 5-7, backfigured from Test PI, are much smaller than those recommended by usual methods (Reese and Wang, 1993; American Petroleum Institute, 1987). Several other researchers, investigating the lateral response of pile foundations in sand using centrifuge tests, have observed a similar trend. Scott (1979) simulated the Mustang Island field tests reported by Reese et al. (1974) in the centrifuge. A comparison of the model test with the prototype lateral load test indicated that at similar loads, scaled model deflections were 50% higher than the prototype deflections. Bouafia and Garnier (1991) performed an experimental study to determine p-y curves for piles in sand. They found that the soil stiffness values (initial and secant modulus of the p-y curves backfigured from the tests) were several times smaller than those recommended in usual methods based on density index and angle of shearing resistance. This discrepancy is attributed to differences between deformability of sands in the field, and sands reconstituted at the same density in laboratory, due to aging, overconsolidation and horizontal stress level effects, as well as to the fact that the field tests were typically done on driven piles while model tests in the laboratory including

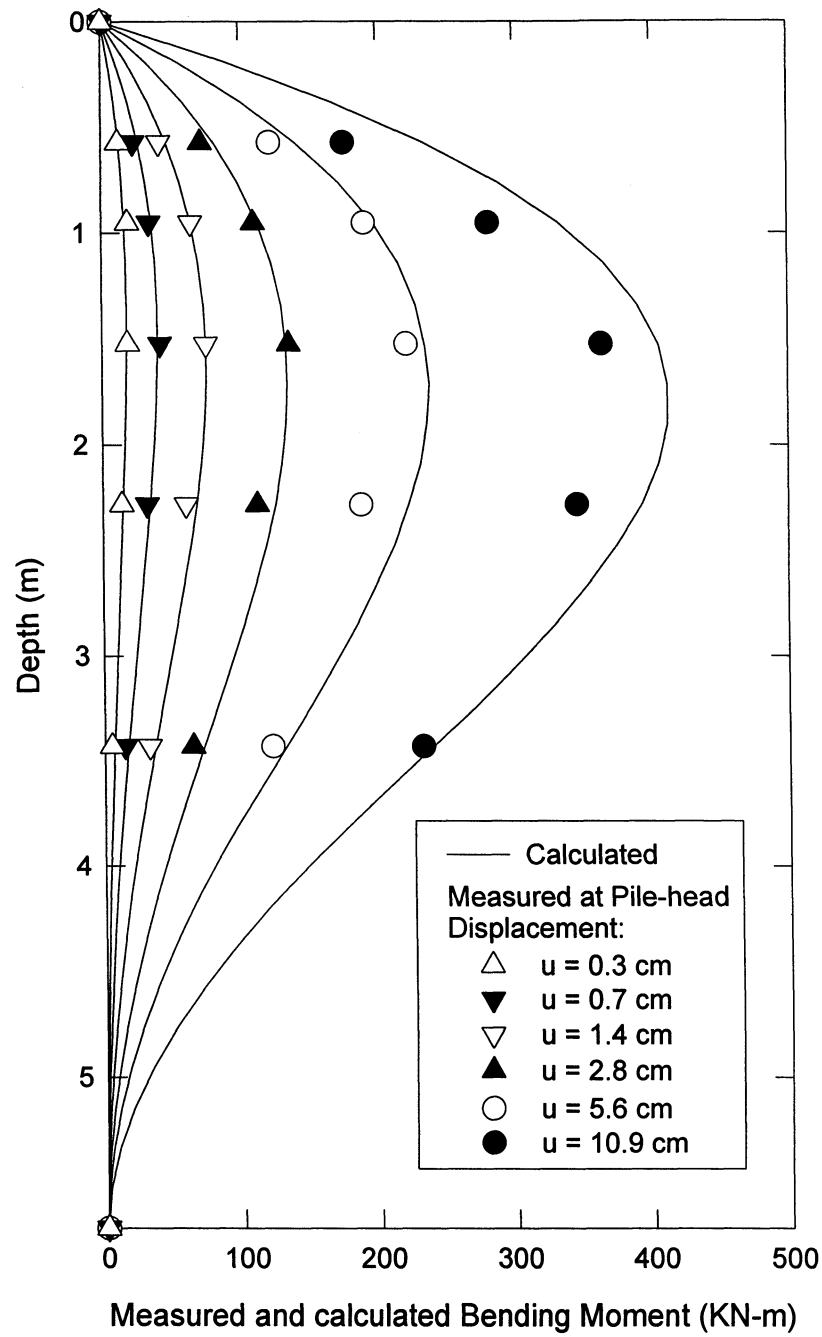


FIGURE 5-8: Measured and calculated bending moments for Test PI.

those reported here, correspond more closely to a drilled pile condition. Bouafia and Garnier give p-y curves, backfigured from a centrifuge test on a single free-head pile in dense dry sand with diameter 0.5 m, flexural rigidity 56 MN-m², and length 5 m in prototype scale. These p-y curves are plotted in figure 5-9 along with the p-y curves backfigured from Test PI. The p-y curves backfigured from Test PI seem to be reasonably consistent with the p-y curves obtained from the results of Bouafia and Garnier.

5.6 COMPARISON OF EXPERIMENTAL RESULTS WITH THEORY

5.6.1 Initial Secant Stiffness

Whitman and Dobry (1993) gave an equation for the equivalent-static horizontal spring stiffness (K_{hf}) of a free-head pile.

$$K_{hf} = K_h - \frac{K_{hr}^2}{K_r} \quad (5-3)$$

where K_h is horizontal stiffness; K_r is the rocking stiffness; and K_{hr} is horizontal rocking coupled stiffness. For a linear homogeneous half-space and a long pile, these stiffness values are, approximately (Whitman and Dobry, 1993; Gazetas, 1991a):

$$K_h \approx d \cdot E_s \cdot \left(\frac{E_p}{E_s} \right)^{0.21} \quad (5-4)$$

$$K_r \approx 0.15 \cdot d^3 \cdot E_s \cdot \left(\frac{E_p}{E_s} \right)^{0.75} \quad (5-5)$$

$$K_{hr} \approx -0.22 \cdot d^2 \cdot E_s \cdot \left(\frac{E_p}{E_s} \right)^{0.50} \quad (5-6)$$

In these equations, E_s and E_p are elastic moduli of soil and pile; and d is pile diameter. These equations are valid for long piles satisfying the following conditions:

$$\frac{L}{d} \geq 10 \quad (5-7)$$

$$\frac{L}{d} \geq 1.5 \left(\frac{E_p}{E_s} \right)^{0.25} \quad (5-8)$$

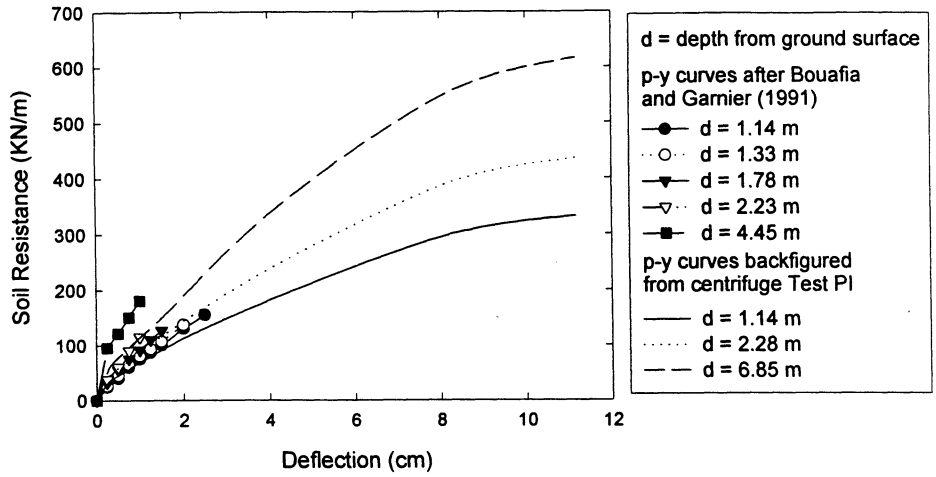


FIGURE 5-9: Comparison of p-y curves backfigured from centrifuge Test PI with the p-y curves modified after Bouafia and Garnier (1991).

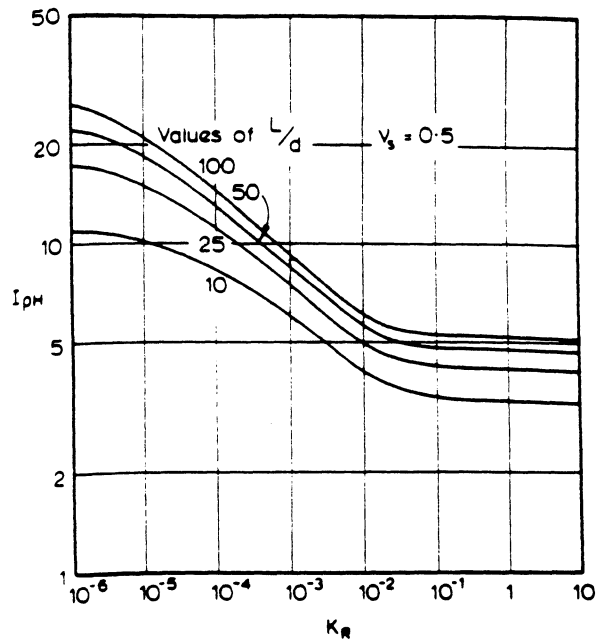


FIGURE 5-10: Correlation chart for $I_{\rho H}$ (after Poulos and Davis, 1980).

where L is the length of the pile. Since the model pile used in centrifuge Test PI was a hollow pipe, the equivalent solid circle Young's modulus E_{pe} must be used in the above equations, where E_{pe} is

$$E_{pe} = \left[1 - (d_i/d_o)^4\right]E_p \quad (5-9)$$

and d_i and d_o are respectively inner and outer diameters of the pile. Using (5-3) to (5-6), and the parameters listed in table 5-4, we get a value of equivalent horizontal stiffness for the free-head pile equal to 111.8 KN/cm, which matches well with the initial secant stiffness value of 117.3 measured in the centrifuge Test PI. These parameters also satisfy the "long pile" criteria given by (5-7) and (5-8). In table 5-4, the soil Young's modulus, $E_s = 11.5$ MPa and the corresponding soil shear modulus $G = 4.26$ MPa were backfigured from the measured initial pile stiffness of 117.3 KN/cm using (5-3) to (5-9) and a Poisson's ratio $\nu = 0.35$. These are equivalent uniform values of elastic soil moduli. The value of shear modulus backfigured from Test PI (4.26 MPa) is about 2.5 times higher than the value obtained from the cap-alone experiments (1.73 MPa) in Section 4 (see Subsection 4.5 and table 4-4). This may be due to the fact that in the test on pile, the lateral resistance is provided by deeper soil strata subjected to higher confining pressures, as compared to the tests on the cap. Also, the shear strain amplitudes in the soil adjacent to the foundation, at least for greater depths, may not be as high as in case of the tests on the cap-alone.

For a pile in linear soil, the horizontal soil spring, K_{hd} , given by (5-2) is approximately proportional to the soil Elastic Modulus, with $K_{hd} = \delta E_s$, where $\delta \approx 1$ to 1.4 (Whitman and Dobry, 1993). The initial values of K_{hd} obtained from the p-y curves shown in figure 5-7 range from 12.4 MPa at the pile-head to 18.8 MPa at the bottom of the pile. Considering an average uniform value of $K_{hd} = 15.6$ MPa, and using the value of soil elastic modulus backfigured in the earlier analysis, $E_s = 11.5$ MPa (table 5-4), we get $\delta = 1.35$, which is within the specified range.

5.6.2 Lateral Load Deflection Characteristics

Poulos and Davis (1980) provided solutions for a floating pile in soil with uniform elastic modulus, E_s , and limiting soil pressure, p_y . For a free-head pile of length L and diameter

TABLE 5-4: Parameters used for initial stiffness calculations.

Pile Parameters:	Length, L	5.715 m
	Outer diameter of the pile, $d = d_o$	38.1 cm
	Inner diameter of the pile, d_i	32.8 cm
	Young's Modulus, E_p	6.9×10^4 MPa
	Flexural Rigidity, $E_p I_p$	3.23×10^{11} N-cm ²
	Equivalent solid circle Elastic Modulus, E_{pe}	3.1×10^4 MPa
Soil Parameters:	Young's Modulus, E_s	11.5 MPa
	Shear Modulus, G	4.26 MPa
	Poisson's Ratio, ν	0.35
	Friction Angle, ϕ	39°

TABLE 5-5: Calculation of lateral load-deflection curve for Test PI according to Poulos and Davis (1980) recommendations.

H (KN)	H/H _u	F _p (from figure 5-11)	ρ (cm) (calculated using (5-10))	ρ (cm) (measured)
32.9	0.04	1	0.35	0.3
58.5	0.08	1	0.62	0.7
102.8	0.14	1	1.1	1.4
195.8	0.27	0.91	2.3	2.8
323.1	0.45	0.72	4.8	5.6
507.0	0.71	0.45	12.0	10.9
571.0	0.8	0.35	17.4	--
643.0	0.9	0.28	24.4	--

d, subjected to a horizontal load H at the top with no eccentric loading, the pile-head displacement is given as:

$$\rho = \frac{H \cdot I_{\rho H}}{E_s L \cdot F_\rho} \quad (5-10)$$

where $I_{\rho H}$ = elastic influence factor for displacement caused by horizontal load; and F_ρ = yield-displacement factor = ratio of pile displacement in elastic soil to pile displacement in yielding soil. The elastic influence factor, $I_{\rho H}$, is a function of L/d ratio for the pile and of the pile-flexibility factor K_R given by:

$$K_R = \frac{E_p I_p}{E_s L^4} \quad (5-11)$$

The yield displacement factor F_ρ is primarily a function of K_R and of the applied load level expressed by the dimensionless ratio H/H_u , where H_u is the ultimate lateral-load capacity of the pile if failure occurs by failure of the soil rather than pile. Correlation charts for $I_{\rho H}$ and F_ρ given by Poulos and Davis (1980) are reproduced in figures 5-10 and 5-11 respectively. For the free-head pile in Test PI, using the parameters in table 5-4, in conjunction with (5-11), we get $K_R = 2.64 \times 10^{-3}$. Using the chart for $I_{\rho H}$ in figure 5-10, for $K_R = 2.64 \times 10^{-3}$ and $L/d = 15$, we get $I_{\rho H} = 7$. Poulos and Davis provide recommendations for obtaining $H_u/p_y L d$ ratio for the soil. This ratio is about 0.4 according to these recommendations, assuming a uniform p_y distribution. Poulos and Davis prescribe the use of Broms's recommendation to get average p_y for soil. Following Broms's (1964) suggestion for cohesionless soil, the average limiting soil pressure p_y is given as $p_y = 3 p_p$, where p_p is the passive pressure halfway along the embedded part of the pile. Using the parameters in table 5-4 in conjunction with the above recommendations, we get a predicted value of ultimate load, $H_u = 714.4$ KN. The subsequent calculations for the load-deflection curves, using (5-10) and figure 5-11, are given in table 5-5. The measured and calculated deflections match well. These measured and calculated load-deflection curves for Test PI are shown in figure 5-12, with excellent agreement.

5.6 CONCLUSIONS

The conclusions of this section from centrifuge Test PI are as follows:

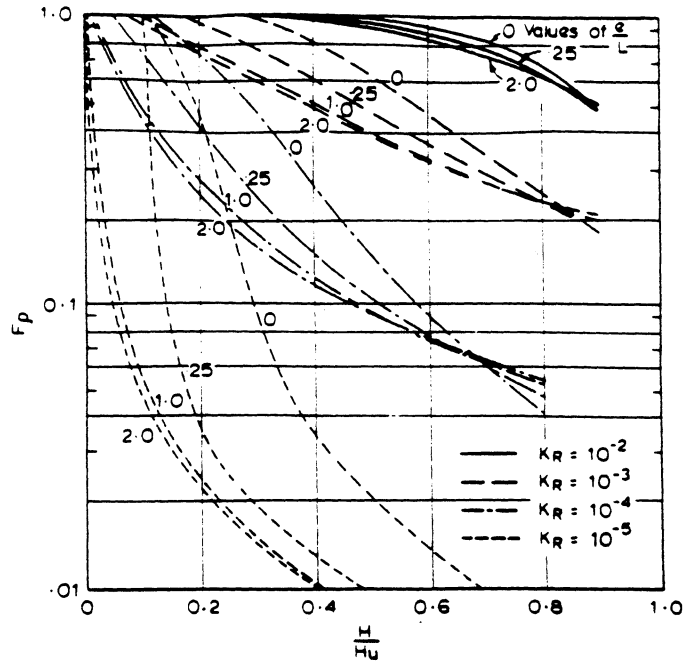


FIGURE 5-11: Correlation chart for F_p (after Poulos and Davis, 1980).

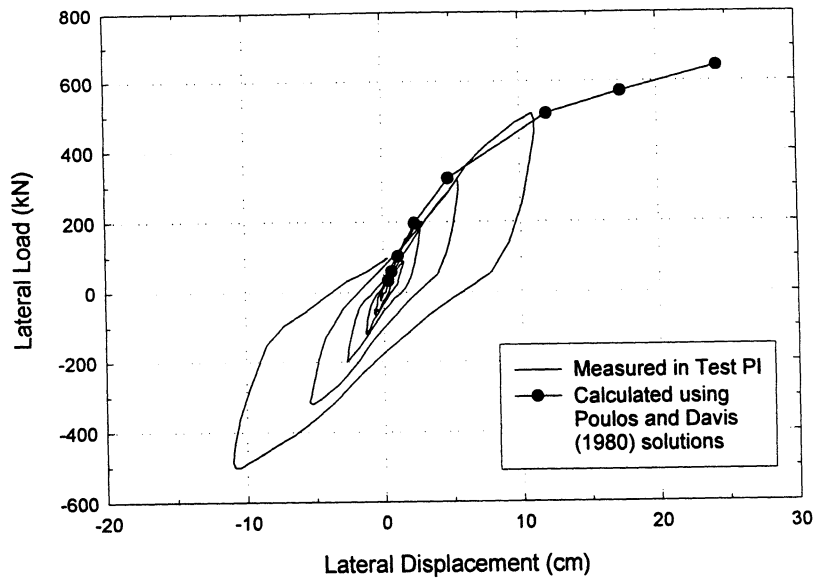


FIGURE 5-12: Measured and calculated load-deflection curves for Test PI.

1. The lateral response of the free-head pile is much more linear than that of the cap-alone.
2. The ultimate capacity of the pile was not reached in the test, but the measured allowable lateral force (corresponding to a static limiting lateral displacement of 0.635 cm), compares well with the observed values in field experiments, as well as values recommended in the literature for this type of piles. The measured lateral load for 2.8-cm lateral displacement (196 KN) matches well with the lateral pile capacity of 178 KN or 40 Kip, specified by the CALTRANS Bridge Design Aids (1988) for a 2.5-cm (1-in) deflection of the standard 40-cm (16-in) diameter pile.
3. For small displacement amplitudes, the measured secant stiffness of the pile is smaller than the measured value for the cap. For displacements greater than about 3 cm, the stiffness of the pile becomes greater than that of the cap. The pile retains much of its stiffness even at large displacements. The measured secant stiffness for 2.8-cm deflection (70 KN/cm) matches well with the value recommended by CALTRANS of 70 KN/cm (40 Kip/in) for the standard pile.
4. A reasonable set of p-y curves at different depths was backfigured from the results of the free-head pile test, which, in conjunction with program LPILE, predicted well both the measured bending moments along the pile, and the measured lateral load-displacement relationship at the pile-head.
5. The measured initial secant stiffness and lateral load-deflection characteristics agree well with the solutions provided in the literature.

SECTION 6

CENTRIFUGE TESTS ON PILE-CAP SYSTEM

6.1 INTRODUCTION

In order to evaluate the response of the entire pile-cap system, two centrifuge tests were performed on a model of the pile-cap foundation system in dry sand. The centrifuge tests conducted on the cap-alone and the free head pile-alone were described in Sections 4 and 5, respectively. A similar experimental setup and dimensions of the pile and cap were used in the tests on the pile-cap system described in this section. This facilitated direct comparison of the results of all centrifuge tests. All centrifuge tests performed on the cap, pile, and pile-cap system are given in table 6-1, repeating some of the information already provided in the previous sections.

In this section, centrifuge Tests PCBSP and PCBSPi performed on models of the entire pile-cap system are described. The results of these centrifuge tests are compared with the corresponding results of the cap-alone and free-head pile experiments.

6.2 MODEL CONFIGURATION

Two centrifuge tests, Tests PCBSP and PCBSPi, were performed on a model of the pile-cap system in dry Nevada sand of 75% relative density, at 30-g centrifugal acceleration. The pile was modeled with an aluminum pipe of external diameter 12.7-mm, wall thickness 0.9-mm, and length 19-cm, representing a prototype pile of diameter 38.1-cm, length 5.72-m, and flexural rigidity 3.23×10^{11} N-cm². The dimensions of the pile were the same as in Test PI of free-head pile, previously reported in Section 5. The cap was modeled with a rigid aluminum block of dimension 38-mm (L) x 38-mm (B) x 28-mm (D), similar to the tests on cap-alone covered in Section 4. Sand was glued to the sides and the base of the cap to simulate a rough concrete surface. Similar to Test CBSP on the cap-alone, all sides and base of the cap were in contact with the soil, with 1-cm soil

confinement above the top rim of the model cap. A confining box similar to the one used in Test CBSP was used to retain the soil above the top edge of the cap.

The pile was rigidly clamped to the cap, with this rigid connection not allowing for any relative rotation of the pile with respect to the cap. The pile-cap system model is shown schematically in figure 6-1. No strain gages were used in Test PCBSP; on the other hand, in Test PCBSP, strain gages were installed on the model pile to measure bending moments along the pile length. The pattern of strain gages used in Test PCBSP and shown in figure 6-1, was similar to that used in Test PI on the free-head pile (see Section 5). This captured the rapid changes in bending moment near the pile-head.

6.3 MODEL CONSTRUCTION AND TESTING PROCEDURE

The procedure for model construction and centrifuge testing was similar to the tests on cap-alone and pile-alone reported earlier. The following steps were used for model construction:

1. Dry sand with relative density of about 75% was deposited in layers of thickness 6 cm or less. The amount of sand needed for each layer to achieve required density was weighed, and sand was rained through air in the container.
2. Once the top surface of the sand reached about 11 cm from the bottom of the box, the model of the pile-cap system with loading rod was placed in the box. The model was held vertical with the help of specially designed clamps. The model and loading rod were positioned such that the loading rod would be in a vertical alignment with the hole in the bearing plate of the lateral loading assembly, when the housing plate was placed on top of the container. Sand was rained around the model, maintaining the required density. The clamps were removed when the sand surface reached near the bottom of the cap.
3. The confining box was placed around the cap to retain soil vertically above the top rim of the cap, similar to Test CBSP on cap-alone. Sand was deposited around the cap and the confining box, until the soil surface reached about 1 cm above the top edge of the cap.

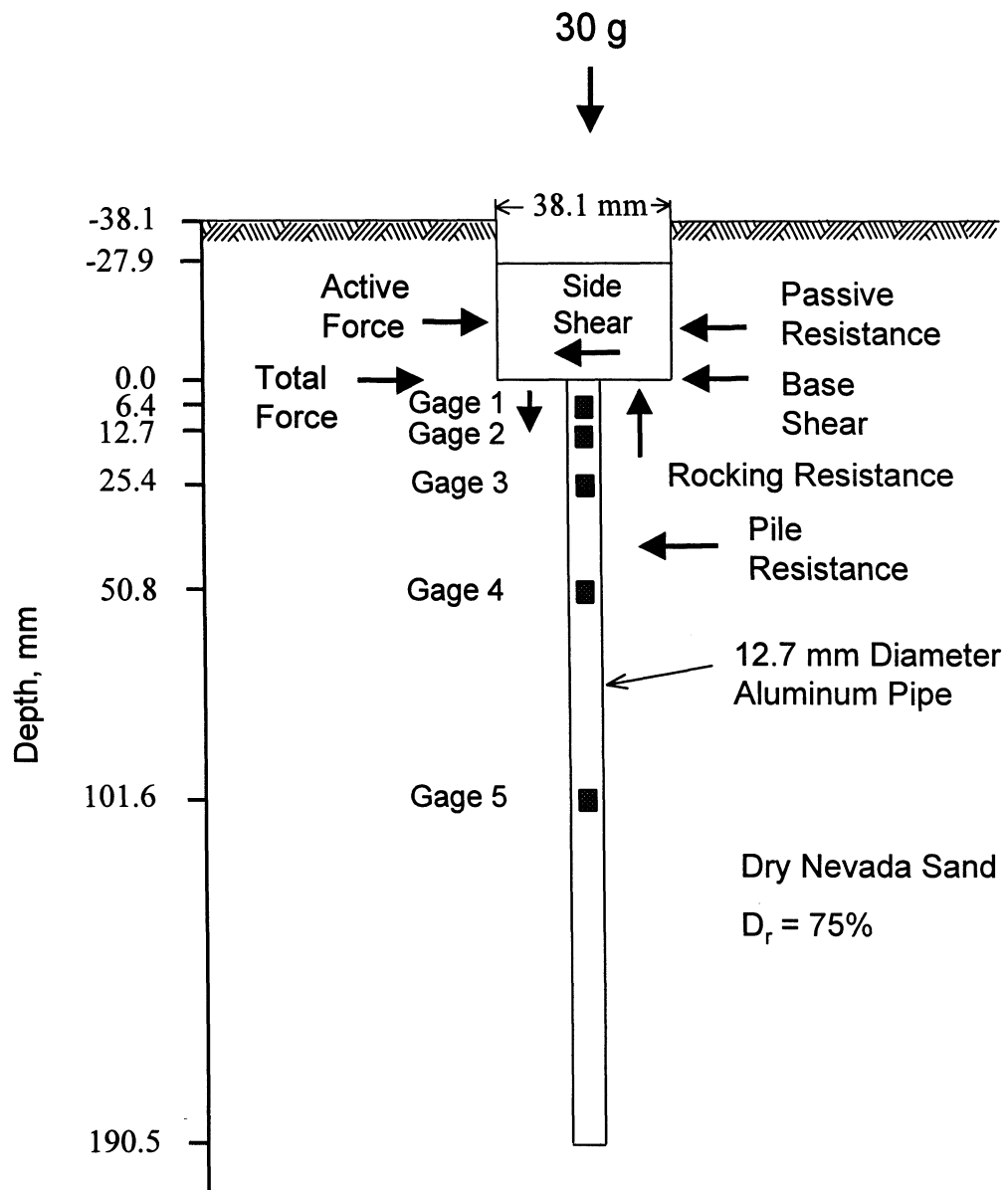


FIGURE 6-1: Model of pile-cap system used in Test PCBSPI.

4. The thick housing plate, bearing the lateral loading assembly, was placed on top of the model container, ensuring that the loading rod was inserted in the central hole of the bearing plate. Specially designed clamps were used to keep the loading rod vertical, and to eliminate any model disturbance during this process. The clamps were removed when the housing plate was secured to the model container.
5. The loading rod was clamped to the bearing plate confirming that the rounded end of the loading rod was located at the pile-head. This arrangement ensured that no moments were transmitted to the pile-head. The housing plate was fitted to the model container with screws. The general final setup is schematically shown in figure 6-2.
6. The model was then transported to the centrifuge basket with the help of a forklift.

The testing procedure for the tests on the pile-cap system was similar to the general procedure for tests on cap-alone described in Section 4, and for the free-head pile in Section 5. Lateral displacement cycles of increasing amplitude were applied to the model, using a servo controlled feedback system. The load-displacement response was recorded using a load-cell and a displacement transducer (LVDT). In addition, in Test PCBSP, the bending moments along the length of the pile were recorded by the strain-gages located on the pile.

6.4 TEST RESULTS

The results of centrifuge Tests PCBSP and PCBSP are presented in this subsection. These results, and the data presented in the following subsections are in prototype scale, unless specified otherwise. Tests PCBSP and PCBSP were identical, except for the fact that in Test PCBSP the pile was instrumented with strain gages, for measurement of bending moments. The load-displacement response measured in Tests PCBSP and PCBSP are given, respectively, in figures 6-3 and 6-4. The response of both tests is similar, which serves to demonstrate test repeatability. The load-displacement loops are sharper than the loops for the tests on the cap-alone, described in Section 4, but flatter than the loops for the test on the free head pile-alone of Section 5. This is reasonable, as the response of the pile-cap system should be a combination of two systems or springs

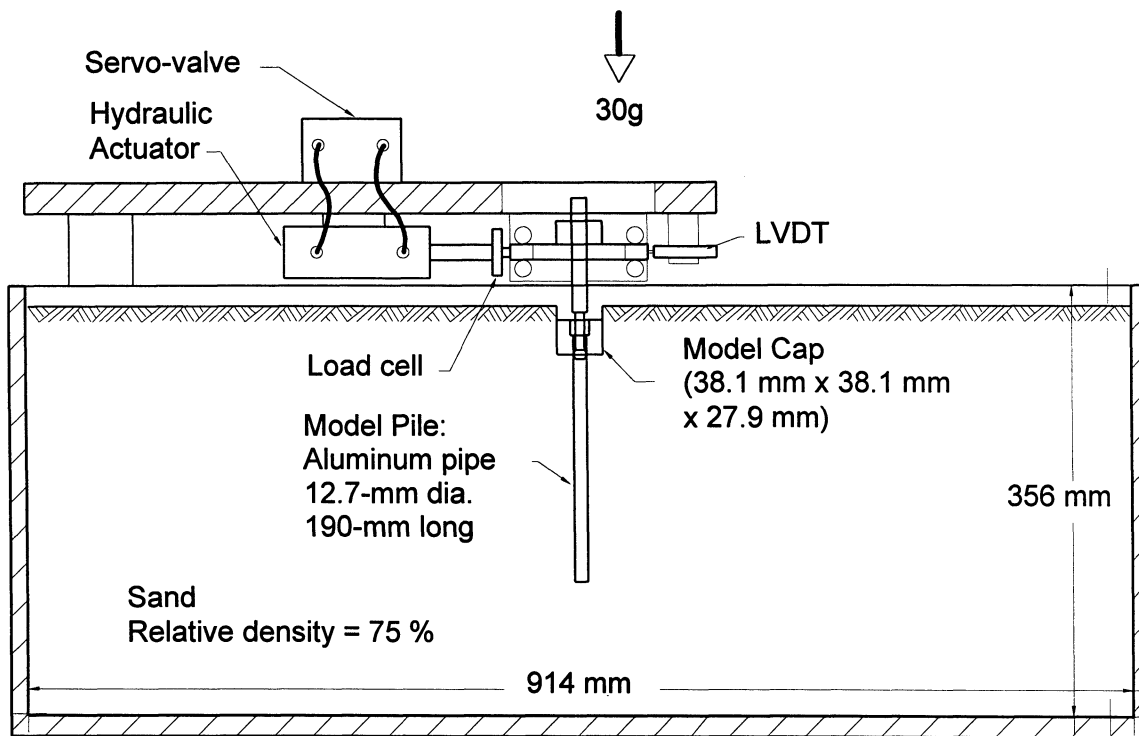


FIGURE 6-2: Set-up for centrifuge tests on pile-cap system.

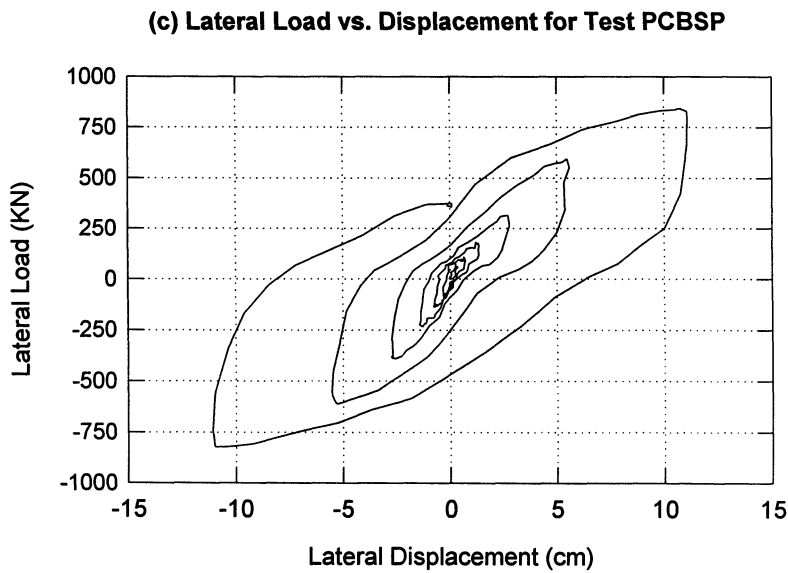
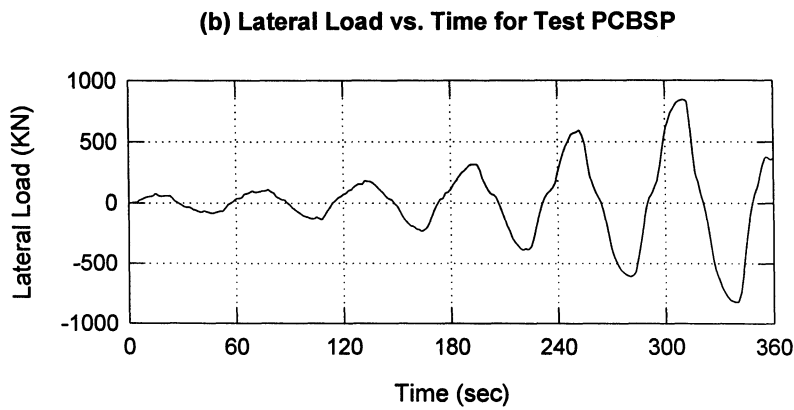
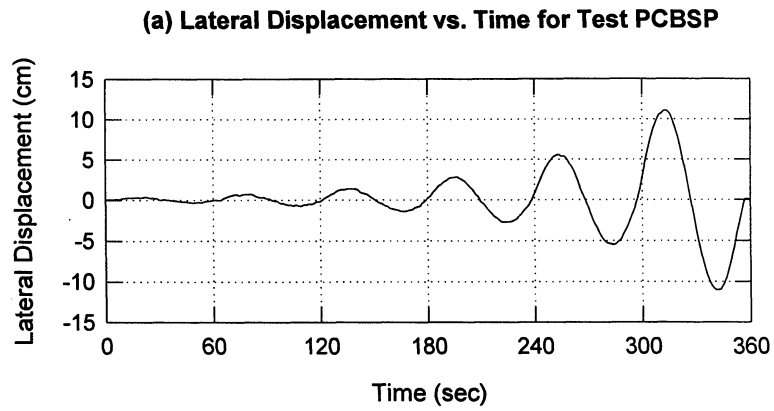
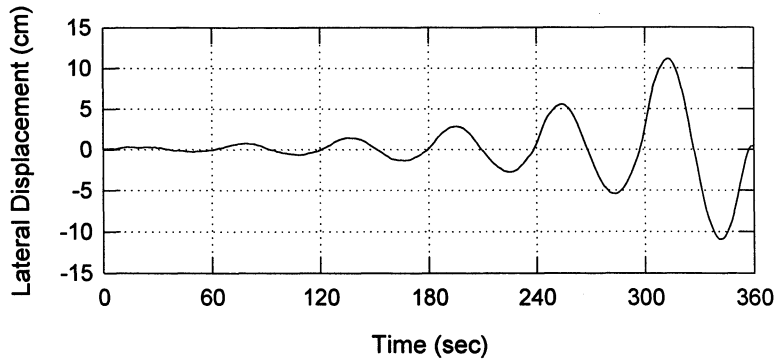
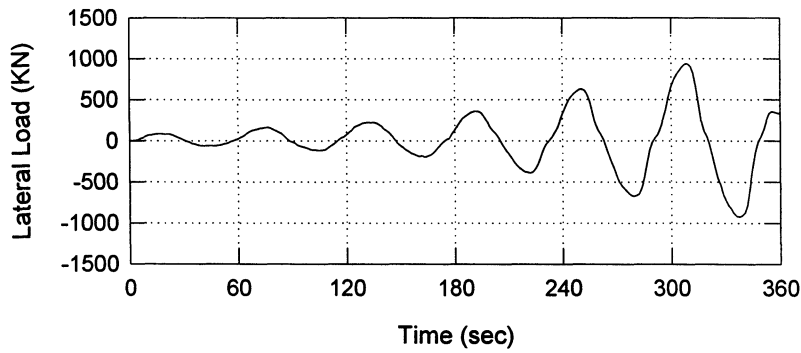


FIGURE 6-3: Measured load-displacement response for Test PCBSP in prototype scale (pile-cap system).

(a) Lateral Displacement vs. Time for Test PCBSP1



(b) Lateral Load vs. Time for Test PCBSP1



(c) Lateral Load vs. Displacement for Test PCBSP1

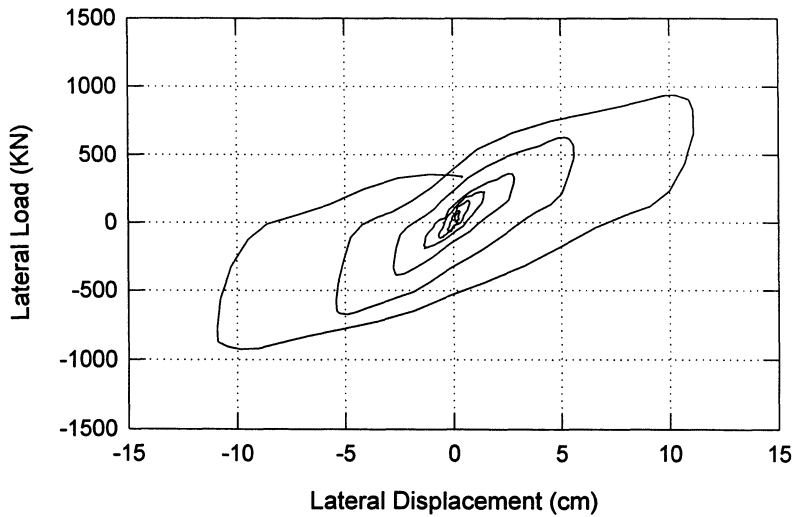


FIGURE 6-4: Measured load-displacement response for Test PCBSP1 (pile-cap system with instrumented pile).

more or less in parallel: the approximately elastoplastic spring representing the cap, and the more or less linear spring representing the pile.

6.4.1 Ultimate Capacity

The measured ultimate capacities of all centrifuge tests are listed in table 6-1. These ultimate capacities are the loads measured at a lateral deflection of about 11-cm. The ultimate capacities for Tests PCBSP and PCBSPI are 841 KN and 908 KN respectively, which are close as expected for identical tests. This capacity of the pile-cap system is about four times the capacity of the cap-alone in Test CBSP (214 KN). This indicates that at this limiting conditions the pile contributes significantly to the total response of the combined pile-cap system. At large displacements, deeper layers of soil around the pile provide lateral resistance, even though the soil at shallow depths around the cap and pile is expected to have failed. The measured ultimate capacities for Tests PCBSP and PCBSPI (841 to 908 KN) were both greater than the addition of the ultimate load values for Test CBSP on the cap-alone, and Test PI on the pile-alone (712 KN).

6.4.2 Secant Stiffness

The secant stiffness values at various displacement amplitudes measured in Tests PCBSP and PCBSPI on the pile-cap system are listed in table 6-2, and plotted in figure 6-5, together with values for Test CBSP on cap-alone, and Test PI on pile-alone. The secant stiffnesses for Tests PCBSP and PCBSPI are similar, again showing good repeatability. Table 6-2 also provides the ratio between the secant stiffness for Test PCBSPI (pile-cap system) and Test CBSP (cap-alone). This ratio starts with a value of 1.7 for the first cycle, and increases subsequently for loops of increasing displacement amplitude to about 4.3 for the last cycle. It can be speculated that as the displacement amplitude increases, the soil around the cap starts yielding, with much of the total stiffness arising from pile contribution.

The percent differences between the sum of stiffness values for Tests CBSP and PI, and the corresponding stiffness for Test PCBSPI are also given in table 6-2. Although the cap

TABLE 6-1: List of Centrifuge Tests Performed.

Test Code	Pile Contribution	Cap Contribution			Vertical Load at base* (KN)	Ultimate Lateral Resistance (KN)	Remarks
		Base Friction	Side wall Shear	Passive /active Force			
CB	NO	YES	NO	NO	53	44	$\mu \approx 0.82$
CBL	NO	YES	NO	NO	108	88	
CS	NO	NO	YES	NO	53	38	$K_s \approx 2.1$
CP	NO	NO	NO	YES	53	124	$K_p \approx 14.3$
CSP	NO	NO	YES	YES	53	165	
CBSP	NO	YES	YES	YES	53	214	
CBSPL	NO	YES	YES	YES	108	245	
PI	YES	NO	NO	NO	-	498	Free-head Instrumented pile
PCBSP	YES	YES	YES	YES	53	841	
PCBSPI	YES	YES	YES	YES	53	908	Instrumented pile

* This includes the cap's self weight and any additional static vertical load applied to the cap.

TABLE 6-2: Secant Stiffness for Loops of Increasing Displacement Amplitude.

Loop No.	1	2	3	4	5	6	
Displacement Amplitude, ρ (cm)	0.3	0.7	1.4	2.8	5.6	10.9	
Stiffness K_{test} (KN/cm)	K_{CBSP}	161	96.1	71.3	53.9	32.1	19.5
	K_P	117.3	87.5	73.5	70	58	45.5
	K_{PCBSP}	271.2	173.7	146.1	126.3	107.9	76.2
	K_{PCBSPI}	271.4	182.4	148.3	132.8	115.6	84.3
$\frac{K_{PCBSPI}}{K_{CBSP}}$	1.7	1.9	2.1	2.5	3.6	4.3	
$\frac{(K_{CBSP} + K_P) - K_{PCBSPI}}{K_{PCBSPI}}$ (%)	2.5	0.7	-2.4	-6.7	-22.1	-22.9	

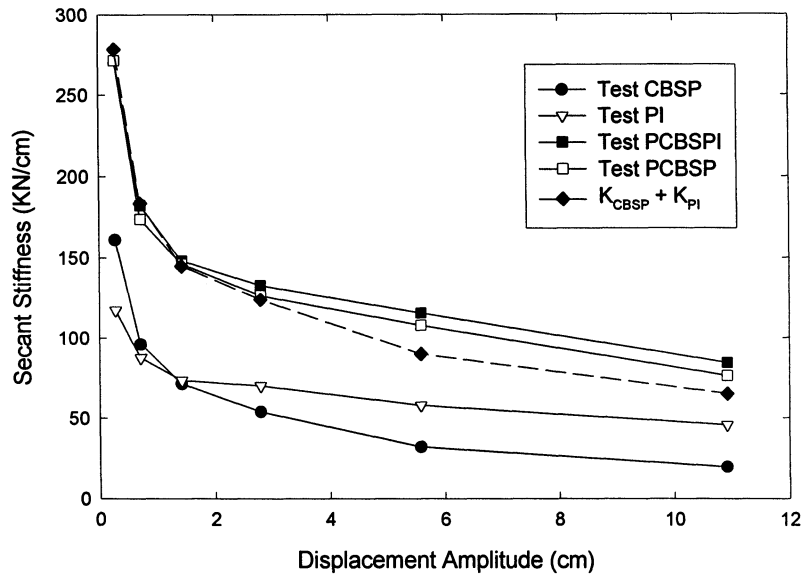


FIGURE 6-5: Measured secant stiffness versus displacement amplitude.

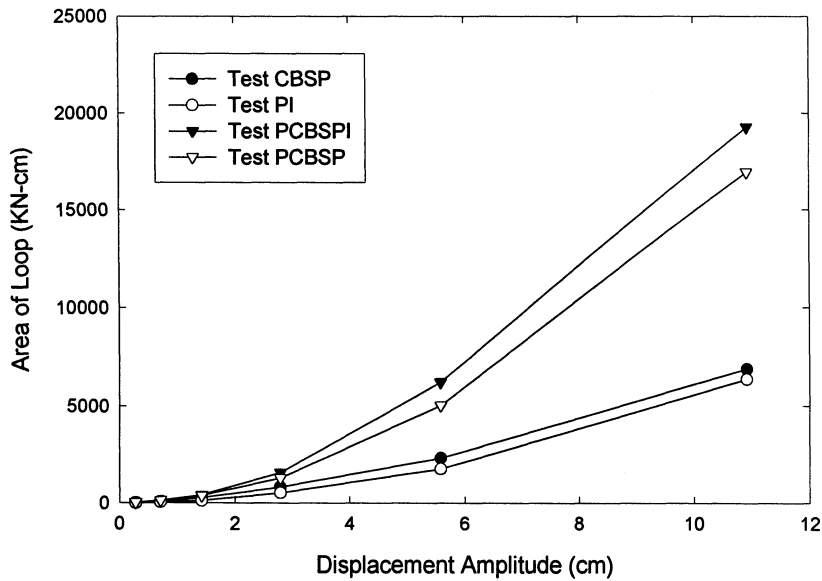


FIGURE 6-6: Measured area of loop versus displacement amplitude.

and the pile might have had different amounts of rotations during these experiments, and thus the validity of this addition rule is by no means guaranteed, for displacements up to 3 cm the difference was within 10 %. For larger displacement amplitudes of 5.6 cm and 10.9 cm, the stiffness for Test PCBSPI is 20-25 % higher than the sum of stiffnesses for Tests CBSP and PI. This fact is also evident from figure 6-5, which includes curve of the sum of secant stiffnesses from Tests CBSP and PI. This curve matches closely the curve for Test PCBSPI up to a displacement of about 2.8-cm, after that the two curves deviate.

6.4.3 Material Damping

The areas of loops for different displacement amplitudes measured in Tests CBSP, PI, PCBSPI, and PCBSPI are listed in table 6-3 and plotted in figure 6-6. Again, the areas of loops for Tests PCBSPI and PCBSPI are close as expected. For displacement amplitudes up to 2.8 cm, the sum of areas of loops for Tests CBSP (cap-alone) and PI (pile-alone) is approximately equal to the corresponding area of loop for Test PCBSPI. This “addition rule” does not hold good for larger displacement amplitudes. The areas of loops for displacements of 5.6 cm and 10.9 cm in Test PCBSPI are higher than the sums of corresponding areas of loops for Tests CBSP and PI. Table 6-3 also lists the equivalent damping ratios calculated using (4-3). As anticipated, the damping ratios for Tests PCBSPI and PCBSPI increase very slowly with amplitude, and are somewhere between the corresponding values for Tests CBSP and PI.

6.4.4 Measured Bending Moments

The bending moments recorded by strain gages at different locations along the length of the pile for Test PCBSPI are plotted in figure 6-7. The moments recorded by gages 2 to 5 were in phase. Shallow strain gage 1 recorded out-of-phase moments for a few initial cycles. However, for the final cycles, the moments recorded by gage 1 were also in phase with the records of the other gages. The external lateral force (displacement) is applied at the pile-head, which in this test is at the bottom of the cap (see figure 6-1). This external force is resisted by both the cap above, and the pile below. As discussed in Section 4, the cap resistance has three components: side shear, active/passive resistance, and base shear.

TABLE 6-3: Material Damping for Loops of Increasing Displacement Amplitude.

Test	Loop	1	2	3	4	5	6
	ρ (cm)	0.3	0.7	1.4	2.8	5.6	10.9
PI	Area (KN-cm)	10.6	51.0	125.5	525.5	1768	6371
	β_{eq}	0.18	0.18	0.13	0.15	0.16	0.19
CBSP	Area (KN-cm)	21.1	83.8	267.5	825.8	2324.2	6880.6
	β_{eq}	0.28	0.30	0.30	0.31	0.37	0.47
PCBSP	Area (KN-cm)	31.5	142.4	376.3	1291.8	5042	16950
	β_{eq}	0.21	0.25	0.21	0.22	0.25	0.30
PCBSPI	Area (KN-cm)	28.1	135.5	411	1569	6219	19285
	β_{eq}	0.22	0.23	0.22	0.24	0.27	0.31

TABLE 6-4: Calculated Negative Bending Moments at the Pile-head in Test PCBSPI.

Displacement Amplitude (cm)	Force due to Side Shear and Passive Resistance of the cap (from test CSP) (KN)	Negative Moment induced at the Pile-head (KN-m)
0.3	32.7	9.15
0.7	46	12.84
1.4	69.6	19.06
2.8	104.6	29.22
5.6	129	36.06
10.9	170	47.47

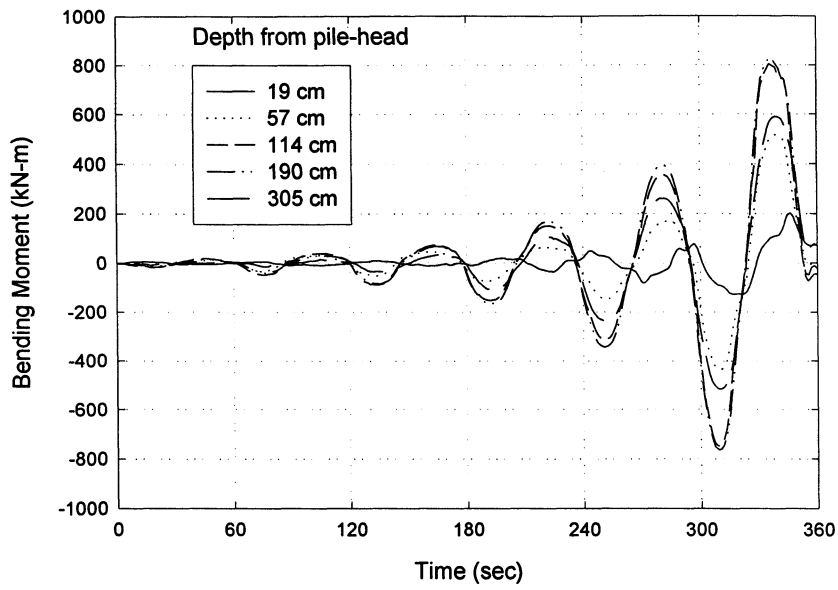


FIGURE 6-7: Measured bending moments versus time in Test PCBSPI in prototype scale.

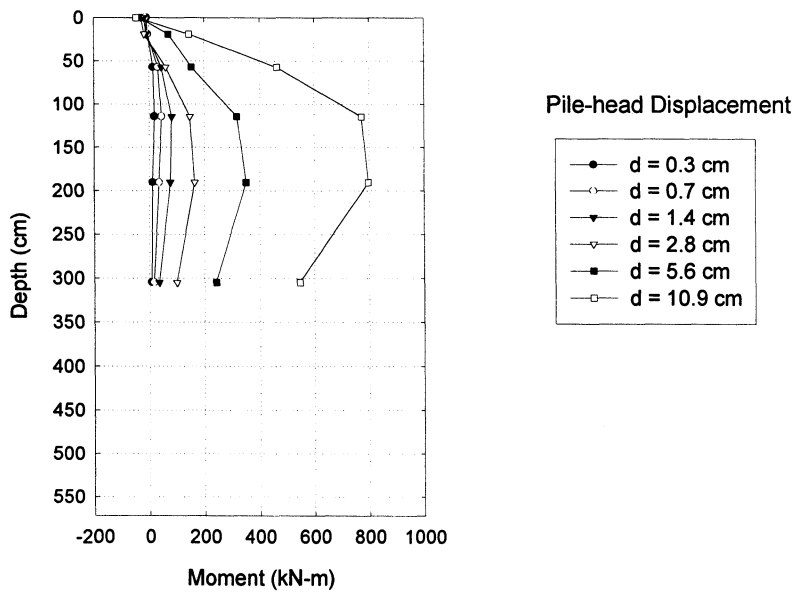


FIGURE 6-8: Measured Bending Moments along the Length of the Pile in Test PCBSPI.

To this must be added the rocking resistance of the soil at the base of the cap due to any tendency of the cap to rotate. The side shear and the active/passive resistances of the cap induce counterclockwise moments at the pile-head in figure 6-1. As the bending moments along a free-head pile due to the total force shown in figure 6-1 were defined as positive in Section 5, the counterclockwise moments due to the side shear and active/passive resistance correspond to a negative bending moment at the top of the pile. Table 6-4 lists these negative moments, calculated for different displacement amplitudes, under the assumption that any tendency of the cap to rotate in Test PCBSPI does not affect these forces and moments obtained in tests of the cap-alone, where the rotation of the cap was zero or negligible. The moments in table 6-4 were calculated assuming that the resultants of both active/passive resistance and side shear resistance of the cap act at an elevation of one third of the cap height, above the bottom of the cap. The values of side shear and active/passive resistances measured in Test CSP (see Section 4), when the cap was alone and the pile was not present, were used in these computations. As both base shear and total force shown in figure 6-1 act at the pile head, they do not induce any moment.

As lateral displacement cycles of increasing amplitude are applied to the pile-cap system, at small displacement amplitudes, the contribution of the cap in resisting the total lateral force is relatively high. As the displacement amplitude increases, the soil around the cap starts yielding, and the relative importance of the cap's contribution decreases (figure 6-5). Hence, at small displacements, due to these relatively high soil forces acting on the cap, the negative bending moment induced at the top of the pile is large enough to generate negative moments down to the depth of shallow strain gage 1. This seems to be the explanation why figure 6-7 shows that for the initial cycles shallow gage 1 records a negative moment, while in the deep gages the recorded moments are positive. At large displacement amplitudes, the soil forces acting on the cap, and the induced negative moment at the pile-head become insignificant, compared to the positive moments generated by the total force in the pile. Thus, at large displacements the negative bending moment region is extremely shallow and does not extend even to the depth of shallow

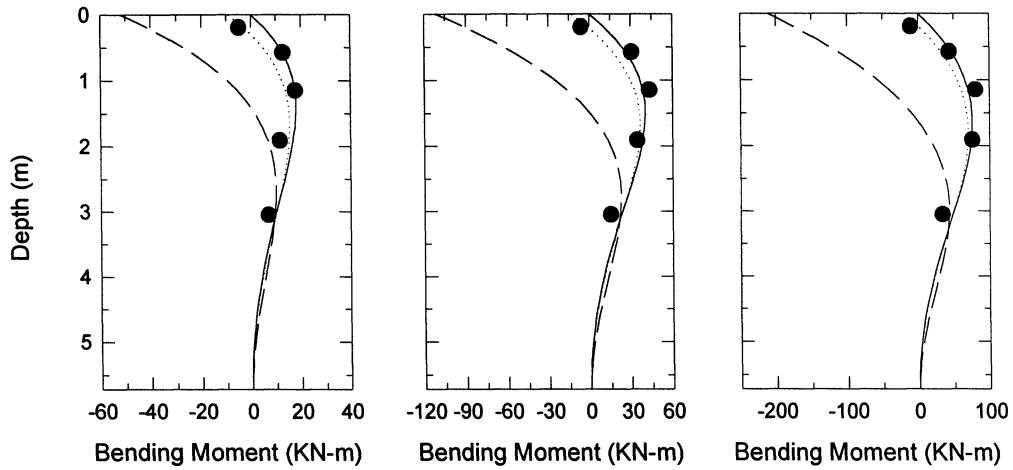
gage 1. This would explain why for the final cycles all strain gages recorded positive moments.

The measured distributions of bending moment along the pile for different displacement amplitudes of the pile-head are shown in figure 6-8 (data points connected by straight lines). The calculated negative moments, listed in table 6-4, are plotted as data points at zero depth in this figure. The bending moments at the other depths (data points at other depths) were acquired from the strain gage measurements. The graph shows consistency between the calculated pile head negative moments and the moments measured by the strain gages.

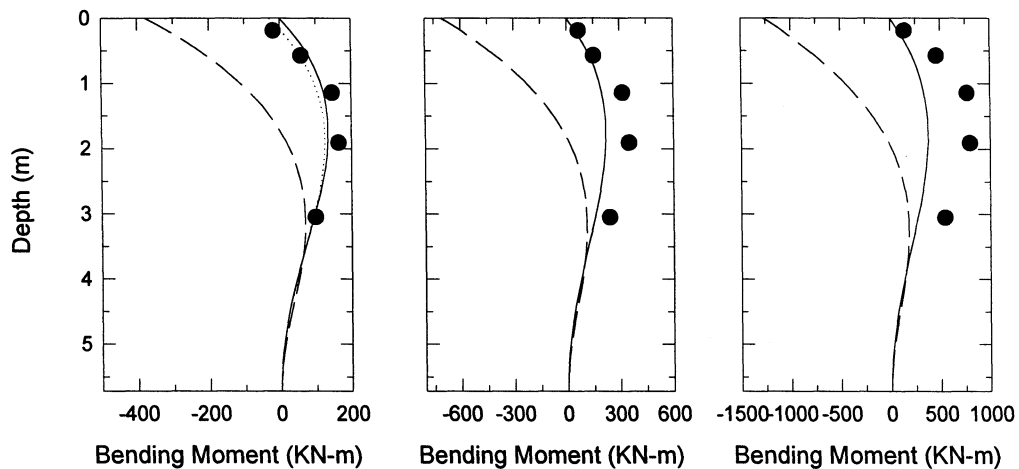
6.5 COMPARISON OF MEASURED AND CALCULATED RESPONSE

The objective of free-head pile Test PI, described in Section 5, was to obtain p-y curves for the soil, so as to predict the lateral response of the pile in Test PCBSPI. The results of Test PI were used to backfigure the p-y curves plotted in figure 5-7. Using those p-y curves, and the computer package LPILE (Reese and Wang, 1993), the lateral response of the pile in the pile-cap Test PCBSPI was predicted for both fixed head and free head conditions, at different displacement amplitudes. This use of p-y curves obtained from Test PI (no cap) to evaluate Test PCBSPI, neglects any possible effect of the vertical load transmitted to the soil through the base of the cap in stiffening the p-y curves near the pile-head. The corresponding two curves are included in figure 6-9 (solid and dashed lines). Also, predictions were made for the lateral response of the pile, when the negative bending moments in table 6-4 and the corresponding lateral displacements were applied simultaneously at the pile-head. The corresponding curves are also included in figure 6-9 (dotted lines). Table 6-5 gives the calculated pile-head moment, shear force, and slope for these different pile-head configurations. These predictions were compared with the measured values in Test PCBSPI.

(a) Pile head Disp. = 0.3 cm (b) Pile head Disp. = 0.7 cm (c) Pile head Disp. = 1.4 cm



(d) Pile head Disp. = 2.8 cm (e) Pile head Disp. = 5.6 cm (f) Pile head Disp. = 10.9 cm



- Computed BM for free-head pile
- - - Computed BM for fixed-head pile
- Measured Bending Moments in Test PCBSPI
- ⋯ BM computed with negative pile-head moment

FIGURE 6-9: Measured bending moments for Test PCBSPI superimposed on moment distributions calculated using p-y curves obtained from Test PI for free-head and fixed-head conditions.

TABLE 6-5: Pile-head Configurations Used for Bending Moment Predictions Using LPILE.

Pile-head condition	Displacement Amplitude, ρ (cm)	0.3	0.7	1.4	2.8	5.6	10.9
Fixed-head	Moment (KN-m)	-51.7	-111.1	-210.2	-375.3	-705.3	-1266
	Shear (KN)	57.8	111.3	195.6	333.8	556.3	1006
	Slope	0.0	0.0	0.0	0.0	0.0	0.0
Free-head	Moment (KN-m)	0.0	0.0	0.0	0.0	0.0	0.0
	Shear (KN)	31.1	61.0	104.6	178.9	289.2	498.4
	Slope ($\times 10^{-2}$)	0.155	0.354	0.701	1.32	2.48	4.60
Free-head with Negative Moment	Moment (KN-m)	-9.2	-12.8	-19.1	-29.2	-36.1	-47.5
	Shear (KN)	36.3	66.7	113.4	189.5	314.0	502.6
	Slope ($\times 10^{-2}$)	0.137	0.316	0.639	1.22	2.36	4.42

TABLE 6-6: Measured and calculated lateral load contribution of pile in Test PCBSPI.

Displacement Amplitude (cm)	Lateral Load (KN)					Contribution of Pile (a)-(b) (KN)
	Calculated from p-y curves		Measured in Centrifuge Tests			
	Fixed-head Pile	Free-head Pile	Test PI	Test PCBSPI (a)	Test CBSP (b)	
0.3	57.8	31.1	32.9	76.1	45	31.1
0.7	111.3	61.0	57.9	129.5	63.6	65.9
1.4	195.6	104.6	102.8	205.6	97.9	107.7
2.8	33.8	178.9	195.8	371.1	150.8	220.3
5.6	556.3	289.2	323.1	646.6	179.3	467.3
10.9	1006	498.4	507.3	920.7	213.2	707.5

6.5.1 Bending Moments

The calculated bending moment distributions for fixed head and free head pile conditions, using LPILE with the p-y curves in figure 5-7, are given in figure 6-9 (solid and dashed lines). Figure 6-9 also includes the curves from the LPILE calculation using free head pile with applied lateral displacements and negative pile-head bending moments (dotted lines). This figure also shows as data points the measured bending moments from Test PCBSPI on the pile-cap system, for different pile-head displacement amplitudes. For small displacement amplitudes (up to 2.8 cm), the measured bending moment distributions are very close to the calculated distributions for a free-head pile condition (figures 6-9a to 6-9d). As the pile connection was very rigid, this suggests that the cap rotated during Test PCBSPI. At the larger displacement amplitudes of 5.6 cm and 10.9 cm, the measured bending moments are much larger than the calculated values for the free-head pile condition. The bending moment distributions for the pile, calculated using the negative bending moments listed in table 6-4 as pile-head moments, are also plotted in figure 6-9 (dotted curves). These distributions are very close to the calculated distributions for the free-head pile condition. It seems that the negative moments generated by the soil resistance around the cap (including positive rocking resistance of the base of the cap, not considered in the calculations) were not high enough to prevent the rotation of the cap and pile-head. Consequently, the pile-head condition was close to a free-head condition in this test.

6.5.2 Lateral Load

The lateral load values calculated for various displacement amplitudes for free-head and fixed-head piles, based on the p-y curves in figure 5-7, along with the measured values for Test PCBSPI (pile-cap system), Test CBSP (cap-alone), and Test PI (free-head pile alone), are tabulated in table 6-6. The difference between the lateral load values measured in Test PCBSPI and Test CBSP is also given in table 6-6 as the contribution of the pile. As shown in the table, this difference is very close to the load measured in the free-head

pile Test PI, for displacement amplitudes up to 2.8 cm. For larger displacements, the difference is greater than the free-head pile value.

6.5.3 Rotation of Cap

In the tests on the cap-alone (see Section 4), the position of the loading rod was adjusted such that there were no moments transmitted to the cap, and the cap had horizontal translation with minimal rotation. In Test PI on the free-head pile, the loading rod was at the pile-head, transmitting zero moment. The slopes at the pile-head in that test, calculated using LPILE and the p-y curves backfigured from Test PI, are listed in table 6-5, for various displacement amplitudes. Based on the comparison of bending moments for Tests PI and PCBSPI, it can be assumed that the pile in Test PCBSPI behaved as a free-head pile. Furthermore, at least for displacements up to 2.8 cm, its response was similar to the pile in Test PI. Since in Test PCBSPI the pile was rigidly clamped to the cap, the cap must have rotated in that test and its rotation must be equivalent to the slope of the pile at pile-head. Apparently, the behavior of the cap may have been different in Test CBSP on cap-alone (minimal cap rotation) and Test PCBSPI on pile-cap system (cap rotation equal to free-head pile rotation). Hence the simple arithmetic operations on lateral loads from these tests performed in the previous subsection may seem questionable. In order to clarify this, nonlinear three-dimensional finite element (FE) analyses were performed and are reported later in Section 7, simulating the cap-alone experiments with different amounts of cap rotations. The results of these FE analyses show that for any displacement amplitude, the lateral load value for the cap with only translation and no rotation, and the value with translation and rotation about its base equal to the slope of the free-head pile for that displacement amplitude, are very close. The values for translation with rotation were only slightly higher. In the pile-cap foundation systems utilized in engineering design, the cap is usually supported by a group of piles, rather than by a single pile, and the rotation of the cap will be much smaller than the slope of a single free-head pile, for any given lateral displacement. Hence, when computing the contribution of the cap to the lateral stiffness of a pile-cap foundation system, as an engineering approximation, the rotational and cross-coupling components

of the cap stiffness may be neglected in this test. The horizontal cap stiffness can be assumed to be equal to the stiffness of an equivalent embedded footing without any rotation. This is consistent with the CALTRANS procedure described by Lam et al. (1991), in which the stiffness of the cap is calculated using simplified equations for the stiffness of a shallow foundation, and the rotational and cross-coupling effects are neglected.

6.5.4 Response at Large Displacements

As seen in the previous subsections, up to about 2.8-cm lateral displacements, the lateral resistance of the pile-cap system (Test PCBSPI) can be obtained, by sum of the lateral loads for the cap-alone (Test CBSP) and the free head pile (Test P). In addition, the bending moment distribution of the pile was almost identical with the distribution for the free-head pile up to 2.8-cm displacement. According to Lam et al. (1991), for normal working load levels in highway bridge foundations, the lateral pile-head deflection ranges from 1.3 cm to 2.5 cm. Hence, the “addition rule” for lateral load is valid for normal working load levels. However, for larger displacement amplitudes of 5.6 cm and 10.9 cm, the lateral loads for Test PCBSPI were larger than the sum of lateral loads for Tests CBSP and PI. Also, the bending moments along the pile at shallow depths in Test PCBSPI are much higher than the moments in Test PI. This indicates that the soil around the pile was providing much more lateral resistance in Test PCBSPI than in Test PI.

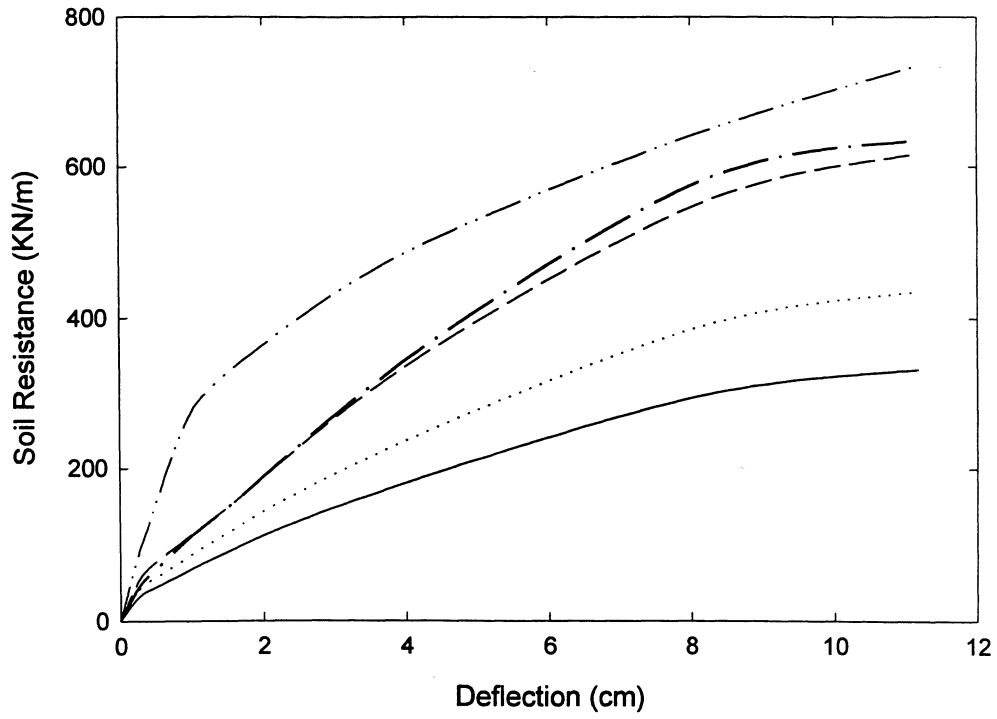
One possible explanation for this phenomenon is that, as the cap rotates in Test PCBSPI, at higher displacements and rotations, its base wedges the soil around the pile, providing additional confinement and additional lateral resistance to the lateral movement of the pile. This results in higher shear forces and bending moments near the pile-head. The zone of influence for the wedging action due to rotation of the base may be assumed to be down to a depth about equal to the width of the cap/foundation. The basis of this assumption is the similitude of this situation with the bearing capacity solution for a footing based on a Rankine wedge (Lambe and Whitman, 1969). The base of the rotating cap forms a passive Rankine wedge at an angle equal to $45^\circ + \phi/2$ from the base, which

pushes the soil downwards and inwards. For the soil internal friction angle of $\phi = 39^\circ$, this makes the depth of the Rankine wedge approximately equal to the side of the cap. Stiffer p-y curves were used for the soil in this zone of influence for obtaining bending moments and lateral loads at higher displacements. These stiffer p-y curves are shown in figure 6-10. The bending moment distributions calculated using LPILE and the stiffer p-y curves of figure 6-10 for displacement amplitudes of 5.6 cm and 10.9 cm are shown in figure 6-11, along with the measured bending moments in Test PCBSPI. The calculated and measured values match reasonably well. The corresponding computed lateral load values of 480.6 KN and 756.5 KN, for displacements of 5.6 cm and 10.9 cm, agree well with the differences of lateral load values between Tests PCBSPI and CBSP (see table 6-6) at corresponding displacements (467.3 and 707.5 KN).

6.6 CONCLUSIONS

The conclusions of this section can be summarized as follows:

1. The lateral response of the pile-cap system is more linear than that of the cap-alone, but less linear than that of the free head pile alone.
2. The contribution of the cap to the lateral stiffness of the pile-cap system, which is more than 50 % at small displacements, decreases as the displacement amplitude increases, and is only about 25 % at a lateral displacement of the system of 11 cm.
3. The measured bending moments along the pile in the pile-cap system model are close to the bending moments measured in the free-head pile tests, for normal working load levels (displacement amplitudes less than 3 cm).
4. For normal working load levels, an addition rule is approximately valid for the secant stiffness in Test PCBSPI, where the stiffness from Test PI (free-head pile alone) plus the stiffness from Test CBSP (cap-alone) is about equal to the stiffness in Test PCBSPI (pile-cap system). This is consistent with the recommendations given in the CALTRANS procedure described by Lam et al (1991).
5. The measured areas of loops, representing material damping, also satisfy an “addition rule” for normal working load levels these tests.



p-y curves for pile-head deflections of up to 2.8 cm for depths from ground surface:

- depth = 1.14 m
- depth = 2.28 m
- - - depth = 5.72 m

— · Modified p-y curve for pile-head deflection 5.6 cm, for depths from 1.14 m to 2.28 m.

— ··· Modified p-y curve for pile-head deflection 10.9 cm, for depths from 1.14 m to 2.28 m.

FIGURE 6-10: p-y Curves Used for Large Displacement Amplitudes.

(a) Pile-Head Displacement = 5.6 cm

(b) Pile-head Displacement = 10.9 cm

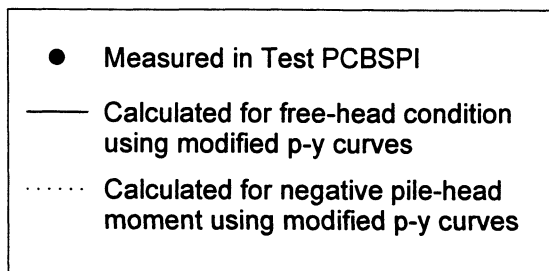
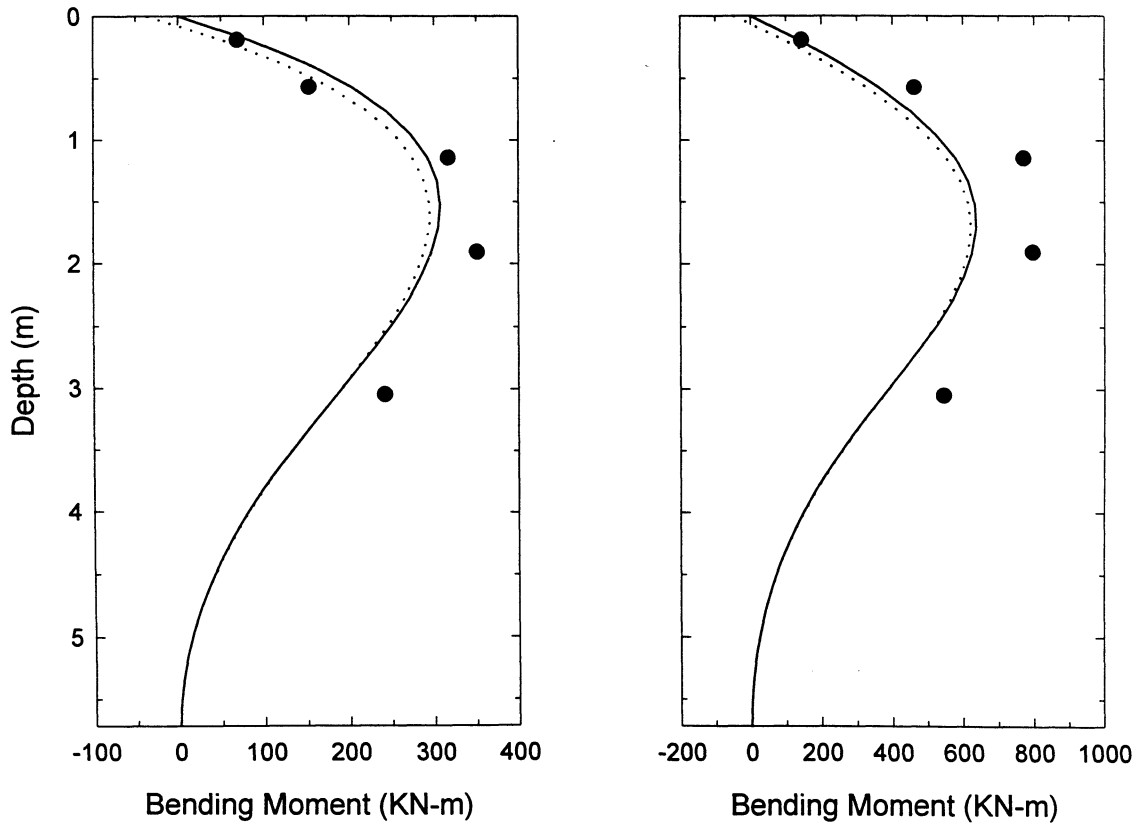


FIGURE 6-11: Measured and Calculated Bending Moments for Test PCBSPI at Large Displacements.

SECTION 7

FINITE ELEMENT ANALYSES OF CAP-ALONE (EMBEDDED FOUNDATION) WITH UNIFORM SOIL MODULUS

7.1 INTRODUCTION

Three-dimensional nonlinear finite element (FE) analyses were conducted to numerically simulate the results of centrifuge tests on the cap-alone (embedded footing) described in Section 4. These FE analyses were then extended to perform a parametric study, in which the shear modulus of the soil and the dimensions of the cap were varied, and the corresponding nonlinear lateral springs were computed.

Previous attempts to evaluate the lateral stiffness of embedded footings using three dimensional FE models seem to have been limited to linear elastic soil (Kuhlemeyer, 1979; Gazetas and Tassoulas, 1987a, b). This section describes the FE model used to simulate the results of the cap-alone experiments, in which all sides and the base of the cap were in contact with the soil (Tests CBSP and CBSPL). Three-dimensional nonlinear static FE analyses were performed, in which the soil was modeled as an elastoplastic material, the cap was modeled as a very stiff elastic material, and the interface between the cap and the soil was modeled with interface friction elements. Uniform soil shear modulus was used in these analyses. The relative contributions of the sides and the base of the cap to the total lateral response are also computed from the results of the FE analyses, and compared to the contributions measured in the centrifuge tests, as described in Section 4. The results of a parametric study performed to investigate the effects of varying the soil shear modulus and the foundation geometry on the nonlinear lateral response are also presented.

7.2 MODEL DESCRIPTION

The FE analyses performed modeled the lateral response of a square embedded foundation in dry sand. The objective was to numerically simulate the results of centrifuge tests on the cap presented in Section 4, and to perform a parametric study to

investigate the influence of soil shear modulus and footing geometry on the lateral response.

The dimensions of the prototype square embedded foundation modeled in the centrifuge experiments are shown again in figure 7-1 **Error! Reference source not found.** The footing had dimensions $2B \times 2B \times H$, and was embedded in sand at a depth D from the ground surface. The top of the footing was at a distance $m = D - H$ from the ground surface. Sand was retained around the top rim of the footing. Sand was glued to all surfaces of the model footing in contact with the sand to simulate a rough concrete foundation. Lateral displacement cycles of increasing amplitude were applied to the footing, and the corresponding loads were measured. The soil and the footing were modeled in the FE analyses with eight node three-dimensional solid elements. The rough interface between the soil and foundation was modeled with eight node interface elements. As the loading in the centrifuge tests was slow, static FE analyses were used. Due to the symmetry of the geometry and loading condition in the horizontal direction, only half of the foundation-soil system was modeled, and symmetric boundary conditions were applied on the vertical plane passing through the center of the footing. No constraints were applied to the soil ground surface. Appropriate horizontal or vertical displacement constraints were applied at the other boundaries of the soil mass. These boundaries were located at distances of more than $10 B$ from the footing, to eliminate any boundary effect on the calculated results. The nodes of the soil elements above the top rim of the footing were constrained to simulate the sand retention system used in the centrifuge tests. A typical FE mesh of the soil-foundation system is shown in figure 7-2. This mesh was generated using the FE analysis package PATRAN (PDA Engineering, 1993), and the FE analyses were performed using the ABAQUS code (Hibbit, Karlsson, and Sorensen, Inc., 1994).

7.2.1 Constitutive Models

Different constitutive models were used to model the behavior of the foundation, soil, and soil-foundation interfaces. Very stiff elastic elements were used to model the rigid foundation. The soil was modeled with the Modified Drucker-Prager Cap model available

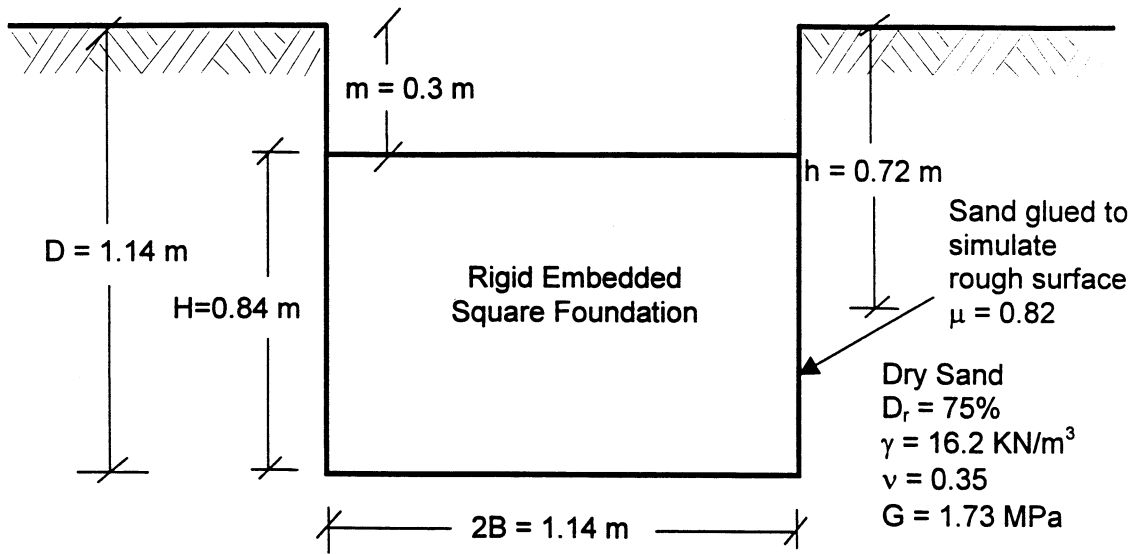


FIGURE 7-1: Dimensions of the square embedded foundation/pile-cap used in basic FE analyses.

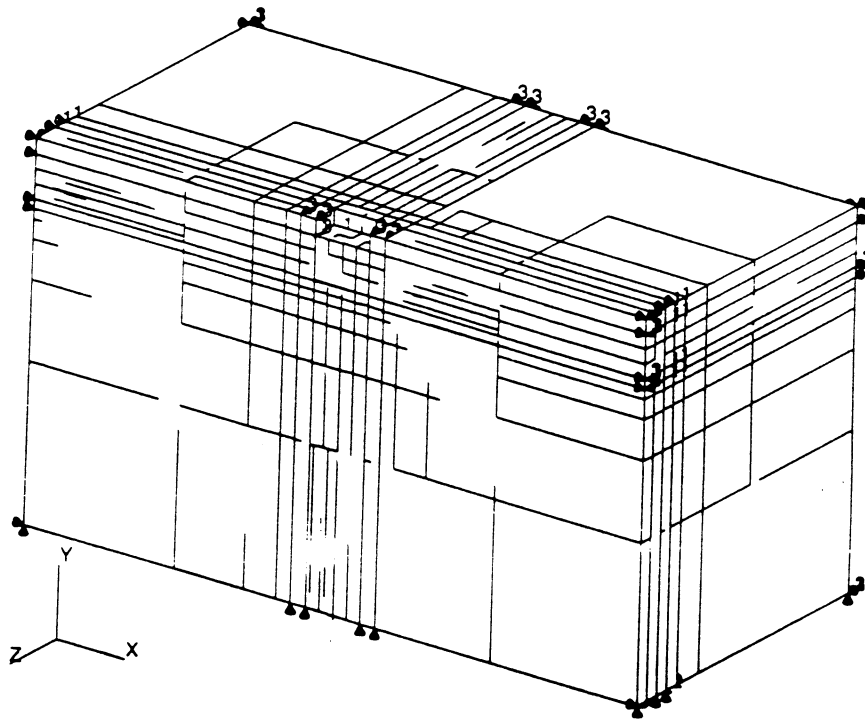


FIGURE 7-2: Finite element mesh simulating set-up for centrifuge tests on cap-alone.

in ABAQUS, and the rough interface between soil and foundation was modeled with interface elements of ABAQUS.

Dry sand response, especially at low confining pressures, is highly nonlinear, with yielding occurring at very low strains. In the centrifuge tests, lateral displacement cycles of increasing amplitude were applied to the footing/cap model, with amplitudes increasing from 0.3 cm in the first cycle to about 11 cm in the last cycle. Linear elastic analyses of these cap-alone experiments show that even at the initial displacement amplitude of 0.3 cm, shear strains of the order of 0.5% were developed in the soil around the cap. Hence, it was decided to use a nonlinear constitutive model for the soil, which could account for plastic yield. The Modified Drucker-Prager/Cap plasticity model available in the ABAQUS code was used for this purpose. This constitutive model is applicable to geological materials which exhibit pressure-dependent yield.

The yield surface defined by the Modified Drucker-Prager Cap model includes two main segments: a shear failure surface, providing dominantly shear flow, and a “cap,” which intersects the equivalent pressure stress axis (figure 7-3). There is a transition region between these segments, introduced so as to provide a smooth surface. The cap bounds the yield surface in hydrostatic compression, thus providing an inelastic hardening mechanism to represent plastic compaction. It also helps to control volume dilatancy when the material yields in shear, by providing softening as a function of the inelastic volume increase created as the material yields on the Drucker-Prager shear failure and transition yield surfaces. The model uses associated flow in the cap region, and nonassociated flow in the shear failure and transition regions.

The model assumes a linear strain increment decomposition such that:

$$d\epsilon = d\epsilon^{el} + d\epsilon^{pl} \quad (7-1)$$

where $d\epsilon$ is the total strain rate, $d\epsilon^{el}$ is the elastic strain increment, and $d\epsilon^{pl}$ is the inelastic (plastic) strain increment.

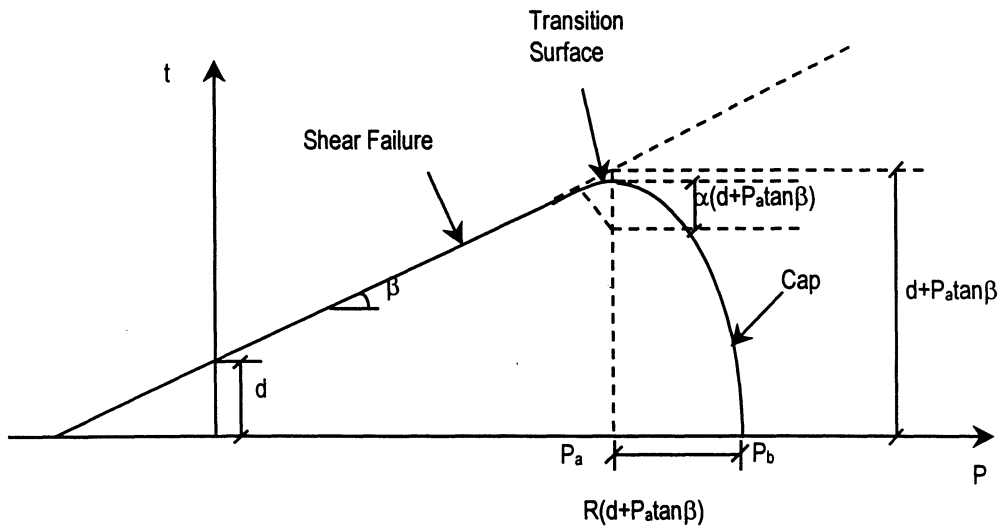


FIGURE 7-3: Modified Drucker-Prager/Cap model: yield surface in the p - t plane (after Hibbit, Karlsson & Sorensen Inc., 1994).

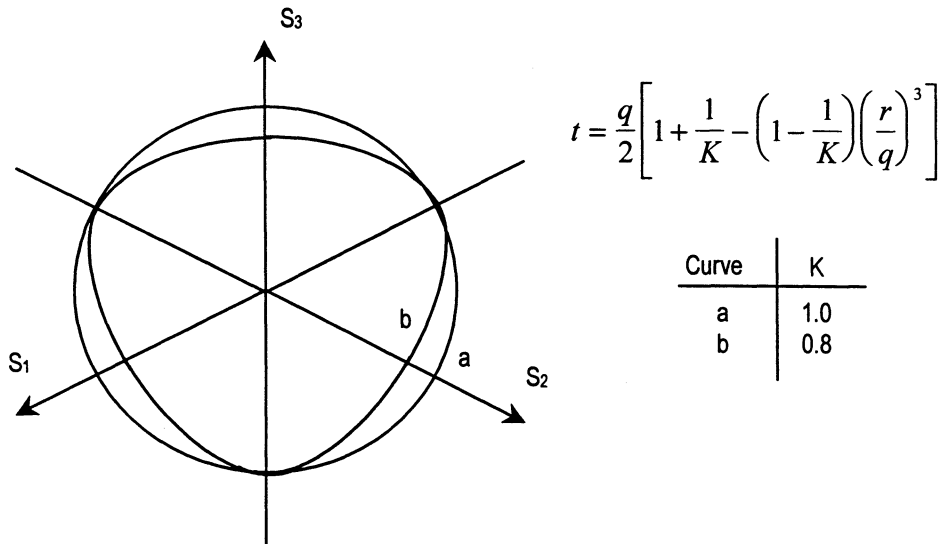


FIGURE 7-4: Modified Drucker-Prager/Cap model: typical yield/flow surfaces in the deviatoric plane (after Hibbit, Karlsson & Sorensen Inc., 1994).

The elastic behavior may be modeled as linear isotropic elastic, in which the total stress σ is related to the total elastic strain ϵ^{el} , through the elastic stiffness matrix \mathbf{D}^{el} such that:

$$\sigma = \mathbf{D}^{el} \epsilon^{el} \quad (7-2)$$

The elastic stiffness matrix can be found based on the Young's modulus and Poisson's ratio for the material, as in this case the relation between stress and strain is supposed to be that of a linearly elastic isotropic solid.

The plastic behavior is defined through the yield/failure surfaces. These are written in terms of the standard three stress invariants: the equivalent pressure,

$$p = -\frac{1}{3} \text{trace}(\sigma) \quad (7-3)$$

the Von-Mises equivalent stress,

$$q = \sqrt{\frac{3}{2} (\mathbf{S}:\mathbf{S})} \quad (7-4)$$

and the third invariant of deviatoric stress,

$$r = \left(\frac{9}{2} \mathbf{S}:\mathbf{S}:\mathbf{S} \right)^{1/3} \quad (7-5)$$

where \mathbf{S} is a stress deviator, defined as

$$\mathbf{S} = \sigma + p\mathbf{I} \quad (7-6)$$

where \mathbf{I} is the identity tensor. As used in mechanics formulations, compressive stresses are defined as being negative. We also define the deviatoric stress measure

$$t = \frac{q}{2} \left[1 + \frac{1}{K} - \left(1 - \frac{1}{K} \right) \left(\frac{r}{q} \right)^3 \right] \quad (7-7)$$

where K is a material parameter. This measure of deviatoric stress is used because it allows matching of different stress values in tension and compression in the deviatoric plane. This provides flexibility in fitting experimental results, and a smooth approximation to the Mohr-Coulomb surface. Since $r/q = 1$ in uniaxial tension, $t = q/K$ in this case, and since $r/q = -1$ in uniaxial compression, $t = q$ in that case. When $K = 1$, the dependence on the third deviatoric stress invariant is removed, and the Von-Mises circle

is recovered in the deviatoric plane: $t = q$. The dependence of t on K is shown in figure 7-4. To ensure convexity of the yield surface, $0.778 \leq K \leq 1.0$.

With this expression for the deviatoric stress measure, the Drucker-Prager failure surface is written as

$$F_s = t - p \tan \beta - d = 0 \quad (7-8)$$

where β and d are parameters related to material friction angle, ϕ , and cohesion, c (see figure 7-3). When matching the triaxial test response, the relations between the Drucker-Prager parameters β , d , and K and Mohr-Coulomb parameters ϕ and c are found to be:

$$\tan \beta = \frac{6 \sin \phi}{3 - \sin \phi} \quad (7-9)$$

$$d = c \frac{6 \cos \phi}{3 - \sin \phi} \quad (7-10)$$

$$K = \frac{3 - \sin \phi}{3 + \sin \phi} \geq 0.778 \quad (7-11)$$

The cap yield surface has an elliptical shape, with constant eccentricity in the meridional (p - t) plane (figure 7-3), and also including dependence on the third stress invariant in the deviatoric plane (figure 7-4). The cap surface hardens or softens as a function of the volumetric plastic strain; volumetric plastic compaction (when yielding on the cap) causes hardening, while volumetric plastic dilation (when yielding on the shear failure surface) causes softening. The cap yield surface is written as

$$F_c = \sqrt{(p - p_a)^2 + \left[\frac{Rt}{(1 + \alpha - \alpha / \cos \beta)} \right]^2} - R(d - p_a \tan \beta) = 0 \quad (7-12)$$

where R is a material parameter that controls the shape of the cap, α is a small number which is defined below, and p_a is an evolution parameter that represents the volumetric plastic strain driven hardening/softening. The hardening/softening law is a user-defined piece-wise linear function, relating the hydrostatic compression yield stress, p_b , and the corresponding volumetric plastic strain ϵ_{vol}^{pl} . The evolution parameter p_a is defined as

$$p_a = \frac{p_b - Rd}{(1 + R \tan \beta)} \quad (7-13)$$

The parameter α is a small number (typically 0.01 to 0.05) used to define a smooth transition surface between the shear failure surface and the cap:

$$F_t = \sqrt{(p - p_a)^2 + \left[t - \left(1 - \frac{\alpha}{\cos \beta} \right) (d + p_a \tan \beta) \right]^2} - \alpha (d + p_a \tan \beta) = 0 \quad (7-14)$$

Plastic flow is defined by a flow potential that is associated in the deviatoric plane, associated on the cap in the meridional plane, and nonassociated on the failure surface and transition surface in the meridional plane. The flow potential surface in the meridional plane is shown in figure 7-5. It is made up of an elliptical portion in the cap region that is identical to the cap yield surface:

$$G_c = \sqrt{(p - p_a)^2 + \left[\frac{Rt}{1 + \alpha - \alpha / \cos \beta} \right]^2} \quad (7-15)$$

and another elliptical portion in the failure and transition regions that provides the nonassociated flow component in the model:

$$G_s = \sqrt{\left[(p - p_a) \tan \beta \right]^2 + \left[\frac{t}{1 + \alpha - \alpha / \cos \beta} \right]^2} \quad (7-16)$$

The two elliptical portions G_c and G_s form a continuous and smooth potential surface.

7.3 NUMERICAL SIMULATION OF CENTRIFUGE TESTS

Two three-dimensional static nonlinear FE analyses were performed to verify the results of the lateral loading experiments on a fully embedded foundation or pile cap. These two analyses correspond to Tests CBSP and CBSPL. The footing and soil were modeled with eight node 3-D solid elements, and the interface between soil and foundation was modeled with eight node interface elements. The geometry of the footing model used in these finite element analyses is shown in figure 7-1 **Error! Reference source not found.**

The FE mesh shown in figure 7-2 had approximately 5,000 degrees of freedom.

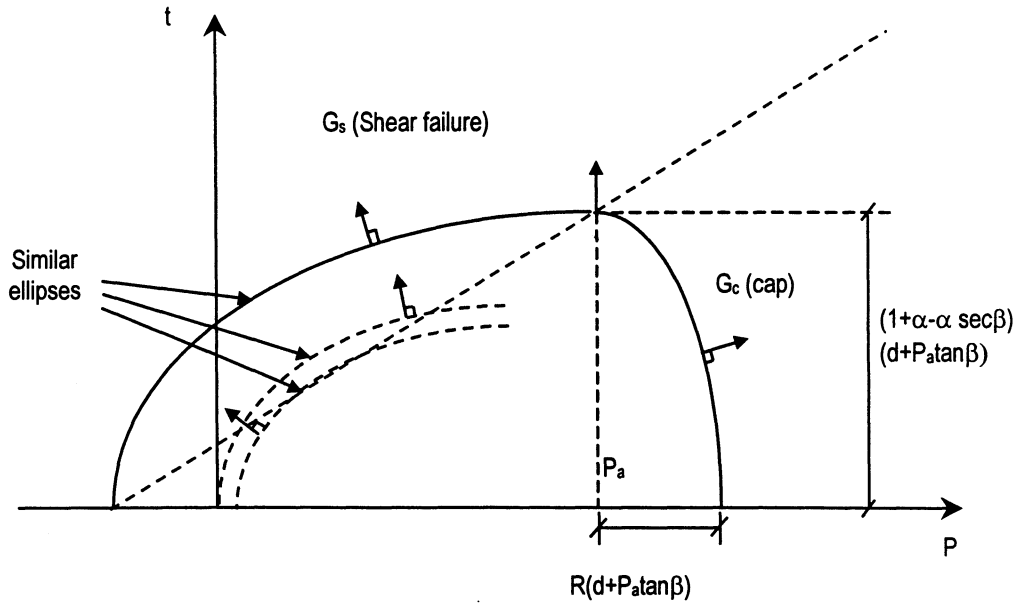


FIGURE 7-5: Modified Drucker-Prager/Cap model: flow potential in the p - t plane (after Hibbit, Karlsson & Sorensen Inc., 1994).

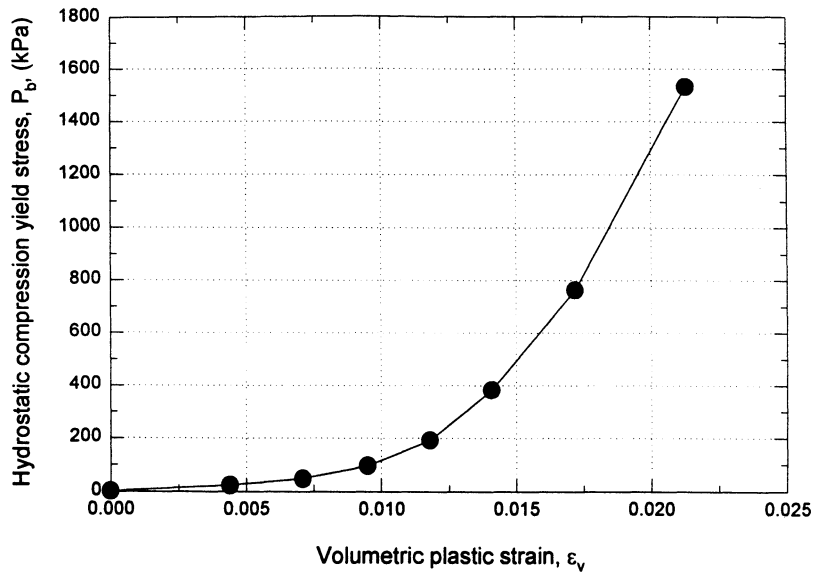


FIGURE 7-6: Cap hardening rule for the sand used in the FE analysis.

The FE analyses simulating centrifuge Tests CBSP and CBSPL were performed in two steps. In the first step, gravity and vertical loading were applied to the FE models, and then the lateral displacement was applied in the second step. All sides and the base were in contact with the soil in these analyses. The vertical load was applied to the foundation by means of its unit weight γ_f . When simulating Test CBSPL, the vertical load on the cap was doubled, similar to what was actually done in this centrifuge experiment, by doubling the unit weight of the cap material. Although cyclic loading was applied to the foundation in the centrifuge tests, monotonic loading was specified in the FE analyses, as unrealistic results would have been obtained for cyclic loading, due to the isotropic hardening behavior specified by the Modified Drucker-Prager cap model.

An elastic FE analysis was first performed on the cap-soil system without the interface elements to check the adequacy of the FE mesh. For Young's modulus $E = 4.67$ MPa and Poisson's ratio $\nu = 0.35$ in the soil (consistent with $G = 1.73$ MPa backfigured at a small displacement for the cap-alone experiments in Subsection 4.5), the value of static horizontal stiffness computed using this linear FE analysis was about 180.1 KN/cm. This matches reasonably well with the value of 168.7 KN/cm computed using elastic solutions provided by Pais-Kausel (1988) and Gazetas and Tassoulas (1987) for this foundation-soil system (see Section 4). This demonstrates that the FE mesh used is adequate, and the soil boundaries are far enough from the foundation to minimize any modeling errors.

7.3.1 Parameters Used in the FE Model

The parameters used in the FE analyses to simulate centrifuge Tests CBSP and CBSPL are listed in table 7-1. The elastic constitutive model was used for the cap/embedded footing with Young's modulus, $E_f = 6895$ MPa and Poisson's ratio, $\nu_f = 0.35$, obtained from the literature for aluminum. This Young's modulus used for the foundation was much higher than the soil modulus, making it a very stiff footing. The soil parameters used for the Modified Drucker-Prager Cap model are also included in table 7-1. The soil Poisson's ratio, $\nu = 0.35$ used in the analysis is a typical value for dry sand. The constant value used of the soil shear modulus, $G = 1.73$ MPa, is that already calibrated in Section 4 with the elastic Pais-Kausel and Gazetas-Tassoulas solutions, using the initial measured

TABLE 7-1: Parameters used in the finite element analyses of centrifuge Tests CBSP.

Foundation Parameters:	Width, $2B$	1.14 m
	Depth of footing base below ground surface, D	1.14 m
	Height of the footing, H	0.84 m
	Elastic Modulus, E_f	6895 MPa
	Poisson Ratio, ν_f	0.35
	Unit Weight, γ_f	48.5 KN/m ³
Soil Parameters:	Shear Modulus, G	1.73 MPa
	Elastic Modulus, E	4.67 MPa
	Poisson Ratio, ν	0.35
	Friction angle, ϕ	35°
	Cohesion, c	0.5 kPa
	Unit weight	16.2 KN/m ³
	Modified Drucker-Prager Cap model parameter K	0.778
	Modified Drucker-Prager Cap model parameter R	0.00041
	Modified Drucker-Prager Cap model parameter α	0.01
Interface Parameters	Friction Coefficient, $\tan \phi_w$	0.82

TABLE 7-2: Comparison of lateral resistance of the cap with no rotation and with rotation equal to the pile-head rotation in the free-head case.

Displacement Amplitude, ρ , cm	Pile-head slope for free-head case, θ , rad.	Computed Lateral load for cap with no rotation, KN	Computed lateral load for cap with cap rotation = θ , KN
0.3	1.55×10^{-3}	39.1	43.5
0.7	3.54×10^{-3}	75.6	80.9
1.4	7.01×10^{-3}	118.8	122.2
2.8	1.32×10^{-2}	159.0	159.9
5.6	2.48×10^{-2}	194.8	196.6
10.9	4.60×10^{-2}	221.1	224.6

stiffness at 0.3 cm displacement. The FE analyses indicated that maximum shear strains of the order of 0.5% were developed in the sand around the model footing, when the lateral displacement of the foundation was 0.3 cm. Therefore, this equivalent linear $G = 1.73$ MPa used is not G_{\max} of the soil; G_{\max} is much larger, as already discussed in Section 4.

A small amount of cohesion (0.5 kPa) was provided to the soil for computational stability, and consequently, the initial friction angle of the soil was reduced from 39° to 35° . These modified values of cohesion and friction angle were chosen to match the soil shear strength at a shallow soil depth in the free field. A similar approach was adopted to model lateral response of piles in sand by Brown and Shie (1990). The cap hardening rule for the sand used in the finite element analyses was derived from available results of one dimensional consolidation-rebound tests on 60 % relative density Nevada sand, reported by Arulmoli et al. (1992). The foundation-soil interface was modeled with 8 node interface elements, which provide for no force transmitted across the interface upon separation and for frictional behavior when the surfaces are in contact. The friction coefficient for the contact elements was specified as 0.82, the value measured in centrifuge Tests CB and CBL (see Section 4).

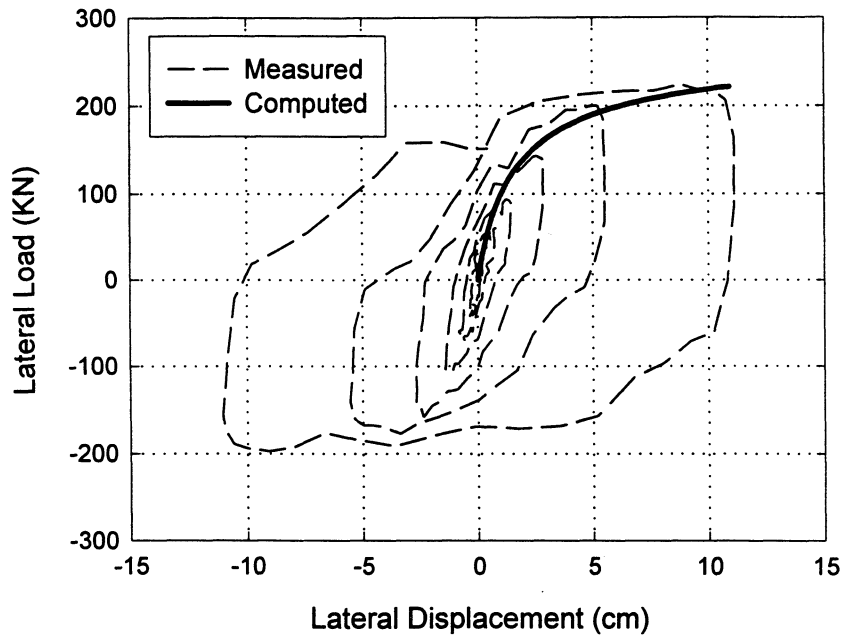
7.3.2 Results of FE Analyses

The load-displacement monotonic curve computed using the FE analyses are compared in figure 7-7, with the load-displacement loops measured in centrifuge tests CBSP and CBSPL. The computed load-displacement curves pass through the apexes of the measured load-displacement loops in both cases, indicating close matching between centrifuge and FE results. The values predicted from the analyses for the ultimate capacity (load corresponding to 11-cm displacement) for Tests CBSP and CBSPL are 221 KN and 263.8 KN, respectively, which match reasonably well with the measured capacities of 214 KN and 245 KN.

7.3.3 Comparison of Computed and Measured Material Damping

While no cyclic loading was imposed in the FE analyses, load-displacement loops for various displacement amplitudes can be generated from the predicted monotonic load-

Test CBSP



Test CBSPL

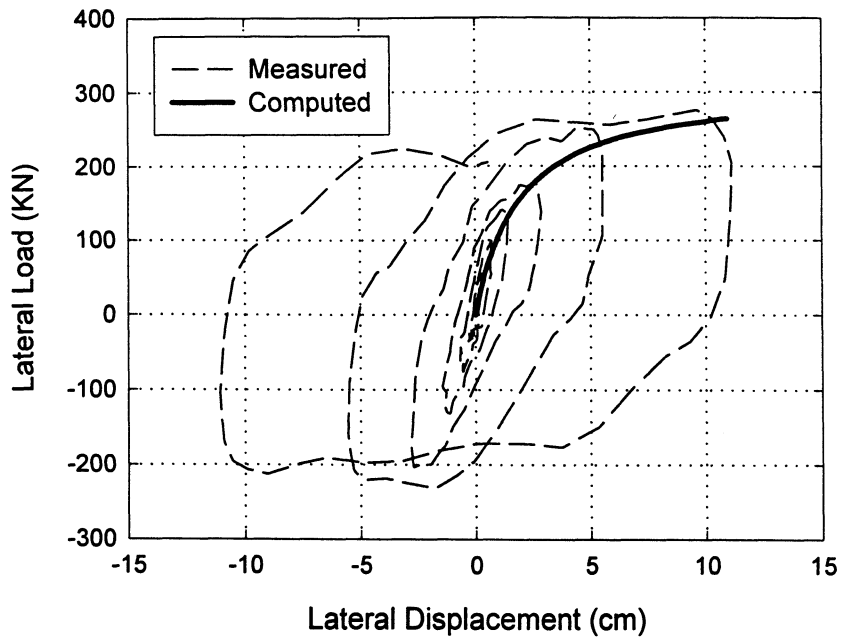


FIGURE 7-7: Measured and computed load-displacement response for Tests CBSP and CBSPL.

displacement backbone curve using the Masing criteria. This Masing behavior, described by Masing (1926), assumes that the loading and unloading curves have the same shape as the backbone curve (with the origin shifted to the loading reversal point), but scaled by a factor of 2. The monotonic load-displacement curve for Test CBSP computed using the three-dimensional nonlinear finite element analysis was used as the backbone curve. The load-displacement loops generated from the FE analysis for various displacement amplitudes are shown in figure 7-8 as solid lines, where they are compared with the measured loops. The computed loops are much sharper than the measured load displacement loops for Test CBSP shown in the same figure as dotted lines. The equivalent damping ratios for the FE loops generated using the Masing criterion, calculated using the expression:

$$\beta_{eq} = \frac{A}{2\pi K_h u^2} \quad (7-17)$$

are shown in figure 7-9, together with the corresponding measured equivalent damping ratios for Test CBSP. The computed damping ratios are much smaller than the measured damping ratios for lower displacement amplitudes (less than 2.5 cm). This is related to the very fast drop-off in load immediately after unloading and reloading associated mainly with the passive face behavior, already discussed in Section 4. For larger displacements, the computed and measured damping ratios become about equal. In engineering design, the damping ratios calculated from the load-displacement loops created using the Masing criteria may perhaps be used as conservative design values.

7.3.4 Contributions of Base and Sides of Cap to Total Lateral Response

The centrifuge tests on cap-alone listed in table 4-1 were performed to isolate the contributions of the base (Test CB), shearing sides (Test CS), and active/passive sides (Test CP) to the total lateral force applied to the cap at a given lateral displacement (Test CBSP). These contributions can also be computed from the results of the nonlinear finite element analysis for Test CBSP. The contribution of the base can be assumed to be equal to the sum of shear forces in the loading direction transmitted through the interface at the base. Similarly, the contribution of the shearing sides is equal to the sum of the shear forces in the loading direction transmitted through the interfaces along the shearing sides.

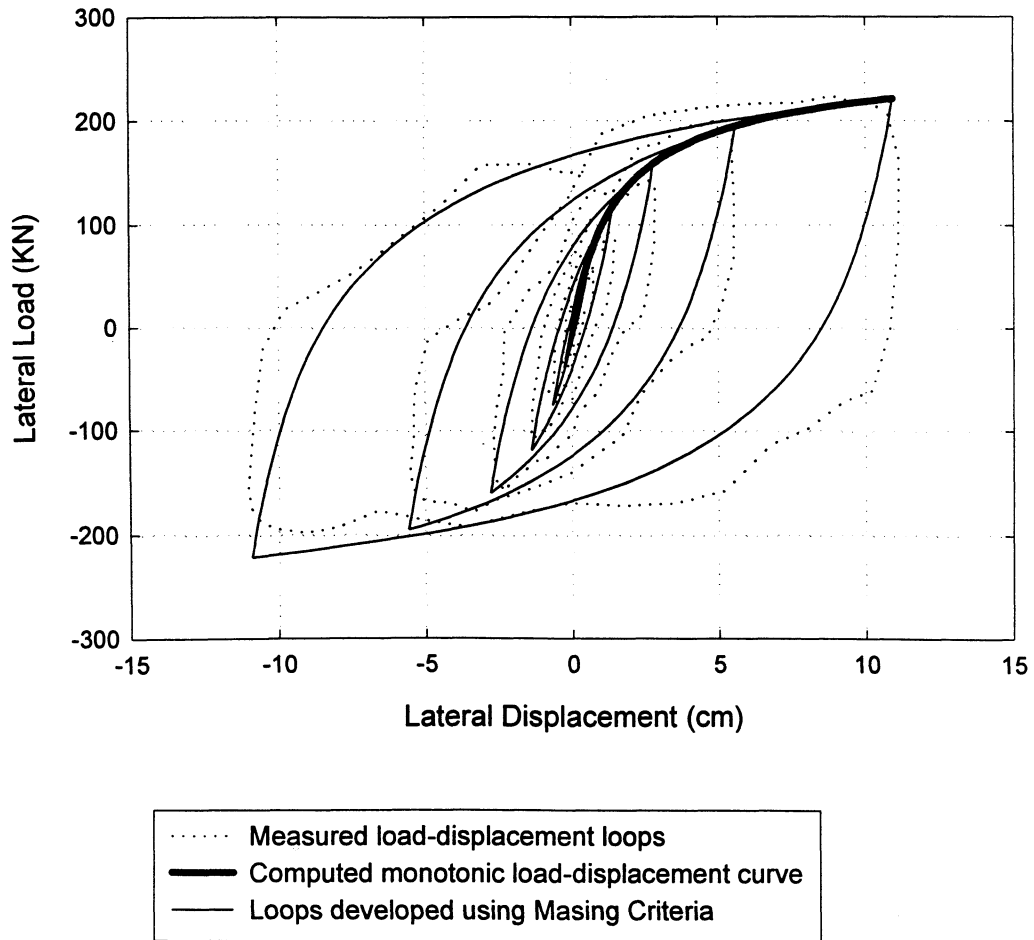


FIGURE 7-8: Load-displacement loops generated for Test CBSP from finite element results using Masing criterion.

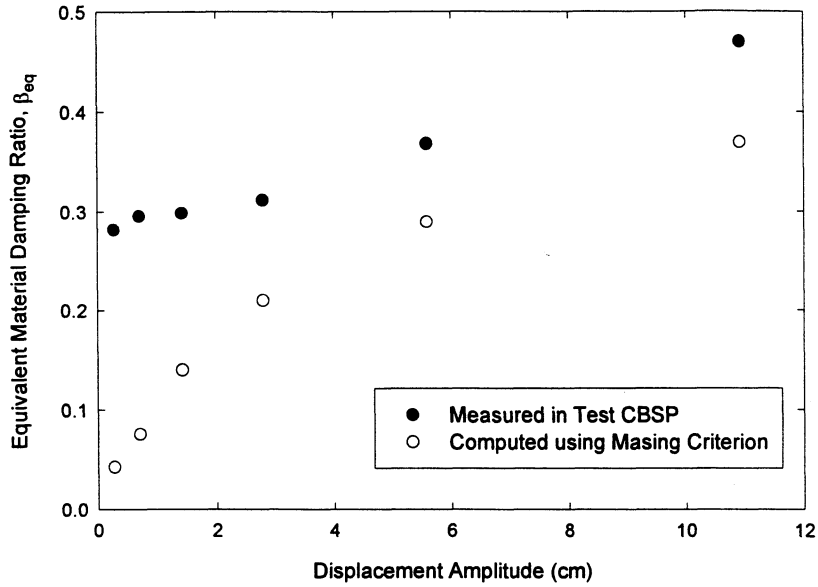


FIGURE 7-9: Measured and computed equivalent damping ratios for Test CBSP.

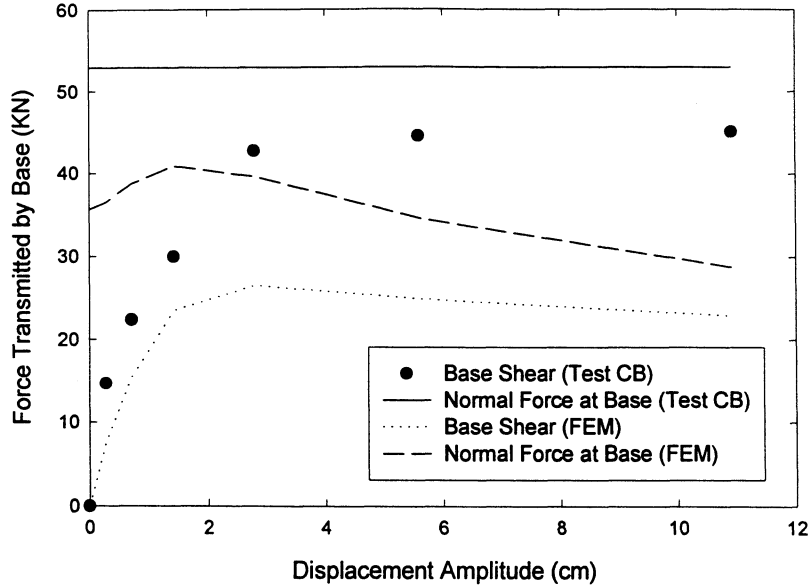


FIGURE 7-10: Shear and normal forces at the base of the cap. (FE results are for Test CBSP with parameters of table 7-1).

The active/ passive contribution can be calculated as the sum of the normal forces transmitted via the interfaces along the active/passive sides. The shear (or normal) force transmitted through each contact element along an interface can be assumed to be approximately equal to the product of the average shear (or normal) stress for that element, which is included in the output information of the FE runs, times the area of the element.

The measured shear and normal forces for centrifuge Test CB, in which only the base of the cap was in contact with the soil, are plotted in figure 7-10 for various displacement amplitudes. The normal force at the base in this test remains constant at about 53 KN for all displacements. The shear force at the base increases with displacement, up to about 40 KN at a 2.5-cm displacement, and shortly afterwards the cap starts sliding without any significant increase in shear force. The friction coefficient obtained from this test was about 0.82 (see Section 4). The shear and normal forces at the base of the cap computed from the finite element analysis simulating centrifuge test CBSP (base and all sides in contact with soil) are also shown in figure 7-10. The total vertical force acting on the cap in Tests CB and CBSP was identical (53 KN) but the FE analysis suggests that in Test CBSP not all of this vertical force was transmitted to the base. Since the sides of the cap are also in contact with the soil in Test CBSP, the sides carry some portion of the total 53 KN vertical force. The calculated normal force at the base increases slightly with displacement and then starts decreasing with increasing displacement amplitude. This is because, with increasing displacement amplitude, the normal forces on the passive and shearing sides increase, and greater and greater fraction of the vertical force is taken by shearing resistance along these sides. The FE results suggest that at small displacements the base shear in Test CBSP increases with displacement. At large displacements the base shear force in loading direction becomes about 0.82 times the normal force transmitted to the base. Up to a displacement of about 1.4-cm the base shear contribution in Test CBSP is predicted reasonably well by Test CB. After a displacement of about 2.5-cm, when the cap starts sliding at the base, the base shear becomes directly dependent on the normal force transmitted to the base. The base shear contribution for Test CBSP, as computed

from FEM results becomes about 60 % of the lateral load taken by the base as measured in Test CB.

The side shear and normal forces computed using the results of the finite element analysis of Test CBSP are shown in figure 7-11, along with the shear forces actually measured in centrifuge Test CS (see Section 4), in which only the shearing sides were in contact with the soil. The computed contribution of shearing sides in Test CBSP agrees well with the measured side shear in Test CS. The ultimate capacity contribution of the shearing sides computed using the FE results (34.5 KN) matches reasonably well with the ultimate capacity measured in Test CS (38 KN). The calculated normal force on the shearing sides for Test CBSP also increases with displacement amplitude. This effect may be attributed to dilation of the dense sand along the shearing sides when it undergoes shear deformation. The final value of computed normal force on the shearing sides in Test CBSP, at a lateral displacement of about 11-cm, is about 43.5 KN. Based on this value normal force, the lateral earth pressure coefficient K_s , calculated using (4-1), is about 1.95, which compares well with the measured $K_s = 2.1$ in Test CS.

The normal forces acting on the active and passive sides of the cap, computed from the FE results for Test CBSP are shown in figure 7-12. This figure also shows the lateral resistance measured in Test CP (described in Section 4) when only the active/passive sides of the cap were in contact with the soil. The normal force on the active side computed from the FE results decreases rapidly with displacement, and becomes zero at displacements larger than about 0.5 cm. The normal force on the passive side increases with displacement. The total lateral resistance contributed by the active/passive sides in Test CBSP can be assumed to be equal to the difference between the computed passive and active normal forces. Thus from figure 7-12 it is evident that the computed lateral resistance contribution of the active/passive sides for Test CBSP agrees very well with the lateral resistance measured in Test CP. The computed ultimate capacity contribution of the active/passive sides (133 KN) for Test CBSP matches well with the ultimate capacity measured in Test CP (124 KN). Subsequently, the passive lateral earth pressure coefficient computed using this capacity contribution of 133 KN and (4-2), $K_p = 15.3$,

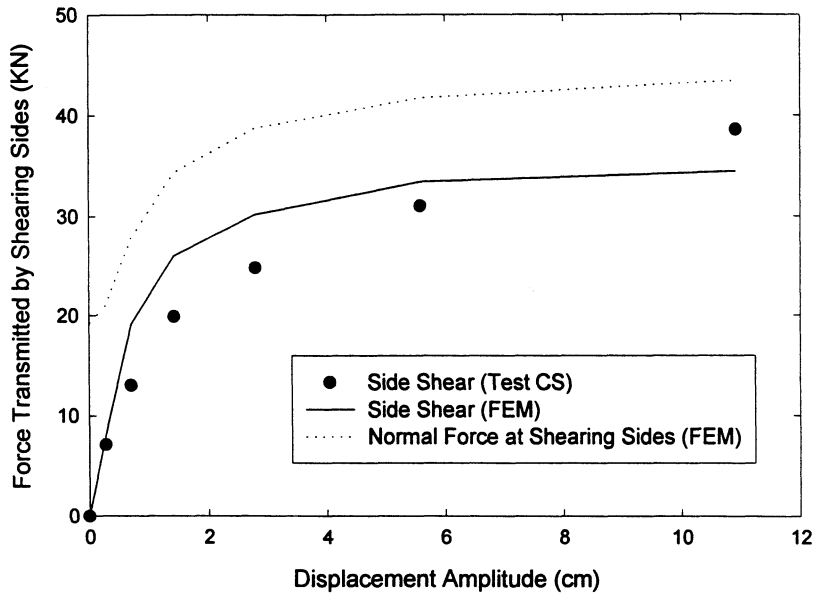


FIGURE 7-11: Shear and normal forces along the shearing sides of the cap (FE results are for Test CBSP with parameters of table 7-1).

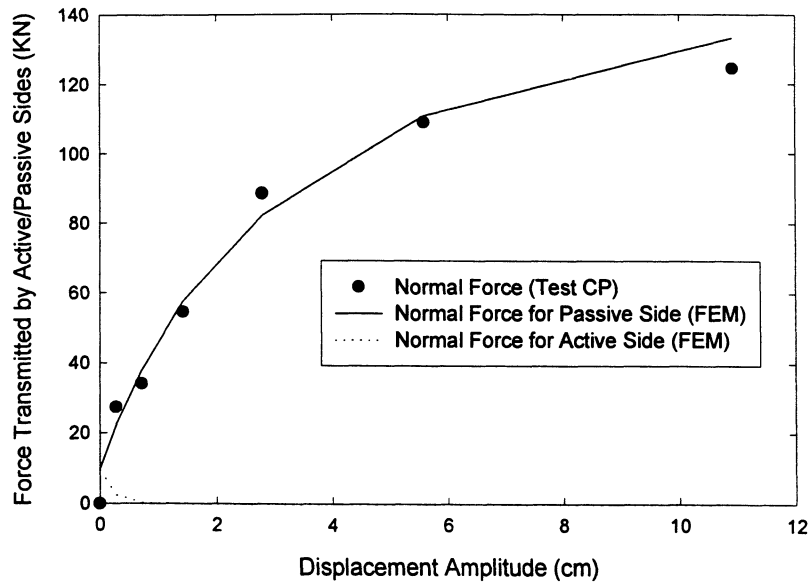


FIGURE 7-12: Normal forces at active/passive sides of the cap (FE results are for Test CBSP with parameters of table 7-1).

agrees reasonably well with $K_p = 14.3$ measured in Test CP. This is interesting, as the aspect ratio of the face considered, $1.14/0.84 = 1.36$, is rather small, as already discussed in Section 4, and reinforces the conclusion in that section that this theoretical K_p obtained from an infinitely long wall assumption is applicable to a rather short footing or cap.

The contributions of the base and sides to the lateral resistance of the cap computed from the FE results for Test CBSP are plotted in figure 7-13, along with the measured lateral resistances for Tests CB, CS, CP and CBSP. The corresponding total and partial, computed and measured, secant stiffnesses are shown in figure 7-14 for various displacement amplitudes. The computed total lateral load (figure 7-7) and stiffness (figure 7-14) for Test CBSP match well with the values measured in centrifuge test CBSP. The computed contributions of the shearing and active/passive sides agree well with the lateral loads and stiffnesses measured in the centrifuge tests with only these sides in contact with the soil (Tests CS and CP). This indicates that the contributions of the shearing and active passive sides in Test CBSP are predicted reasonably well by Tests CS and CP. As mentioned earlier, the computed contribution of the base to the lateral force and corresponding stiffness of the cap in Test CBSP is lower than lateral force and stiffness measured in Test CB. The error in predicting the total lateral resistance of the footing in Test CBSP using Test CB is not large because the overall contribution of the base to the total lateral resistance/stiffness in Test CBSP is very small.

The corresponding computed lateral load contributions from the base and sides of the cap from the FE analysis for Test CBSPL are plotted in figure 7-15. In this test the total vertical load on the cap was doubled compared with Test CBSP. The lateral loads actually measured in Tests CBL, CS, CP and CBSPL are also plotted in figure 7-15. The secant stiffnesses corresponding to these lateral load contributions are plotted in figure 7-16. The computed load-displacement response and secant stiffnesses for Test CBSPL match quite well with the measured values. Also, Test CS and CP predict well the contributions of the shearing and active/passive sides. The computed contribution of the base in Test CBSPL is much lower than the lateral resistance/stiffness measured in Test

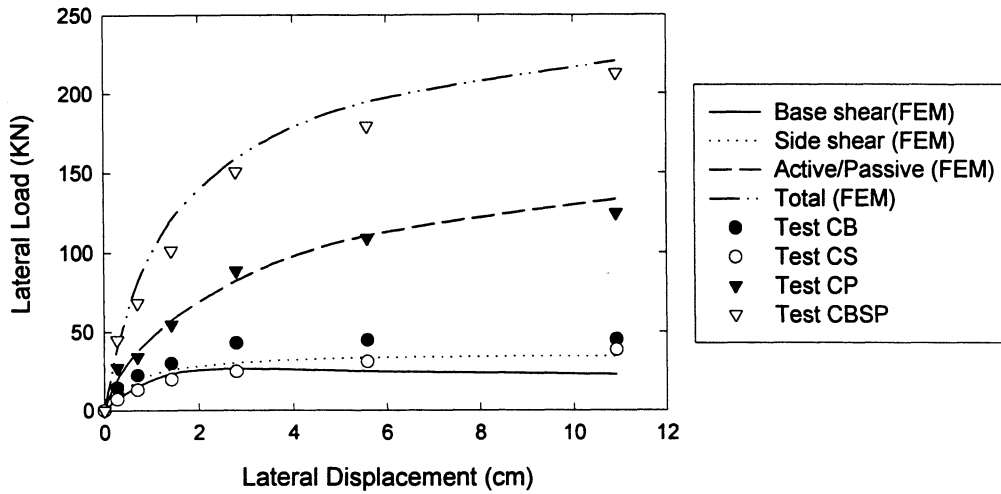


FIGURE 7-13: Measured and computed contributions to the load-displacement response of the cap. (FE results are for Test CBSP with parameters in table 7-1).

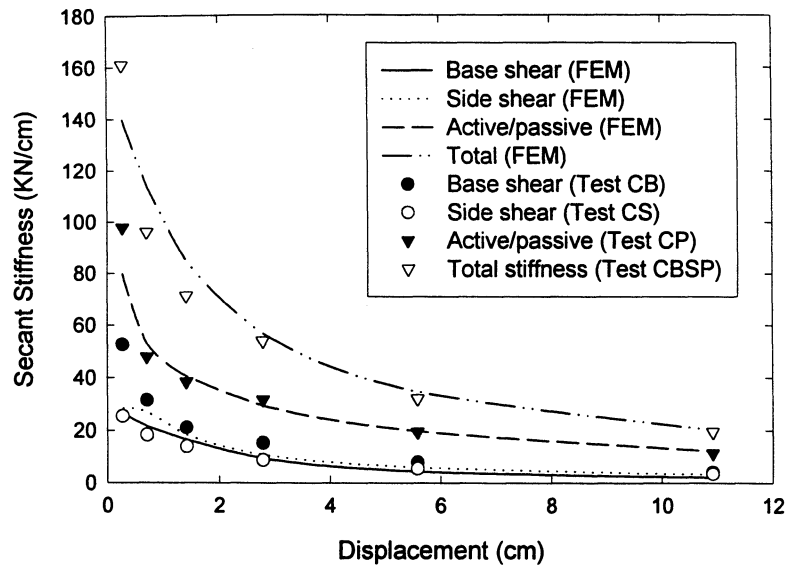


FIGURE 7-14: Measured and computed secant stiffness contributions versus displacement amplitude. (FE results are for Test CBSP with parameters in table 7-1).

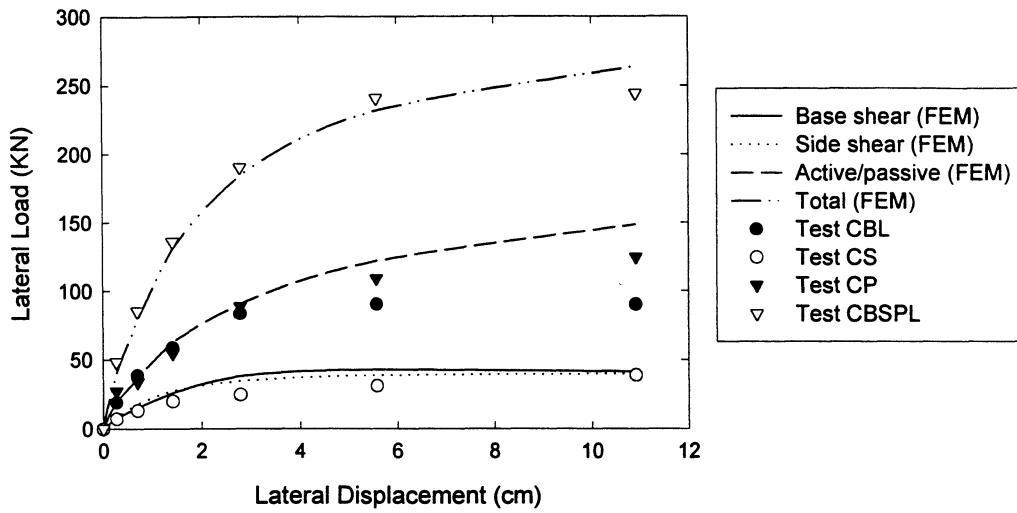


FIGURE 7-15: Measured and computed contributions to the load-displacement response of the cap. (FE results are for Test CBSPL with parameters in table 7-1).

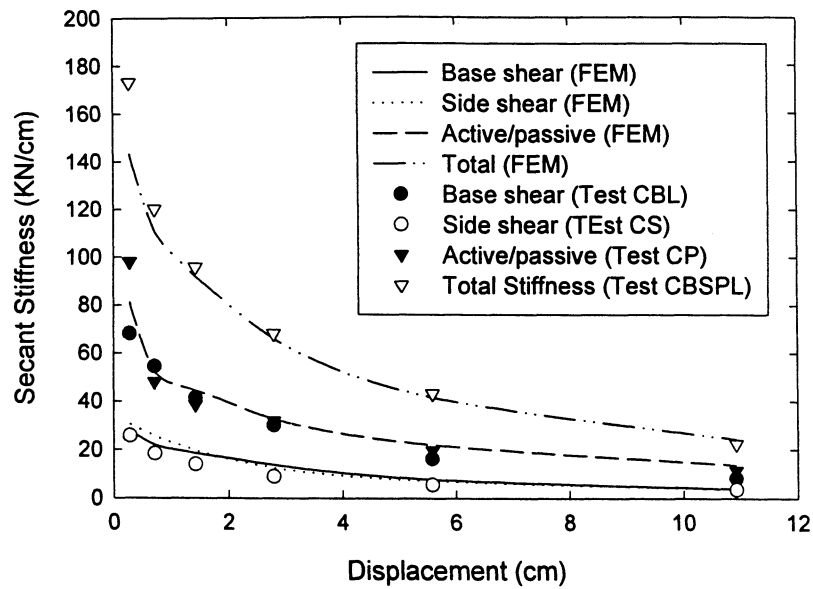


FIGURE 7-16: Measured and computed secant stiffness contributions versus displacement amplitude. (FE results are for Test CBSPL with parameters in table 7-1).

CBL. These observations are consistent with the interpretations made from the FE results of Test CBSP.

7.4 COMPARISON OF LATERAL RESPONSE OF CAP IN TESTS CBSP AND PCBSPI

Centrifuge Test CBSP was performed on the cap-alone, while Test PCBSPI was performed on the pile-cap foundation system. In both tests, all sides and the base of the cap were in contact with the sand. In Test CBSP, the total lateral load was applied at a distance of about one third of the height of the cap from the bottom to minimize the rotation of the cap. In Test PCBSPI, the total lateral load was applied at the pile-head. A comparison of the bending moment distribution measured on the piles in Test PCBSPI (pile-cap system) and Test PI (free-head pile alone), shows that in Test PCBSPI, up to a displacement amplitude of about 2.8 cm, the pile behaved as a free-head pile similar to Test PI. Hence, in Test PCBSPI, the cap must have rotated. Since the cap was very stiff and was rigidly clamped to the pile, the rotation of the cap can be assumed to be equal to the pile-head rotation. Table 7-2 gives the values of pile-head slopes for various displacement amplitudes computed using LPILE for the free-head pile condition (see also Section 6, tables 6-5 and 6.6 and corresponding discussion). Static finite element analyses similar to those described in Subsection 7.3 were performed on the cap model, in which the cap was subjected to lateral displacement with and without a rotation equal to that of table 7-2 for the free-head pile. The computed lateral load values for various lateral displacement amplitudes of cap with and without rotation are listed in table 7-2. For any value of lateral displacement, the computed lateral load values for cap with and without rotation are very close. It should be noted, however, that these analyses were conducted with uniform shear modulus independent of the mean normal stress. In reality, at least at larger displacement amplitudes, the lateral load taken by the cap with and without rotation may be different due to high confining stresses developed under the cap with rotation associated with the wedging action described in the previous subsection.

In pile-cap foundation systems utilized in engineering design, the cap is usually supported by a group of piles rather than a single pile and the rotation of the cap will be

much smaller than the slope of a single free-head pile for any value of lateral displacement. Consequently, the error in neglecting the rotation of the cap in the analysis of the lateral response of pile-cap systems will be even lesser. Hence, when computing the contribution of the cap to the lateral stiffness of pile-cap foundation systems, at least at smaller displacement amplitudes, as an engineering approximation, the rotational and cross-coupling components of the cap stiffness may be neglected. The horizontal cap stiffness can be assumed to be equal to the stiffness of equivalent embedded footing without any rotation.

7.5 PARAMETRIC FE STUDY FOR LATERAL RESPONSE OF CAP/FOOTING

7.5.1 Effect of Soil Modulus on Lateral response

The effect of the soil shear modulus on the lateral response of the foundation was studied by repeating twice the finite element analysis of Test CBSP described in Subsection 7.3, but with the soil modulus increased by 25 % and 50 % respectively. The geometry and other parameters for the foundation-soil system used for these FE analyses, was the same as shown in figure 7-1. **Error! Reference source not found.** The load-displacement responses obtained from these FE runs are shown in figure 7-17. All three curves fall within a narrow range, with the ultimate capacities computed in all cases being almost identical. The horizontal secant stiffnesses computed based on these curves are plotted in figure 7-18 for all displacement amplitudes. The measured and computed stiffnesses also fall within a narrow range. There is some scatter in the stiffnesses up to displacement amplitudes of about 2.5 cm, but beyond that the horizontal stiffness is not very sensitive to the shear modulus used. At large displacements, it could be expected that the soil strength parameters should govern the response of the foundation rather than its shear modulus. For the three FE analyses, the cohesion and friction angle of the soil were not altered, and hence the response at large displacements did not change.

7.5.2 Effect of Foundation Geometry on Lateral Response

Parametric nonlinear finite element analyses were performed in which the square footing/cap's side (W) and the embedment depth (D_f) were varied. A total of eight FE analyses were performed by combining four different values of footing width and two

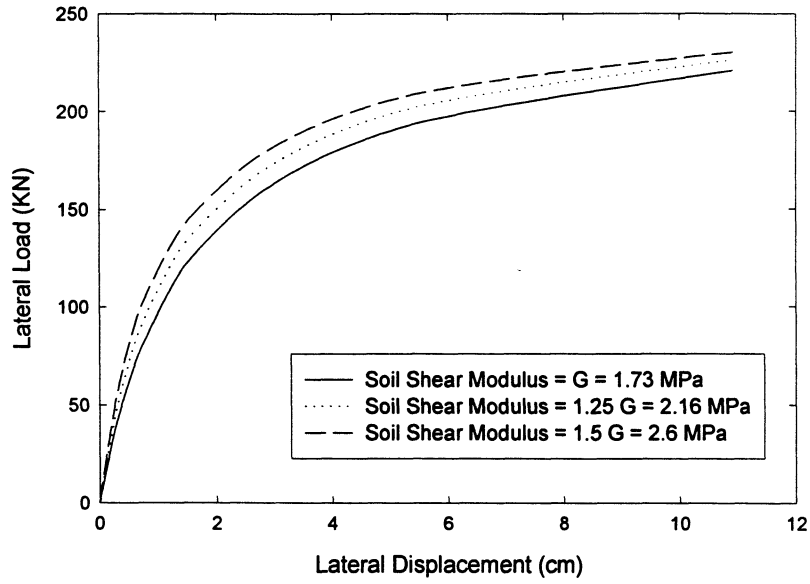


FIGURE 7-17: Computed load-displacement responses for Test CBSP with different soil shear moduli.

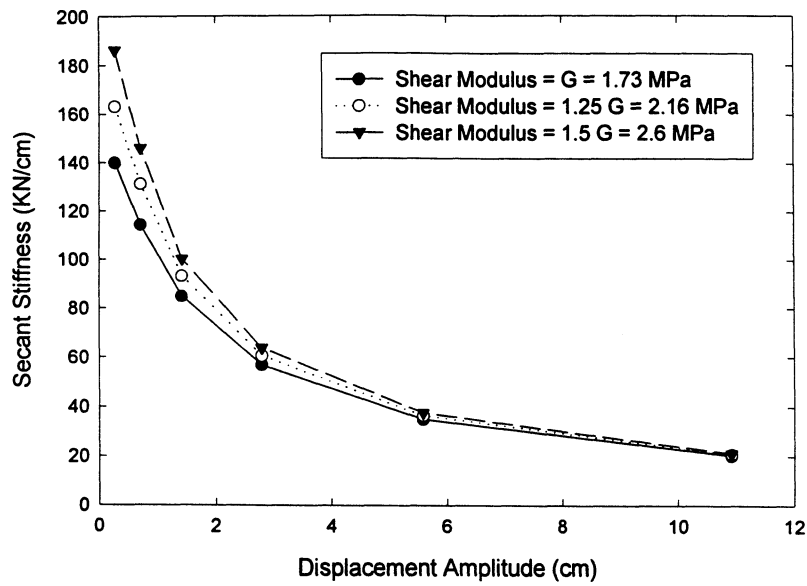


FIGURE 7-18: Computed horizontal secant stiffness versus displacement amplitude for Test CBSP with different soil shear moduli.

TABLE 7-3: Comparison of ultimate capacity calculated by adding contributions of different sides with the capacity obtained using FE analyses. (Note: 2B = 1.14 m, D = 1.14 m, G = 1.73 MPa).

Footing Dimensions (W x W x D _f)	Contribution to Ultimate Capacity (KN)			Ultimate Capacity (KN)	
	Base (a)	Shearing Sides (b)	Passive Side (c)	(a + b + c)	Computed using FEM
2B x 2B x D	44	38	124	206	221
4B x 4B x D	176	76	266	518	520
6B x 6B x D	396	114	372	882	856
8B x 8B x D	704	152	496	1352	1281
2B x 2B x 2D	88	152	496	736	606
4B x 4B x 2D	352	303	992	1647	1609
6B x 6B x 2D	792	455	1488	2735	2552
8B x 8B x 2D	1408	607	1984	3999	3577

TABLE 7-4: Comparison of initial secant stiffness computed in the FE parametric study with the stiffness calculated using Pais-Kausel and Gazetas-Tassoulas solutions. (Note: 2B = 1.14 m, D = 1.14 m, G = 1.73 MPa).

Footing Dimensions (W x W x D _f)	Stiffness of surface footing calculated using Pais-Kausel (1988) solution, K _{sur} KN/cm	Gazetas-Tassoulas (1987a) factors		Stiffness of embedded footing, K _h , KN/cm	
		Trench factor I _{tre}	Sidewall factor I _{wall}	K _{sur} I _{tre} I _{wall}	Computed using FEM at 0.3-cm deflection
2B x 2B x D	55.0	1.21	2.53	168.7	140.0
4B x 4B x D	110.0	1.15	1.88	237.8	234.3
6B x 6B x D	164.9	1.12	1.64	302.7	318.2
8B x 8B x D	219.9	1.11	1.51	366.1	400.1
2B x 2B x 2D	55.0	1.30	3.67	262.3	229.3
4B x 4B x 2D	110.0	1.21	2.53	337.5	339.2
6B x 6B x 2D	164.9	1.17	2.11	407.5	438.1
8B x 8B x 2D	219.9	1.15	1.88	475.4	528.2

values of embedment depths. The ratio m/D_f was maintained constant in all FE runs. The dimensions of the footing for the base case of $W = 2B$ and $D_f = D$ are shown in figure 7-1. The material properties for the foundation and the soil were kept constant in all cases. These material properties are listed in table 7-1.

The ultimate capacities computed from the FE analyses for the eight cases are listed in table 7-3. In general, the ultimate lateral capacity of the footing increases with its dimensions. Table 7-3 also lists the capacities calculated by adding the contributions of the base and the shearing and active/passive sides calculated using some simplified engineering rules developed from the centrifuge tests. The ultimate base shear is calculated in table 7-3 by multiplying the total vertical load by the frictional coefficient $\mu = 0.82$. The ultimate side shear is equal to the normal soil thrust on the shearing sides times the frictional coefficient μ . The normal thrust on these shearing sides is obtained by utilizing the dilatational side-shear earth-pressure coefficient $K_s = 2.1$. The limiting lateral passive thrust is calculated using of lateral passive earth-pressure coefficient $K_p = 14.3$. That is, the following expressions were used to calculate the various contributions to the ultimate capacity of footings listed in table 7-3.

$$\text{Ultimate Base Shear} = \mu \gamma_f (H W^2) \quad (7-18)$$

$$\text{Ultimate Side Shear} = \mu K_s (\gamma m H + \frac{1}{2} \gamma H^2) 2W \quad (7-19)$$

$$\text{Ultimate Passive Resistance} = K_p \cos \phi_w (\gamma m H + \frac{1}{2} \gamma H^2) W \quad (7-20)$$

In these equations W is the width of the square footing, $W = 2B$ in the base case; H is the height of the footing; and $m = D_f - H$ is the depth of the top rim of the footing from ground surface where D_f is the embedment depth of the footing, $D_f = D$ in the base case. These dimensions are shown in figure 7-1 for the base case. The friction and earth pressure coefficients and wall friction angle ($\mu = 0.82$, $K_s = 2.1$, $K_p = 14.3$, and $\phi_w = 39^\circ$) were determined in Section 4 using the results of centrifuge tests on cap-alone (See table 4-1). Other foundation and soil parameters used are given in table 7-1 **Error! Reference source not found.** Comparison of the ultimate lateral capacities calculated using (7-18) to (7-20) with the capacities computed by FE analyses shows that the maximum error in

using (7-18) to (7-20) in conjunction with the addition rule is only of the order of 10 %. Hence the above equations furnish a very good design approximation to calculate the ultimate lateral capacity of square foundations or pile caps in engineering practice. This is especially interesting considering that a unique $K_p = 14.3$, consistent with an infinite aspect ratio of the passive wall, is used for the range of aspect ratios from 1.36 to (4) (1.36) = 5.4, always with good agreement.

The initial secant stiffness computed using the finite element analyses for the eight cases considered in the parametric study are listed in table 7-4. These secant stiffnesses are computed for 0.28-cm lateral displacement, which was the amplitude of the first lateral displacement cycle in the centrifuge tests. As mentioned earlier in Section 4, the elastic stiffness K_h , for a square embedded foundation of side W can be calculated by making use of Pais-Kausel (1988) and Gazetas-Tassoulas (1987a) equations.

$$K_h = K_{sur} I_{tre} I_{wall} \quad (7-21)$$

where K_{sur} is the lateral stiffness of an equivalent surface footing given by,

$$K_{sur} = \frac{4.6WG}{(2 - \nu)} \quad (7-22)$$

and I_{tre} and I_{wall} are factors incorporating the trench and sidewall effects:

$$I_{tre} = 1 + 0.15 \sqrt{D_f / (W / 2)} \quad (7-23)$$

$$I_{wall} = 1 + 0.53 \left(\frac{hA_w}{(W / 2)^3} \right)^{0.40} \quad (7-24)$$

where W is the width of the footing; D_f is the embedment depth; A_w is the vertical area of the footing sidewall actually in contact with the soil; and h is the depth from ground surface of the centroid of the sidewall area in contact with the soil. The initial stiffnesses calculated for the eight cases using (7-21) to (7-24) are listed in table 7-4. Comparison of these stiffness values with the initial secant stiffnesses computed using the FE analyses shows that the error in using the Pais-Kausel and Gazetas-Tassoulas solution to estimate the initial secant stiffness of the footing is of the order of 15%. Thus, the Pais-Kausel and Gazetas-Tassoulas solutions may be used to determine the initial stiffness of an embedded foundation or pile-cap, in the absence of measurements or FE calculations.

The secant stiffness versus displacement amplitude for all eight cases considered are plotted in figure 7-19.

7.6 CONCLUSIONS

Following are some of the conclusions that may be drawn based on the FE study of lateral response of square footings/ pile caps presented in this section:

1. The Modified Drucker-Prager Cap model available in the code ABAQUS can be conveniently used to study nonlinear soil-structure interaction problems. The load-displacement responses for the centrifuge tests CBSP and CBSPL on a fully embedded foundation in full contact with soil at the base and around the walls agree well the results of 3-D nonlinear FE analyses.
2. The equivalent material damping ratios, calculated from the monotonic load-displacement curves obtained from FE analyses using the Masing criteria are much lower than the damping ratios measured in the centrifuge tests.
3. The contributions of the shearing and active/passive sides to the lateral response of the footing/cap computed using results of the nonlinear FE analyses match well with the centrifuge Tests CS and CP, in which respectively only the shearing and active passive sides were in contact with the soil.
4. When computing the contribution of the cap to the lateral stiffness of pile-cap foundation system, at least at small lateral displacement amplitudes, as an engineering approximation, the rotational and cross-coupling components of the cap stiffness may be neglected. The horizontal cap stiffness can be assumed to be equal to the stiffness of equivalent embedded footing without any rotation.
5. The secant stiffness of the foundation depends on the shear modulus at small displacements. At large displacements, the influence of the shear modulus on the secant stiffness is negligible.
6. A parametric nonlinear FE study conducted to understand the effect of the footing geometry on the lateral response shows that the ultimate lateral capacity of a footing can be very well approximated, by adding contributions of its base and sides derived from simple basic formulations incorporating friction and lateral earth pressure coefficients. The initial secant stiffnesses computed using these FE analyses agree

reasonably well with those predicted using the Pais-Kausel and Gazetas-Tassoulas solutions, and an appropriate value of the soil modulus.

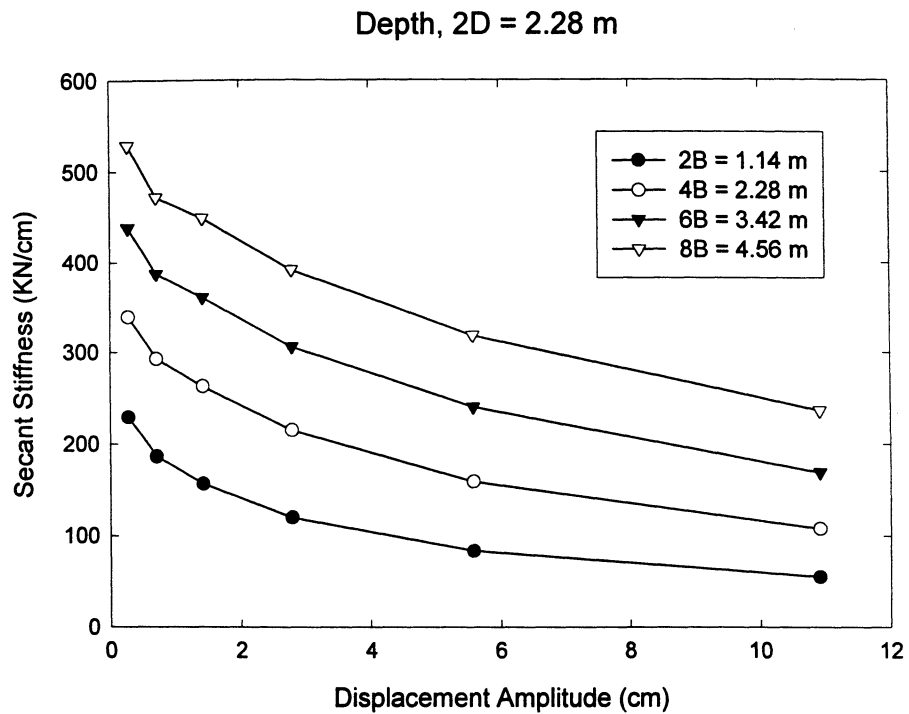
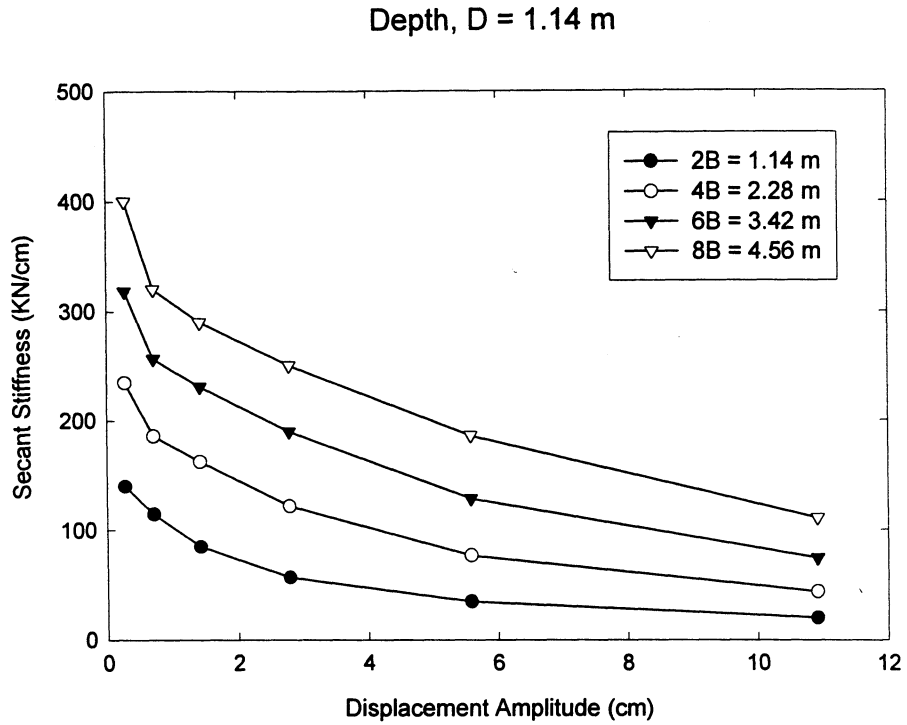


FIGURE 7-19: Results of parametric FE analyses conducted to study the influence of footing geometry on lateral secant stiffness. (FE analyses performed with $G = 1.73$ MPa).

SECTION 8
FINITE ELEMENT ANALYSIS OF CAP/FOOTING WITH SOIL MODULUS
DEPENDENT ON MEAN NORMAL STRESS

8.1 INTRODUCTION

Three-dimensional nonlinear finite element (FE) analyses similar to those described in Section 7, but with the soil shear modulus now dependent on the initial mean normal stress, were performed. These FE analyses were utilized to numerically predict the results of centrifuge tests on the cap-alone described in Section 4. The centrifuge tests were performed with dry Nevada sand of 75% relative density. Since in sands the shear modulus depends on the confining pressure, the constant shear modulus throughout the soil mass used in Section 7 can be only a first approximation. To allow the shear modulus to vary through the soil mass according to the mean normal stress should be a better approximation.

Several researchers have found that in dry sands the small-strain shear modulus G_{\max} is approximately proportional to the square root of the mean normal stress σ_o (Hardin and Drnevich, 1972; Richart et al., 1970; Seed and Idriss, 1970).

$$G_{\max} = A\sigma_o^{0.5} \quad (8-1)$$

where A is a constant of proportionality. Richart et al. (1970) give the following expression for G_{\max} in uniform sands with rounded particles:

$$G_{\max} = 6900 \frac{(2.17 - e)^2}{1 + e} \sigma_o^{0.5} \quad (8-2)$$

where both G_{\max} and σ_o are in KPa and e is the void ratio of the sand. For Nevada sand of relative density 75% used in the centrifuge tests, $e = 0.605$. Using (8-1) and (8-2), the constant of proportionality A for this sand is $A = 10529$ in SI units.

This section presents the results of nonlinear FE analyses performed to numerically simulate centrifuge Tests CBSP and CBSPL on the cap-alone, when all sides and the base

of the cap were in contact with the soil. These FE analyses are similar to those described in Section 7, but with the soil shear modulus now dependent on the mean normal stress. A parametric study was also performed to evaluate the effect of the cap geometry on the lateral stiffness, analogous to the one presented in Section 7, but in this case with the soil shear modulus given by (8-1). The results of this parametric study are also presented in this section.

8.2 NUMERICAL SIMULATION OF CENTRIFUGE TESTS CBSP AND CBSPL

Nonlinear three-dimensional FE analyses were performed to predict the results of centrifuge Tests CBSP and CBSPL. An elastic constitutive relation was used for the cap/foundation material, while the Modified Drucker Prager Cap model described in Section 7, was used to describe the behavior of the soil elements. Similar to what was done in Section 7, the interface between the soil and the footing/cap was defined using interface elements with a friction coefficient of 0.82.

8.2.1 FE Analyses

In the centrifuge tests, the loading of the model cap involved two stages. In the first stage the model was subjected to gravity and vertical force on the cap, and in the second stage lateral displacement cycles were applied to the cap. All sides and the base of the cap were in contact with the soil in Tests CBSP and CBSPL. The finite element analyses presented in this section were performed with the soil shear modulus proportional to the square root of the initial mean normal stress, at the end of the first stage of loading, using (8-1). This was accomplished through an iterative process. The steps involved in this process are:

1. In the first iteration, a nonlinear FE analysis was performed for gravity and vertical loading of foundation (no lateral loading) using the parameters of table 7-1 and an initial value of soil shear modulus of 1.73 MPa specified for all soil elements.
2. The three effective principal stresses σ_1 , σ_2 , and σ_3 for all soil elements were obtained from this FE analysis and the mean normal stress σ_o for each soil element was calculated as:

$$\sigma_o = \frac{\sigma_1 + \sigma_2 + \sigma_3}{3} \quad (8-3)$$

3. The shear modulus for each soil element was recalculated using (8-1), and the nonlinear FE analysis for gravity and vertical loading, described in step 1, was repeated with these calculated shear moduli specified for the respective soil elements.
4. Steps 2 and 3 were repeated, until a close agreement between the calculated soil moduli for all soil elements in two consecutive iterations was achieved.
5. The lateral displacements were then applied to the cap, with the mean-normal-stress-dependent soil moduli specified in each soil element throughout the soil mass.

Nonlinear finite element analyses were first performed for Test CBSP using $A = 10529$ for G_{\max} obtained from Richart et al. equation (8-2). The computed monotonic load-displacement response is shown in figure 8-1 (dashed line), along with the measured response for Test CBSP. The load-displacement response computed with $A = 10529$ is much stiffer than the measured response. Hence, a smaller value of $A = 584$ was backfigured to fit the computed load displacement response with the measured response in Test CBSP. The new load-displacement monotonic curve computed using $A = 584$ is also shown in figure 8-1. This curve passes through the apexes of the measured load-displacement loops, indicating excellent agreement of measured and computed response. The measured load displacement loops for Test CBSPL, in which the total vertical load on the cap was doubled, along with the computed response for that test with $A = 584$ are shown in figure 8-2. Again, the computed response curve passes through the apexes of the measured loops, demonstrating good agreement.

The measured variation of secant stiffness with lateral displacement amplitude for Test CBSP is shown in figure 8-3, along with the values computed with: (i) a uniform soil shear modulus $G = 1.73$ MPa (Section 7), (ii) variable shear modulus dependent on mean normal stress $G = A \sigma_o^{0.5}$ with $A = 10529$ (Richart et al value), and (iii) variable shear modulus with $A = 584$ (backfigured value). The measured stiffnesses match very well with the computed stiffnesses both in the case of uniform $G = 1.73$ MPa and stress-dependent G with $A = 584$ at all displacement amplitudes. At small displacements, the computed stiffnesses with non-uniform G and $A = 10529$ are much higher than the measured stiffnesses. At larger displacement (greater than 2.5 cm), the secant stiffnesses

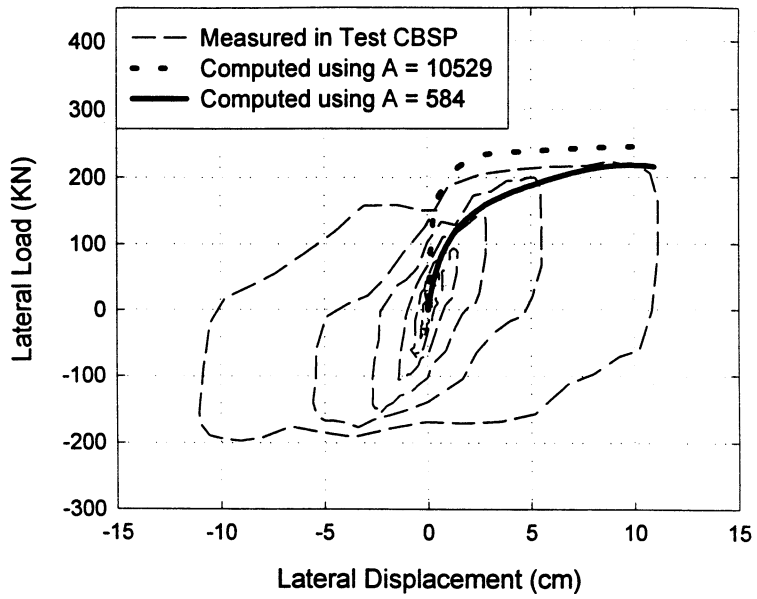


FIGURE 8-1: Measured and computed load-displacement response for Tests CBSP.

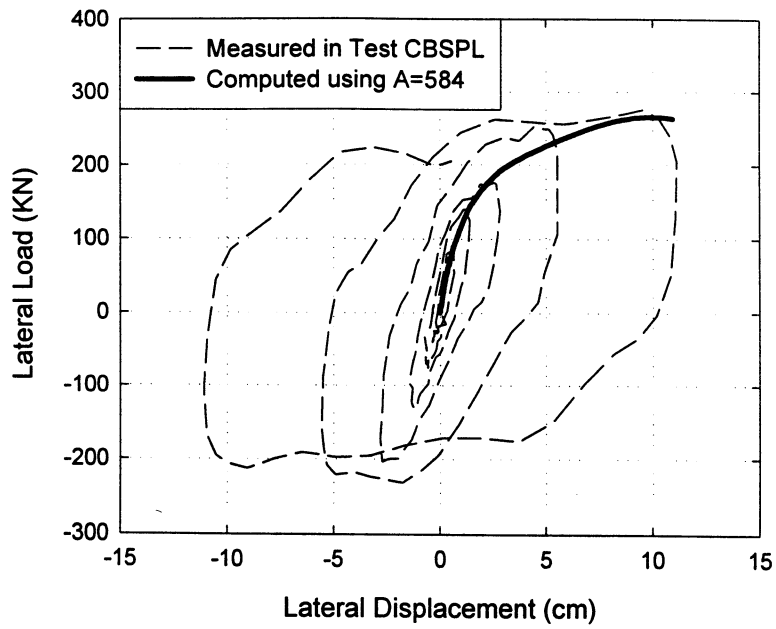


FIGURE 8-2: Measured and computed load-displacement response for Test CBSPL.

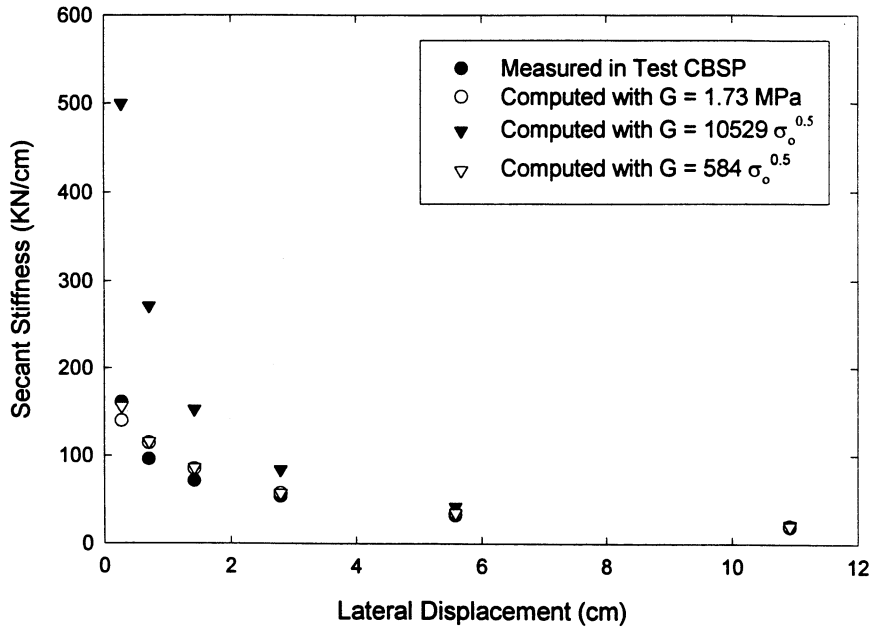


FIGURE 8-3: Measured and computed secant stiffness for Test CBSP.

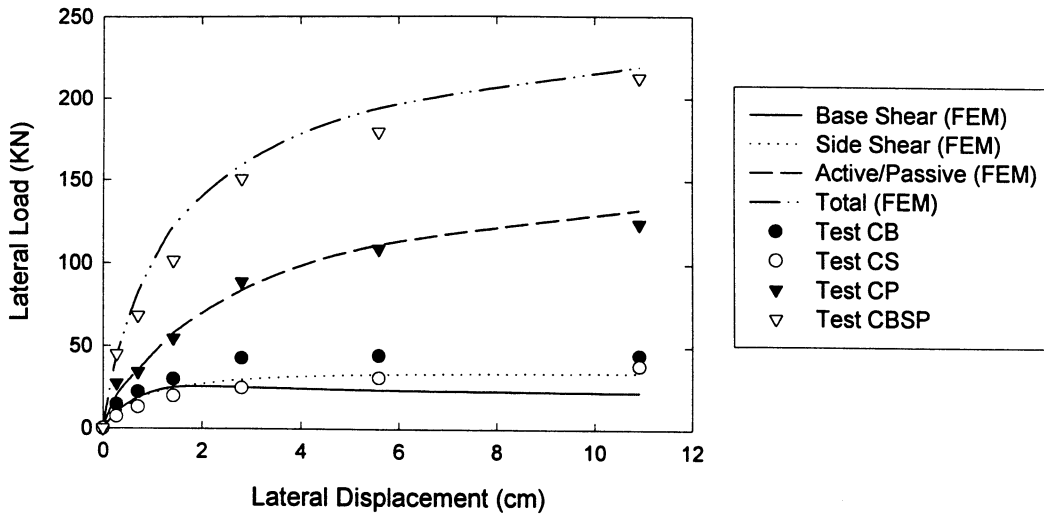


FIGURE 8-4: Measured and computed contributions to the load displacement response in Test CBSP. (FEM analyses are with $G = 584 \sigma_0^{0.5}$).

tend to become independent of the initial soil modulus used. It is interesting that the value of $A = 584$, which was found to provide the best match for G at small lateral displacement, in conjunction with $A = 10529$ corresponding to G_{\max} , provide a $G/G_{\max} = 584/10529 = 0.06 < 0.10$, consistent with the discussion on G and G/G_{\max} for Test CBSP in Subsection 4.5.

8.2.2 Contribution of Base and Sides of Cap to Total Lateral Response

The contributions of the base and sides of the cap to the total lateral force, computed from the FE analysis of Test CBSP with $G = 584 \sigma_o^{0.5}$, are shown in figure 8-4. These contributions were computed from the FE results by the same procedure described in Section 7. This figure also plots the peaks of the measured load-displacement loops for centrifuge Tests CB, CS, CP and CBSP. The corresponding computed and measured secant stiffnesses are shown in figure 8-5. The computed total load-displacement response, as well as the secant stiffnesses for the cap match well with the values measured in Test CBSP. Also, very good agreement is observed between the computed contributions of the shearing and active/passive sides, and the measured responses in Test CS and CP in which these sides were exclusively contributing. The computed contribution of the base in Test CBSP is lower than the measured response for Test CB in which only the base of the cap was in contact with the soil. This may be because unlike Test CB, not all the vertical load in Test CBSP is transmitted to the base.

The computed contributions of the base and sides of the cap to the load-displacement response of Test CBSPL are plotted in figure 8-6. The peaks of the measured load-displacement loops for Test CBL, CS, CP and CBSPL are also plotted in the same figure. The corresponding secant stiffnesses are plotted in figure 8-7. The computed total response and the contributions of the shearing and active/passive sides conform to the measured responses for Tests CBSPL, CS and CP, respectively. The measured response for Test CBL is lower than the computed contribution of the base. Similar trends were observed earlier in Section 7, when the computed lateral response contributions from FE analyses of Tests CBSP and CBSPL with uniform $G = 1.73 \text{ MPa}$, were compared with the corresponding measured responses.

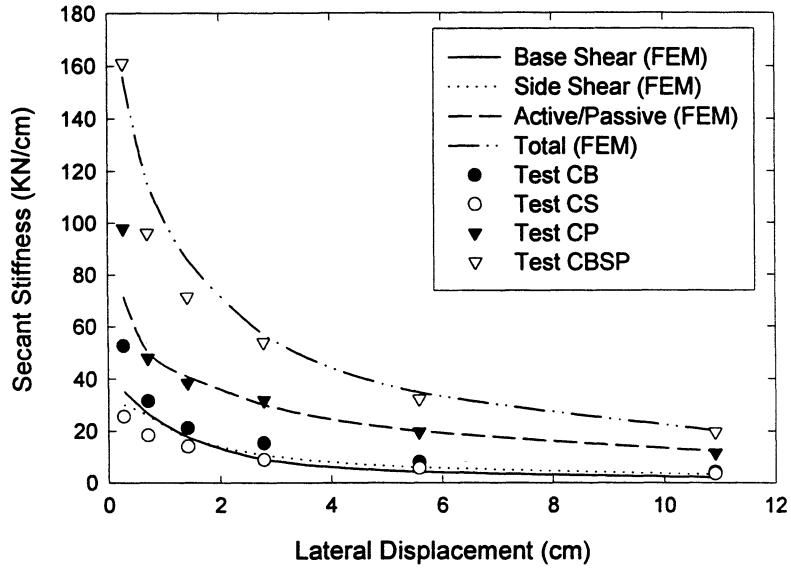


FIGURE 8-5: Measured and computed contributions to secant stiffness in Test CBSP (FEM analyses are with $G = 584 \sigma_0^{0.5}$).

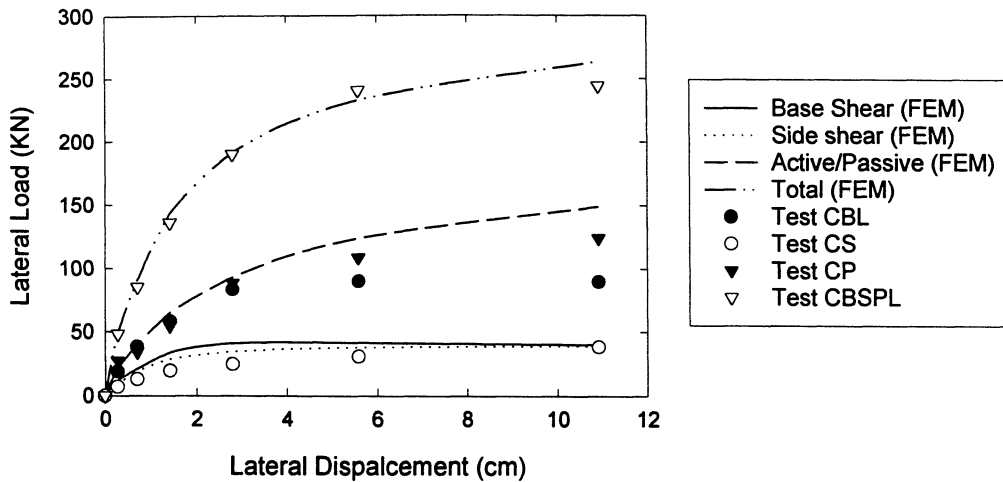


FIGURE 8-6: Measured and computed contribution to load-displacement response in Test CBSPL (FEM analyses are with $G = 584 \sigma_0^{0.5}$).

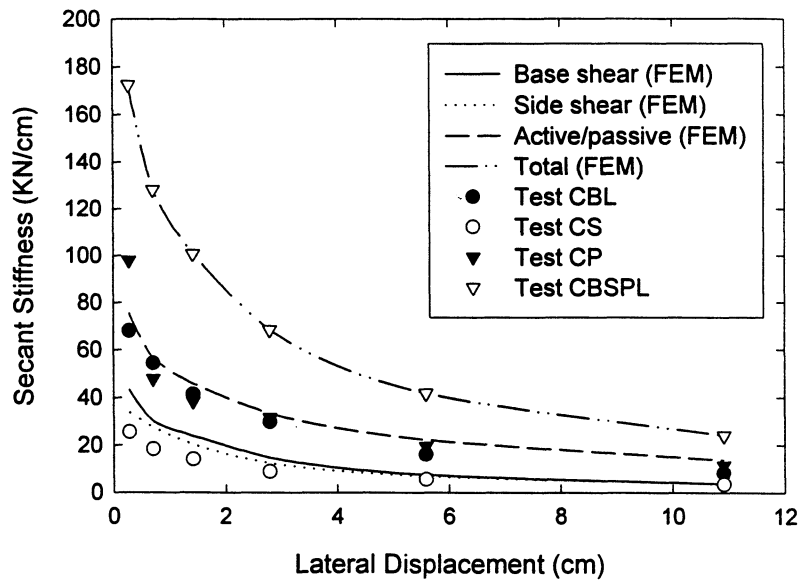


FIGURE 8-7: Measured and computed contributions to secant stiffness of Test CBSPL. (FEM analyses are with $G = 584 \sigma_o^{0.5}$)

8.3 EFFECT OF FOUNDATION GEOMETRY ON LATERAL RESPONSE

Parametric nonlinear FE analyses were performed, in which the square footing/cap's side (W) and embedment depth (D_f) were varied. A total of eight FE analyses were performed with combinations of four different values of footing-width and two values of embedment depths. The ratio m/D_f was maintained constant in all FE runs. The dimensions of the footing for the base case of $W = 2B$ and $D_f = D$ are shown in figure 7-1. All FE analyses were performed with the soil modulus proportional to the square root of the mean effective stress given by $G = 584 \sigma_o^{0.5}$. This was accomplished in each case through an iterative process similar to the one described in Subsection 8.2. Other soil and foundation parameters used in these FE runs may be found in table 7-1. The unit weight of the foundation and soil was constant in all FE runs. Thus, in all cases the ratio between apparent foundation pressure (total foundation load divided by base area), and vertical soil pressure at the level of the base of the foundation (unit weight of soil times depth of foundation) was maintained constant.

The ultimate capacities computed using FE analyses for the eight cases are listed in table 8-1. In general, the ultimate capacity of the footing increases with its dimensions. Table 8-1 also lists the capacities calculated by adding the contributions of the base and the shearing and active/passive sides. These contributions are calculated using the procedure described in Section 7. The ultimate base shear is calculated by multiplying the total vertical load by the friction coefficient μ . The ultimate side shear is equal to the horizontal normal soil thrust on the shearing sides times the frictional coefficient μ . This normal thrust on the shearing sides is obtained by utilizing the dilatational side-shear earth-pressure coefficient $K_s = 2.1$. The limiting lateral passive thrust is calculated making use of the lateral passive earth-pressure coefficient K_p . Equations (7-18) to (7-20) were used to calculate different contributions to the ultimate capacity of footings in table 8-1. The friction and earth pressure coefficients ($\mu = 0.82$, $K_s = 2.1$, and $K_p = 14.3$), determined in Section 4 using the results of centrifuge tests on the cap-alone (See table 4-1), were used. Other foundation and soil parameters are explained in table 7-1 and figure 7-1. Comparison of the ultimate lateral capacities calculated using (7-18) to (7-20) with

TABLE 8-1: Comparison of ultimate capacity calculated by adding contributions of different sides with the capacity obtained using FE analyses. (Note: $2B = 1.14$ m, $D = 1.14$ m, $G = 584 \sigma_o^{0.5}$)

Footing Dimensions (W x W x D _f)	Contribution to Ultimate Capacity (KN)			Ultimate Capacity (KN)	
	Base (a)	Shearing Sides (b)	Passive Side (c)	(a + b + c)	Computed using FEM
2B x 2B x D	44	38	124	206	240
4B x 4B x D	176	76	266	518	521
6B x 6B x D	396	114	372	882	855
8B x 8B x D	704	152	496	1352	1280
2B x 2B x 2D	88	152	496	736	875
4B x 4B x 2D	352	303	992	1647	1673
6B x 6B x 2D	792	455	1488	2735	2663
8B x 8B x 2D	1408	607	1984	3999	3690

TABLE 8-2: Comparison of initial secant stiffness at 0.3-cm deflection computed with $G = 1.73$ MPa and $G = 584 \sigma_o^{0.5}$. (Note: $2B = 1.14$ m, $D = 1.14$ m.)

Foundation Dimensions (W x W x D _f)	Initial stiffness of embedded footing K_h computed at 0.3 cm deflection (KN/cm)		Ratio of computed initial stiffnesses (b)/(a)
	$G = 1.73$ MPa (a)	$G = 584 \sigma_o^{0.5}$ (b)	
2B x 2B x D	140.0	155.9	1.11
4B x 4B x D	234.3	283.1	1.20
6B x 6B x D	318.2	401.7	1.26
8B x 8B x D	400.1	509.1	1.27
2B x 2B x 2D	229.3	305.4	1.33
4B x 4B x 2D	339.2	488.4	1.44
6B x 6B x 2D	438.1	669.8	1.53
8B x 8B x 2D	528.2	847.3	1.60

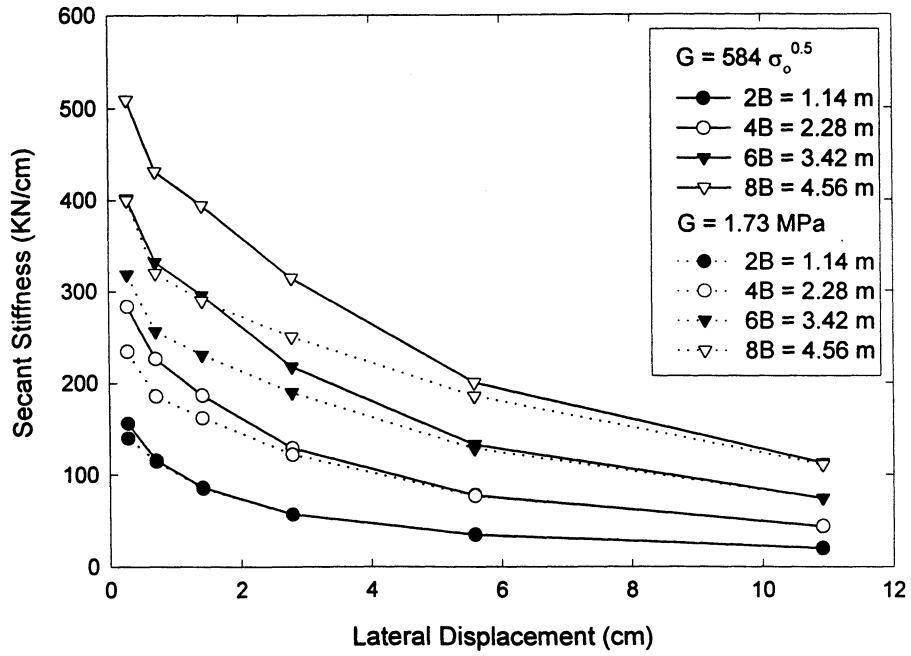
the capacities computed by FE analyses shows that the maximum error in using (7-18) to (7-20) is only of an order of 10 %. Hence, these equations furnish a very good design approach to calculate the ultimate lateral capacity of square foundations or pile caps in engineering practice.

The reduction of secant stiffnesses with displacement amplitude computed from the FE analyses for all eight cases with $G = 584 \sigma_0^{0.5}$ are shown in figure 8-8 (solid lines). This figure also shows the secant stiffness reduction curves for the eight cases computed in Section 7 with a uniform value of $G = 1.73$ MPa (dotted lines). For the base case of $W = 2B = 1.14$ and $D_f = D = 1.14$, the secant stiffness reduction curves are almost identical for both definitions of G . This is because the constants in both definitions of G were backfigured to fit the experimental results of the centrifuge Test CBSP. For all other cases, at large displacements the secant stiffnesses computed using both definitions of G are also nearly the same. This independence of secant stiffnesses at large displacements on the distribution of soil shear modulus is consistent with the independence of secant stiffness on the value of soil modulus noticed in the parametric FE studies performed in Section 7. The reason is clearly that large displacement stiffness depends on capacity, and thus on c and ϕ of the soil and not on G . At small displacements the secant lateral stiffnesses computed with $G = 584 \sigma_0^{0.5}$ are higher than the stiffnesses calculated using $G = 1.73$ MPa. This fact becomes evident in table 8-2, which compares the initial secant stiffnesses computed using a uniform value of $G = 1.73$ MPa and $G = 584 \sigma_0^{0.5}$. Stiffnesses computed using non-uniform G are 10 to 60 % higher than the stiffnesses computed using uniform G .

In Section 7 it was observed that the Pais-Kausel (1988) and Gazetas-Tassoulas (1987a) solutions give fairly accurate estimate of the initial secant stiffnesses computed using FE analyses with uniform soil shear modulus. The horizontal secant stiffness K_h of a square foundation of side W , embedded in an elastic half-space with uniform soil shear modulus G can be expressed using these solutions as:

$$K_h = \frac{4.6WG}{(2-\nu)} I_{tre} I_{wall} \quad (8-4)$$

Depth, $D_f = D = 1.14$ m



Depth, $D_f = 2D = 2.28$ m

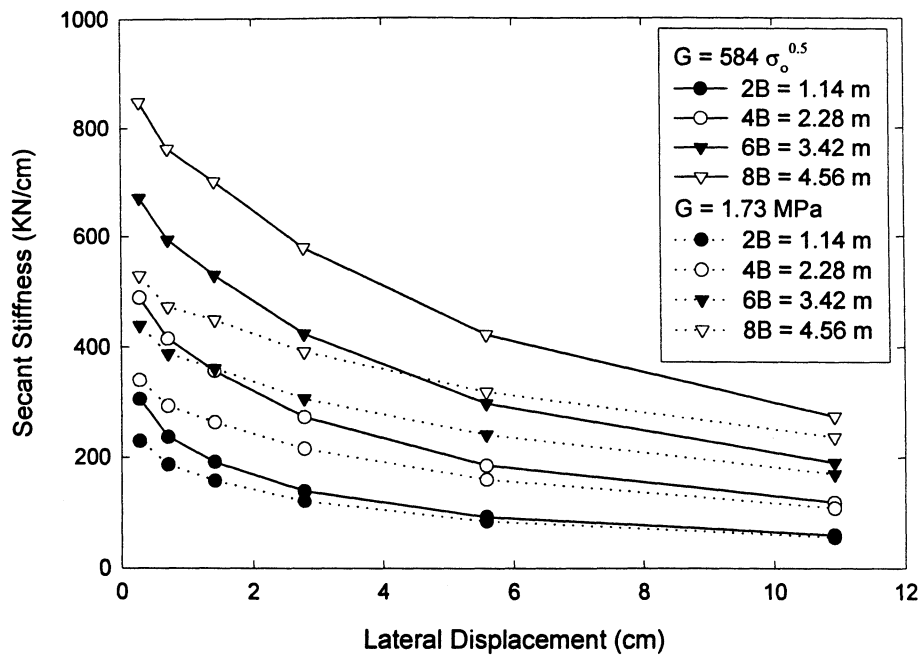


FIGURE 8-8: Results of parametric FE analyses conducted to study the influence of footing geometry on lateral secant stiffness.

where I_{tre} and I_{wall} are the trench and sidewall factors respectively, given by Gazetas and Tassoulas (see Subsection 7.5). This equation can be used to back-calculate an equivalent uniform soil shear modulus, G_{eq} from the initial secant stiffnesses computed using FE analyses with $G = 584 \sigma_o^{0.5}$. The G_{eq} values calculated for all eight cases considered in this parametric study using (8-4) are listed in table 8-3. These values range from 1.6 MPa to more than 3 MPa as opposed to the value of 1.73 MPa backfigured from centrifuge Test CBSP.

The FE analyses performed for this parametric study assumed that the soil shear modulus proportional is to the square root of the mean normal stress, $G = 584 \sigma_o^{0.5}$. The mean normal stress in the soil in free-field is equal to

$$\sigma_o = \frac{(1 + 2K_o)\sigma_v}{3} \quad (8-5)$$

where σ_v is the vertical stress; and K_o is the coefficient of earth pressure at rest. Assuming $K_o = 0.5$, an equivalent depth D_{eq} , such that $\sigma_v = \gamma D_{eq}$, can be computed from the value of equivalent uniform soil shear modulus G_{eq} in table 8-3 using the above equations in each case. This is the depth at which an equivalent uniform soil shear modulus satisfying $G = 584 \sigma_o^{0.5}$ should be selected, so that the Pais-Kausel and Gazetas-Tassoulas equations predict accurately the initial secant lateral stiffnesses computed using FE analyses with $G = 584 \sigma_o^{0.5}$. The equivalent depths D_{eq} computed for all eight cases are listed in table 8-3. These depths range from 0.7 m to 2.6 m for the range of foundation dimensions considered in this parametric study. The normalized equivalent depth D_{eq}/D_f is plotted against the normalized half width $(W/2)/D_f$ of the footing for each case in figure 8-9, where D_f is the depth of the foundation from the ground surface. In general, as $(W/2)/D_f$ increases, D_{eq}/D_f also increases.

8.4 CONCLUSIONS

The results of three-dimensional nonlinear FE analyses with soil modulus dependent on the mean normal stress ($G = A \sigma_o^{0.5}$) performed in this section lead to the following conclusions:

TABLE 8-3: Equivalent uniform soil shear modulus for the FE analyses with $G = 584 \sigma_0^{0.5}$ (Note: $2B = 1.14 \text{ m}$, $D = 1.14 \text{ m}$.)

Foundation Dimensions (W x W x D _f)	Computed initial Stiffness with $G = 584 \sigma_0^{0.5}$ K_h (KN/cm)	Gazetas-Tassoulas (1987a) factors		Equivalent uniform soil shear modulus G_{eq} (MPa)	Depth of Equivalent soil shear modulus D_{eq} (m)
		Trench factor I_{tre}	Sidewall factor I_{wall}		
2B x 2B x D	155.9	1.21	2.53	1.61	0.70
4B x 4B x D	283.1	1.15	1.88	2.06	1.15
6B x 6B x D	401.7	1.12	1.64	2.29	1.43
8B x 8B x D	509.1	1.11	1.51	2.39	1.54
2B x 2B x 2D	305.4	1.30	3.67	2.01	1.10
4B x 4B x 2D	488.4	1.21	2.53	2.51	1.71
6B x 6B x 2D	669.8	1.17	2.11	2.84	2.20
8B x 8B x 2D	847.3	1.15	1.88	3.08	2.58

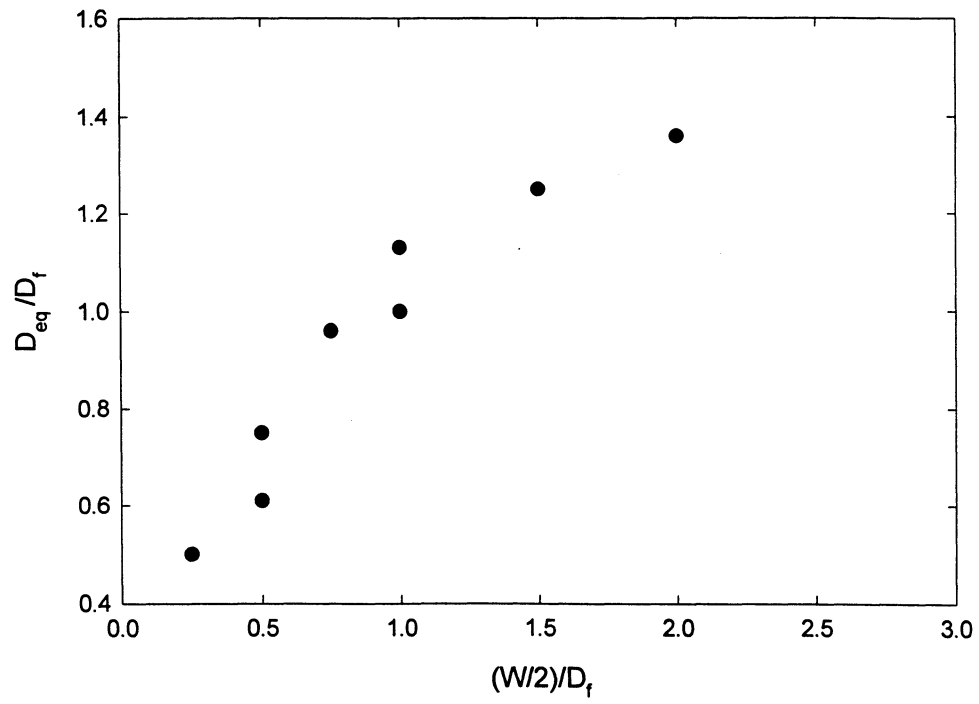


FIGURE 8-9: Normalized equivalent depth versus normalized side of the footing ($m/D_f = 0.26$).

SECTION 9

CENTRIFUGE TESTS ON SEAT-TYPE MODEL ABUTMENTS

9.1 INTRODUCTION

Determination of the lateral stiffness and capacity of bridge abutments is an important issue in the seismic design of highway bridge structures. The lateral response of an abutment is highly nonlinear. Lateral abutment movements of an order of 6 cm or more have been observed during strong earthquake shakings, without major damage to the structure (Lam et al., 1991).

Most specifications and guidelines for earthquake design of highway bridges require that abutment-soil system be included in the analytical model as discrete equivalent linear springs (CALTRANS, 1988 and 1989; ATC-6, 1981; AASHTO-83, 1988). In design applications, these springs are typically determined based either on simplified rules and an iterative process or from abutment capacity in conjunction with the expected deformation during ground shaking. It is not entirely clear how well the stiffness value thus determined represents the complex behavior of the abutment-soil system, which is influenced by soil-structure interaction and nonlinear behavior of the soil.

Wilson (1988), Levine and Scott (1989), and Wilson and Tan (1990) proposed theoretical linear models for determining abutment stiffness based on the soil properties and abutment dimensions. However, these models do not include the significant effect of nonlinear soil behavior (Siddharthan et al., 1995). Several researchers have attempted to determine abutment stiffness and/or vibration properties from field vibration tests on highway bridges (Crouse et al., 1987; Gates and Smith, 1982; Douglas et al., 1990; Ventura et al., 1995). However, such small amplitude tests lead to results that can not be easily extrapolated to the design conditions for intense earthquake motions, as the abutment stiffness depends on the level of shaking. Recognizing this limitation of small-amplitude tests, several investigators have estimated abutment stiffness from motions of bridges recorded during earthquakes (Maroney et al., 1990, McCallen and Romstad,

1994; Werner et. al, 1994; Goel and Chopra, 1997). Maroney et al. (1994) describe the results of a half scale load test on a monolithic abutment tested to failure. Based on these results, Martin et al. (1996) developed a modeling procedure to simulate abutment stiffness, capacity and damping characteristics for use in seismic response analysis of bridge structures. Results of centrifuge tests on monolithic bridge abutments have also been presented (Hushmand et al., 1986), showing that centrifuge modeling can be an effective tool to study lateral abutment response at large displacements.

In order to understand better the lateral response of seat-type abutments, and to verify the current design procedures used for estimation of abutment stiffness and capacity, three lateral loading centrifuge experiments were performed on abutment models supported by dry Nevada sand of 75 % relative density. This section presents the results of these tests with focus on the horizontal secant stiffness and ultimate capacity of seat-type bridge abutments. While these lateral load centrifuge tests were slow, it is believed that for dry sand results are not rate dependent, and hence are applicable to faster earthquake loadings. The stiffness and capacity results of these centrifuge tests are compared with the CALTRANS and AASHTO-83/ATC-6 design procedures, as well as with some relevant theoretical predictions, and with the conclusions obtained by other authors from analysis of actual abutment response to earthquakes.

9.2 TESTING PROGRAM: SCOPE AND IMPLEMENTATION

9.2.1 Model of Seat-Type Abutment

The same steel abutment model was used for all these centrifuge tests presented in this section. Schematic drawings of the model abutment with backfill, in actual model units, are shown in figures 9-1 to 9-3. The length of the model abutment was about 11.4 cm (4.5 in), and the height of backfill in model scale was about 3 cm (1.2 in). Thus the aspect ratio of the model abutment was $11.4/3 = 3.75$. Dry Nevada sand of 75% relative density was used in all these experiments. Properties of this sand can be found in Section 3. The abutment model did not extend along the entire width of the model container and steel angles were used beyond the extent of the model abutment to maintain different elevation of the sand at both sides of the model abutment as shown in figures 9-1 to 9-3. The model

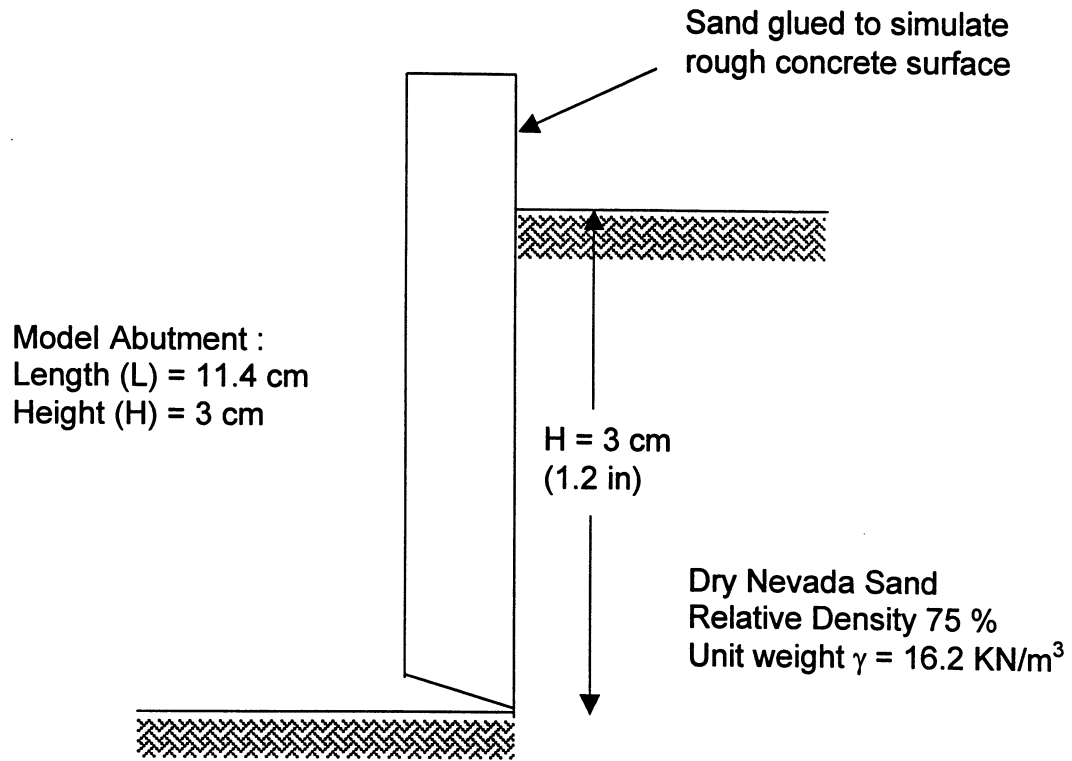


FIGURE 9-1: Schematic view of model abutment.

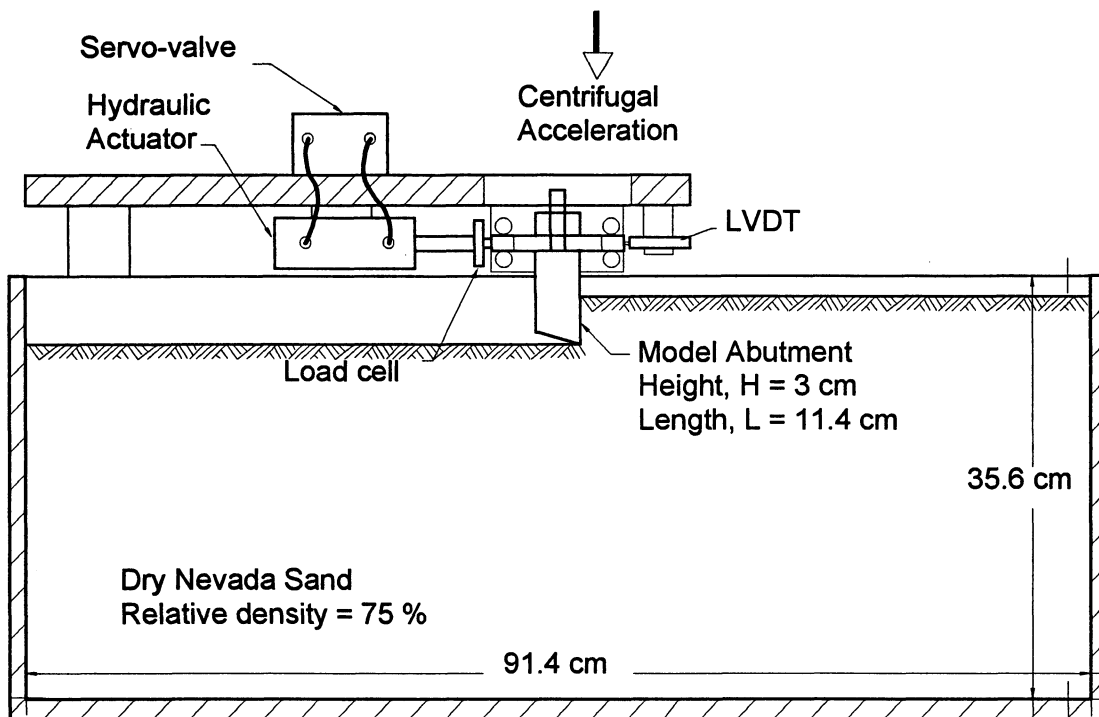


FIGURE 9-2: General setup for centrifuge tests on abutments.

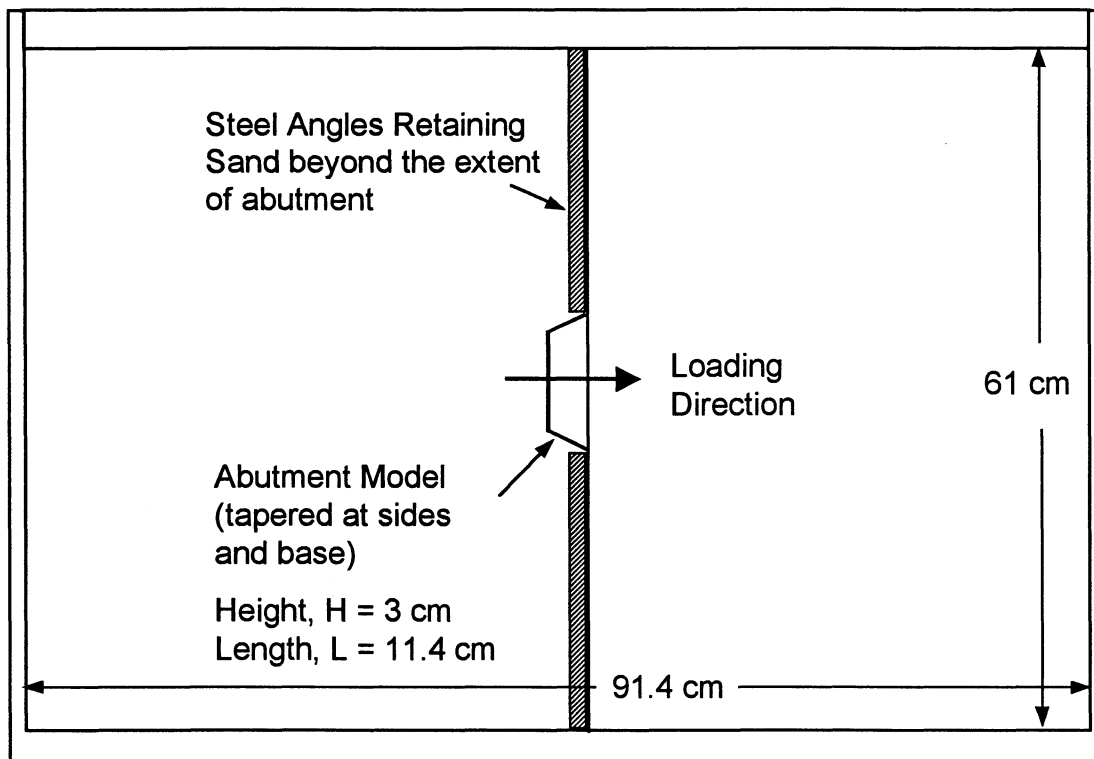


FIGURE 9-3: Plan view of model abutment used in centrifuge tests.

abutment was tapered at the base and sides to minimize the contact with the sand along these surfaces. In addition, Teflon was glued to the sides and base to reduce any friction. Thus, the lateral resistance provided was essentially due to the passive resistance of the sand against the face of the abutment model. Sand was glued to this abutment-backfill interface to simulate a rough “concrete surface.” A rigid aluminum box of dimensions 914-mm (L) x 610-mm (B) x 356-mm (D), described in Section 3, was used as model container in all these tests. The setup of all these centrifuge experiments is shown in figure 9-2. The model abutment is shown in plan view in figure 9-3. The steel model abutment was about 3.8 cm thick, which made it very stiff, and minimized any rotation or bending of the abutment in the loading plane during the lateral loading operation.

9.2.2 Centrifuge Tests Performed

The three centrifuge tests performed using the model abutment of figure 9-1 and the test setup of figure 9-2 are listed in table 9-1. These are centrifuge tests AB50g, AB80g and AB100g conducted at centrifugal accelerations of 50-g, 80-g and 100-g respectively. The prototype heights and lengths of the abutments simulated in these three tests are given in table 9-1. The ratio of length to height (L/H) was maintained at 3.75 in all three tests. That is, the effect of L/H on abutment response was not studied in this research. At 80-g, the model represents a 2.44-m (8-ft) high prototype abutment, which is reasonably representative of a typical California abutment geometry (Lam et al., 1991). The abutment-sand model was not re-used after lateral loading, but a new model was constructed with sand re-deposited for each one of the three tests.

9.2.3 Lateral Loading

The same lateral loading assembly previously used for the centrifuge tests on the pile-cap foundation system was utilized for these tests on abutments. The description of this system can be found in Section 3. This system consists of a servo-controlled hydraulic actuator with a feedback displacement transducer (LVDT) and a load cell. This system, mounted on the model container, is shown schematically in figure 9-2.

The centrifuge tests were performed to study the response of seat-type bridge abutments, which involve loading only in the passive direction. Hence, lateral displacement half-

TABLE 9-1: Centrifuge tests performed on abutments.

Test Code	Abutment Dimensions in Prototype Scale (m)		Measured Ultimate Capacity* F_{ult} (KN)	Passive Earth Pressure Coeff.*, K_p	Ultimate capacity per unit area* (KPa)	Soil capacity using Goel and Chopra's (1997) Procedure (KPa)
	Height, H	Length, L				
AB50g	1.52	5.72	1510	18.6	174	190
AB80g	2.44	9.14	4250	>12.5	>191	240
AB100g	3.05	11.43	6872	>10.3	>197	268

* The abutment capacity was defined as the load corresponding to a lateral displacement of 11 cm. For Tests AB80g and AB100g, the true ultimate capacity was not attained. The initial K_o condition of the backfill in these tests has been neglected.

TABLE 9-2: Analysis of negative forces measured in the final displacement cycle of centrifuge tests on abutments.

Test Code	Centrifugal acceleration, n (g)	Measured Prototype Negative Force, F_p (KN)	Negative Force in Model Scale, $F_M = F_p/n^2$ (N)	Net Active Force on Abutment Model, F_a (N)	Negative Force due to Passive Wedging $F_M - F_a$ (N)	$(F_M - F_a)/n$
AB50g	50	115	46	9	37	0.74
AB80g	80	785	121	15	106	1.32
AB100g	100	1676	167	18	149	1.49

cycles of increasing amplitude were applied to the model abutments. Six lateral displacement half-cycles with amplitudes increasing from 0.3 cm prototype in the first cycle to about 11 cm in the last cycle were applied to the abutment in each test. Thus, determination of lateral abutment stiffnesses at various levels of displacement was possible. In order to avoid interaction between the responses in two consecutive half cycles, each half-cycle was followed by a period of no displacement (see the measured displacement responses for the centrifuge tests in figures 9-4 to 9-6). There is a slight difference between the abutment loading specified by these half cycles and the abutment-loading pattern observed in actual seat-type highway bridge abutments during earthquakes. In highway bridges with seat-type abutments, the bridge deck is supported (seated) by the abutment on a bearing (see figure 2-2). During cyclic earthquake shaking, as the deck moves laterally towards the abutment/back wall, it applies a lateral compressive force in the passive direction. This compressive force is released when the deck moves away from the abutment during this cyclic shaking operation, resulting in some permanent lateral displacement of the abutment (gap formation) due to the nonlinearity of the abutment-backfill system. Thus, during actual earthquake loading, the seat-type abutment moves back only a little under the active force. However, in the centrifuge tests on the seat-type abutments described in this section, the specified displacement half-cycles force the abutment back to the mean position (zero displacement) at the end of each half-cycle. Nevertheless, this discrepancy in the abutment-loading pattern is believed to have no significant effect on the lateral secant stiffnesses and ultimate capacity of the abutment. The frequency of the displacement half-cycles applied in the centrifuge tests was 0.5 Hz in model scale, which is equivalent to 0.01 Hz, 0.00625 Hz and 0.005 Hz in prototype scale for Tests AB50g, AB80g and AB100g, respectively. Hence, the strain rate in these tests was slow and no significant inertia forces were generated in the system. The lateral displacement half-cycles were applied using the servo controlled hydraulic actuator, and the corresponding loads were measured using the load cell.

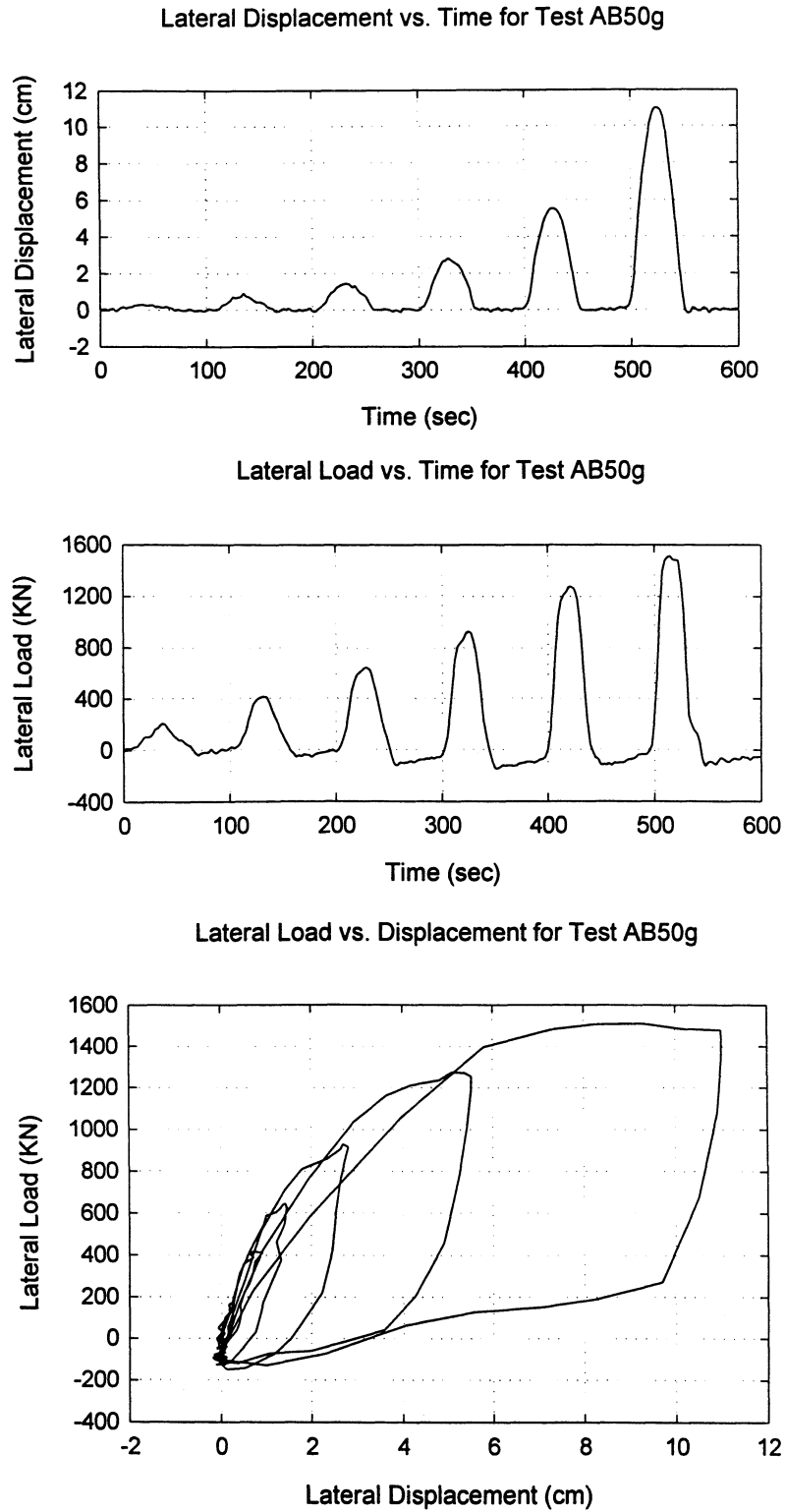


FIGURE 9-4: Measured load-displacement response for Test AB50g in prototype scale.

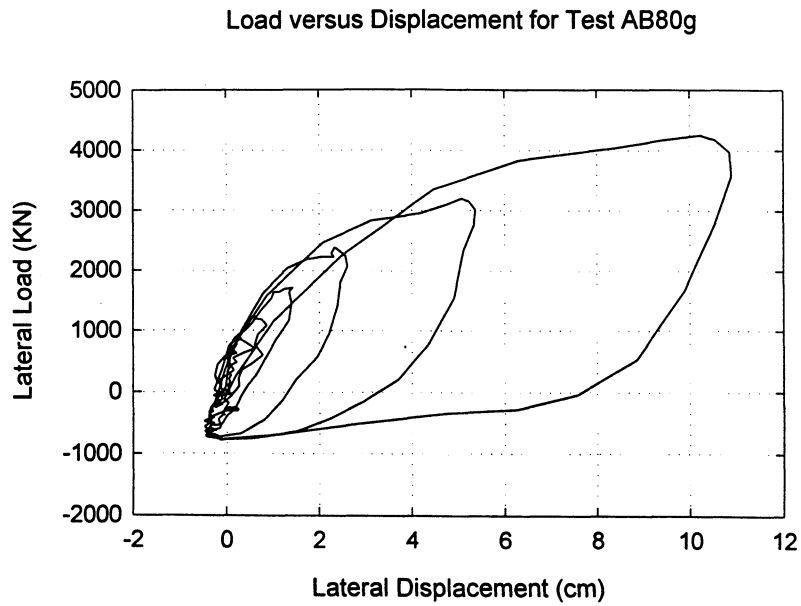
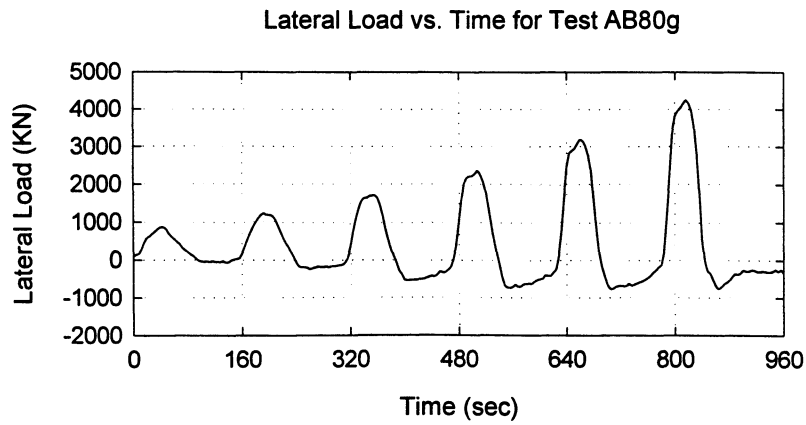
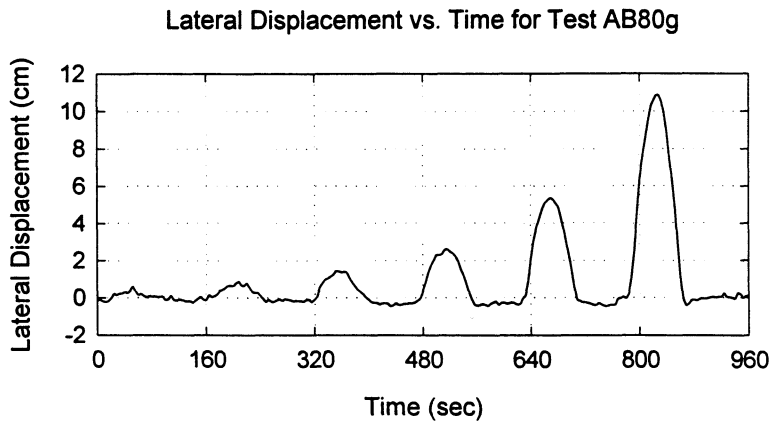


FIGURE 9-5: Measured load displacement response for Test AB80g in prototype scale.

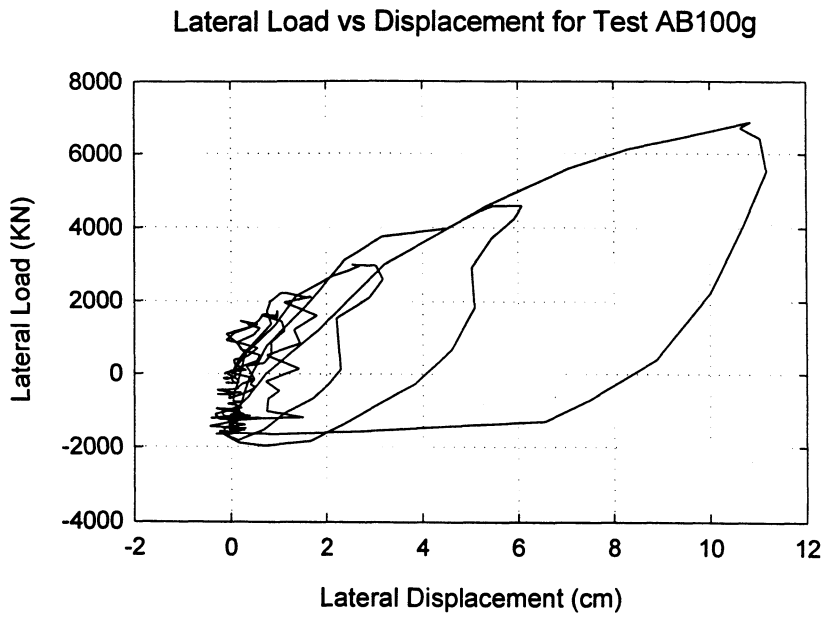
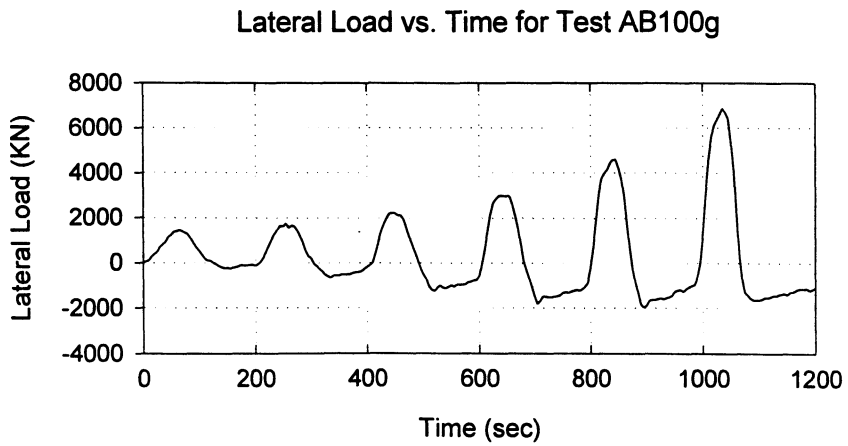
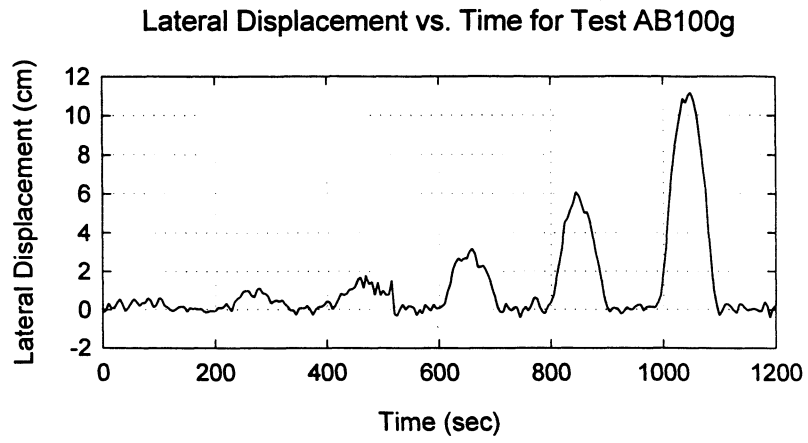


FIGURE 9-6: Measured load-displacement response for Test AB100g in prototype scale.

9.3 MODEL CONSTRUCTION AND TESTING PROCEDURE

The model construction and testing procedures used for the three centrifuge tests on abutments are similar to the procedures used in the centrifuge experiments on the pile-cap foundation system, described in Sections 4, 5 and 6. These procedures are explained in the following subsections.

9.3.1 Model Construction

The general procedure of model construction for the centrifuge tests on abutments is as follows:

1. Dry sand with relative density of about 75% was deposited in layers of thickness 6 cm or less. The amount of sand needed for each layer to achieve required density was weighed, and sand was placed in the container by a raining technique.
2. Once the height of the sand layer reached to the estimated level of the bottom of the abutment, the model abutment with the loading plate was placed on the box. At this point, the abutment model was hanging from the bearing plate of the lateral loading assembly, and no vertical load was transmitted to the soil from the abutment.
3. Sand was deposited along one side of the abutment maintaining the required density until the top of the soil surface was about 3 cm above the base of the abutment, making the height of the backfill in model scale equal to 3 cm. Steel angles were used to retain the soil beyond the extent of the abutment on both sides (figure 9-3).
4. The model was then transported to the centrifuge basket with a forklift.

9.3.2 Testing Procedure

1. The model was placed on the centrifuge basket very gently.
2. The data acquisition computers were turned on.
3. Signal conditioners, amplifiers, and servo-control system on the arm of the centrifuge were powered to warm up the system.
4. The load-cell and the displacement transducer (LVDT) were connected to the data acquisition panel on the centrifuge arm. The cord of the feedback LVDT was adjusted to the mean position. The servo valve was connected to the servo controller system.

5. Video cameras in the centrifuge room and the video monitors in the control room were turned on to observe model in-flight.
6. The centrifuge was spun to the required centrifugal acceleration.
7. The hydraulic pump was started, and an input signal was sent to the servo-control system.
8. Lateral displacement half- cycles of increasing amplitudes were applied to the abutment through the hydraulic actuator. The displacements were monitored through the feedback LVDT and the corresponding loads were measured through the load-cell.

9.4 TEST RESULTS

Results of the three centrifuge tests of table 9-1, performed on models of seat-type bridge abutments are presented in this subsection. The data presented in this and following subsections are in prototype scale, unless specified otherwise. Load displacement responses for the three centrifuge tests are plotted in figures 9-4 to 9-6. Several general trends can be observed from these results. The lateral response of the abutments is highly nonlinear. After full unloading there is in all cases a significant permanent displacement, as anticipated due to the nonlinear hysteretic behavior of soil. Clear yielding can be observed in Test AB50g at a lateral displacement of about 8-cm. In Tests AB80g and AB100g, the load-displacement loops do not show clear yielding even at the final displacement amplitude of 11 cm.

In all centrifuge tests negative forces are measured after unloading when the abutment is forced back to the mean position (zero displacement), as shown in figures 9-4 to 9-6. Table 9-2 lists the negative force, F_P in prototype scale, measured in each test after unloading in the last displacement cycle. This force F_P can be transformed back to the force in the model scale, F_M by using $F_M = F_P/n^2$, where n is the centrifugal acceleration for the corresponding test. The model construction procedure described in subsection 9.3 suggests that the backfill soil was in “at-rest” or K_o condition before the application of the lateral displacement cycles. Hence the “zero-load” measured at the beginning of the lateral loading actually corresponds to lateral thrust of the backfill soil at rest. For a soil

internal friction angle of $\phi = 39^\circ$ (see Section 4) the coefficient of lateral earth pressure at rest, $K_o \approx 1 - \sin 39^\circ = 0.38$ (Lambe and Whitman, 1969). After the application of displacement half-cycles when the abutment was forced back to the mean position, the lateral earth pressure condition in the backfill soil was probably closer to “active” rather than “at-rest.” For a wall friction angle of $\phi_w = 39^\circ$, and also using an internal friction angle of soil, $\phi = 39^\circ$ (see Section 4), the active earth pressure coefficient $K_a = 0.21$ (Lambe and Whitman, 1969). Thus, one of the sources of the negative force measured in all tests after the final displacement half cycle may be the difference between the lateral force on the abutment wall due to the backfill soil at rest and with the backfill soil in an active state. This net horizontal active force on abutment wall, F_a is given by,

$$F_a = \frac{1}{2}(K_o - K_a \cos \phi_w)\gamma H^2 W \quad (9-1)$$

This force F_a in model scale can be obtained by substituting in the above equation values of unit weight $\gamma = (16.2 \times n)$ KN/m², model abutment height $H = 0.03$ m and width $W = 0.114$ m. The calculated values of F_a in model scale for all tests are listed in table 9-2. For all tests, this calculated negative force contribution of the active force F_a is much less than the actual measured negative force in model scale F_M also listed in table 9-2. Since there was essentially no friction at the sides and at the base of the abutment model during these tests, this additional negative force ($F_M - F_a$) presumably arises due to the passive wedging of the sand infiltrated under the tapered base of the model during test (see figures 9-1 and 9-2). Assuming the same pattern of sand-infiltration in each test, this negative force ($F_M - F_a$) due to passive wedging of the infiltrated sand should be approximately proportional to the centrifugal acceleration, n . Table 9-2 gives the ratio $(F_M - F_a)/n$ for each test, which should be about constant if the above hypothesis is true. Despite some scatter, this ratio falls in a relatively narrow range of 0.74 to 1.49, substantiating the above hypothesis that the additional negative force arose due to the passive wedging of the sand infiltrated under the tapered base of the model abutment during lateral loading. These measured values of negative force, if due to active thrust and wedging of sand, should not affect the positive lateral forces and stiffnesses measured in the centrifuge experiments.

9.4.1 Ultimate Capacity

The ultimate lateral capacity F_{ult} for the different tests was defined as the maximum load measured in the last displacement cycle of amplitude of about 11 cm. These ultimate capacities are listed in table 9-1. It should be noted however, that while the ultimate capacity is attained at this displacement for the abutment in Test AB50g, the abutments in Tests AB80g and AB100g do not show clear yielding. Thus the true capacity for the abutments in these tests must be higher than the measured lateral load corresponding to 11-cm displacement. As expected, the abutment in Test AB100g has the highest capacity (6872 KN), followed by the abutments in Tests AB80g (4438 KN) and AB50g (1510 KN). Neglecting the fact that the initial “zero load” in these tests actually corresponds to the lateral thrust of the backfill at rest, these measured ultimate capacities are primarily due to the passive thrust of the soil. As already mentioned, sand was glued to the surface of the model abutment in these tests to simulate a rough concrete surface, similar to the centrifuge tests on the pile-cap (Section 4). Hence, the wall friction angle ϕ_w for the abutments can be assumed to be equal to $\tan^{-1}0.82 = 39^\circ$ (obtained from the measured soil-base friction coefficient $\mu = 0.82$ in Tests CB and CBL on the pile cap-alone in Section 4). The coefficient of passive earth pressure K_p can be calculated in each test as:

$$K_p = \frac{F_{ult}}{\cos \phi_w \gamma H^2 L} \quad (9-2)$$

where $\gamma = 16.2 \text{ KN/m}^3$ is the unit weight of the sand; and H and L are respectively the height and the length of abutment. The values of K_p calculated for all three tests are given in table 9-1. As mentioned earlier, since the true ultimate capacity is not attained in Tests AB80g and AB100g, the K_p values in these tests must be larger than the values of 13 and 10.3 listed in table 9-1, and thus these values are indicated as lower bounds in the table. The measured K_p value of about 18 in Test AB50g is somewhat higher but within 25% of $K_p = 14.3$ measured in Test CP on the cap-alone in Section 4. Also, using a wall friction angle of $\phi_w = 39^\circ$ and an internal friction angle of $\phi = 39^\circ$ for the soil, we get a theoretical $K_p \approx 14$, again neglecting the difference between a short and long wall (Caquot and K erisel, 1949; Lambe and Whitman, 1969), which agrees reasonably well with the values measured in the centrifuge tests. The measured K_p values for all tests are much greater

than the coefficient of earth pressure at rest, $K_o = 0.38$ for the sand, indicating that the assumption of neglecting the initial K_o condition in the above calculations of K_p is reasonable. Table 9-1 also gives the measured ultimate capacities per unit area of abutment for the three tests. These values fall in a relatively narrow range between 170 KPa and 200 KPa. For static loading, CALTRANS (1988) has recommended a soil capacity of 240 KPa (5 Ksf) for typical California abutment-backfill conditions (2.4-m height of the backfill, backfill soil with shear wave velocity of about 240 m/sec). For other backfill depths Goel and Chopra (1997) suggest that this capacity may be modified by multiplying by the factor $(H/2.4)^{0.5}$, where H is the actual depth of the backfill in meters. Table 9-1 gives the ultimate soil capacities computed using the CALTRANS procedure and the suggestion of Goel and Chopra (1997). Comparison of the calculated values with the values measured in centrifuge experiments shows that the CALTRANS recommended value of 240 KPa is comparable and slightly greater than the measured soil capacity. Since the design values for the abutment capacity from the AASHTO-83/ATC-6 and the CALTRANS procedure are identical, the above-noted conclusion also applies to the recommendations of AASHTO-83/ATC-6.

9.4.2 Secant Stiffness

The secant stiffnesses measured in the three centrifuge tests on abutments for various levels of displacements are plotted in figures 9-7 to 9-9, and are listed in table 9-3. These stiffnesses were calculated by dividing the maximum load for each half-cycle by the maximum displacement of that half-cycle. In general, for each of the three tests the secant stiffness reduces as the displacement amplitude increases. This is as expected for this nonlinear system, and is analogous to the reduction in secant shear modulus in soils with increased shear strain.

In Goel and Chopra's (1997) interpretation of the CALTRANS procedure, the design value of the abutment stiffness is computed as the ratio between its design capacity and the acceptable deformation. Two values of the acceptable deformation are considered: 2.5 cm (1 in) and 6.1 cm (2.4 in). The first represents the deformation at which the soil pressure reaches its peak value of 240 KPa (5 Ksf), and the latter represents the limiting

value corresponding to incipient damage to the abutment (CALTRANS 1988 and 1989). The design values of the abutment stiffness are summarized in table 9-3. These values are plotted in figures 9-7 to 9-9 along with the values measured for the centrifuge tests. The design values obtained by Goel and Chopra's interpretation of the CALTRANS procedure for a 2.5-cm deformation are larger than the values measured in the centrifuge for that displacement. Similarly, the design values for 6.1-cm deformation are also slightly greater than the measured values at that displacement.

In the AASHTO-83 and ATC-6 procedures, which are identical, two estimates –initial and final – are made for the design value of the abutment stiffness (Goel and Chopra, 1997). The initial estimate of the abutment stiffness is obtained by adding the contributions of the backfill and of the piles (Lam and Martin, 1986). Since the abutment stiffness in the centrifuge tests was entirely due to the backfill, only the contribution of the backfill needs to be considered. The estimated stiffness due to backfill is $0.425 \times E_s \times L$, where $E_s = 1440 \text{ Ksf}$ (69 MPa) is the estimated elastic modulus of the soil, and L is the effective length of the backwall in feet. The final stiffness is computed by an iterative procedure in which the abutment stiffness is successively reduced until the computed abutment force is about equal to the abutment capacity. The initial estimates of abutment stiffnesses for the three centrifuge tests computed using this AASHTO-83/ATC-6 procedure are listed in table 9-3. These values are much larger than the measured stiffnesses for a design lateral displacement of 2.5-cm. The final values of abutment stiffnesses obtained from the AASHTO-83/ATC-6 procedure are identical with the stiffnesses computed using the CALTRANS procedure (Goel and Chopra, 1997).

The secant stiffnesses per unit length of the abutments measured in the three centrifuge tests are plotted in figure 9-10 against the corresponding displacement amplitudes. At small lateral displacements (less than about 1 cm) the secant stiffness per unit length increases with height of abutment. At larger displacements of more than about 2 cm, the secant stiffnesses for Tests AB80g and AB100g remain in a narrow range. The CALTRANS Bridge Design Aids (1988) recommended an abutment-backfill interaction stiffness of 1150 KN/cm/m (200 Kip/in/ft) as a starting point for iterative analysis for typical California abutment-backfill conditions (material with shear wave velocity of

about 240 m/s and approximately 2.4 m of effective height of abutment walls). Although CALTRANS engineers no longer use this procedure (Goel and Chopra, 1997), it is instructive to compare this recommended value with the stiffnesses measured in the centrifuge tests. Test AB80g represents the typical California abutment-backfill conditions. The secant stiffnesses per unit length measured in this centrifuge test are much lower than this old recommended value of 1150 KN/cm/m (see figure 9-10) for all displacement amplitudes.

The secant stiffnesses per unit area of the abutments measured in all three-centrifuge tests are shown in figure 9-11 for different levels of lateral displacements. The measured secant stiffnesses per unit area increase with height of abutment for the first displacement amplitude of 0.3-cm. For displacements larger than about 0.7 cm, the measured secant stiffness per unit area is independent of abutment dimensions, and depends only on the level of lateral displacement. Hence, the lateral stiffness per unit area may serve as a good specified parameter in seismic design guidelines for highway bridge abutments.

9.4.3 Normalized Non-dimensional Backbone Curve

Maroney et al. (1994) describe the results of a half-scale lateral load test on a monolithic abutment tested to failure during research conducted at the University of California, Davis. The backfill soil was comprised of cohesive clayey silt with an estimated undrained cohesion of about 95 KN/m^2 (2 Ksf). The dimensions of the abutment were 1.68 m (H) x 2.59 m (L) (5.5 ft x 8.5 ft) and the measured ultimate capacity was about 1440 KN (325 Kips). Based on the results of this test, Martin et al. (1996) developed a modeling procedure to simulate abutment stiffness, passive capacity and damping characteristics for use in seismic response analysis of bridge structures. In this procedure, the UC Davis load-displacement curve is used to develop a non-dimensional load displacement curve shape where the measured force values were divided by the ultimate force capacity and the measured deflection values were divided by the wall height. This non-dimensional curve can then be extrapolated to abutments of other dimensions, using the ultimate force capacity of the abutment estimated based on the shear strength characteristics of the backfill soil and the appropriate passive earth pressure theory. The

non-dimensional backbone curve developed using the UC Davis data is shown in figure 9-12. A similar non-dimensional backbone curve was developed in this work by normalizing the load-displacement curve for the centrifuge Test AB50g (shown in figure 9-4), with the measured ultimate capacity value (1510 KN) and abutment height (1.52 m). This normalized backbone curve is also shown in figure 9-12.

In figure 9-12, for normalized non-dimensional force values less than 0.77 the normalized UC Davis backbone curve is much stiffer than the backbone curve obtained from Test AB50g. This may be due to the fact that while the load-displacement response in the centrifuge tests is associated essentially with the abutment-backfill interaction, the UC Davis load-displacement curve was also influenced by the presence of abutment piles, which are thought to have failed at a load of about 1112 KN (250 Kips) (Maroney et al., 1994) corresponding to a normalized non-dimensional force of about 0.77 in figure 9-12. Beyond this value, the normalized UC Davis backbone curve matches well with the backbone curve obtained from the results of the centrifuge Test AB50g. This agreement is especially good and may be fortuitous considering that the backfill soil types in these two tests were very different; cohesive clayey silt in the UC Davis test and dense dry sand in the centrifuge test. Further research is needed to compare normalized backbone curves for abutments with backfill soils of various types with the curves plotted in figure 9-12.

Normalized curves were not plotted for centrifuge Tests AB80g and AB100g because, as explained in Section 9.4.1, the true capacity was not attained in these tests. If normalized curves had been plotted for these tests using the lower bound capacity values listed in table 9-1, they would be stiffer than the curve for Test AB50g in figure 9-12, as expected.

9.5 CONCLUSIONS

Three centrifuge lateral loading tests were performed on models of bridge abutments of different prototype dimensions in dense dry sand to study the lateral response at various levels of displacement. Analysis of the results of these centrifuge tests and comparison of

the measured abutment capacities and stiffnesses with various design procedures, and theoretical and field measurement results, lead to the following conclusions.

1. The ultimate capacity of the abutment increases with abutment dimension. Neglecting the initial K_0 condition within the sand, the values of passive earth pressure coefficients (K_p) measured in the three centrifuge tests are all larger than 10, and in one of the tests is $K_p = 18.6$, which is in reasonable agreement with the theoretical value of $K_p \approx 14$.
2. The value of ultimate backfill resistance per unit area of abutment, obtained at the maximum abutment displacement of 11 cm, falls in a relatively narrow range of about 170 KPa to 200 KPa. The CALTRANS recommended value of 240 KPa is comparable and slightly greater than these measured capacity values.
3. The secant stiffness measured in all centrifuge tests decreases with the amplitude of lateral displacement. The secant stiffnesses computed using Goel and Chopra's interpretation of the CALTRANS procedure (identical to the AASHTO-83/ATC-6 recommendations for estimating the final abutment stiffness) for the three abutment configurations employed in the centrifuge tests are larger than the measured secant stiffnesses in the centrifuge tests.
4. The secant stiffnesses per unit area seem to be independent of the dimensions of the abutment for these centrifuge tests for displacements larger than about 0.7 cm.
5. The normalized load-displacement backbone curves obtained from the centrifuge Test AB50g matches reasonably well with the normalized backbone curve obtained from the half-scale lateral load test described by Maroney et al. (1994).

TABLE 9-3: Measured and computed stiffnesses for centrifuge tests on abutments.

	Displacement Amplitude (cm)	Lateral Stiffness (KN/cm)		
		Test AB50g	Test AB80g	Test AB100g
Measured in centrifuge tests	0.3	696	2280	4843
	0.7	593	1528	2483
	1.4	459	1198	1587
	2.7	332	906	1073
	5.5	232	595	821
	11	137	404	625
Calculated using CALTRANS procedure as interpreted by Goel and Chopra (1997)	2.5	666	2156	3369
	6.1	277	898	1403
Initial estimate of abutment stiffness using Goel and Chopra's (1997) interpretation of AASHTO-83/ATC-6 procedure	-	1673	2678	3347

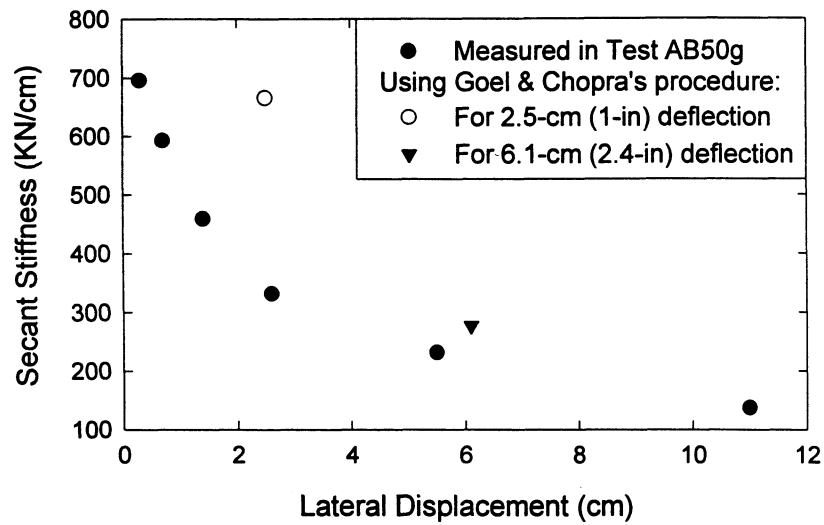


FIGURE 9-7: Measured and computed secant stiffnesses for Test AB50g.

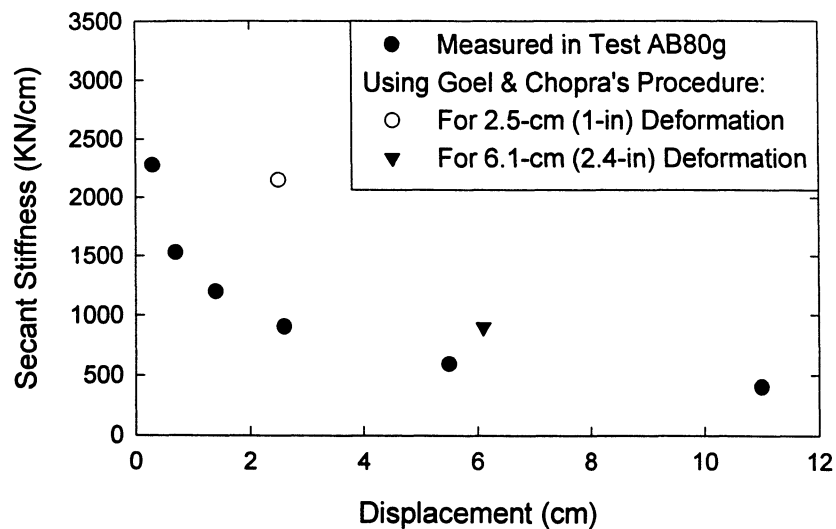


FIGURE 9-8: Measured and computed secant stiffnesses for Test AB80g.

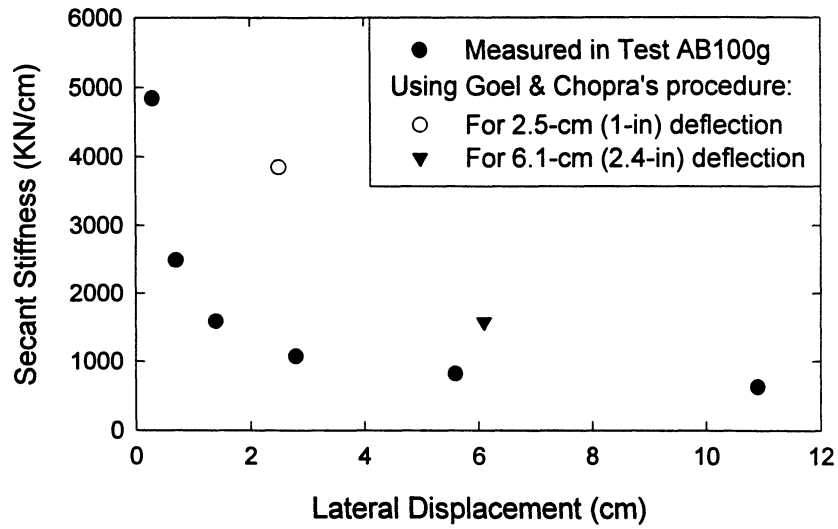


FIGURE 9-9: Measured and computed secant stiffnesses for Test AB100g.

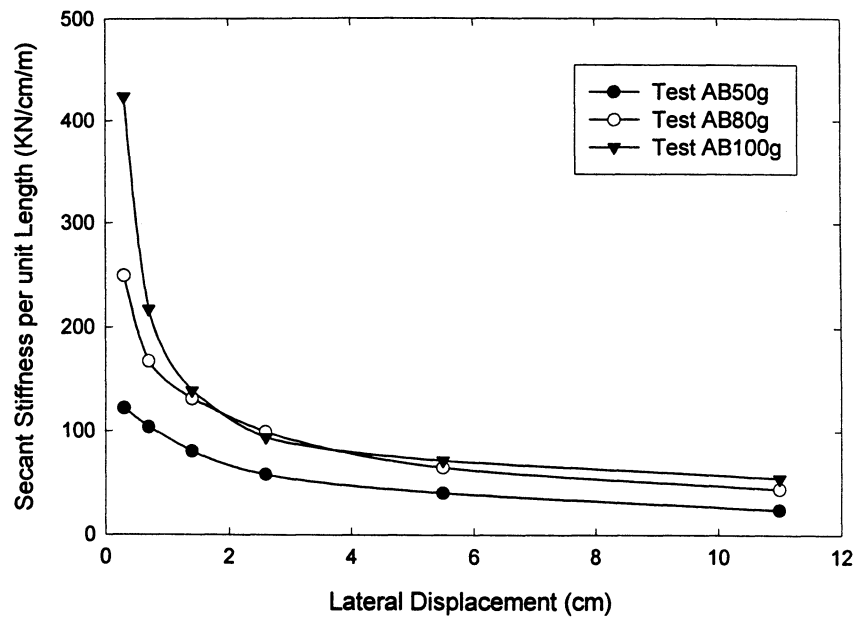


FIGURE 9-10: Measured secant stiffness per unit length for centrifuge tests on abutments.

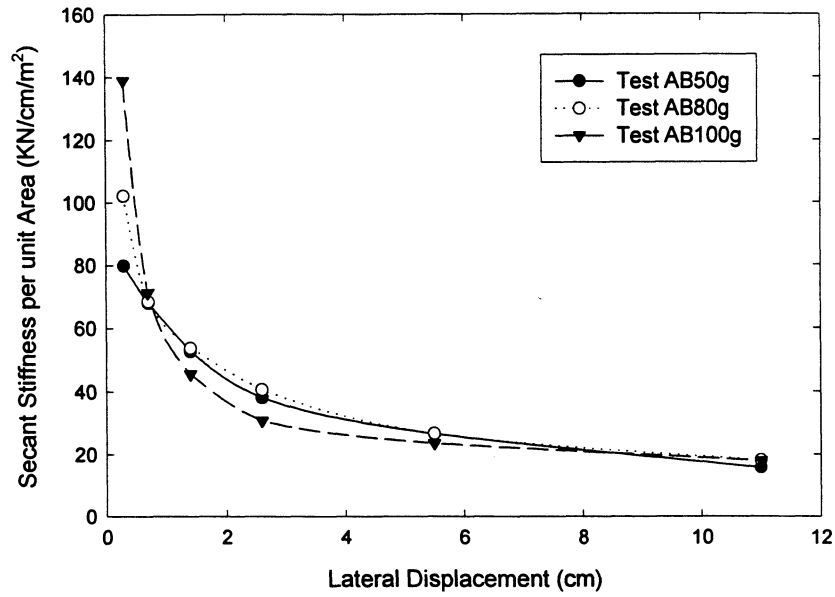


FIGURE 9-11: Measured secant stiffness per unit area for centrifuge tests on abutments.

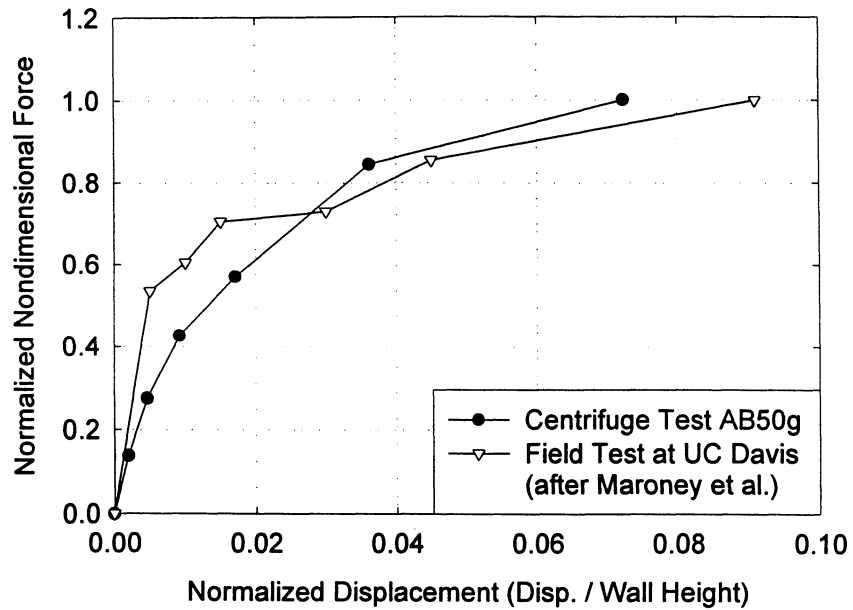


FIGURE 9-12: Normalized backbone curves obtained from the centrifuge tests and the half-scale load test described by Maroney et al. (1994).

SECTION 10 CONCLUSIONS

The results of thirteen lateral-loading centrifuge tests conducted on models of the pile-cap system and seat-type bridge abutments in dense dry sand were reported in the previous sections. Nonlinear finite element (FE) analyses performed to verify numerically the results of centrifuge tests on the cap-alone/embedded footing, when all sides and the base of the cap were in contact with the sand were also presented. Also reported were the results of parametric FE studies, performed to understand the influence of the value and distribution of the soil shear modulus and of the cap/footing geometry on the nonlinear lateral response of the footing. Table 10-1 summarizes the thirteen centrifuge tests and FE analyses performed in this research task and some of the main conclusions. Some of these major conclusions drawn from the results of the centrifuge tests and FE analyses are as follows:

1. This work clearly demonstrates that lateral-load centrifuge testing is an effective tool to study the lateral response of pile-cap foundation systems and bridge abutments, at various levels of displacements. Consistent results are obtained from all centrifuge tests, which also agree reasonably well with the available information in the literature.
2. For the seven tests on the cap-alone, which is equivalent to an embedded footing, the measured values of ultimate lateral capacity agree reasonably well with theory and also satisfy the expected limiting equilibrium condition.
3. In tests on the cap/embedded footing, there is little interaction between the stiffness contributions of the base, shearing sides, and active/passive sides, with an addition rule for secant stiffness being approximately valid. The measured areas of loops, representing energy dissipated as material damping, also satisfy the “addition rule.”
4. For all parameters measured in tests on the model cap/footing (ultimate capacity, lateral stiffness, and material damping), the contribution of the passive side accounts for more than half of the total.
5. The measured initial secant stiffness values for the cap/footing, including their increase when the foundation walls make contact with the surrounding soil, agree

well with the available elastic solutions in the literature, if an equivalent linear shear modulus at a shallow depth is selected.

6. For the test on the free-head pile, the measured lateral secant stiffness and lateral force corresponding to allowable lateral displacement match well with the values recommended by CALTRANS for this pile. A reasonable set of p-y curves at different depths was backfigured, which predicts well both the measured bending moments along the pile, and the lateral load-displacement characteristics at the pile head.
7. The relative contribution of the cap to the lateral stiffness of the pile-cap system, which is high at small displacements, decreases as the lateral displacement amplitude increases.
8. For normal working load levels (lateral displacements less than about 3 cm), the single pile in the pile-cap system tested roughly behaved as a free head pile. It was found that the addition rule is approximately valid for secant stiffness, that is the stiffnesses of the free-head pile and the cap-alone can be added to get the corresponding stiffness of the whole pile-cap system. A similar addition rule also works for the measured areas of loops representing material damping, for normal working load levels.
9. The Modified Drucker-Prager Cap model, available in the code ABAQUS, can be conveniently used to study nonlinear soil-structure interaction problems. The load-displacement responses for centrifuge tests on a fully embedded cap/footing agree well with the results of three-dimensional nonlinear FE analyses.
10. The secant stiffness of the cap/footing depends on the soil shear modulus at small displacements. At large displacements, the influence of both the value and distribution of soil modulus on the secant stiffness is negligible.
11. A parametric FE study to understand the effect of the footing geometry on the lateral response shows that the ultimate lateral capacity of a footing/cap can be well approximated by adding the contributions of its base and sides. These contributions can be derived from simple formulations incorporating basic soil parameters, such as friction and lateral earth pressure coefficients. The initial secant stiffnesses computed

using the FE analyses agree reasonably well with the elastic solutions available in the literature if an equivalent soil shear modulus at a shallow depth is selected.

12. Results of the centrifuge tests performed on models of seat-type bridge abutments show that the measured capacity values are comparable and somewhat smaller than the values obtained by usual design procedures, recommended by CALTRANS, AASHTO-83, and ATC-6. The measured stiffnesses in the centrifuge tests are smaller than those computed from available design procedures.
13. For the centrifuge tests on abutments, the secant stiffness per unit area of the abutment seems to be independent of the dimensions of the abutment for displacements larger than about 0.7 cm.

TABLE 10-1: Summary of centrifuge tests and FE analyses performed.

	Test	Test Characteristics	Main Conclusions
Cap-alone/ Embedded footing	CB	-Base shear.	- $\mu = 0.82 = \tan 39^\circ$
	CBL	-Base shear with additional load.	
	CS	-Side shear.	- $K_s = 2.1$
	CP	-Active/passive force.	- $K_p = 14.3$, agrees with theory
	CSP	-Side shear & active/passive contributions.	-"Addition rule" valid for contributions of base and sides to stiffness, material damping, and capacity.
	CBSPL	-All sides and base.	
	CBSPL	-All sides & base with additional load.	
Free-head pile	PI	-Instrumented pile.	-Reasonable set of p-y curves
Pile-cap system	PCBSP	-Pile rigidly clamped to cap.	-"Addition rule" valid for contributions of cap and pile to stiffness and damping up to lateral deflection of 2.5 cm.
	PCBSPI	-Instrumented pile rigidly clamped to cap.	
Cap-alone/ Embedded footing	3-D Non-linear FE analyses	-Prediction of centrifuge tests. -Parametric studies for effect of variation in shear modulus and cap geometry.	-Simple formulations for contributions of base and sides to ultimate capacity. -Initial stiffness can be approximated by elastic solutions if modulus at shallow depth is selected.
Seat-type bridge abutments	AB50g		-Measured capacity and stiffness values comparable or smaller than the values recommended by the usual design procedures.
	AB80g	-Typical California abutment-backfill geometry.	
	AB100g		

SECTION 11

RECOMMENDATIONS

Some engineering recommendations based on the research presented in this report, as well as suggestions for future work, are given in this section.

11.1 ENGINEERING RECOMMENDATIONS

Engineering recommendations that are directly derived from the results of the centrifuge tests on the pile-cap system and seat-type bridge abutments, and from the nonlinear FE analyses of the cap-alone experiments are as follows:

1. Centrifuge testing can and should be used more often as a tool to study complicated soil-structure interaction problems, such as the lateral response of pile-cap foundation systems and abutments. The results of centrifuge tests can also be used to calibrate various analytical and numerical models.
2. The ultimate lateral capacity of embedded spread footings/pile-caps in dense sand, may be assessed by simply adding the contributions of the base, shearing sides, and active/passive sides, derived from some simple formulations incorporating basic soil parameters, such as friction and lateral earth pressure coefficients.
3. The initial secant stiffness of embedded spread footings/pile-caps in sand can be roughly estimated with available elastic solutions, if an equivalent linear soil shear modulus at a shallow depth is selected.
4. The cap's contribution is substantial, and should not be neglected in the analysis of the lateral response of a pile-cap system.
5. At least in a pile-cap system with a single pile, the lateral stiffness of the system can be approximated by adding the contributions from the pile and cap, for lateral displacements of up to 3 cm. The rotational and cross-coupling terms in the cap's stiffness may be neglected in this calculation. This recommendation is consistent with the current CALTRANS design procedure.
6. The current earthquake design procedures for highway bridges (CALTRANS, 1988,1989; ATC-6, 1981; AASHTO-83, 1988) somewhat overestimated the measured lateral capacity of bridge abutments in the centrifuge tests. Available

procedures also seem to overestimate the measured lateral stiffnesses. Additional research is recommended to investigate these differences.

7. The results of the centrifuge tests on abutments show that the lateral stiffness per unit area of abutment does not depend on the dimensions of the abutment for displacements larger than 0.7 cm. Hence, the lateral stiffness per unit area may serve as a good specified parameter in seismic design guidelines for highway bridge abutments.

11.2 SUGGESTIONS FOR FUTURE WORK

The authors would like to recommend the following research areas to extend this study on the lateral response of pile-cap foundation systems and abutments:

1. Additional centrifuge tests may be performed on pile-cap systems with various dimensions of caps and piles to reinforce the conclusions derived from the centrifuge tests presented in this thesis. These tests can also be utilized to calibrate better the nonlinear finite element model presented in this research.
2. Lateral loading centrifuge tests on pile groups with embedded cap need to be performed to study the pile-group interaction, as well as the role of an embedded cap in the lateral response of a pile-group.
3. Additional lateral loading centrifuge tests on abutments with different aspect ratios may be useful to compliment the results of the centrifuge test on abutments presented in this report, and to generate better seismic design guidelines for bridge abutments.

SECTION 12
REFERENCES

- AASHTO-83, 1988, *Guide Specifications for Seismic Design of Highway Bridges*, American Association of State Highway and Transportation Officials, Washington, D. C.
- ATC-6, 1981, *Seismic Design Guidelines for Highway Bridges*, Applied Technology Council, Berkley, CA, October.
- Abcarius, J. L., 1991, "Lateral load test on driven pile footings," *Proc. Third Bridge Engineering Conference*, Denver, Colorado, TRB Record No. 1290, Vol. 2.
- American Petroleum Institute, 1987, *Recommended Practice for Planning, Designing, and Constructing Fixed Offshore Platforms, API Recommended Practice 2A (RP 2A)*, Seventeenth Edition, April 1, 1987.
- Applied Technology Council, 1986, *Seismic Design Guidelines for Highway Bridges*, Applied Technology Council, Redwood City, CA.
- Arulmoli, K., K. K. Muraleetharan, M. M. Hossain and L. S. Fruth, 1992, *Verification of Liquefaction Analysis by Centrifuge Studies Laboratory Testing Program Soil Data Report*, Report from The Earth Technology Corporation, Irvine, California.
- Banerjee, P. K., and R. Sen, 1987, "Dynamic Behavior of Axially and Laterally Loaded Piles and Pile Groups," In: *Dynamic Behavior of Foundations and Buried Structures: Developments in Soil Mechanics and Foundation Engineering*, Chapter 3, Elsevier Applied Science, New York, NY.
- Barton, Y. O., 1984, "Response of Pile Groups to Lateral Loading in the Centrifuge," *Proc. Symp. Application of Centrifuge Modelling to Geotechnical Design*, Manchester, 16-18 April 1984, W. H. Craig (ed.), pp. 457-473.
- Barton, Y. O. and G. N. Pande, 1982, "Laterally Loaded Piles in Sand: Centrifuge Tests and Finite Element Analysis," *Inst. For Num. Methods in Engineering C/R/413/82*, also *Proc. Inst. Symp. On Numerical Models in Geomechanics*, Zurich.
- Bouafia, A. and J. Garnier, 1991, "Experimental Study of p-y Curves for Piles in Sand," *Proc. Int. Conf. Centrifuge 91*, Boulder, Colorado, 13-14 June, 1991, Hon-Yim Ko and Francis G. McLean (eds.), pp. 261-268.
- Broms, B. B., 1964, "Lateral Resistance of Piles in Cohesionless Soils," *J. S. M. F. D., ASCE*, Vol. 90, SM3, pp. 123-156.

- Brown, D. A., and C. F. Shie, 1990, "Three Dimensional Finite Element Model of Laterally Loaded Piles," *Computers and Geotechnics*, Vol. 10, pp. 59-79.
- CALTRANS, 1988, *Memo to Designers 5-1*, California Department of Transportation, Division of Structure, Sacramento, CA, September.
- CALTRANS, 1989, *Bridge Design Aids 14-1*, California Department of Transportation, Sacramento, CA, October.
- Caquot, A., and J. Kérisel, 1949, *Traite de Mechanique des sols*, Gauthier-Villars, Paris.
- Cox, W. R., L. C. Reese, and B. R. Grubbs, 1974, "Field Testing of Laterally Loaded Piles in Sand," *Proc. 6th Annual Offshore Technology Conf.*, Paper OTC 2079, Houston.
- Crouse, C. B., G. C. Liang, and G. R. Martin, 1985, "Experimental Foundation Impedance Functions," *Journal of Geotechnical Engineering*, ASCE, Vol. 111, No. 6, pp. 819-822.
- Crouse, C. B., B. Hushmand, and G. R. Martin, 1987, "Dynamic Soil-Structure Interaction of a Single Span Bridge," *Earthquake Engineering and Structural Dynamics*, Vol. 15, pp. 711-729.
- Crouse, C. B., B. Hushmand, E. Luco, and H. L. Wong, 1990, "Foundation Impedance Functions: Theory versus Experiment," *Journal of Geotechnical Engineering*, ASCE, Vol. 116, No. 3, pp. 432-449.
- Dickin, E. A. and M. J. Wei, 1991, "Moment Carrying Capacity of Short Piles in Sand," *Proc. Int. Conf. Centrifuge 91*, Boulder, Colorado, 13-14 June, 1991, Hon-Yim Ko and Francis G. McLean (eds.), pp. 277-284.
- Dobry, R. and G. Gazetas, 1986, "Dynamic Response of Arbitrarily Shaped Foundations," *Journal of Geotechnical Engineering*, ASCE, Vol. 112, No. 2, pp. 109-135.
- Dobry, R., V. Taboada, and L. Liu, 1995, "Centrifuge Modeling of Liquefaction Effects During Earthquakes," *Proc. First Intl. Conf. on Earthquake Geotechnical Engineering*, Tokyo, Japan.
- Dobry, R., E. Vicente, M. J. O'Rourke, and J. M. Rosset, 1982, "Horizontal Stiffness and Damping of Single Piles," *Journal Geotechnical Engineering*, ASCE, Vol. 108, No. 3, pp. 439-459.
- Dobry, R., R. V. Whitman, J. M. Roesset, 1971, *Soil Properties and the One-Dimensional Theory of Earthquake Amplification*, Research Report R71-18, Dept. of Civil Eng., M. I. T., Cambridge, MA.

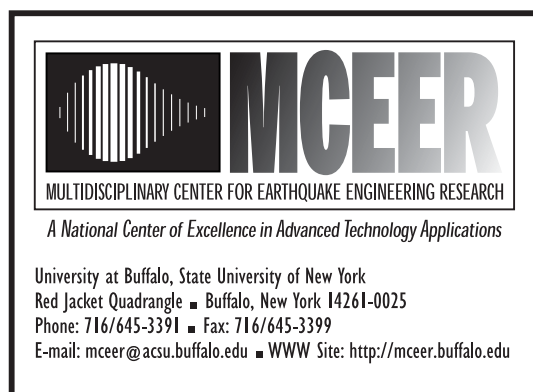
- Dominguez, J., 1978, *Dynamic Stiffness of Rectangular Foundations*, Res. Rept. R78-20, Civil Engineering Dept., Massachusetts Institute of Technology, Cambridge, MA.
- Douglas, B. M., E. A. Maragakis, S. Vrontino, and B. J. Douglas, 1990, "Analytical Studies of the Dynamic Response of the Meloland Road Overcrossing," *Proceedings of Fourth US National Conference on Earthquake Engineering*, Vol. 1, Palm Springs, CA, May, pp. 987-996.
- Elgamal, A.-W., R. Dobry, P. Van Laak, and J. Nicolas-Font, 1991, "Design, Construction, and Operation of 100 g-ton Centrifuge at RPI," *Proc. Int. Conf. Centrifuge 91*, Boulder, Colorado, 13-14 June, 1991, Hon-Yim Ko and Francis G. McLean (eds.), pp. 27-34.
- Gates, J. H., and M. J. Smith, 1982, *Verification of Dynamic Modeling Method by Prototype Excitation*, FHWA/CA/SD-82/07, California Department of Transportation, Office of Structures Design, Sacramento, CA, November.
- Gazetas, G., 1991a, "Foundation Vibrations," *Foundation Engineering Handbook*, 2nd Ed., Chapter 3, H. Y. Fang (ed.), Van Nostrand Reinhold, New York, NY, pp-553-593.
- Gazetas, G., 1991b, "Formulas and Charts for Impedances of Surface and Embedded Foundations," *Journal of Geotechnical Engineering*, ASCE, Vol. 117, No. 9, pp. 1363-1381.
- Gazetas, G. and K. H. Stokoe II, 1991, "Free Vibration of Embedded Foundations: Theory versus Experiment," *Journal of Geotechnical Engineering*, ASCE, Vol. 117, No. 9, pp. 1382-1401.
- Gazetas, G., and J. L. Tassoulas, 1987a, "Horizontal Stiffness of Arbitrary Shaped Embedded Foundations," *ASCE J. Geotechnical Engineering*, Vol. 113, No. 5, pp. 440-457.
- Gazetas, G., and J. L. Tassoulas, 1987b, "Horizontal Damping of Arbitrary Shaped Embedded Foundations," *ASCE J. Geotechnical Engineering*, Vol. 113, No. 5, pp. 458-475.
- Goel, R. K., and A. K. Chopra, 1997, "Evaluation of Bridge Abutment Capacity and Stiffness during Earthquakes," *Earthquake Spectra*, Vol. 13, pp. 1-23.
- Hardin B. O., and V. P. Drnevich, 1972, "Shear Modulus and Damping in Soils: Design Equations and Curves," *ASCE J Soil Mechanics and Foundations Division*, Vol. 98, No. SM7, pp. 667-692.
- Hibbit, Karlsson & Sorensen, Inc., 1994, *ABAQUS/Standard Theory Manual, Version 5.4*, Hibbit, Karlsson & Sorensen, Inc. Pawtucket, RI.

- Hushmand, B., C. B. Crouse, J. H. Wood, and G. F. Martin, 1986, "Centrifuge Testing of a Bridge-Soil Model," In: *Seismic Design of Monolithic Bridge Abutments*, Report by the Earth Technology Corporation, Long Beach, CA.
- Johnson, G. R., P. Christiano, and A. M. Epstein, 1975, "Stiffness Coefficients for Embedded Footings," *Journal of Geotechnical Engineering*, ASCE, Vol. 101, No. 8, pp. 789-800.
- Kausel, E., and J. M. Rosset, 1975, "Dynamic Stiffness of Circular Foundations," *Journal of the Engineering Mechanics Division*, ASCE, Vol. 101, No. 6, pp. 771-785.
- Kooijman, A. P., 1989, Comparison of an Elastoplastic Quasi Three Dimensional Model for Laterally Loaded Piles with Field Tests," *Proc. 3rd Int. Conf. on Numerical Methods in Geomechanics (NUMOG III)*, Niagara Falls, Canada, pp. 675-682.
- Kuhlemeyer, R. L., 1979, "Static and Dynamic Laterally Loaded Floating Piles," *Journal of Geotechnical Engineering*, ASCE, Vol. 105, No. 2, pp. 289-304.
- Lam, I. G. and G. R. Martin, 1986, *Seismic Design of Highway Bridge Foundations*, FHWA/RD-86/102, Vol. II, U.S. Dept. of Transportation, Washington, DC.
- Lam, I. G., G. R. Martin, and R. Imbsen 1991, "Modeling Bridge Foundations for Seismic Design and Retrofitting," *Proc., Third Bridge Engineering Conference*, Denver, Colorado, pp. 1-14.
- Lambe, T. W., and R. V. Whitman, 1969, *Soil Mechanics*, John Wiley & Sons, New York.
- Levine, M. B., and R. F. Scott, 1989, "Dynamic Response Verification of Simplified Bridge-Foundation Model," *Journal of Geotechnical Engineering*, ASCE, Vol. 115, No. 2, pp. 246-260.
- Liu, L. and R. Dobry, 1995, "Effect of Liquefaction on Lateral Response of Piles by Centrifuge Model Tests," *NCEER Bulletin*, Buffalo, NY, pp. 7-11.
- Martin, G. R., and I. P. Lam, 1995, "State of the Art (SOA4) Seismic Design of Pile Foundations: Structural and Geotechnical Issues," *Proceedings, 3rd International Conference on Recent Advances in Geotechnical Earthquake Engineering and Soil Dynamics*, Vol. III, St. Louise, MO, April, pp. 1491-1515.
- Martin, G. R., I. P. Lam, L. Yan, M. Kapuskar, and H. Law, 1996, "Bridge Abutments – Modeling for Seismic Response Analysis," *Proceedings, 4th CALTRANS Seismic Research Workshop*, Sacramento, CA, July.
- Masing, G., 1926, "Eigenspannungen und Verfertigung beim Messing," *Proc., 2nd International Congress on Applied Mechanics*, Zurich.

- Maroney, B., K. Romstad, and M. Chajes, 1990, "Interpretation of Rio Dell Freeway Response During Six Recorded Earthquake Events," *Proceedings of Fourth US National Conference on Earthquake Engineering*, Vol. 1, Palm Springs, CA, May, pp. 1007-1016.
- Maroney, B., B. Kutter, K. Romstad, Y. H. Chai, and E. Vanderbilt, 1994, "Interpretations of Large Scale Bridge Abutment Test Results," *The Third Annual Seismic Research Workshop*, Sacramento, June.
- McCallen, D. B., and K. M. Romstad, 1994, "Dynamic Analysis of a Skewed Short-Span Box-Girder Overpass," *Earthquake Spectra*, Vol. 10, No. 4, pp. 729-755.
- McNulty, J. F., 1956, "Thrust Loading on Piles," *ASCE J. S. M. F. D.*, Vol. 82, No. SM4, paper 1081.
- McVay, M., Casper, R., and T. I. Shang, 1995, "Lateral Response of Three-Row Groups in Loose to Dense Sands at 3D and 5D Pile Spacing," *Journal of Geotechnical Engineering*, ASCE, Vol. 121, No. 5, pp. 436-441.
- Nasim, M. A., and M. J. O'Rourke, 1987, "Lateral Impedance of Contact Pile Foundations," *Dynamics of Structures, Proceedings of Structures Congress '87*, ASCE, Orlando, FL.
- Nogami, T. (ed.), 1987, "Dynamic Response of Pile Foundations – Experiment, Analysis and Observation," *Geotechnical Special Publication No. 11*, ASCE, New York, NY. (*Proceedings, ASCE Convention, Atlantic City, NJ, April*)
- Nogami, T., J. Otani, and H. L. Chen, 1992, "Nonlinear Soil-Pile Interaction Model for Dynamic lateral Motion," *Journal of Geotechnical Engineering Division*, ASCE, Vol. 118, No. 1, pp. 89-106.
- Oldham, D. C. E., 1985, "Experiments with Lateral Loading of Single Piles in Sand," *Proc. Symp. Application of Centrifuge Modelling to Geotechnical Design*, Manchester, 16-18 April 1984, W. H. Craig (ed.), pp. 121-141
- Pais, A., and E. Kausel, 1988, "Approximate Formulas for Dynamic Stiffness of Rigid Foundations," *Soil Dynamics and Earthquake Engineering*, Vol. 7, No. 4, pp. 213-227.
- Poulos, H. G., and E. H. Davis, 1980, *Pile Foundation Analysis and Design*, John Wiley & Sons, Inc., New York, NY.
- PDA Engineering: PATRAN Division, 1993, "PATRAN User's Manual, Version 1.2," PDA Engineering, Costa Mesa, CA.

- Reese, L. C., W. R. Cox, and F. D. Koop, 1974, "Analysis of Laterally Loaded Piles in Sand," *Proc. 6th Annual Offshore Technology Conf.*, Paper OTC 2079, Houston.
- Reese, L. C. and S. T. Wang, 1993, *Documentation of Computer Program LPILE version 4.0*, Ensoft, Inc., Austin, Texas.
- Richart, F. E., Jr., J. R. Hall, and R. D. Woods, *Vibrations of Soils and Foundations*, Prentice-Hall, Englewood Cliffs, NJ, 1970.
- Saada, A., 1988, "A Brief Revue of Constitutive Models," *Proc. Int. Workshop on Constitutive Equations for Granular Non-Cohesive Soils*, 22-24 July, Cleveland, OH, pp. 7-10.
- Scott, R. F., 1979, "Laterally-Loaded Pile Tests in a Centrifuge," In: *Centrifuge Modeling of Geotechnical Problems*, ASCE National Convention, Atlanta, Georgia, pp. 1-13.
- Seed, H. B., and I. M. Idriss, 1970, *Soil Moduli and Damping Factors for Dynamic Response Analysis*, Report No. EERC 70-10, University of California, Berkley.
- Siddharthan, R., M. El-Gamal, and E. A. Maragakis, 1995, "Influence of Free-Field Strains on Nonlinear Lateral Abutment Stiffness," *Proceedings of 7th Canadian Conference on Earthquake Engineering*, Montreal, Canada, June, pp. 739-746.
- Stokoe, K. H., and F. E. Richart, 1974, "Dynamic Response of Embedded Machine Foundations," *Journal of Geotechnical Engineering Division*, ASCE, Vol. 100, No. 4, pp. 427-447.
- Sweet, J., and K. B. Morrill, 1993, "Nonlinear Soil-Structure Interaction Simulation of the Painter Street Overcrossing," *Proc. of the Second Annual CALTRANS Seismic Research Workshop*, Sacramento, CA, March.
- Terashi, M., M. Kitazume, A. Maruyama, and Y. Yamamoto, 1991, "Lateral Resistance of a Long Pile in or near the Slope," *Proc. Int. Conf. Centrifuge 91*, Boulder, Colorado, 13-14 June, 1991, Hon-Yim Ko and Francis G. McLean (eds.), pp. 245-252.
- Van Laak, P., 1996, *Development of Dynamic Capability for Geotechnical Centrifuge Model Studies*, Ph. D. Thesis, Dept. of Civil Engineering, RPI, Troy, NY.
- Ventura, C. E., W. D. L. Finn, and A. J. Felber, 1995, "Ambient Vibration Study of the Painter Street Overpass," *Proceedings of the 7th Canadian Conference on Earthquake Engineering*, Montreal, pp. 787-794.
- Werner, S. D., C. B. Crouse, L. S. Katafygiotis, and J. L. Beck, 1994, "Use of Strong Motions Records for Model Evaluation and Seismic Analysis of a Bridge Structure,"

- Proceedings of Fifth US National Conference on Earthquake Engineering*, Vol. 1, Chicago, IL, pp. 511-520.
- Whitman, R. V., and R. Dobry, 1993, *Soil Dynamics*, Class notes, Rensselaer Polytechnic Institute, Troy, NY.
- Wilson, J. C., 1988, "Stiffness of Non-Skewed Monolithic Bridge Abutments for Seismic Analysis," *Earthquake Engineering and Structural Dynamics*, Vol. 14, pp. 339-354.
- Wilson, J. C. and B. S. Tan, 1990, "Bridge Abutments: Formulation of Simple Model for Earthquake Response Analysis," *Journal of Engineering Mechanics*, ASCE, Vol. 116, No. 8, pp. 1828-1856.
- Wong, H. L., and J. E. Luco, 1978, *Tables of Impedance Functions and Input Motions for Rectangular Foundations*, Report No. CE78-15, Univ. of Southern California.
- Wolf, J. P., 1988, *Soil Structure-Interaction Analysis in Time Domain*, Prentice-Hall, Inc. Englewood Cliffs, NJ.



ISSN 1520-295X